Legacy of sulfide ore mining in the Friuli Venezia Giulia region: geochemical behaviour of potentially toxic trace elements and their impact on environmental compartments

NICOLÒ BARAGO | DEPARTMENT OF MATHEMATICS AND GEOSCIENCE | UNIVERSITY OF TRIESTE

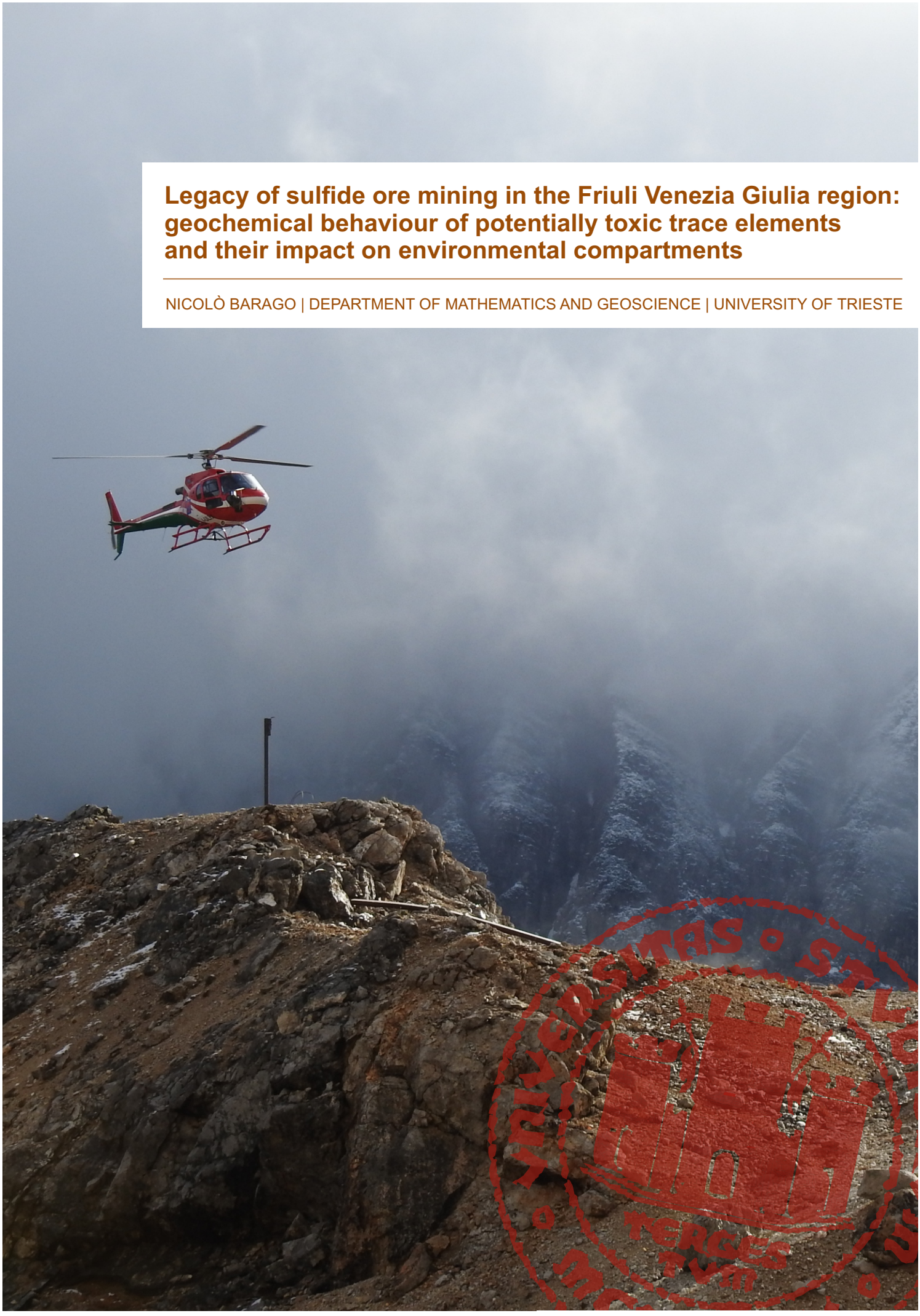

UNIVERSITÀ
DEGLI STUDI
DI TRIESTE

UNIVERSITÀ DEGLI STUDI DI TRIESTE

XXXV CICLO DEL DOTTORATO DI RICERCA IN

Scienze della Terra, Fluidodinamica e Matematica. Interazioni e Metodiche

Risorse del Dipartimento di Eccellenza (DMG, UNITS) 2018-2022

Legacy of sulfide ore mining in the Friuli Venezia Giulia region: geochemical behaviour of potentially toxic trace elements and their impact on environmental compartments

Settore scientifico-disciplinare: **GEO-08 Geochimica e Vulcanologia**

DOTTORANDO
NICOLÒ BARAGO

COORDINATORE
PROF. STEFANO MASET

SUPERVISORE DI TESI
PROF. DAVIDE LENAZ

CO-SUPERVISORE DI TESI
PROF. STEFANO COVELLI

ANNO ACCADEMICO 2021/2022

TABLE OF CONTENTS

1 INTRODUCTION

1.1 New challenges

Climate change is one of the biggest issues of the 21st century. Climate change has as its main cause anthropogenic emissions of greenhouse gases into the atmosphere and can cause a series of consequences on the environment and the society including: droughts, floods, more frequent extreme meteorological events, increase in global temperatures and sea levels, and more. Climate change is being tackled in recent years, with more or less decisiveness and effectiveness by the world states. Fortunately, the topic is increasingly a priority, and the knowledge of the problem is now widespread among the population. One of the main solutions to this global problem lies in the so-called "energy transition", through which, due to a progressive abandonment of fossil fuels in favour of renewable energies (solar, wind, geothermal, hydroelectric), the society should arrive to a hypothetical "zero emission" to limit climate change. However, since, in many cases, the power of renewable energies is not constant over time and all over the planet, the use of renewable sources must be accompanied by infrastructures and energy storage systems, to be able to manage it when and how energy is most needed.

An example of the energy transition is the automotive industry. In this regard, countries such as those members of the European Union are finally committing to reduce greenhouse gas emissions by at least 55% by 2030 (compared to 1990 levels) to become climate neutral by 2050[1]. In fact, the European Commission has declared that "all new cars and vans registered in Europe will be zero-emission by 2035" (European Commission, 2022). The transition include the switch to electric cars vehicles whose "fuel" should be energy produced from future renewable energy supplies (European Commission, 2022). Another example is Italy, which is committed to almost doubling the power (MW) produced from renewable sources starting, for example, from 9,410 MW produced by the wind power sector in 2016, to reach 20,200 MW produced by 2030 (onshore and offshore)[2].

Although the objective is clear, it remains less clear how to achieve these goals, since the realization of this transition requires large amounts of natural resources, even rare that are not present in all the world regions. In the newspaper "The Conversation", Prof. Pablo Higueras from Castilla-La Mancha University (Spain) writes: "A common 3 MW wind turbine needs on average more than 1 ton of neodymium (Nd) and about 100 kg of dysprosium (Dy). (...) These two rare earth group metals, a group of elements that are extracted only in certain regions of the world (...) are indispensable for the technologies needed to the renewable energy and electrify transport." In fact, such elements are rather rare that means they are not find in sufficient concentrations for extraction in nature and there are few producing states of these elements, thus determining their high. For example, the cost of neodymium in the period 2015-2022 was 50,000-240,000 dollars/ton (compared to 1,500-4,500 dollars/ton for a base metal such as zinc) (Higueras et al., 2022).

Moreover, many resources are not currently extracted in the European Union (EU) and the supply of many critical elements come from imports from geopolitically unstable countries (e.g. Democratic Republic of Congo) or potentially competing states (e.g. China, Russia) of the EU, and it is unclear whether there are other substitutes or alternatives for such resources (Leonard et al., 2021). In addition, the demand for these resources is growing. In this regard, the European Commission (2020) states: "Pressure on resources will increase - due to increasing global population, industrialisation, digitalisation, increasing demand from developing countries and the transition to climate neutrality with metals, minerals and biotic materials used in low emission technologies and products. OECD forecasts that global materials demand will more than double from 79 billion ton today to 167 billion tonnes in 2060. Global competition for resources will become fierce in the coming decade. Dependence of critical raw materials may soon replace today's dependence on oil." Therefore, for European strategic security reasons, 30 critical raw materials have been recognised.

[1] 2030 Climate target plan; https://climate.ec.europa.eu/eu-action/european-green-deal/2030-climate-target-plan_en (visited 11/01/2023)

[2] National Integrated Energy and Climate Plan. 2019. Ministry of Economic Development, Ministry of the Environment and Protection of the Territory of the Sea and Ministry of Infrastructure and Transport, Italy.

Table 1: List of Critical Raw Materials for the European Commission (2020)

2020 Critical Raw Materials (30)			
Antimony	Fluorspar	Magnesium	Silicon Metal
Baryte	Gallium	Natural Graphite	Tantalum
Bauxite	Germanium	Natural Rubber	Titanium
Beryllium	Hafnium	Niobium	Vanadium
Bismuth	HREEs[1]	PGMs[3]	Tungsten
Borates	Indium	Phosphate rock	Strontium
Cobalt	Lithium	Phosphorus	
Coking Coal	LREEs[2]	Scandium	

[1] Heavy Rare Earth Elements
[2] Light Rare Earth Elements
[3] Platinum Group Metals

1.2 Mining and environmental legacy

Although recycling and development of new technologies, which do not require critical elements, are the preferrable option for environmental sustainability, the traditional way to supply these elements is mining. In fact, the European Union (2022) states: "Mining has a central role in the EU's Green Deal and the green transition", therefore not extracting resources from the earth in the EU does not seem a choice. However, industrial extraction and processing of mineral resources is one of the major anthropogenic global sources of contamination and pollution from potentially toxic trace elements in the environment. Also because the volume of global mine waste production is massive, i.e., it was estimated to exceed five gigatons in the 1996 alone (ICOLD, 1996; Vallero and Blight, 2019). Due to the exponentially growing global demand for mineral resources (especially for Rare Earth Elements (REE) and precious metals) and improvements in the separation techniques of the economic minerals from gangue, mining companies currently exploit even low-grade ore bodies than in the past (Vriens et al., 2020), where up to 99% of the material may be discarded. This requires managing higher volumes of potentially toxic mining waste. However, mining is still one of the most ancient and necessary industries of the world. Hence, no sentence can better summarize the paradox of mining than "Mining activities are full of controversies. Modern societies need the product of mining. Nobody, however, wants to have a mine in their backyard or nature conservation area. The tension between global needs and transitions and local mining activities is evident" (European Union, 2022). In fact, in the last few years exploration and future exploitation are currently done even in EU where many states abandoned or dramatically reduced the mineral exploration in the last 30 years such as the examples of the Per Geijer REE ore deposit near Kiruna (Sweden), the Jadar Li ore deposit in Serbia or the Gorno Pb-Zn mine in Lombardia (Italy). However, last news report that for the Jadar and Gorno ore deposits, licenses were cancelled or not given due to protests and/or environmental incompatibility indicating that the future about mining in the EU is not clear.

1.3 Mineral resources in Friuli Venezia Giulia, Italy

Nowadays, 31 years have passed since the closure of the last major mine in Friuli Venezia Giulia (FVG), the Raibl mine. Mines in Italy are generally closed from few decades and the mining art is being lost, together with the workers and technicians and experts of the mining sector. Recent Italian scientific literature in this field has also declined, until today. But the needs driven by progress and the search for elements to carry out the energy transition and the recent conflicts and the world geopolitical framework have perhaps awakened the need to study the existing mineral deposits and find new ones and reconstitute experts in the art of mining. This thesis work was therefore difficult at first, as there are few people who still know the art of mining whereas information on the geochemistry of mineral deposits and, in general, the knowledge about this issue are fragmented.

Thanks to the work of Dino Di Colbertaldo, and others (including Luciano Brigo and Roberto Zucchini) who continued the study and research on regional mining sites (Figure 1), there are different scientific works that have handed down this knowledge.

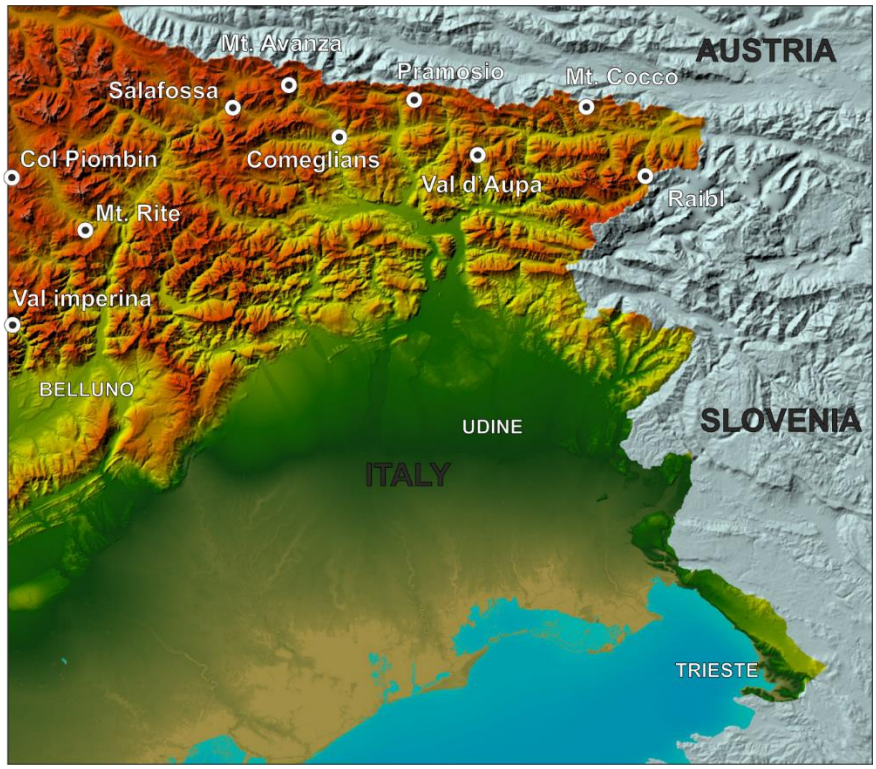

Figure 1 – Map of the metallic deposits of the Southeastern Alps

The geological-mining framework of Friuli Venezia Giulia is provided by Di Colbertaldo (1960), who was likely the first, starting from 1943, studying the Raibl field from a scientific point of view. In the article "*Le risorse di minerali metallici in Friuli*", he identifies the stratigraphic horizons in which the main metallic ore bodies have been found (Table 2, Figure 2), which in order from the oldest to the most recent are:

1. Silurian limestones at Orthoceras (e.g., Iron, manganese)
2. Devonic limestones in contact with the metapelites of the Carboniferous (copper, antimony, lead, zinc, barium)
3. Upper Permian dolomitic limestones (lead, zinc, copper)
4. Early Triassic arenaceous limestones (arsenic)
5. The limestone of the upper Ladinian in contact with the Carnian (zinc, lead, germanium, cadmium, fluorine; author's note: thallium, arsenic)

Other metalliferous horizons near middle Anisic dolostones, Permian magmatic rocks or Prepaleozoic shales and phyllades which are found in Veneto and Trentino Alto Adige, are missing in FVG.

Di Colbertaldo, in the early 60s, indicated that the mining activity in FVG, except for Raibl, was rather mediocre. In fact, while Raibl reached its historical production peaks (with about 550,000 tons/year of extracted ore, of which around 50,000 tons/year of mostly zinc and less lead concentrate), the rest of the mines were already decommissioned. However, he stated that the ores are present but it was necessary to start from the beginning with modern and rational mining methods, since the ancient mining research and exploitation had been conducted without rules, and the difficulties, especially logistical, were not negligible.

From that moment, no new deposits were exploited, although, on several occasions, mining explorations were conducted in the region, for example in the Carnic Alps with focus on: Cu-Sb mineralization at the Devonic-Carboniferous contact, among which Monte Avanza; baryte deposits at Coccau (nearby Tarvisio); Au presence which, however, was not found. Moreover, works of reorganization of the knowledge about mineralisations were conducted. Then, the exploration was concluded in the 90s. At present, mining sites are attracting only for environmental, touristic, historical and scientific interest.

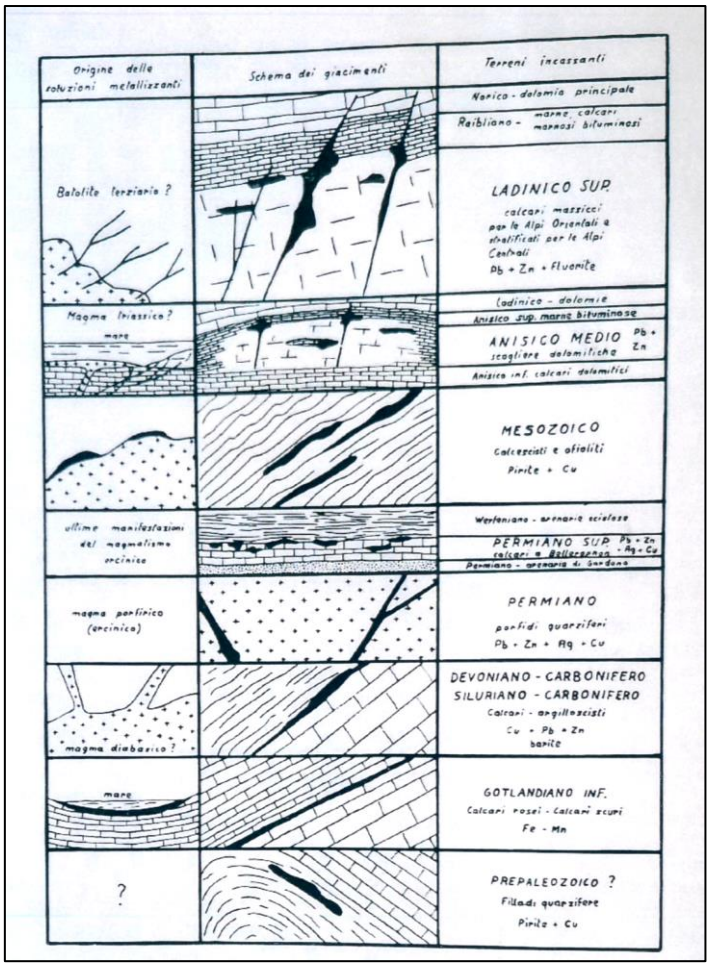

Figure 2 - Diagram of metal deposits in the eastern Italian Alps (Di Colbertaldo, 1960)

Table 2: modified from Colbertaldo (1960)

Geological eras and periods (old classification)		Host rock	Resource	Deposits in the Eastern Italian Alps	
				Veneto – Trentino Alto Adige	Friuli
Triassic	Upper Ladinian - Carnic	Dolostones, calcareous marly, bituminous limestone	Pb-Zn (As-Tl-Ge-Cd), pyrite, fluorite	Salafossa (Belluno)	Raibl Val d'Aupa, Val Uque
	Middle anisic	Serla Dolomite	Pb-Zn (Ag)	District of Auronzo, M. Rite, Col Duro, Val Inferno, Col Piombin	-
	Lower Trias	Sandstones - limestones	As	-	Val Bartolo
	Mesozoic in general	Limestone to Bellerophon	Cu + pyrite	Prettau (Bolzano)	-
Permian	Upper Permian	Quartz porphyries	Pb-Ag (Zn-Cu)	District of M. Calisio	Val Bartolo
	Early Permian	Limestones - clay schists	Pb-Zn-Ag (Cu)	Terlano, Nogarè (Trento)	-
	Devonic in contact with the Carboniferous	Limestones - clay	Cu-Sb-Ag-Zn-Ag-Ba	-	Monte Avanza, Comeglians, Ravascletto, Pramosio
	Upper Silurian	Limestone in Orthoceras	Fe-Mn	-	Monte Cocco
	Precambrian	Quartz Clays	Pyrite + Cu	Val Imperina (Agordo), Calceranica (Trento)	-

Regarding environmental aspects, the Raibl mine has been intensively monitored by the Environmental Protection Regional Agency (ARPA) due to the dispersion of potentially toxic elements in the groundwater and surface water of the area following the decommissioning of the mine. Also, accumulation of Tl in fish has been reported in Austrian Rivers, possibly due to the impact of the former extraction activities at Raibl. Therefore, fishing in the main watercourse was prohibited. In fact, not only the area is currently undergoing reclamation, but also the universities of Trieste and Udine have been commissioned to carry out specific studies on 1) the mobility and the behaviour of thallium (Tl), a mobile and very toxic element, and other metal(loid)s to mitigate dispersion outside the mining area, and 2) the possibility of implementing phytoremediation techniques, which use plants to limit contamination and erosion of spoil heaps.

From a scientific point of view, numerous studies in international peer-reviewed journals regarding environmental biogeochemistry or aspects of hydrogeological risk of Raibl have been published in recent years or presented at national and international conferences (e.g. Barago et al., 2021; Calligaris et al., 2017; Fellet et al., 2012; Meriggi et al., 2008; Petrini et al., 2016), whereas others, also concerning other mining sites, are currently in progress. Other studies have been recently carried out on mineralogy or other aspects of the FVG deposits (e.g. Bortolozzi et al., 2015a, 2015b, 2018; Ciriotti et al., 2006; Frangipani, 2013; Giarduz et al., 2015)

Some mines have been currently secured for tourism, also becoming important sites such as Raibl. Other abandoned mines rediscovered for tourism purposes are, for example, Cludinico (coal) and Resartico (oil shale) which can currently be visited, even if only minimally (i.e. Resartico).

From the historical point of view, the Natural History Museum of Udine have published several articles concerning the history and scientific aspects of mining areas of FVG in the recent years. Among them, of considerable importance is the 1998 book by Roberto Zucchini entitled "*Miniere e mineralizzazioni in provincia di Udine*", which is the main text of the history of the regional mining activity.

2 AIM OF THE THESIS

In the recent decades, we are witnessing an increasing demand for natural resources, driven by demographic and technological development, and now also for the energy and digital transition. This need translates into more increased extraction and production of larger volumes of resources from the Earth, where the mining industry is already active. Yet, in those countries where the mining industry has been stopped, interest is growing. However, although past, present, and future mining activity is always indispensable, it is never free from potential long-lasting environmental issues or disasters and conflicts with the populations living around the mining sites.

The contamination of the environment from the mining activity is a geochemical issue. Geochemical research at mining sites allows to assess the environmental impact of mining activities on the surrounding ecosystem and human health as well as to understand the mechanisms of release, attenuation and in general partitioning between different environmental compartments of potentially toxic elements (PTEs) and other contaminants. The geochemical knowledge allows to 1) identify and characterize the sources of contamination; 2) understand the chemical behaviour of elements through their speciation and possibly transport processes even over long distances; 3) assess environmental impacts such as contamination of soils and water; 4) monitor environmental quality over time; 5) understand natural attenuation processes of the contamination; 6) help for remediation and mitigation strategies and techniques.

The occurrence of PTEs in the environment due to the presence of the mining activity is a well-known issue. However, only the behaviour of the most common elements has been extensively studied, i.e. zinc (Zn), lead (Pb), arsenic (As). In contrast, less common but equally potentially dangerous elements, such as thallium (Tl), received less attention. Thallium is a quite uncommon element in nature but also an emerging contaminant due to its potential toxicity to ecosystems and human beings, which is also often disregarded by national regulations. In freshwaters, Tl is highly mobile and toxic at very low concentrations ranging from a few μg/L to mg/L.

The present doctoral thesis aims to study the environmental legacy of two mining sites in the Friuli Venezia Giulia region (Italy), now closed for more than 30 years. The two mines studied here, The Pb-Zn Raibl and the Cu-Sb(-Ag) Mt. Avanza mines, are relevant from an environmental, historical or political point of view. For example, the Raibl mine is currently under reclamation due to problems of cross-border contamination issues of potentially toxic elements (PTEs), among which major concerns are about high concentrations of Tl in the riverine waters. In contrast, other less important sites such as the Cu-Sb(-Ag) Monte Avanza mine, nowadays are being completely abandoned.

Hence, since environmental issues are different among different types of ore deposits and adopted processing systems, the objectives of this PhD thesis, through two case studies (Pb-Zn carbonate-hosted mine, and a Cu-Sb(-Ag) fahlore mine), are:

1) To reconstruct the history of the mining sites, focusing on the interactions between mining and the environment
2) Evaluating analytical methods for geochemical and contamination assessments.
3) To evaluate the impact of mining in the two main mines of FVG by potentially toxic trace elements in different environmental matrices (water, soils, mining waste, atmosphere)
4) To study the distribution, the temporal variations and the behaviour of thallium and other PTEs with focus on geochemical similarities and differences in several environmental compartments of sites affected by the mining activity. Particular attention was given to the release and natural attenuation processes of PTEs.
5) Making a step for creating or improving geoenvironmental models (Plumlee et al., 1999; Seal II and Foley, 2002), (i.e., models used to predict the effects on the environment characteristics for different ore types) for carbonate-hosted Pb-Zn and Cu-Sb fahlore mining sites.

3 STUDY AREA

As already mentioned before, the study areas are focused on two mines of the Friuli Venezia Giulia region, in Italy. The Zn-Pb Raibl and the Cu-Sb(-Ag) Mt. Avanza mines (Figure 3).

1) The decommissioned Raibl mine located at Cave del Predil, near Tarvisio (Udine) was a very important site for the extraction of lead and zinc (Pb-Zn) base metals. The mineralization is hosted in dolostones of Ladinian age, Middle Triassic. The first documents of mining are dated at least in 1320 and mining continued almost uninterruptedly until 1991. The peak of production occurred in the 60s of the XX century, with 1132 workers, about up to 550 000 tons / year of raw ore extracted with a production of Zn concentrate around 45 000 tons / year and Pb concentrate equal to about 5000 tons / year. Nowadays, it is under reclamation due to the release of trace elements, Tl and Pb among the others, into the riverine waters of the Rio del Lago.

2) The Monte Avanza mine is a rare example of a mostly monomineralic tetrahedrite ore deposit. It is characterised by a copper-antimony mineralization (Cu-Sb) and a paragenesis mainly composed of tetrahedrite, from which Cu and silver (Ag) were extracted. The deposit is hosted at the contact between Devonic metacalcareous rocks and Carboniferous metapelites. The first documents of mining seem to be dated to 778 AD and the production continued intermittently until the Second World War. In the second half of the '900, only some mining explorations were perpetuated, until 1995, when the interest for the mine dropped. Towards the end of the activities, in 1952, there were about 7070 tons / year of raw ore extracted with a production of concentrate equal to 90 tons.

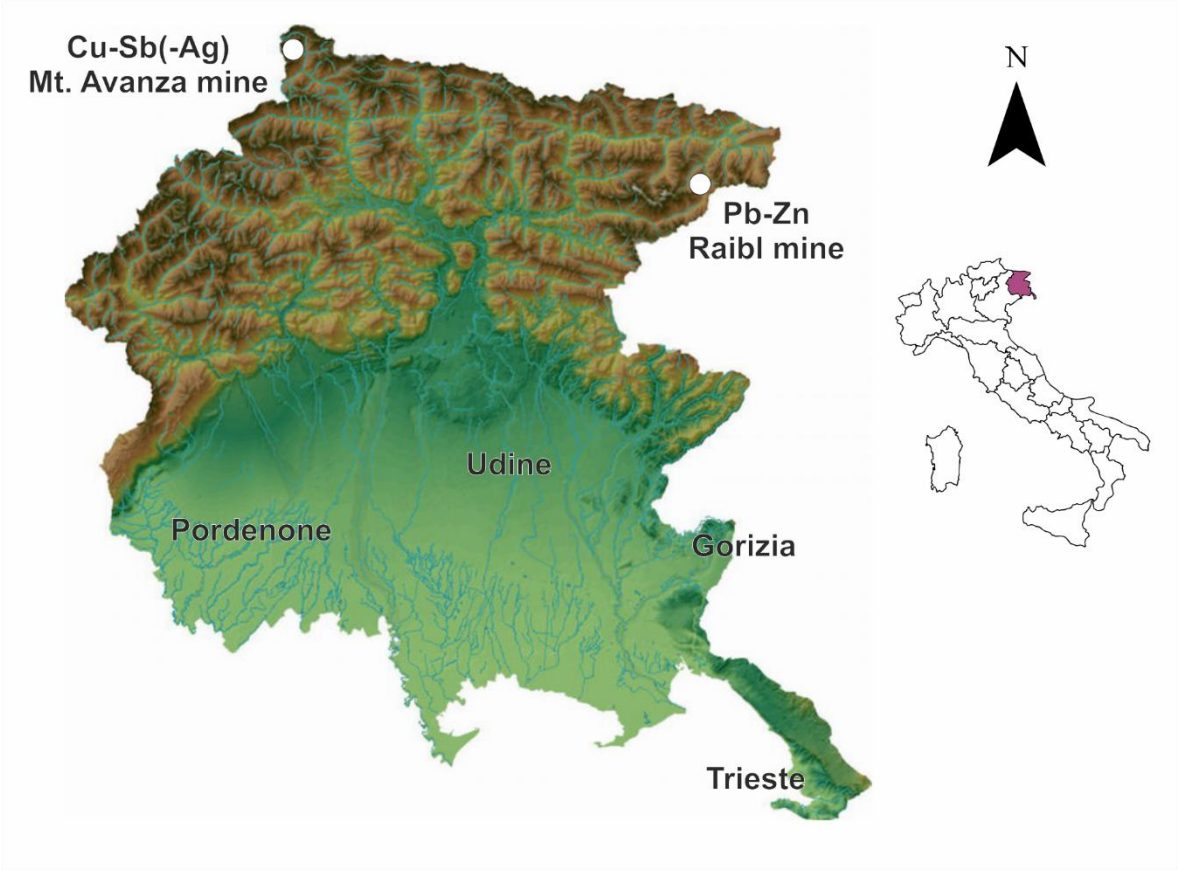

Figure 3 - Map of the Friuli Venezia Giulia region with location of the two investigated mines.

3.1 Raibl mine

From Middle Ages to 1991

Vague hints regarding the zinc-lead mine of Raibl (Figure 4), in today's Cave del Predil village (Figure 5), in the province of Udine (Friuli Venezia Giulia, Italy), date back to 1006, whereas the first documents of mining activity in Raibl are dated to 1320. No documents from Roman times have been found, although the presence of Roman roads in Cave del Predil suggests that the mines could have been exploited as early as that period. It is reasonable to think that the presence of exposed mineralization, with the red-ochre alteration colour of iron (Fe) had attracted attention and led to a metallurgical activity in Roman or pre-Roman times. The name Raibl is attributed to Oswald Rabel, a rich local landowner of the 15th century.

Figure 4 - Raibl mine at Cave del Predil; picture from June 2022. Left: “Clara” main shaft; center: main entrance of the mine; right: mineralurgical plant.

Although mining, in recent years, was mainly aimed at the extraction of Zn, Pb, and some lesser-known trace elements such as germanium (Ge), mining was initially oriented towards Pb and Fe. Iron was, in fact, used to feed the forges of the Valcanale valley and, starting from the fifteenth century, of the Fusine area (which means forges and, at that time, was called Weissenfels). On the contrary, Zn was transported to nearby Austria, to Arnoldstein, as early as the 16th century, for the production of brass.

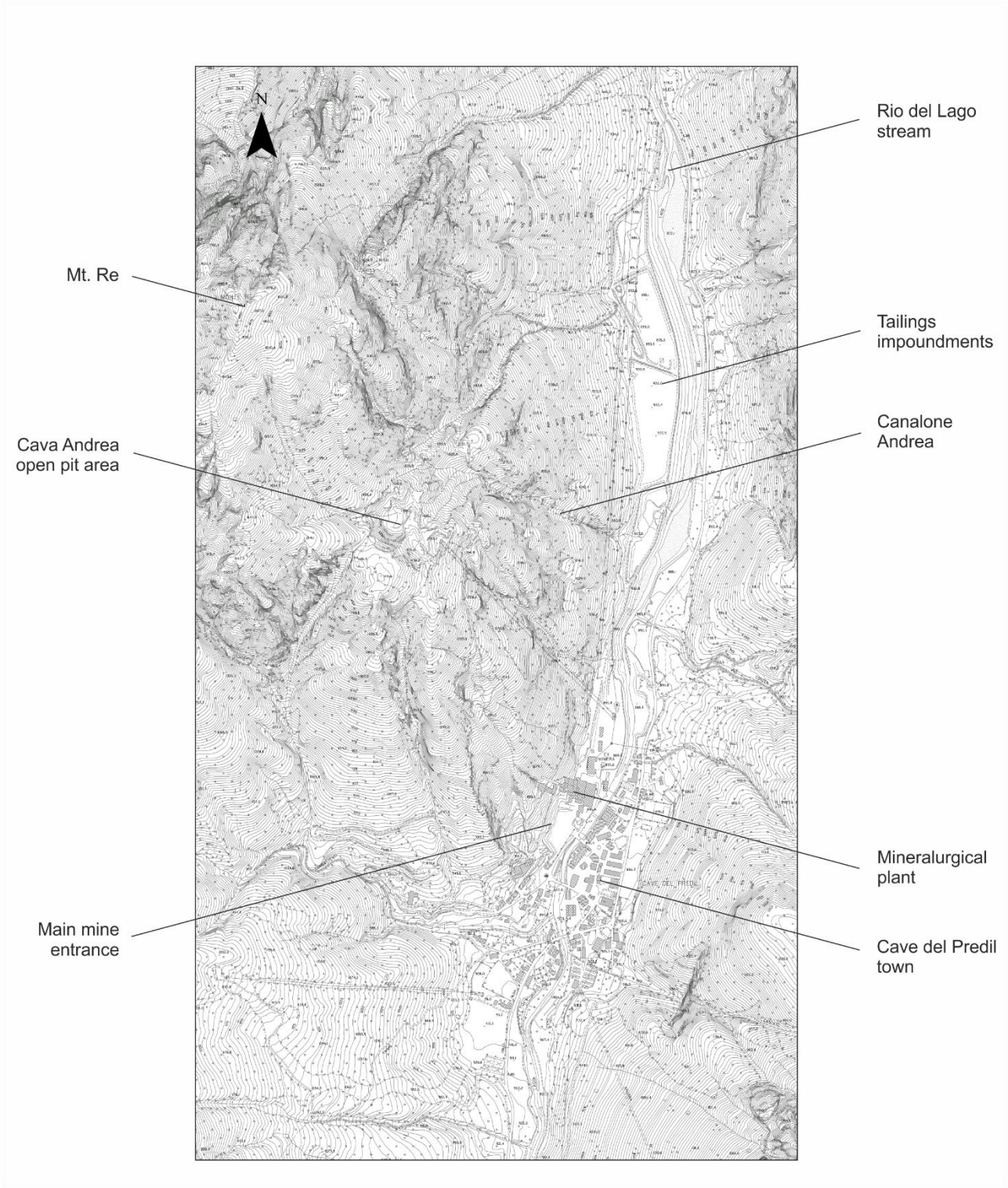

Figure 5 - Cave del Predil - Raibl mine area topographic map (1:5000 CTR FVG)

In 1678, the Raibl mine increased its importance, although to a lesser extent than Bleiberg, which produced three times more Pb than the Raibl mine. Until 1854, exploitation was limited to a depth of about 189 m (from level zero which corresponds to the village of Cave del Predil). With new exploration techniques, including the use of dynamite, and new knowledge, the lower portion of the ore deposit was also reached, greatly increasing the available reserves. Thus, the importance of mine grew considerably. By 1857 the number of mines had increased to 6 (Raibl I-VI). In Zucchini's treatise, reference is also made to a melting furnace owned by the company Erben Cyprian Struggl with blende (ZnS) and galena (PbS), whose location is not mentioned.

In 1893, Olinto Marinelli wrote that the ore was not processed at Raibl. Here, the ore was only sorted by hand and by mechanical means *on site*, and then transported to other locations for further processing. In fact, the galena (PbS) was brought to Kaltwasser (Riofreddo) (Figure 6) located 3 km downstream of the mine and the sphalerite, likely, to Celje (Slovenia), where there was a Zn smelter plant that was active from 1873 to 1970 (Žibret et al., 2018). The slags of the Riofreddo smelter plant can still be seen in the very small village located at the confluence of the Rio Freddo with the Rio del Lago. Also the chimney of the oven resting on the hydrographic left side of the homonymous stream is still visible. The ancient smelting plant of Riofreddo was presumably abandoned in the early '900. From what the miners learned, in recent times, the galena concentrate (PbS) was then sent across the border to Arnoldstein (Austria), whose plants also received the galena of Bleiberg. Zucchini (1998) also reports that some forges were operating in Tarvisio.

Figure 6 - Left: area of the former smelter plant of Riofreddo; right: detail of the slags; below a historical photo of the village and the active smelter plant[3].

The Bretto gallery, located at the XIII level at about 240 m below the village of Cave del Predil (or level zero) drains the waters of the lower levels of the mine (Figure 7) which are then discharged directly to the Koritnica River (Slovenia) which is a tributary of the Isonzo (Soča, in Slovenian) River flowing into the Gulf of Trieste. This straight gallery, almost 5 km long and with a slope of 2 ‰ was inaugurated by the Austrians in 1905, after 6 years of work. In 1917, during the First World War, the Bretto gallery was adapted to a railway line. The Austrian army used to bring

[3] Courtesy of Roberto Zucchini

soldiers, armaments and supplies also decisive for the defeats that Italy suffered. In the post-war period, the gallery represented a state border and an access to the lower mine levels for Slovenian workers directly from the village of Log pod Mangarton (in Italian: Bretto).

Figure 7 - Gallery of Bretto, 240 m deep from lv. zero, XIII level[4].

After the First World War, the Valcanale valley and its mines, with the treaty of Saint-Germain-en-Laye (10 September 1919) and Rapallo (12 November 1920), were annexed to Italy. In 1924, the Italian State become the sole owner of the mine and the company in charge of the thirty-year operation of the mine was the *Società Anonima Miniere Cave del Predil*, directed by Ing. Bernardino Nogara. In these years, there was a rational reorganization of exploitation. Numerous fillings were carried out of mine galleries of the war years, abandoned after "robbery" exploitation.

However, the effects of the 1929 crisis led to the closure of the mine in 1931. The mine was reopened only in 1933 as a result of the fascist autarchic politics, which were aimed to the economic independence of Italy. At that time, the successor company, *Società Mineraria del Predil S.p.A*. was led by the nephew of the previous director Giovanni Nogara. This led to significant changes in the efficiency of concentrate production. In fact, during this time, the sink and float" gravity concentration system was introduced in the mineralurgical plant (Figure 8). It consisted of a modern system of separation of the ore from gangue using dense liquids, in which the ore floated and the gangue sank allowing the separation of the valuable ore. Before the adoption of the *Sink and Float* system, sorting was done by manual picking by women.

[4] Picture: Omniaevo S.r.l.

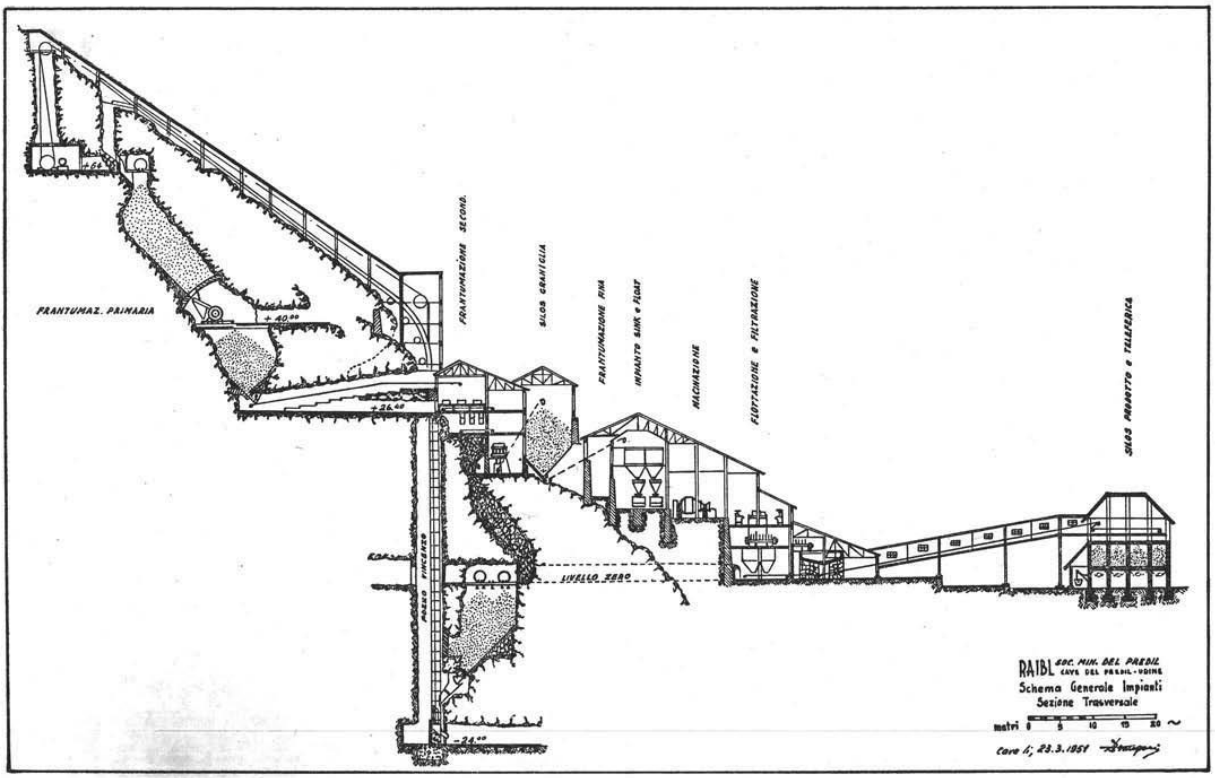

Diagramma n. 1. — Schema generale dell'impianto di concentrazione della Miniera di Raibl.

Figure 8 - photo at present (above) and scheme (below) of the mineralurgical plant (Mancini, 1950).

The first documented environmental issues date back to 1935. In an exchange of letters between the mine and the "Consortium for the Protection of Fisheries in Venezia Giulia" (ARFVG, 1935), the mine was called to perform analysis on the waters and provide data on the production and management of "mine water drainages" to answer the accusations of damage to fishing. As often happened, in the following decades, the mine recalled the right of discharge into the waters of the Rio del Lago as provided for by the treaty of Saint-Germain-en-Laye. The specific article, recalled several times in history, is art. 44 of Law 1322/1920: "*Austria also recognizes the right of Italy to the free use of the waters of Lake Raibl and its outlet, and the right to derive these waters to the Korinitza River*".

Figure 9 - Overview of Lake Predil upstream the Raibl mine[5].

[5] Picture: Friulioggi.it

Only in the years following the Second World War (1952), an agreement was made between the mine and the Consortium as follows: the damage was recognised and reimbursed by the Mine through the annual sowing of 100,000 juvenile trout to allow the repopulation of the waters upstream of the mine (presumably in Lake Predil, Figure 9) and the payment of a sum of 1,900,000 lire to the Consortium.

In the period between 1939 and 1941, the slurry discharged into the Rio del Lago stream was on average 370 tons / day, which testifies to a greater exploitation and production, compared to previous years, also for necessity of the war industry. It is reasonable to think that environmental issues were not the main concern at that time.

During the Second World War, episodes of sabotage by Slovenian partisans, occupations by Slavic bands, lack of personnel, exodus of German inhabitants from Raibl to Germany and general difficulties related to the war period (also in relation to the border position in which the mine was located) put at risk the continuation of mining activities. With the end of the war, in 1947 the new border between Italy and Yugoslavia was established, which passed in the middle of the Bretto gallery, perhaps the only example of an underground state border of the time.

In those years, the Tarvisio hydroelectric plant (which replaced the Plezzut plant) came into operation together with the Rutte basin (Figure 10) waters of the Rio del Lago were derived through an underground channel. In the Rutte basin, part of the waste from the mineralurgical plant was also deposited. The coarser fraction of sediments deposited in the Rio del Lago stream, and the suspended material left arrived at the Rutte basin, where the coarser fraction of these sediments deposited, as a second sedimentation step. The finer fraction, however, was transported from the Rutte basin to further downstream, entering the Tarvisio hydroelectric plant and then directly discharged into the waters of the Slizza stream. The Rutte basin had a capacity of about 311,000 m^3 and 20,000 m^2 of surface. However, this basin was often subject to muddying phenomena with the formation of layers of fine material, which had to be disposed of every 1–2 years. A 1952 report describes: "*The muddying of the Rutte basin is very strong. Indeed, during the February-April period in 1952, it reached a volume of about 10,000 cubic meters, corresponding to about 20,000 tons, where the material derived from river erosion can be considered zero. [...] Well, therefore, it can be said that the Rutte basin retains in a year [...] 66,500 tons of tailings, if we want to fix it, the period necessary for the emptying and cleaning of the basin is two months*" (ARFVG, 1952). The tailings were then discharged into riverine waters. As evidence of this, the director of the mine wrote in 1964: "*at the time of cleaning it is necessary to warn Bleiberger that it stops its plant so as not to have inconvenience for the influx of material discharged from the basin and everything ends there*" (ASTs, 1964). Therefore, this basin was primarily designed to create a "greater jump" for the plant and prevent muddying of the hydroelectric plants, rather than limiting the discharge of mining wastes into the river. The only produced effect was to decrease the turbidity of the waters of the Rio del Lago during the year, causing large dispersions of contaminants in a short time.

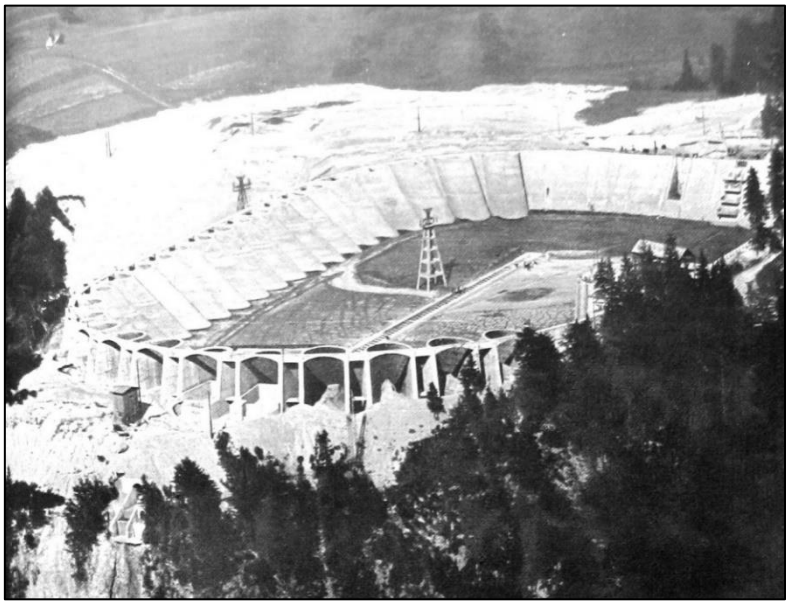

Figure 10 - Rutte basin just completed in 1952[6].

[6] Picture: Wikipedia

In addition to these works, a further damming of the Slizza stream (called "III jump") is mentioned. However, it is not known if it was built and where it was located (Figure 11). This should have constituted a second large basin that prevented the waste from being transported downstream, so that theoretically only 6% of the tailings, namely the very fine grains, could reach the Gail river (ARFVG, 1952). In conclusion, it can be said that until the construction of the tailings impoundments in 1976, there was no sufficient mine waste management. The only operations that did not involve the dispersion of tailings in the environment were the filling operations of abandoned underground galleries, with waste rock or tailings and the use of these materials for construction purposes.

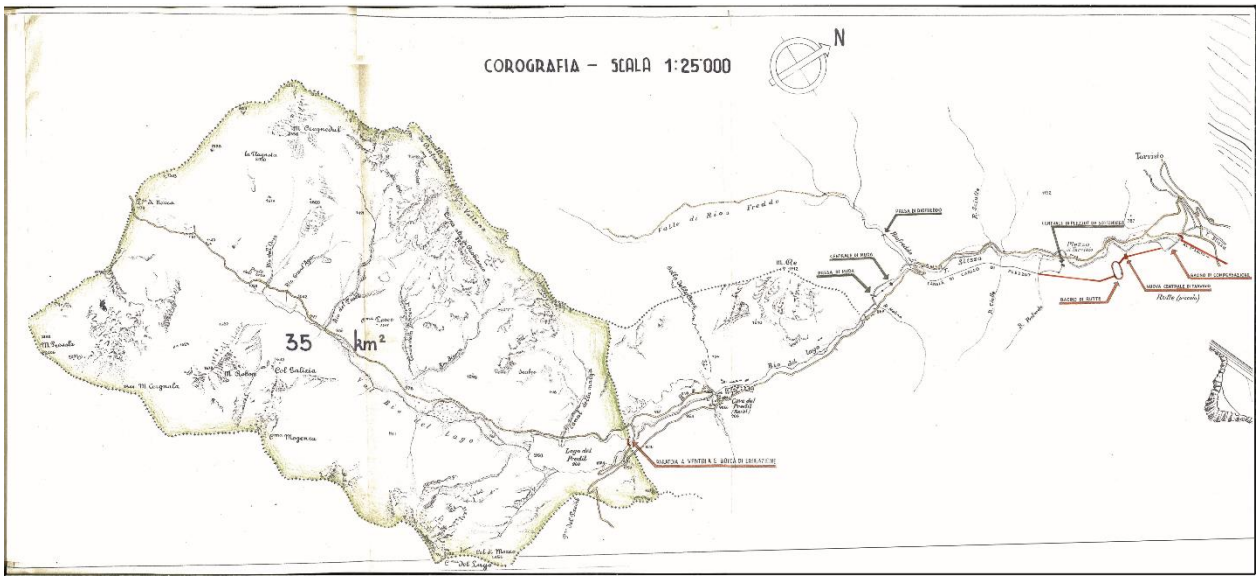

Figure 11 - Chorography of the valley of the Rio del Lago - Slizza in 1952 (ARFVG, 1952).

In 1952, following continuous solicitations from Austria, which claimed that Raibl's mining activity seriously affected fishing in the Austrian Gail River, the Water Magistrate allowed the riverbed area on the left bank of the Rio del Lago (the current area where the tailings impoundments are located) for the storage of tailings of the ore processing plant. However, the work was not realised. In response to the Austrians, the "*Corpo delle Miniere*" of Trieste responded by recalling, as in the past, the treaty of Saint-Germain-en-Laye and adding that the contamination of the Gail River was to be attributed to the waste of the chemical industries and the foundries of Arnoldstein, and the Pb-Zn mine of Bleiberg, that was more productive than Raibl, which discharged into the Nötch stream (a tributary of the Gail River in Austria).

In 1956, the mine passed under the private control of the "*Società Mineraria e Metallurgica Pertusola*". In those years, production was greatly increased and there was a peak in employment with 1,132 employees. In these years the production reached about 550,000 tons / year of ore extracted, with about 45,000 tons / year of sphalerite concentrate and 5000 tons / year of galena concentrate. However, this productivity was paid for by very heavy work rhythms, introduction of piecework, indiscriminate exploitation of the deposit and lack of attention to safety conditions, increasing accidents and mortality. In these years, the increase in production was accompanied by tensions with the workers.[7]

In 1963, the concession to the private company Pertusola expired, and the mine passed to AMMI (*Azienda Mineraria Metallurgica Italiana*) of the EGAM Group (*Ente Gestione Aziende Minerarie*). With the establishment of the Friuli Venezia Giulia Region, the Region acquired the mine, authorizing a twenty-year concession to AMMI in 1968. During this period, AMMI made improvements to the mineralurgical plant system.

Fatal accidents at the Raibl mine were frequent, and the arrival of the state-owned company was well received by the miners. As testified by the session of Tuesday, June 13th 1967 in the Italian Chamber of Deputies, the problem of rock bursts at the Raibl mine was well known. Rock can accumulate large amounts of energy, induced by the purely lithostatic load and the presence of excavations, galleries and voids in the rock. The rock bursts are instantly energy releases due to strong accumulation of the tensions in an elastic state in the dolomite rock. They are such as small and local seismic events. The effects of these events could vary from cracking to collapses of the gallery walls, with collapses for an extension of 2-3 meters in height and even of 1000 m^3 of volumes. Therefore, at the end of 1972, the excavation technique

[7] Archivio di Stato di Trieste.

for "descending cuts with cemented filling" was introduced, which gave greater stability to the galleries, limiting the possibility of rock bursts. Improving safety was mandatory but, from another point of view, the cemented filling introduced other costs, which would have contributed to weighing on the company finances in the following years until the definitive closure of the mine[8].

Between 1964 and 1965, the Rutte basin was emptied for the last time before being decommissioned. The reason was a collapse of the buttresses, which occurred on November 7th, 1965, which triggered a flood in the Slizza stream, without any victims. From that moment, the Rutte basin was never again used for mining purposes.

The construction of the tailings impoundments and, therefore, of the dams that store the flotation tailings, took place in the 70s. In fact, the drafting of the project dates back to 1972; the concession (*Disciplinare* n° of Rep. 12439 of 16/12/75) is of December 1975 and Magistrate Decree (n° 486/1 of 9/04/76) is of April 1976 (Ismes & Aquater, 1990). The construction of the tailings impoundments (Figure 12) involved the partial occupation of the bed of the Rio del Lago stream. As the dams are ubicated on its sediments, it caused a little significant deviation of the stream and constituting, *de facto*, the new left bank of the stream. Initially, the entire work consisted of 3 ponds (or impoundments), then became 4, which develop in succession, with a trend that, even altimetrically, follows the general morphological trend of the valley. The dams of the ponds were made in a single solution, and were completed prior to the discharge operations, using mostly the coarser waste rock produced from the mine. The subdivision of the ponds was achieved through the construction of internal transverse dams which connect the external dams with the left side of the *Piccolo Monte Re*. Currently, the tailings impoundments extend for a length of about 1200 meters in S-N direction, from the village of Cave del Predil (S) to the locality Muda (N).

In 1978, SAMIM (*Società Azionaria Minero-Metallurgica*) of the ENI group acquired the concession of Raibl. From this year SAMIM carried out interventions of restoration, upgrading and mineral exploration. Direct testimonies from miners about that the exploration under Mount *Cinque Punte* (on the opposite side of valley and of the mine), where for years miners looked for ore and hydrothermal springs, following the experience of Bleiberg, unfortunately was not successful.

In 1987, the SIM (*Società Italiana Miniere*) of the ENI group took over the management of the mine, until its closure in 1991. We learn from the Ismes-Aquater report that in 1988 interventions were carried out to raise the impoundments, to reach a maximum height of 25 and 23 meters for ponds N° 2 and N° 3 (current name), respectively, whereas they were waived for pond No. 4. At the same time, following the tragic experiences of the dam failure of the Prestavel mine in the Stava valley (Trentino Alto Adige, Italy), the slope of the dams was reduced and regularised up to a slope of 24.7°, from the previous average slope of 30° - 38°. Before, the discharge of the tailings was in a direction N-S parallel to the valley. The slurry was discharged in the basin N° 2, with passage, for further clarification, to the subsequent lower basins (N°3 and 4), and finally discharged into the Rio del Lago stream (Ismes & Aquater, 1990), downstream of basin n°4. We learn that, from 1988, the management of the slurry changed. In fact, the discharge took place in the basin in operation at that time, using the basins separately one at a time. In addition, the points of the slurry discharges were rationally moved on the external dams, with the aim of favouring the formation of "beaches" of sand near the external dam and to reduce the formation of water stagnations near them (Figure 13). In each basin, various discharge points were set up, about 50 meters apart each, which were varied during each weekly phase of discharge, in order to obtain a certain uniform distribution of the tailings in each basin. We also learn from the technical report that, in periods prior to 1985, the basin N° 1 (now N° 2) had been partially emptied, and the removed material was used for fillings and for the substrate of the motorway.

Even if the potential of the mine was never fully exploited, several factors contributed to the closure of mine. However, Raibl was the only one to operate in Friuli Venezia Giulia in the second half of the '900. Currently, the memory of mining is kept by a museum known as *Polo Museale di Cave del Predil*, where the opportunity to live the history of Raibl is offered, illustrated with great competence thanks to the support of the mining community.

[8] The technique consisted of removing the mineralization and filling the cavity with inert rock material and cement.

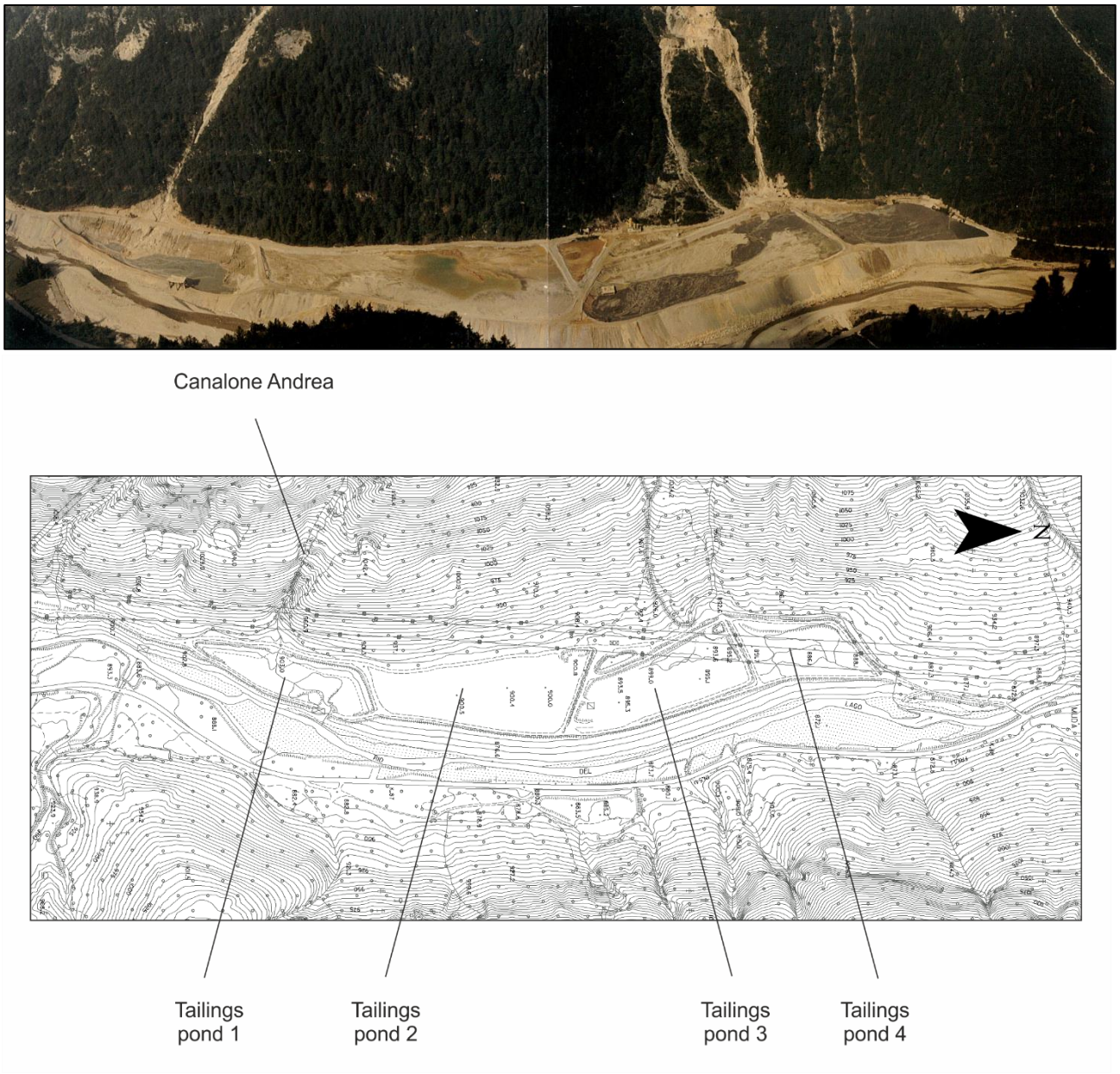

Figure 12 – (Top) Raibl tailings impoundments in 1988. The upstream area where the main entrance of the mine is located, is on the left. Source: archives from the FVG Geological Survey. (Bottom) Tailings impoundments, topographic map (1:5000 CTR FVG)

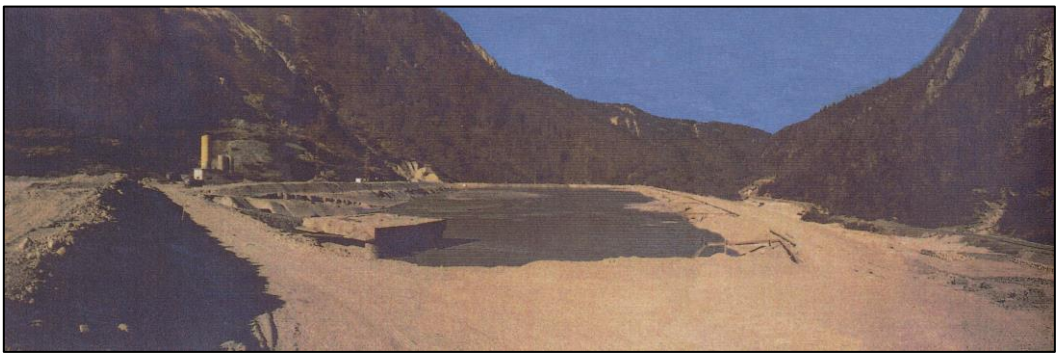

Figure 13 - Overview from N to S of pond N° 3. They are distinguished from the left: concrete plant, reinforced concrete platform, tailings discharge pipe in operation. Source: archives from the FVG Geological Survey

After 1991, reclamation and environmental studies

Following the closure of the mine in 1991, the works are not regulated either by Royal Decree (R.D.) n. 1443/1927, which regulates the research and exploitation of mines, nor by the Decree of the President of the Republic (D.P.R.) n. 128/1959 "*Norme di polizia delle miniere e delle cave*".

With Law no. 388 of 23-12-2000 (*Legge finanziaria* 2001), the Article 18 of Law no. 349 of 8 July 1986 "*Istituzione del Ministero dell'ambiente e norme in materia di danno ambientale*" was modified, inserting in the plan for the reclamation of the industrial area of Bagnoli a list of priority industrial areas, including former mining activities. Among the sites in the list subject to environmental reclamation, was also included the Raibl mine at Cave del Predil, belonging to the Municipality of Tarvisio.

On December 16th 2005, the Ministry of the Environment and Protection of Land and Sea (MATTM), the Friuli Venezia Giulia Region (FVG Region), the Province of Udine and the Municipality of Tarvisio signed an Agreement "for the reclamation and environmental restoration of the former mining site of the Raibl mine at Cave del Predil" by which the reclamation of the tailings impoundments area was planned (Figure 14) with the allocation of € 1,000,000 by the MATTM. This agreement defined the measures aimed at limiting the dispersion of contaminants and reducing their presence to the regulatory limit values in order to mitigate the effects of contamination on the environment.

Figure 14 - Tailings pond n° 1. Left: particular erosion of the pond and failure of the dam, right: view from the north (Iadarola and Viso, 2009).

In 2007 the Regional Agency for Environmental Protection (ARPA FVG) assessed the contamination by means of chemical analyses on various environmental matrices, including soils and surface and groundwaters. In addition, 7 boreholes were carried out, 4 of them in the 4 tailings impoundments. The cores were then subsampled in sections which were analysed for determining concentrations of potentially toxic elements (Figure 15).

Figure 15 - Realization of a core in the tailings impoundments (Imprefond, 2007)

In 2008, the University of Udine carried out a study concluding that there should be no risk of instability of the tailings impoundments following earthquakes (up to magnitude 6.4) and intense rainfall (Meriggi et al., 2008).

The FVG Region, as owner of the area, activated on its own initiative the procedures for the "emergency securing" (MISE), reclamation and environmental restoration, making use of the commissioner management referred to in Regional Law 18 January 1999, n. 2, the figure of its Deputy Commissioner, as well as the off-budget management and the autonomous administration of the fund called "*Fund for the restoration of the mining area of Cave del Predil*". It should be emphasised that the agreement was signed under Ministerial Decree 471/99 and, therefore, the design phase had not included the modelling of the risk analysis. With the entry of Legislative Decree no. 152/2006 (on 29/4/2006), the project phases concerning the "permanent securing" (MISP) have been adapted to the *titolo V* of the decree D. lgs 152/2006.

On 20th June 2009, the Deputy Commissioner for the restoration of the mining area of Cave del Predil transmitted the "Characterization Plan for the area of tailings impoundments", for approval by the Authorities which, following requests for documentary additions, with the Decree No. 43 UD/BSI/134 of 22nd January 2010, approved the plan.

With the note dated 10th January 2011, Prot. 4/11, received on 14th January 2011, the Deputy Commissioner for the recovery of the mining area of Cave del Predil, Dr. Luciano Baraldo, sent the "site-specific risk analysis" document, for approval by the Authorities. By decree of 18th January 2012 No. 74/UD/BSI/134, the document itself was approved. In the characterization plan and in the risk analysis, the tailings impoundments are identified as the main source of contamination of the Rio del Lago.

In 2012, Fellet et al. (2012) published the first article related to environnental contamination at Raibl where the authors reported zinc and lead concentrations in several metallophyte plants, including the hyperaccumulator of thallium *Biscutella laevigata L.* (Figure 16), from several sites of the mining area.

Figure 16 - Thallium (Tl) hyperaccumulator: *Biscutella laevigata L.* Picture from the Salafossa mine, 2014.

On 1st July 2013, the "operational securing" project was submitted and, on 12th November, the operational project of the "permanent securing" interventions - first phase for its approval was resubmitted, ratified by decree n.109 / UD / BSI / 134 of 28/01/2015.

With a note dated 29th October 2015, the Deputy Commissioner transmitted the variant to the general operational project of the interventions for the permanent securing of the tailings impoundments of the Raibl mine (Cave del Predil).

After the phases of characterization and modelling of risk analysis, with decree of the director of the service n.109 / UD / BSI / 134 dated 28/01/2015, the operational project of the interventions of permanent securing of the area of the impoundments was approved. This project, provided for the following interventions:

- construction of an external barrier in bored piles
- installation on the upstream side of a waterproof plastic diaphragm
- coverage of the four tailings impoundments according to Legislative Decree 36/2003
- restoration of the tailings dams
- installation of a permeable Zero Valent Iron reactive barrier
- planting on restored areas

The total cost of the whole work accounts for 19,750,000 €.

During the first phase of the permanent securing activities, capping of ponds N° 3 and 4 were carried out, and with Decree of the Director of the service n. 1134 / UD / BSI / 134 dated 16/5/2016, the second phase of the permanent securing activities (MISP) was approved and it provides, in addition to the above, a better regulation of the waters coming from the “Cava Andrea”, the open pit area on the top of the *Monte Re* (Figure 5, Figure 17), through a gully known as "Canalone Andrea" that descend towards the impoundments from *Monte Re*.

Figure 17 - Open-pit mining area "Cava Andrea".

Petrini et al. (2016) found high concentrations of thallium in the waters of the Rio del Lago and in the main drainage waters of the mine, although they appeared diluted by riverine waters. The authors suggested to better investigate the behaviour of this element, and its possible effects on the aquatic ecosystem and on the water resources used by the population.

By decree no. 32 dated 19th December 2014 of the President of the Autonomous Region of Friuli Venezia Giulia, the Deputy Commissioner delegated for hydrogeological risk approved the final executive project of the intervention "Works of defence and hydraulic regulation of Rio del Lago in Cave del Predil" for the amount of 3,500,000 €. This intervention was completed in 2017 and involved the construction, along the tailings dam, of a 9 m high barrier of bored piles, for a total length of 947 m. The piles were set at the foundation level of the dam, overlapping each other for a few centimetres at the point of contact, in order to create a joint with characteristics of filtration with positive effects on the containment of contaminated residual materials, preventing their dispersion through the sub-riverbed (Figure 18).

Figure 18 - Realization of the external barrier at the foot of the tailings dams (Protec, 2017).

In the same year, in 2017, a study informed that the tailings pond No. 1 would interact with potential landslides and debris flow, due to mining residues eroded by the "Cava Andrea" (Calligaris et al., 2017).

From 2019 to 2023, as a part of this doctoral thesis and as part of a study called "Definition of the geochemical behaviour of potentially toxic trace elements in the Cave del Predil area" the University of Trieste reports that flood events of the Rio del Lago are responsible for greater leaching and transport processes of potentially toxic elements including thallium in the waters of the mining area, especially in groundwater entrapped in the tailings impoundments.

In 2021, the University of Trieste presented the internal geometries of the tailings ponds N° 2-3 and a method to estimate the concentrations of zinc (and other trace elements) in the impoundments starting from geoelectric geophysical surveys described in Barago et al. (2021).

In 2022, capping of tailings ponds 1 and 2 was accomplished.

From 2022, two new studies in progress by the University of Trieste will investigate: 1) the mechanisms responsible for potential release and partitioning of trace elements from the different minerals that constitute flotation tailings of the impoundments and 2) the genesis of the Pb-Zn Raibl deposit. These new studies will not only examine aspects of scientific interest on this centenary site, but perhaps also offer new opportunities for the Raibl mining area.

3.2 Mt. Avanza mine

The Monte Avanza mine (Lat: 46.618763°, Long: 12.755203°) (Figure 19) is located in the western Carnic Alps, near the municipality of Forni Avoltri (UD) in the North West of the Friuli Venezia-Giulia region, very close to the border with Austria and about 4 km from the Veneto region (Figure 20). More specifically, the area is located on the southern slope of the Avanza and Navastolt mountains, of the Monte Avanza group. The Monte Avanza group develops in an East-West direction, characterised by transversal valley incisions. Due to its location, the Monte Avanza mine is located at an altitude between 1650 and 1800 m a.s.l.

Figure 19 - Monte Avanza mine, “Pietra Verde” open pit area[9].

As for Raibl, the main text consulted is "*Miniere e mineralizzazioni in provincia di Udine*" (Zucchini, 1998 and references therein). The beginning of the mining activity dates back to the year 778 AD. The exploitation, although not continuous, continued until the mid-seventeenth century when the Monte Avanza mine was abandoned for years until the nineteenth century.

[9] Picture: Geopark Carnic Alps

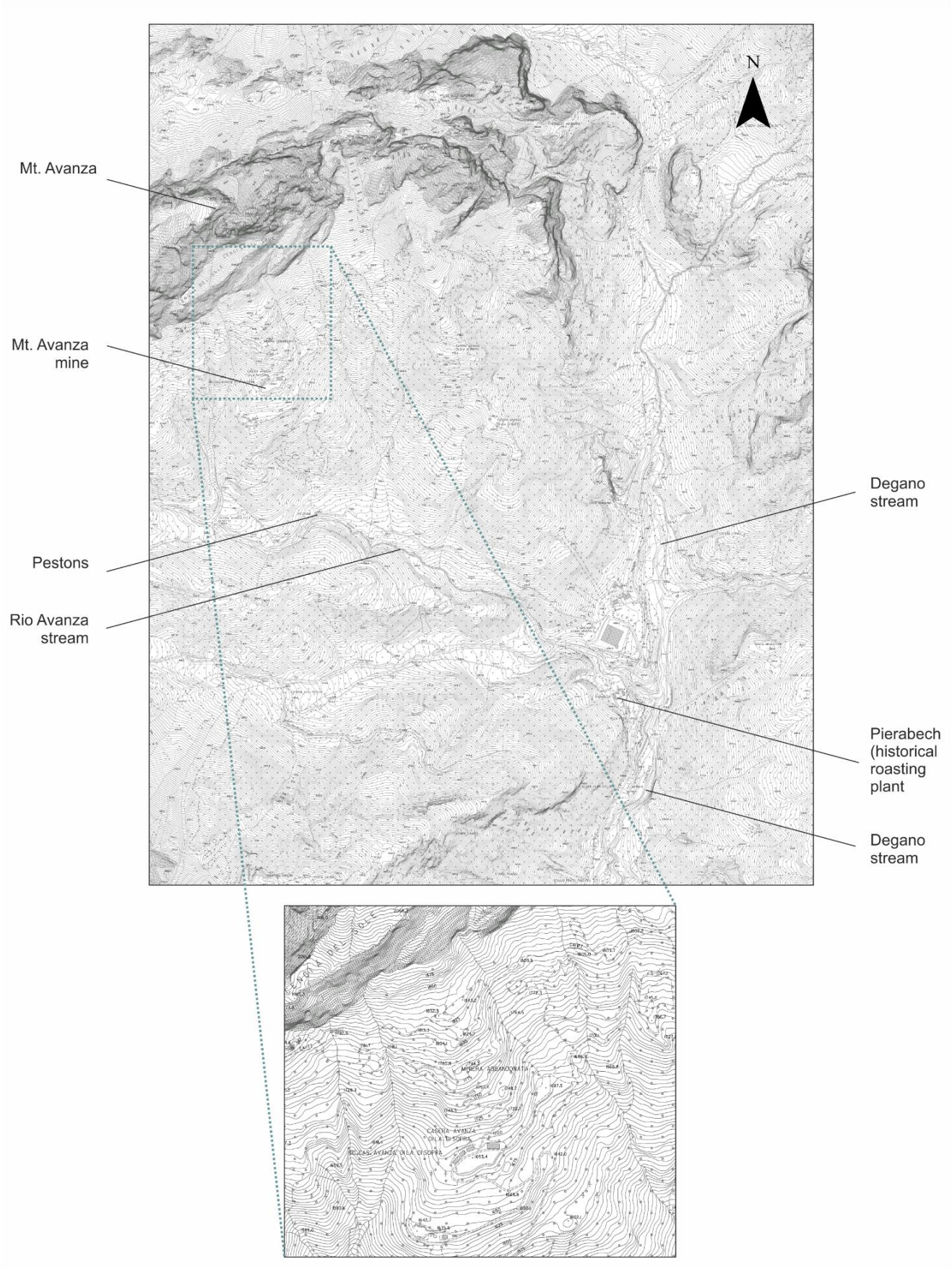

Figure 20 – (Top) Avanza – Degano valley, topographic map. (Bottom) zoom of the mine area (1:5000 CTR FVG).

In 1813, thanks to the discovery of a rich mineralised vein, interest in the tetrahedrite deposit was revived.

In the period between 1858 and 1865, the works in the Monte Avanza mine were managed by the *Società Veneta Montanistica* (SVM) which built the Bauer gallery in 1862 and expanded some ancient galleries. In 1863, the active galleries were the following: Bauer, Errera, Schieling, Comello, O'Conor, Mulazzani, Biringaccio and Sella (Figure 21) intercepting the ore body on the contact between the Carboniferous metapelites and the Devonian carbonates.

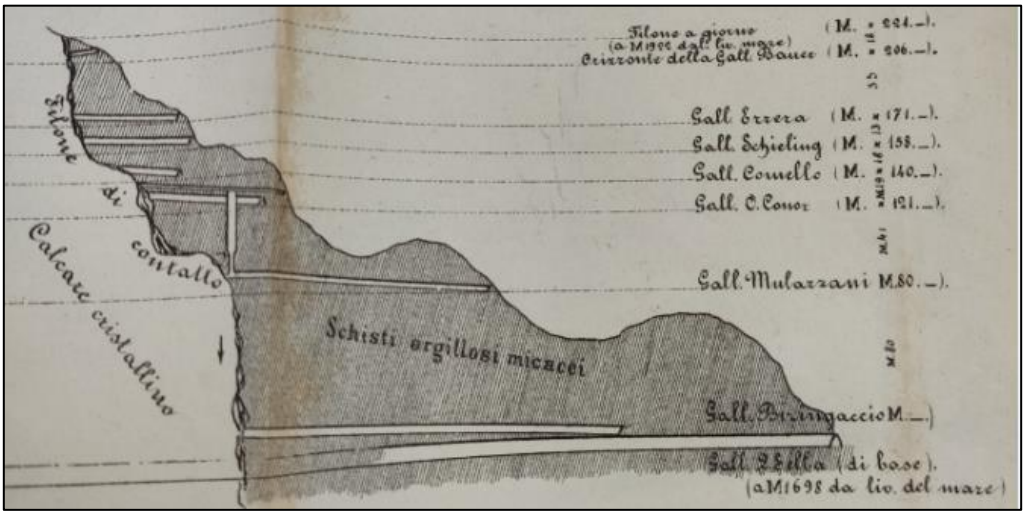

Figure 21 – Section of the Mt. Avanza mine (Marinoni, 1876)

The investments then went into the construction of dormitories, tenements and shelters for the numerous miners, in new road connections, in the construction of ore processing plants, in the construction of furnaces and offices of employees in the locality "Pier a Bec" (now Pierabech) at an altitude of 1062 m above sea level (Marinelli, 1906).

In this period, ore processing for the production of concentrates consisted of several phases (Grignani, 1868). Initially, the ore extracted from the mine was subjected to a first crushing and sorting, which was carried out in the space in front of the mine adit of the Sella gallery (q. 1686 m s.l.m.) through which the mineral considered poor (waste rock) was discarded (Figure 22). Through sorting were obtained: 1) rich ore, 2) poor ore, 3) poor and rich lead, 4) spar (presumably barite), 5) gangue.

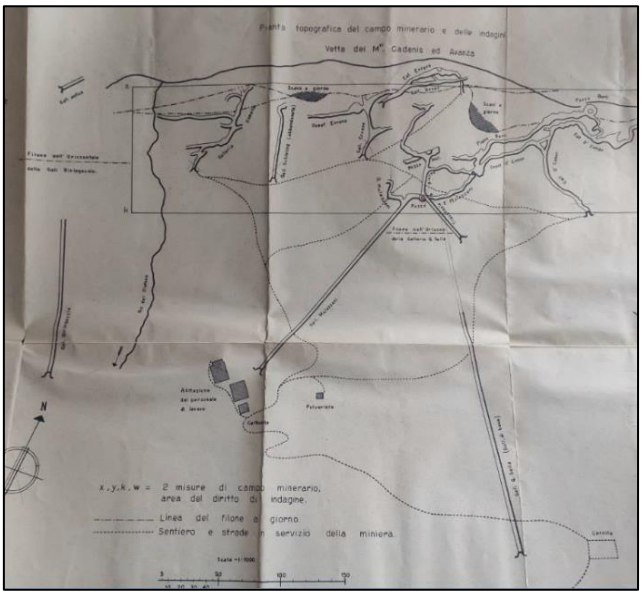

Figure 22 - Plan of the Monte Avanza mine in 1876. The Sella gallery at the bottom right of the plan had not yet reached mineralised contact

After that, the ore was transported by road and then by means of a 540 m long wooden unloader to a mill system at Pestons, located next to the homonymous creek where the ore was milled and sorted. Here, the ore was ground, washed and sieved thanks to the action of the waters of the Rio dei Pestons. The "pistons" plant consisted of 15 pistons in three divisions moved by a water wheel (a watermill); each piston beat 60 hits per minute. The rich ore with a content > 6 % was directly crushed and ground and before passing to the metallurgical forge. The poor ore was instead pulverised and passed to concentration. The rest of the processing steps took place in Pierabech.

The product of this phase was a "*slicco*" (from the German Schlick, "mush"), that is, a concentrate constituted by ground and granulometrically fine material that contained about 4 - 5% copper and about 400 mg/kg silver. This concentrate was roasted in 3 steps in the reverberation furnace at Pierabech (Figure 23): 1) 8 hours for drying, 2) 8 hours for desulfurization and 3) about 8 hours at 850 degrees to obtain copper and silver chlorides (presumably adding sodium chloride).

Figure 23 - Historical photo of the ore roasting area (Pierabech).

From the reverberation furnace, the products passed into tanks with filters containing a solution of 25 % sodium chloride, 14 % sulfuric acid and 22 % hydrochloric acid. The objective was to dissolve sulfosalts (the tetrahedrite) by forming soluble chlorides. Afterwards, the solution was circulated first through copper grains, on which the silver precipitated, and then on scrap and ferrous materials precipitating copper. After that, mercury was used for the separation of silver, with which forms the amalgam. Once the amalgam was roasted (at 123 °C) and mercury evaporated, silver was obtained and mercury was subsequently distilled and recovered. The silver was then liquefied and refined and sold in rods.

About production:

In 1864, 2500 kg of copper and 18 kg of 90% pure silver were produced.

In 1865, 10 tons of copper and 75 kg of 0.86% pure silver had been mined.

In 1866 they found veins increasingly rich in chalcopyrite so that the processing plant was modified. In this year 13 tons of copper and 20 kg of silver were produced.

In 1867 a silver galena vein was found, with little tetrahedrite and chalcopyrite.

However, due to the low economic value of the mining veins, the difficulties related to the processing of minerals other than tetrahedrite, the limited fuel and wood resources, the technical problems of excavation due to high quartz quantities and a huge negative balance also due to the critical Venetian economy at that time, the company reduced their activities starting from 1865 until the works were suspended in 1876. Once the concession expired, in the following decades only sporadic mining research and maintenance of galleries and infrastructures were conducted, alternating with periods of abandonment of the mine.

In 1917, the mill system of Pestons were destroyed during World War I.

In 1921, exploration and maintenance began again but without extraction during the concession of Mr. Petrosini.

In 1923, with the creation of the Province of Friuli, the mine was grouped to the Mining District of Trieste. However, it remained inactive until 1933 due to ore deposit interests in Yugoslavia (Zucchini, 1998).

In 1939, the *Società Anonima Miniere del Monte Avanza* (SAMMA), obtained licenses for the exploration and then later a concession for the exploitation of the well-known copper, antimony, silver, zinc, lead, mercury and arsenic deposits. Thus, the mining activity restarted reactivating almost all the existing infrastructures and galleries. The company promoted the construction of external plants, buildings, staff accommodation, new electrical systems and a flotation plant of 100 tons/day, as well as a 12 t/h material ropeway (Feruglio, 1966). Of this plant, once located in the locality "Pian della Guerra", now only the basic ruin remains. There were also extensions of the galleries and levels to follow the intermittent mineralisations (Cecchi, 1986).

In 1942, 3,500 tons ore with 2% of copper were produced (Zucchini, 1998). After the World War II, the production stopped until 1952 when SAMMA lost the concession and abandoned the area (Figure 24). Before the end of operations, raw ore production was estimated at approximately 7070 t for raw ore (0.3% – 1% Cu) and approximately 90 t of concentrate (21% – 23% Cu).

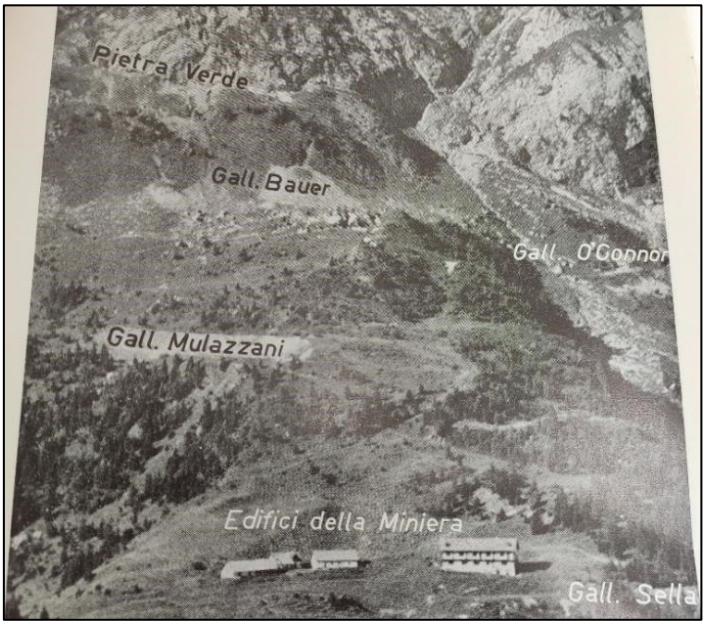

Figure 24 – The area of the Monte Avanza mine showing the main galleries and the mine village (Feruglio, 1966).

In 1975, the company Finsepol S.p.A. of Trieste began an ambitious program of geological and mineral prospecting. Following the successful prospecting, in 1985, the construction of new infrastructures began, including the current "*Villaggio minerario"*, the improvement of road connections and the excavation of the Finsepol gallery, which is at an altitude of 1640 m a.s.l., located at the lowest altitude and is the longest of all the galleries of the mine (Figure 25). The waste rock produced from the excavation of the Finsepol gallery (or at least part of it) was stored in the waste rock pile that now constitutes the square of the Mining Village (Figure 26). A drainage water purification system for the Finsepol gallery was also built by means of an hydrocyclone, and the waters were channelled and discharged into the Rio Avanza (Figure 27). However, the company concluded the research with negative results and, in 1995, it abandoned the area proceeding towards environmental restoration works, such as the planting of native trees. Nowadays, the area is completely abandoned again.

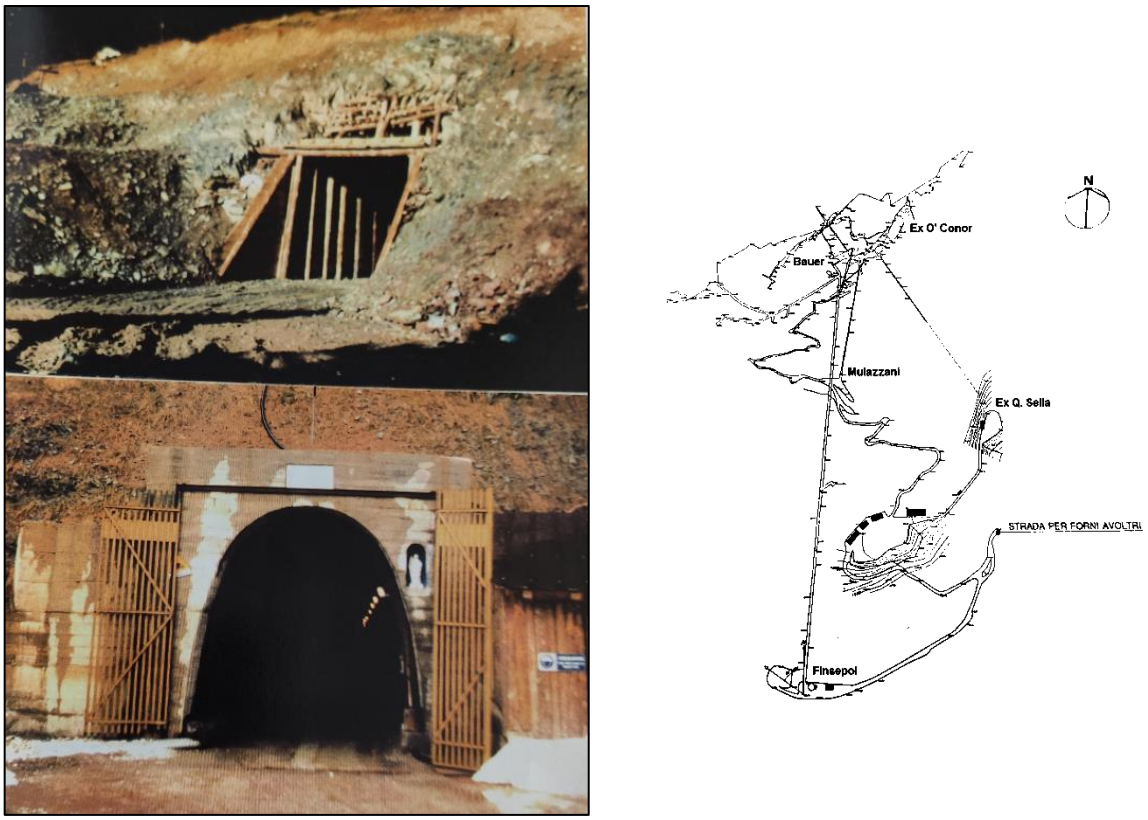

Figure 25 - (top left) excavation in 1986 and (below left) work completed in 1989 of the Finsepol gallery (Brusca, 1996); (right) planimetry during the last stages of mining exploration (90s). Location of the waste rock piles at the Sella gallery and the Mining Village are shown.

Figure 26 - (left) Storage of waste rock at the "*Villaggio minerario"* in 1989; (right) "*Villaggio minerario" today*[10].

[10] Picture: Geoparco Alpi Carniche

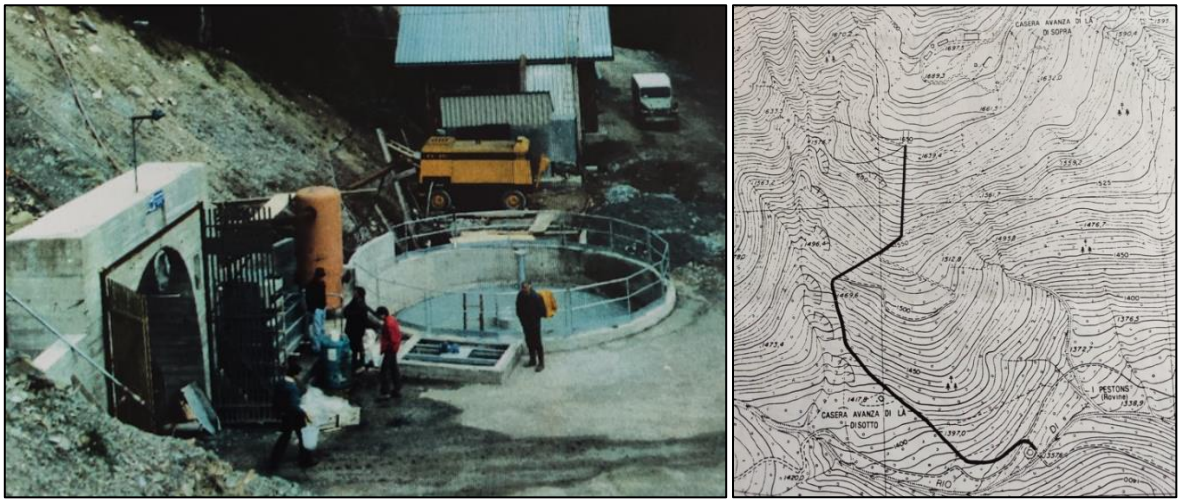

Figure 27 - (Left) construction of the Finsepol gallery drainage water clarification plant; (right) project for the drainage water discharge pipe of the Finsepol gallery (Valle, 1997)

4 SUMMARY OF PAPERS

4.1 Paper I - Hydrogeochemistry of thallium and other potentially toxic elements in neutral mine drainage at the decommissioned Pb-Zn Raibl mine (Eastern Alps, Italy)

Authors: Barago N., Pavoni E., Floreani F., Crosera M., Adami G., Lenaz D. and Covelli S.

Journal: Journal of Geochemical Exploration, 245, 107129. https://doi.org/10.1016/j.gexplo.2022.107129

Summary: Study on the hydrogeochemistry of PTEs, in the Pb-Zn mining area of Raibl. The area is of particular interest because it is subjected to remediation due to a prolonged process of cross-border contamination and represents one of the few case studies regarding Tl in abandoned mining areas. Given this, geochemical data of waters have been monitored for more than two years and it was observed that tailings impoundments are the main source of Tl in the surface and groundwaters in the mining area. Moreover, for this element no particular natural attenuation processes are expected, whereas for zinc (Zn), lead (Pb), arsenic (As) and antimony (Sb) the release could be attenuated by absorption processes on Fe-oxyhydroxides and precipitation of Zn carbonates. In general, the impact is strongly spread throughout the valley of the Rio del Lago - Slizza. However, the concentrations of PTEs in the waters of the area are quite high and further studies and interventions must be conducted to limit the contamination of the area.

4.2 Paper II - Thallium and PTE distribution and mobility in solid matrices at the Zn-Pb Raibl mining site (NE Italy)

Authors: Barago, N., Pavoni, E., Crosera, M., Adami, Floreani F., G., Lenaz, D. and Covelli, S.

Journal: Manuscript

Summary: This part of the thesis describes a study on the distribution and mobility of various metal(loid)s at Raibl, with attention to critical issues and opportunities. Via laboratory tests (partial extraction with HCl 0.5 M) it was possible to evaluate the mobility of potentially toxic elements present in the solid matrix (e.g., soils, sediments, mining waste) under moderately acidic conditions. The median value (%) of the labile fraction was found in the following order: Mn ≈ Cd > Co > Zn > Ni > Tl > Sb > Cu > Pb > Cr > V ≈ As ≈ Fe. Antimony was found more mobile than As, although often both were found in their higher concentrations in the residual fraction. It has been observed that most of the mining residues can release high concentrations of many PTEs under moderately acidic conditions. However, comparing these results with those of the real chemistry of the waters, it is noted that Tl remains mobile even in weakly alkaline conditions (along with Cd and Zn). This evidence confirms what was observed by hydrogeochemical study of the waters. However, the diluted HCl partial extraction seems 1) to overestimate Pb mobility and 2) to strongly affect dissolution of secondary Zn carbonate minerals. These results indicate that the HCl partial extraction may inhibit some natural attenuation processes of Pb and Zn availability in dissolved forms such as (co-precipitation) and sorption on Hydrous Ferric Oxides (HFOs). It is also noted that the concentrations of some landfills are so high that they may be worthy of further processing, to extract useful metals and remove them from the environment. In general, the impact is strongly widespread throughout the valley of the Rio del Lago – Slizza.

4.3 Paper III - Composition of mine tailings: a microanalytical study (Pb-Zn Raibl mine)

Authors: Barago N., Covelli S., Turco G., Lenaz D.

Journal: Manuscript

Summary: Quantitative chemical microanalysis on flotation tailings, residues of the Raibl mineral processing plant, with particular attention to the occurrence of metal(loid)s in different mineral phases. These results constitute the first study in

the area regarding speciation of elements in flotation tailings. The absence of primary sulfide minerals such as sphalerite (ZnS) and galena (PbS), very scarce quantities of pyrite (FeS_2) and great abundance of iron oxyhydroxides (Fe) and Zn carbonates, discarded during the separation phases and formed by oxidation processes of primary sulfide minerals, was observed. Regarding potentially toxic elements (PTEs), no minerals with As-Cd-Ge-Sb-Tl as major element were found indicating that those elements are hosted in other phases. In addition, the abundant presence of Fe-oxyhydroxides very rich in Zn and Pb supports and confirms the hypothesis of absorption of PTEs on them, whereas the abundance of Zn carbonates supports the hypothesis of Zn precipitation due to oversaturation of Zn in waters and stability of carbonate forms of this element. These processes of natural attenuation are crucial for environmental considerations. The mineralogical-geochemical results might also contribute to design a dedicated flotation tailings treatment plant, as traditional systems are based on the separation of minerals.

4.4 Paper IV - Environmental impact of potentially toxic elements on soils, sediments, waters and air nearby an abandoned Hg-rich fahlore mine (Mt. Avanza, Carnic Alps, NE Italy)

Authors: Barago N., Mastroianni C., Floreani F., Pavoni E., Floreani F., Parisi F., Lenaz D. and Covelli S.

Journal: Environmental Science and Pollution Research (accepted)

Summary: The study in the Cu-Sb(-Ag) mining area of Monte Avanza was focused on the distribution of other PTEs or elements of economic interest, such as mercury (Hg), antimony (Sb), copper (Cu) and arsenic (As). The characterization of different environmental matrices such as water, solids (soils, mining residues, sediments) and air allows to study the partitioning of various PTEs among different matrices. Interestingly, Tl and Ge were associated with the "lithogenic component" and not to sulfide minerals. Although mine drainage water often slightly exceeded the national regulatory limits for Sb and As, with Sb being more mobile than As, their relatively low dissolved concentrations indicate a moderate stability of the tetrahedrite. Mercury showed weak solubility but the potential evasion of Gaseous Elemental Mercury (GEM) into the atmosphere also appears to be characteristics of Hg also in non-cinnabar ores. The other studied elements were not mobile and therefore prefer to partition in the solid phase. In general, the impact is strongly localised close to in the extraction area.

4.5 Paper V - Portable X-ray Fluorescence (pXRF) as a Tool for Environmental Characterisation and Management of Mining Wastes: Benefits and Limits.

Authors: Barago, N., Pavoni, E., Floreani, F., Crosera, M., Adami, G., Lenaz, D., Larese Filon, F. and Covelli, S.

Journal: Applied Sciences 12, 12189. https://doi.org/10.3390/app122312189

Summary: The validation of portable X-ray fluorescence analytical data (pXRF) on solid samples of the two sites under examination (Raibl and Mt. Avanza), by comparison with results from traditional benchtop multielemental analytical methods (ICP-OES, ICP-MS) indicate that as far as a thorough QA/QC protocol is followed, pXRF can be a powerful method for determining the concentration of potentially toxic elements as well as elements of economic interest, in a fast and accurate manner. In fact, As, Cu, Fe, Hg, Mn, Pb, Sb, Zn reached a good data quality level in at least one of the two sites, if the concentrations were sufficiently high. However, pXRF produced false-positive results, which should be manually removed via spectral interpretation. At low concentrations the reliability of the pXRF analysis decreased for some elements such as As, Cu and Fe.

6 CONCLUSIONS

In summary, this work is aimed to understand the impact on the surface environment of the legacy of past mining activities, starting from their historical reconstruction and investigating the geochemical behaviour of potentially toxic trace elements present in the different analysed matrices, in terms of spatial and temporal variability. Two mining sites located in the Friuli Venezia Giulia Region (Northern Italy) were studied: the carbonate-hosted Zn-Pb mine, (Mississippi Valley or Alpine-type) at Raibl, and the fahlore Cu-Sb(-Ag) mine, at Monte Avanza.

In this three-year research, various environmental and geological matrices, such as air, water, soils, sediments and mine waste from the two mine sites were investigated through chemical and mineralogical analyses. The results obtained provided a series of information highlighting aspects and dynamics concerning potentially toxic trace elements, especially thallium, that are still little known, and can be summarised hereafter.

History

Although both mines were active from the Middle Age, the Raibl mine was two orders of magnitude more productive than the one at Mt. Avanza, this translates in higher volumes of mining waste. In fact, whereas Mt. Avanza site shows few water drainages and limited volumes of waste rock piles, in the Zn-Pb mine of Raibl, a flotation plant produced millions of tons of tailings and waste rocks. Part of them (more or less 4 million tons) are still stored in the impoundments on the Rio del Lago stream bank thus representing a source of contamination for the main watercourse, which flows towards Austria, and matter of concern for the quality of water resources and the aquatic ecosystem.

Various analytical techniques, including also pXRF after thorough QA/QC (quality assurance / quality control) protocols, helped to assess the impact of the two mines discussed below:

Zn-Pb Raibl mine

In the Raibl mine, the main source of contamination of waters are the tailings impoundments, where high concentrations of potentially toxic elements (PTEs) such as thallium (Tl), lead (Pb) and zinc (Zn) are present and leached by the groundwaters and released in the Rio del Lago stream. Time series reveal that leaching and the subsequent dispersion of PTEs are promoted during periods of intense rainfall and high flow river conditions. During such events the concentrations of PTEs in the groundwaters entrapped in tailings impoundments can be heavily increased by one order of magnitude, whereas the total dissolved load (TDL) in the main watercourse, the Rio del Lago, can be magnified by three orders of magnitude. Not only is the water contaminated, but also the compositional characteristics of the stream sediments testify to a long-term impact on the riverine aquatic environment. In fact, the geoaccumulation index (I_{geo}) applied to the stream sediments indicate that the Rio del Lago is heavily to extremely contaminated by As, Cd, Pb, Sb, Tl and Zn. In addition, since the natural soils of the area are often mixed with mining waste (i.e., waste rocks), a wide range of PTE concentrations was found in the Pb-Zn mining area of Raibl: up to > 100 mg/kg for Tl, Sb, Cd and Ge; > 1,000 mg/kg for As; > 1 % wt. for Pb and > 10 % wt. for Zn. Seventeen years have passed since the reclamation of the Raibl mine site began in 2005. Moreover, the high concentrations and release of PTEs persist despite almost 30 years of flushing after extraction and processing activities shut down. A suggestion for a possible remediation of the Raibl area, and other decommissioned or active mining areas, is to consider the reprocessing of mining waste, especially tailings, not only to recover elements of economic value but also to reduce potential contamination of water resources and other environmental compartments. Since reprocessing is based on the separation of different mineral phases, a microanalytical study on tailings minerals was conducted. The results indicate that the external portion of tailings are constituted by iron (Fe) secondary minerals (probably Fe oxy-hydroxides) containing even high concentrations of Zn and Pb (> 10% wt.) and Zn secondary minerals (probably carbonates such as smithsonite or hydrozincite). Further specific investigations on tailings could provide confirmation and, in general, more information on these mineral phases.

Cu-Sb(-Ag) Mt. Avanza mine

The geochemical signature of the past mining activity at the Cu-Sb-Ag Mt. Avanza fahlore ore deposit was evidenced by notable concentrations of the elements associated with the (Hg-Zn)-rich tetrahedrite in mine wastes, soils and stream sediments (max concentrations: Cu = 4019 mg/kg, Sb = 1049 mg/kg, Pb = 1216 mg/kg, Zn = 1204 mg/kg, As = 654 mg/kg and Hg = 473 mg/kg). Conversely, notable amounts of PTEs in the stream sediments appeared to be restricted to the mining area. Although mine drainages often exceeded the national regulatory limits for Sb and As, relatively low

dissolved concentrations of the main metal(loid)s were observed, suggesting the moderate stability of the tetrahedrite and other minor ore-bearing minerals.

Geochemical insights

Tl: the element was found abundant in the Pb-Zn mine associated to sulfide minerals, whereas in the fahlore mine was found associated to the "lithogenic component", thus possibly associated to K-bearing silicates. At the Raibl site, anomalous high concentrations of Tl were found in mining waste (up to 908 mg/kg of Tl) along with surface and, particurlarly, groundwaters affected by leaching of post-flotation tailings (max 120 μg/L), with Tl/Zn ratios 3–4 fold higher with respect to mine drainage and riverine waters. This is reasonably supported by the modelling results since negligible natural attenuation processes are expected for Tl, which appeared to be mainly present in its ionic mobile form Tl(I). This is also consistent with the results obtained from the single-step partial extraction (diluted 0.5 M HCl) applied to solid matrices. An increase of up to an order of magnitude of the Tl labile fraction was observed in mining wastes and ore gossan sediments compared to soils. Indeed, the Tl extractable fraction was found up to 58.7% of the total concentration in samples of the ore gossan sediments, up to 41.9% in waste rock and up to 46.1% in tailings.

Zn: the elements is the main metal extracted at Raibl (from sphalerite) and is only present as a trace element in the Mt. Avanza, although the main mineral is a (Zn-Hg)-rich tetrahedrite. At the latter site, Zn do not represent an element of concern or interest. In contrast, at Raibl, Zn in waters may be more abundant than the common major components, such as K, showing dissolved concentrations up to 14,933 μg/L in the tailings impoundments groundwater. Such high dissolved concentration may trigger even precipitation to hydrozincite minerals, as well as to be absorbed on Fe oxy-hydroxides. These two processes, together to pH-dependent speciation, were found as the three main natural attenuation processes of Zn. Total concentrations of Zn falling in the range of 1-4 % wt. are easily found in mining waste, with max concentrations of 11.5 % wt. thus indicating that reprocessing of mining waste could be evaluated as a possible strategy of metal recovering. About Zn partitioning, it was found that the element can be hosted in sphalerite (ZnS), Zn secondary minerals (smithsonite and hydrozincite carbonates) and Fe secondary minerals (Fe oxy-hydroxides). Secondary minerals appear to be the most important phases in regulating Zn dissolved concentrations in the mining area, although secondary minerals act as a temporary sink because they can be easily mobilizable via a moderate acid extraction. In order to evaluate a possible reprocessing, Zn carbonate should be a target for planning of the mineral separation.

Pb: the element was the second main metal extracted at Raibl and it was a minor constituent of the Cu-Sb(-Ag) Mt. Avanza ore body in galena. At the latter site, Pb is found at relatively low concentrations. In contrast, at Raibl site, Pb is one of the targets of the remediation plan since it was found in high concentrations both in the solid (up to 5.0 % wt.) and the dissolved (up to 96.3 μg/L) matrices. Lead is hosted in galena, associated to Fe and Pb secondary minerals. In fact, Pb dissolved concentrations in waters were likely attenuated due to sorption on Fe oxy-hydroxides and pH-dependent speciation. Precipitation of cerussite ($PbCO_3$) is less likely expected although the mineral was previously identified at Raibl. Thanks to SEM and EMPA microanalyses, Pb was found extensively bound to Fe oxy-hydroxides. However, these three processes were found as the main natural attenuation pathways for Pb. In general, Pb was found less mobile than Cd, Tl and Zn.

Cd: the element was found both at Raibl and in the Mt. Avanza ore deposits. However, the highest concentrations of Cd at Raibl (up to 196 mg/kg in mining waste) do not appear to be a primary concern for water resources, although high concentrations in some water bodies of Raibl were found (up to 13.6 μg/L). Cadmium showed high extractability, and may be slightly mobilizable from stream sediments, indicating that further studies should be conducted on the potential bioaccumulation along the aquatic trophic chain. The low concentrations in water could be related to the very high mobility and preference of Cd for liquid phase partitioning. Also, possibly most of Cd was hosted in sphalerite and contained in the Zn concentrate (final product of the mineral processing), whereas flotation tailings appeared to be depleted.

As and **Sb**: both metalloids were found in the two mining sites. Arsenic was more abundant at Raibl, whereas Sb at Mt. Avanza. At the Mt. Avanza site, the two elements constitute the main ore mineral: tetrahedrite ($Cu_{12}Sb_4S_{13}$), which can host notable amounts of As being called tennantite $Cu_{12}As_4S_{13}$. At Raibl, no As- or Sb-minerals are expected thus, the two elements are hosted in primary sphalerite, galena or pyrite/marcasite. It cannot be excluded that they may also be strongly absorbed to Fe oxy-hydroxides. However, at both sites, Sb was found to be slightly more mobile than As. Besides, always at both sites, the two elements do not represent an issue of concern except for the main mine drainages, where they can be found with concentrations higher than the regulatory limits. In fact, it is believed that pH > 8 and long residence times can promote As mobilization due to desorption from Fe oxy-hydroxides.

Hg: the metal was not found at Raibl, whereas it is a minor constituent of tetrahedrite in the Mt. Avanza mining area. Here, concentrations up to 473 mg/kg of Hg were found in waste rock piles, whereas very low concentrations of dissolved Hg (13.2 ng/L) suggest that Hg is poorly mobile from tetrahedrite. In contrast, Hg was found in its elemental gaseous form (GEM) in atmosphere around the mine waste rock piles and the outside the mine adits (concentrations up to 25.4 ng/m^3). This evidence reveals that Hg from tetrahedrite may prefer volatilization over transfer to the aqueous phase, similar to what has been reported for the more common Hg mineral, cinnabar, in other environmental contexts.

Future research

However, as is often the case, some answers obtained by this work are followed by further questions that will constitute targets for further research which is already planned:

1) the actual extent of the contamination of the Slizza-Gail-Drava river basin
2) the mobility of PTEs at neutral-weakly alkaline pH, similar to real water conditions
4) PTEs retention (absorption, adsorption, co-precipitation) from secondary minerals which are product of temporary natural attenuation processes
5) the potential bioaccumulation of Tl and Cd in the aquatic trophic chain of the contaminated Rio del Lago – Slizza watercourse.
6) a more detailed geochemical and mineralogical characterization of tailings

7 REFERENCES

ARFVG, 1952. I rifiuti della miniera erariale per Pb e Zn "Raibl", in comune di Tarvisio, prov. di Udine, e le acque del fiume austriaco Gail, affluente del fiume Drava. Archivio Regione Friuli Venezia Giulia - ex Distretto Minerario.

ARFVG, 1935. Lettera al Corpo Reale delle Miniere, Distretto di Trieste. Archivio Regione Friuli Venezia Giulia - ex Distretto Minerario.

ASTs, 1964. Inquinamento acque Rio Lago. Archivio di Stato di Trieste.

Barago, N., Covelli, S., Mauri, M., Oberti di Valnera, S., Forte, E., 2021. Prediction of Trace Metal Distribution in a Tailings Impoundment Using an Integrated Geophysical and Geochemical Approach (Raibl Mine, Pb-Zn Alpine District, Northern Italy). Int. J. Environ. Res. Public. Health 18, 1157. https://doi.org/10.3390/ijerph18031157

Bortolozzi, G., Ciriotti, M.E., Bittarello, E., Möckel, S., 2015a. Monte Avanza, Forni Avoltri, Carnia (Udine, Friuli-Venezia Giulia): conferme e nuovi ritrovamenti. Micro 13, 2–39.

Bortolozzi, G., Pondrelli, M., Vidus, L., 2015b. I minerali della Creta di Timau (Lago Avostanis, Paluzza, Udine): riscoperta di un'antica località mineraria. Gortania 37, 15–31.

Bortolozzi, G.M., Bracco, R., De Tuoni, F., Vidus, L., Bittarello, E., Marengo, A., Ciriotti, M.E., Zorzi, F., 2018. Antiche miniere e affioramenti metalliferi a Comeglians (Val Degano, Friuli Venezia Giulia): recenti ritrovamenti. Micro 16.

Brusca, C., 1996. Relazione sui lavori effettuati e sui risultati conseguiti. Unità Mineraria di Monte Avanza, Forni Avoltri, pp. 23-26.

Calligaris, C., Nicola, G., Casagrande, G., Zini, L., Cucchi, F., 2017. Debris Flow Hazard Assessment (Cave del Predil—NE Italy), in: Mikoš, M., Casagli, N., Yin, Y., Sassa, K. (Eds.), Advancing Culture of Living with Landslides. Springer International Publishing, Cham, pp. 369–376.

Cecchi, A., 1986. La ricerca operativa "Monte Avanza", Forni Avoltri (Udine). Ind. Mineraria 33–42.

Ciriotti, M.E., Möckel, S., Blaß, G., Bortolozzi, G., 2006. Cualstibite: ritrovamenti italiani. Micro 19–24.

Di Colbertaldo, D., 1960. Le risorse di minerali metallici in Friuli. Ind. Mineraria 559–569.

European Commission, 2022. Zero emission vehicles: first 'Fit for 55' deal will end the sale of new CO2 emitting cars in Europe by 2035.

European Commission, 2020. Study on the EU's list of Critical Raw Materials.

European Union, 2022. Social and environmental impacts of mining activities in the EU. Policy Department for Citizens' Rights and Constitutional Affairs, European Parliament.

Fellet, G., Pošćić, F., Casolo, V., Marchiol, L., 2012. Metallophytes and thallium hyperaccumulation at the former Raibl lead/zinc mining site (Julian Alps, Italy). Plant Biosyst. - Int. J. Deal. Asp. Plant Biol. 146, 1023–1036. https://doi.org/10.1080/11263504.2012.703250

Feruglio, G., 1966. Il giacimento cuprifero del Monte Avanza in Carnia. Symp. Internazionale Sui Giacimenti Minerari Delle Alpi Mendola Trento Ital.

Frangipani, E., 2013. La miniera della Val D'Aupa in un contesto più ampio di provincia metallogenica triassica situata nelle Alpi Orientali. Atti Mus Civ St Nat Trieste 56, 17–26.

Giarduz, M., Iob, S., Bittarello, E., Ciriotti, M.E., Fassina, B., 2015. Mallestigite di Monte Avanza: Terzo ritrovamento mondiale. Micro 13, 25.

Grignani, L., 1868. Il paese di Forni Avoltri con la sua miniera di Avanza.

Higueras, P., Salazar Jaramillo, D., De Toro, J.A., 2022. Materias primas críticas para la transición verde: ¿es posible obtenerlas sin dañar el medio ambiente? The conversation.

Iadarola, F., Viso, Y., 2009. Piano della caratterizzazione dei bacini di decantazione del distretto minerario di Cave del Predil ai sensi del D.M. 471/99. Tech. Rep.

ICOLD, 1996. A guide to tailings dams and impoundments. International Commission on Large Dams. bullettin.

Imprefond, 2007. Indagini geognostiche finalizzate alla caratterizzazione stratigrafica e geotecnica delle scorie di miniera accumulate durante gli anni lungo la sponda sinistra del Rio del Lago immediatamente a valle del comune di Cave del Predil e dell'imbocco della miniera di Raibl. Rapporto delle indagini e relazione geologico-tecnica.

Ismes & Aquater, 1990. Studio di dettaglio dei bacini di filtrazione della miniera di Raibl.

Leonard, M., Pisani-Ferry, J., Shapiro, J., Tagliapietra, S., Wolff, G., 2021. The geopolitics of the European Green Deal – European Council on Foreign Relations. ECFR. URL https://ecfr.eu/publication/the-geopolitics-of-the-european-green-deal/ (accessed 11.29.22).

Mancini, I., 1950. La laveria di Raibl. VII Congr. Naz. Mineral.

Marinelli, G., 1906. Guida della Carnia. Arnaldo Forni Editore, Ristampa dell'edizione di Tolmezzo. ARFVG, archivio ex distretto minerario, Regione Friuli Venezia Giulia.

Meriggi, R., Del Fabbro, M., Blasone, E., Zilli, E., 2008. Dynamic slope stability analysis of mine tailing deposits: The case of Raibl mine. AIP Conf. Proc. 1020, 542–549. https://doi.org/10.1063/1.2963882

Petrini, R., Cidu, R., Slejko, F.F., 2016. Thallium Contamination in the Raibl Mine Site Stream Drainage System (Eastern Alps, Italy). Mine Water Environ. 35, 55–63. https://doi.org/10.1007/s10230-015-0346-4

Plumlee, G.S., Smith, K.S., Montour, M.R., Ficklin, W.H., Mosier, E.L., 1999. Geologic controls on the composition of natural waters and mine waters draining diverse mineral-deposit types, in: The Environmental Geochemistry of Mineral Deposits, Part B. Case Studies and Research Topics. Society of Economic Geologists, Littleton, CO, pp. 373–432.

Protec, 2017. Lavori di messa in sicurezza degli argini dei bacini di deposito sul Rio del Lago a Cave del Predil in comune di Tarvisio. Certificato di collaudio amministrativo.

Seal II, R.R., Foley, N.K., 2002. Progress on geoenvironmental models for selected mineral deposit types. U.S. Geological Survey Open-File Report 02-195.

Valle, G., 1997. Progetto per la messa in sicurezza di alcune strutture della ex miniera di Monte Avanza che possono costituiree pericolo. Monte Cocco S.r.l., Unità Mineraria di Monte Avanza, Forni Avoltri, Udine.

Vallero, D.A., Blight, G., 2019. Mine Waste: A Brief Overview of Origins, Quantities, and Methods of Storage, 2nd ed, Waste. Elsevier Inc. https://doi.org/10.1016/b978-0-12-815060-3.00006-2

Vriens, B., Plante, B., Seigneur, N., Jamieson, H., 2020. Mine waste rock: Insights for sustainable hydrogeochemical management. Minerals 10, 1–38. https://doi.org/10.3390/min10090728

Žibret, G., Gosar, M., Miler, M., Alijagić, J., 2018. Impacts of mining and smelting activities on environment and landscape degradation—Slovenian case studies. Land Degrad. Dev. 29, 4457–4470. https://doi.org/10.1002/ldr.3198

Zucchini, R., 1998. Miniere e mineralizzazioni nella provincia di Udine. Aspetti storici e mineralogici. Cat. Della Collezione Mineral. Mus. Friul. Storia Nat. Miner. Friulani n. 40.

ACKNOWLEDGMENTS

I thank professors Stefano Covelli and Davide Lenaz for making this work possible and giving me the opportunity to grow as a researcher, always giving me maximum support and availability.

I also thank the colleagues of the Mercurilab research group: Federico Floreani, for sharing this journey, and Elena Pavoni and Elisa Petranich for teaching and advising me.

I thank Prof. Angelo De Min who has always offered me valuable advice and shown what is the spirit of research.

I thank Mara Mauri, Sara Oberti di Valnera, Rosella Marcon, Lucia Serra and Luca Pizzino of the Friuli Venezia Giulia Region, Waste and Contaminated Sites Service and Geological Service, for having instructed me since 2018 on mining sites, on environmental legislation and for having made available the knowledge and bibliographic material, without which this work would not have been complete. I also thank the Extraordinary Commissioner for the restoration of the mining area of Cave del Predil Guglielmo Berlasso as well as the Director of the Waste and Contaminated Sites Service of the Region Flavio Gabrielcig, for the active and valuable support to the realization of this study.

I thank Efrén Garcia Ordiales for teaching me how to research and achieve goals from my first day in Spain. I thank him, along with Jorge Loredo Pérez, Rodrigo Álvarez García, Pablo Cienfuegos, Maria Almudena Ordoñez Alonso for giving me hospitality in Oviedo and a place to return to as well as having educated me on mining engineering.

I thank Alessandro Acquavita, Nicola Skert, Nicola Bettoso, Sergio Predonzani, Carlo Viola, Andrea Cicogna and Claudia Meloni of ARPA – OSMER FVG for having contributed and made available resources for the realization of the study.

I thank the Raibl mining community, including Valerio Rossi and Claudio Squor, for passing on to me part of the direct experience of the Raibl mine.

I thank the guides of the Raibl International Geomining Park: Ilenia Cimenti and Igor Černuta for dedicating their time to accompany us in the mine during the sampling and for always welcoming me with great kindness and sympathy in Cave del Predil during the first 2 years of sampling.

I thank for the enormous expertise handed down to me and for the willingness to build a collaboration with the main experts of the regional mines of the Friulian Museum of Natural History of Udine: Roberto Zucchini, Giuseppe Muscio and Luigi Vidus.

I thank all the students who with their thesis work have helped to realize this study: Cristiano Mastroianni, Samuel Princi, Michele Revelant, Eleonora Amadio, Rossana De Faveri, Josipa Repanić.

I thank my parents Paolo and Rosalinda for giving me the support without which this goal would probably not have been possible, the family of Via Santi Martiri and finally Martina Marzolla for sharing with me this last period of difficulty and joy.

Journal of Geochemical Exploration 245 (2023) 107129

Contents lists available at ScienceDirect

Journal of Geochemical Exploration

journal homepage: www.elsevier.com/locate/gexplo

Hydrogeochemistry of thallium and other potentially toxic elements in neutral mine drainage at the decommissioned Pb-Zn Raibl mine (Eastern Alps, Italy)

Nicolò Barago [a,*], Elena Pavoni [a], Federico Floreani [a,b], Matteo Crosera [c], Gianpiero Adami [c], Davide Lenaz [a], Stefano Covelli [a]

[a] Dipartimento di Matematica e Geoscienze, Università di Trieste, Via Weiss 2, 34128 Trieste, Italy
[b] Dipartimento di Scienze della Vita, Università di Trieste, Via Licio Giorgieri 5, 34127 Trieste, Italy
[c] Dipartimento di Scienze Chimiche e Farmaceutiche, Università di Trieste, Via Licio Giorgieri 1, 34127 Trieste, Italy

ARTICLE INFO

Keywords:
Thallium
Environmental impact
Carbonate-Hosted Pb-Zn
Tailings impoundments
Contamination
Long-term monitoring

ABSTRACT

Decommissioned mines represent a worldwide concern due to the potential long-term effects related to the dispersion of potentially toxic elements (PTEs) in the environment. In this study, 176 water samples were collected in the period 2018–2021 at the carbonate-hosted Pb-Zn Raibl mine which is affected by neutral mine drainage (NMD). The post-flotation tailings are the main source of PTEs (Zn, Pb and especially Tl) in the river drainage system. Compared to other dissolved PTEs (Zn, Pb, Cd), Tl was found to be more mobile, reaching concentrations up to 120 μg L^{-1} in waters flowing in the tailings impoundments. Modelling results suggest that Tl is mainly present in the Tl(I) ionic and mobile form thus suggesting that relevant natural attenuation processes for this element are not expected in the investigated area. In contrast, Zn and Pb attenuation pathways appeared to be governed by pH-dependent speciation and sorption processes, whereas elevated Zn concentrations were likely also limited by hydrozincite precipitation. Metalloids such as As and Sb were almost entirely released into the slightly alkaline waters of the mine drainage system, which are generally characterised by longer residence time or standing waters whereas As and Sb concentrations were negligible in the tailings-seepage waters. However, intense rainy events may increase PTE concentrations of one order of magnitude, especially in the tailings impoundment groundwater as a result of a rise in the water table, and PTE total dissolved loads of three orders of magnitude, in the main stream during high flow events, thus representing the most critical factor in regulating the remobilisation and downward dispersion of PTEs in the river drainage system.

1. Introduction

In the last decade there has been growing worldwide concern regarding Thallium (Tl) as an emerging natural or anthropogenic contaminant. In spite of its potential toxicity to ecosystems and humans through natural geological pathways (Peter and Viraraghavan, 2005; Campanella et al., 2019), this element is often given little thought by the regulation authorities. Thallium (Tl) is a relatively rare heavy metal with an average concentration of 0.9 mg kg^{-1} (Rudnick and Gao, 2003) in the upper continental crust. The chemical behaviour of Tl resembles that of chalcophile elements (Cu, Pb, Zn, Hg, Sb and As) on the one hand and that of the alkali metals (K, Rb, Cs and Na) on the other (Liu et al., 2016). In freshwater, Tl is highly mobile and toxic at very low concentrations ranging from a few μg L^{-1} to mg L^{-1} (Peter and Viraraghavan, 2005; Tatsi et al., 2015; Belzile and Chen, 2017) and is found in two oxidation states, the most abundant monovalent Tl(I) (Vink, 1993) and the most uncommon, toxic but less bioavailable trivalent Tl (III) (Ralph and Twiss, 2002). Bioaccumulation and biomagnification along the trophic chain can occur in areas affected by elevated geochemical anomalies due to both natural and anthropogenic sources, posing a potential issue for environmental quality. For this reason, the areas affected by high Tl concentrations in several environmental matrices need to be investigated in the field to identify the main sources of contamination, focusing on the main geochemical mechanisms in regulating the behaviour and fate of Tl along with other associated potentially toxic trace elements (PTEs).

* Corresponding author.
E-mail address: nicolo.barago@phd.units.it (N. Barago).

https://doi.org/10.1016/j.gexplo.2022.107129
Received 18 May 2022; Received in revised form 24 October 2022; Accepted 20 November 2022
Available online 25 November 2022

In general, the mineral phases that can host notable amounts of Tl mainly belong to sulphide and sulfosalt ore deposits, among which the most relevant are sphalerite, which may have a Tl concentration up to 1800 mg kg^{-1} (Henjes-Kunst et al., 2017; Pimminger et al., 1985), galena (George et al., 2016), pyrite (George et al., 2019) and other Fe sulphides, jarosite (Garrido et al., 2020) or Tl-bearing sulfosalt minerals (Pimminger et al., 1985; Biagioni et al., 2013). Thallium (Tl) can also be found in K-bearing minerals, such as alkali feldspars or micas, and in coal (Kaplan and Mattigod, 1998 and references therein).

Primary sources of Tl in the environment are related to mining, burning coal, cement plants, electronics, etc. (Belzile and Chen, 2017). The contamination deriving from mining activities is one of the major global sources of PTEs in the environment, affecting several environmental matrices including soils, sediments, water, air, and biota even in very large areas (e.g., Acquavita et al., 2022; Barago et al., 2020; Giani et al., 2012; Hudson-Edwards et al., 2011). In Europe, mining of carbonate-hosted Pb-Zn ores such as those from the Alpine (Barago et al., 2021; Brigo et al., 1977; Pimminger et al., 1985) and Silesian districts (Viets et al., 1996), or of the volcanogenic hydrothermal deposits from the Serbo-Macedonian metallogenic province (Bačeva et al., 2014), which have largely been decommissioned, can represent one of the major sources of Tl in the environment. The ores in these mining sites, from which PTEs can be released, still contain high amounts of Tl as a trace element posing a potential environmental risk.

The water-rock interaction in decommissioned mine galleries as well as the weathering of waste rocks or tailings deposits produced during mining and metallurgical activities may favour the release of dissolved Tl and other PTEs, reaching concentrations well above the suggested values from the available environmental and toxicological guidelines (Casiot et al., 2011; Ghezzi et al., 2019; Jabłońska-Czapla et al., 2016; Pavoni et al., 2017, 2018). In fact, such guidelines are often missing in the case of Tl. In Italy, threshold limits for Tl are only provided for groundwaters (2 μg L^{-1}), whereas no quality guidelines are defined in the case of surface freshwaters. Generally, regarding freshwater quality guidelines (CCME, 1999), some authors suggest that these guidelines should be revised downward (e.g. to 0.087 μg L^{-1}) since scientific evidence has highlighted the serious toxic effects on a wide variety of aquatic organisms, even at lower Tl concentrations (Campanella et al., 2019; Tatsi et al., 2015). Since the remediation of decommissioned mining districts is usually very difficult to manage, as well as being expensive, the potentially harmful effects related to the occurrence of Tl and other PTEs may persist in these areas for decades, for example, the Montevecchio Pb-Zn mining district (Cidu et al., 2011) where PTE concentrations are still remarkably high even after almost 50 years of flushing.

The potentially harmful effects caused by mining mainly depend on the chemical composition, the mineralogical assemblage of the ore deposit, and the mineral processing steps adopted to recover the elements of economic interest. The release of PTEs in water draining decommissioned mining districts is mainly due to physico-chemical alteration processes at the water-rock interface of the ore as well as leaching of waste-rocks, tailings or smelter slags. Moreover, the mobility of PTEs is governed by several factors including mineral stability, Eh-pH boundary conditions and exposure to weathering among the most important water parameters. The physico-chemical boundary conditions, especially in terms of pH and Eh, can control PTE speciation in water. Oxidising conditions and higher values of pH, derived from the dissolution of carbonate host rocks, which have a crucial role in buffering acid mine drainages (AMD), can promote the oxidation and carbonatation of sulphides to more stable mineral forms (e.g., galena to cerussite: PbS - > $PbCO_3$) with subsequent attenuation of the release of PTEs in the dissolved phase.

The adsorption of PTEs to Fe oxy-hydroxides (from amorphous ferrihydrite to crystalline goethite) has been widely investigated as this process strongly influences the cation hydrochemistry by limiting the mobility and dispersion of dissolved PTEs (Dzombak and Morel, 1990). High pH values usually promote the transformation of Fe sulphides (e.g., pyrite: FeS_2) to oxidised forms (e.g. ferrihydrite) which can notably scavenge PTEs from solution through sorption processes. PTE adsorption occurs at different pH values, as reported for ferrhydrite: $Cr^{+3} > Pb^{+2} > Cu^{+2} > Zn^{+2} > Cd^{+2} > Ag^{+} > Ca^{+2} \approx Tl^{+}$, from the most to the less sorbed cations (Coup and Swedlund, 2015; Gustafsson, 2009). However, PTEs are only transitorily scavenged since low pH values can induce the dissolution of Fe oxy-hydroxide minerals with subsequent release of previously adsorbed PTEs.

The purpose of this research was to investigate the water chemistry in a Mississippi Valley-type (MVT) carbonate-hosted Pb-Zn decommissioned mine in the Alpine district, focusing on the geochemical behaviour of Tl and other PTEs in a complex environment notably affected by mining. In particular, the objectives were: a) to monitor the occurrence of dissolved PTEs in surface freshwaters, in waters draining abandoned mine galleries and groundwaters into the tailings impoundments b) to investigate the temporal variability of dissolved PTEs and their relation to local hydrological features c) to understand the role of different hydrological conditions on Tl and other PTE mobility from the mine galleries and tailings impoundments to the river drainage system.

1.1. Environmental setting

The Raibl mining district is located in a narrow north-south (N-S) trending valley near the village of Cave del Predil (Friuli Venezia Giulia, Italy; lat. 46.44150, long. 13.56904; 900 m a.s.l.) close to the borders with Slovenia and Austria in the Julian Alps, a south-eastern sector of the Alps (Fig. 1). The Rio del Lago is the stream which flows along the valley from S to N and, after the confluence with the Rio Freddo stream, it becomes the Slizza River which conveys into the Gail–Drava–Danube River system. The average annual rainfall in the period from 2007 to 2021 was 2240 mm/year, with a min-max rainfall of 1490–2980 mm/year and the average annual air temperature was 7.8 °C (ARPA FVG – OSMER and GRN data set; http://www.meteo.fvg.it). Summer and winter are the driest seasons, and autumn and spring the rainiest.

Although the Raibl mining district may have been active from the pre-Roman Era, the first documented activity dates from 1320 and the mine has been closed since 1991. The mine galleries extend inside Monte Re for 500 m and 480 m above and below the village of Cave del Predil, respectively, organised with 19 underground levels below the village for a total of >120 km of galleries. The galleries below the 13th level (−240 m from level zero) were flooded when the dewatering system was recently interrupted. The main water outflow of the underground mine system is the Bretto gallery (sampling site DBR: 250–300 L/s; Fig. 1), a 5 km gallery starting from the 13th level, which discharges directly into the Koritnica River, which flows into the Isonzo/Soča River, in Slovenia. In contrast, a part of the mine drainage system above the level of the village of Cave del Predil (sampling site: DPL) drains into the Rio del Lago stream, which flows in Italy towards Austria. An estimated 4 million metric tons of mineralised waste-rocks and tailings from the flotation plant operating at the Raibl mining district were disposed from 1976 to 1991 in tailings impoundments set up on the western bank of the Rio del Lago stream. Those impoundments are located 1.5 km N with respect to the mine entrance and are characterised by the following dimensions: 1200 m length, 100 m width and a maximum height of 25 m (Barago et al., 2021). Currently, the potential dispersion of water enriched in PTEs from the tailings impoundments to the Rio del Lago stream represents an issue of concern.

The early Mesozoic carbonate-hosted Pb-Zn (Sangster, 1976) mining district of the Eastern Alps represents one of the most historical and studied metallogenic provinces in Europe. The four Pb-Zn mines of Bleiberg (Austria), Mežica (Slovenia), Raibl and Salafossa (Italy) produced >75 % of the total Pb and Zn extracted from the Alps (Brigo et al., 1977). Currently, these deposits are of subeconomic interest, and the mines were decommissioned at the end of the twentieth century.

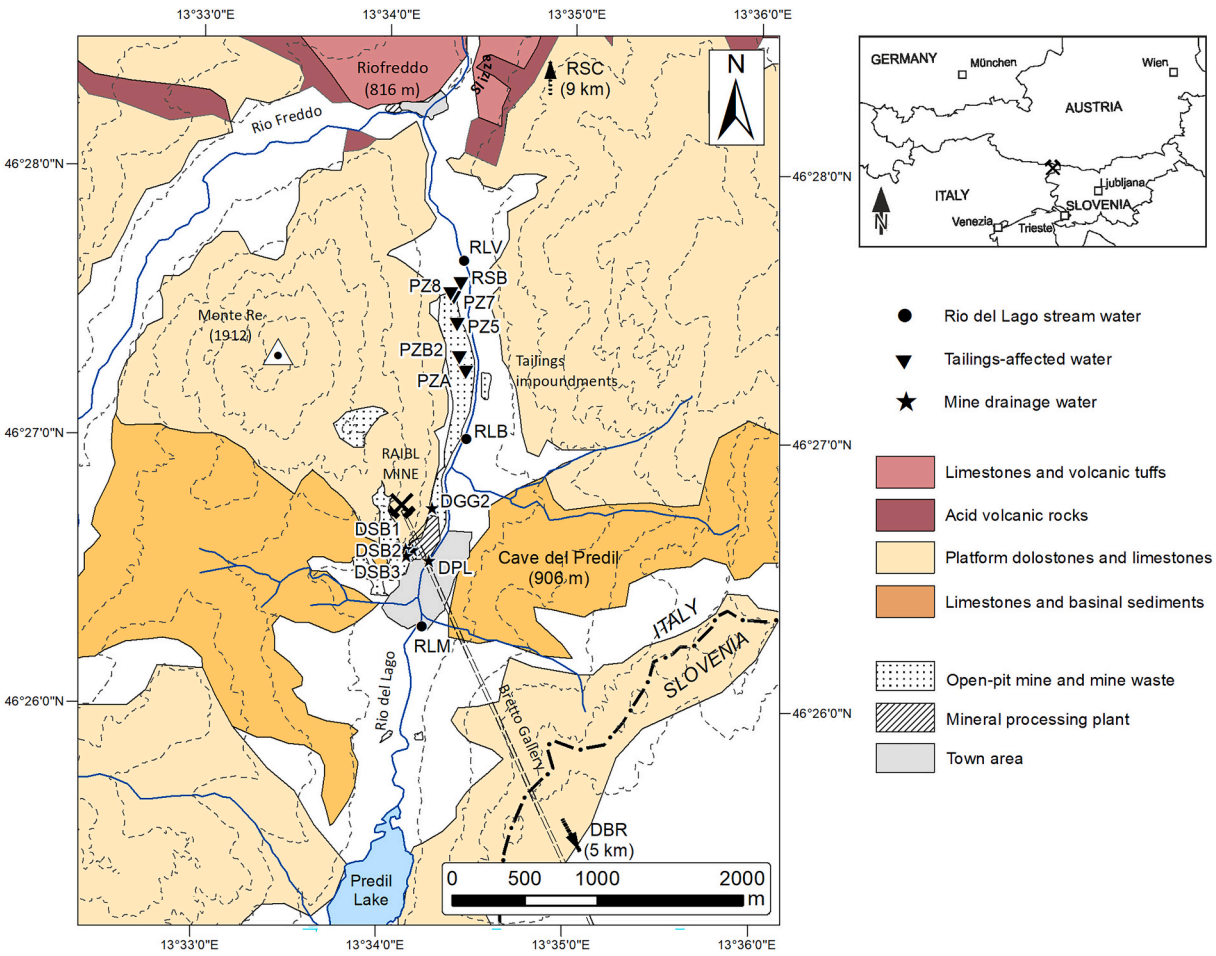

Fig. 1. Geological map of the Raibl mining district (modified after Desio et al., 1967) with the names and locations of the sampling stations related to various waterbodies.

This study is focused on the Triassic carbonate-hosted strata-bound Pb-Zn Raibl mine. The classification of these ore deposits is still controversial (Brigo et al., 1977; Henjes-Kunst et al., 2017; Leach et al., 2010; Schroll, 2005). The MVT (or Alpine-type) low-temperature hydrothermal Pb-Zn ore deposit of Raibl is hosted in thick and massive Triassic dolomitic reefs located on the Adriatic passive continental margin. Other lithologies such as marls and volcanic rocks are notably less abundant in the study area. Structurally, the deposit of Raibl is similarly controlled by the Triassic to Early Jurassic extensional fault activity associated with the Pangea breakup (Doglioni, 1988). The paragenesis of the ore deposits is mainly composed of primary sulphides such as sphalerite (ZnS), galena (PbS) and iron sulphides (mainly pyrite and marcasite: FeS_2). Regarding the occurrence of Tl, the element appears to be preferentially hosted in colloform sphalerite, and likely to a lesser extent in galena and Fe sulphides (Brigo and Cerrato, 1994; Melcher and Onuk, 2019; Schroll et al., 1994). Unusually, elevated Tl-content in inclusions found in dolomite and sphalerite could presumably be related to Tl-bearing jordanite ($Pb_4As_2S_7$) microphases (Brigo and Cerrato, 1994; Pimminger et al., 1985; Venerandi, 1966). An upper oxidised zone is mainly constituted by Fe oxy-hydroxide secondary minerals such as ferrihydrite or goethite. Similarly, the deepest areas of the deposit present abundant secondary carbonate minerals (e.g., smithsonite: $ZnCO_3$, hydrozincite: $Zn_5(CO_3)_2(OH)_6$ and cerussite: $PbCO_3$) formed by leaching of the primary sulphides under ambient conditions. Among gangue minerals, dolomite and barite prevail (Brigo et al., 1977).

2. Materials and methods

2.1. Sampling strategy

In this research, 16 sampling sites were selected at the decommissioned mining district and monitored between 2019 and 2021. In detail, 14 stations were sampled monthly for 1 year, including 3 piezometers (PZB2, PZ5, PZ7), which were sampled monthly for 2 years and 2 stations (DGG2, RSC), which were only sampled sporadically. In addition, results from two preliminary sampling campaigns performed in 2018 were also included in this study for a total of 176 water samples.

The sampling stations were divided into three groups (Fig. 2): (a) *mine galleries and drainage water*: drainage water outflowing into the Rio del Lago stream in front of the mine entrance (DPL) and in the Koritnica River (Slovenia) from the Bretto gallery (DBR), respectively; seepage water flowing from the upper sector of the mine (DGG2); water from three distinct mine galleries at the "zero-level" (DSB1, DSB2, DSB3) which converge in the main outflow (DPL). (b) *Tailings-affected water*: groundwater from the tailings impoundments taken from the external and internal tailings dams mainly consisting of waste rocks (PZA, PZB2, PZ5, PZ7 and PZ8) and a creek at the northern side of the impoundments (RSB). (c) *Surface freshwater from Rio del Lago - Slizza stream*: upstream from the mining site (RLM), immediately downstream from the mine and the tailings impoundments (RLB and RLV, respectively), and further downstream in the Slizza River (RSC) just before the border with Austria, 9 km N. The stream in RLM and RLB stations was found often

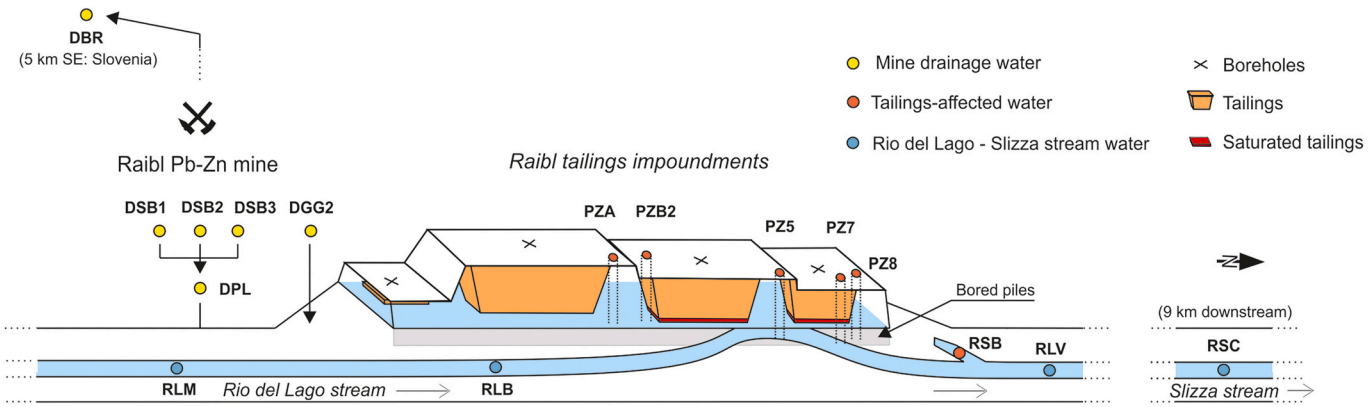

Fig. 2. Schematic representation of the decommissioned Raibl mining district showing the location of the monitored stations for different groups of water. The orange area represents the possible volumes of tailings stored in the ponds based on boreholes and geophysics (Barago et al., 2021).

dry.

Groundwater sampling was performed in dynamic mode using a full submersible pump, which was inserted into each piezometer. In detail, groundwater samples were collected following 15 min of purging for the stabilisation of the physico-chemical parameters. All the water samples were filtered *in-situ* (syringe filters Millipore Millex HA, 0.45 μm pore size, mixed cellulose esters) and three aliquots of 100 mL each were collected for different chemical analyses in pre-conditioned (hot suprapure HNO_3 (VWR), ≥ 69 %, 10 % v/v, heated at 50 °C for 12 h and rinsed with Milli-Q water and the water sample before sample collection) PTFE containers. Moreover, blank samples were collected on each sampling day. Water samples for PTEs and major cation determinations were acidified (1 % *v*/v) with HNO_3 (69 % v/v, VWR). Samples were transported to the laboratory in a cooler filled with ice packs and then stored at a temperature of 4 °C in a cold, dark room. In addition, the main physico-chemical parameters (temperature, pH, oxidation/reduction potential (ORP), dissolved oxygen (DO), electrical conductivity (EC) and total dissolved solids (TDS)) were measured *in situ* using a portable multiprobe meter (Hanna HI98194). Total dissolved load (TDL) was calculated as the product between the dissolved PTE concentration in the filtered water sample and the water discharge from the gauge station located downstream from the tailings impoundments as per data provided by the Deputy Commissioner for the Raibl mining area.

2.2. Analytical measurements

The concentrations of Ca, Mg, K, Na and Zn were determined using an Optima 8000 ICP-OES Spectrometer equipped with an S10 Autosampler (PerkinElmer, USA). The instrument was calibrated using standard solutions (ranging between 1 and 100 mg L^{-1}) prepared by the dilution of a multistandard solution for ICP analysis (Periodic Table MIX5, Merck). Quality control was done by 1) analysing laboratory-fortified samples that are a subset of the samples prepared by spiking multistandard solutions with known amounts of trace elements (depending on the trace element concentrations in the samples) (Periodic Table MIX1, Merck) in actual water samples; and 2) by laboratory-fortified blanks which consist of a multistandard solution prepared by dilution. Both control solutions were analysed every 10 samples with recoveries ranging between 74 and 130 %. Concentrations of PTEs (As, Ba, Cd, Fe, Ge, Mn, Pb, Sb, Tl, Zn) were quantified using an ICP-MS Spectrometer (NexION 350x, PerkinElmer, USA) equipped with an ESI SC Autosampler. The instrument was calibrated using standard solutions (ranging between 0.5 and 500 μg L^{-1}) prepared by dilution from a multistandard solution for ICP analysis (Periodic Table MIX1 and MIX2, Merck). The analysis was performed in KED (Kinetic Energy Discrimination) mode to avoid and minimise cell-formed polyatomic ion interference. Quality control was performed in the same manner as ICP-OES with a multistandard solution (Multi-element quality control standards for ICP, VWR) prepared by dilution, with recoveries ranging between 83 and 92 %. Moreover, Sc, Y and Ho were used as internal standards for quality control in order to evaluate potential matrix effects. The precision of the ICP-OES and ICP-MS analyses expressed as RSD% was <5 % and 3 %, respectively.

Major anions were determined on bulk samples by Ion Chromatography (IC) using a Dionex ICS-3000 equipped with an ASRS 300 electrolytic suppressor. The precision of the IC analysis expressed as RSD% was <10 %. The IC was calibrated with standard solutions (ranging from 0.1 to 100 mg L^{-1}) prepared via the dilution of two different 100 mg L^{-1} standards (Anion multi-element standard I e II, Merck). Quality control was done by analysing of a different multistandard (Dionex™ Retention time standards for Ion Chromatography, ThermoFisher) every 10 samples, with recoveries ranging between 85 and 101 %. Regarding alkalinity, CO_3^{2-} and HCO_3^- were determined by titration with 0.01 N HCl (APAT and IRSA-CNR, 2003).

2.3. Geochemical modelling

Saturation indexes (SI) and chemical speciation were calculated with the chemical equilibrium models provided by Visual Minteq (Gustafsson, 2014). The SI parameters, calculated from the ion activity product (IAP) and the solubility product (K_{sp}), indicate whether elements could precipitate in determined mineral phases starting from a solution with known physico-chemical parameters and chemical composition. Only the water samples where all the parameters were measured were used to simulate speciation.

2.4. Exploratory multivariate data analysis

A 3-way principal component analysis (3W-PCA) obtained using the Tucker-3 algorithm (Smilde et al., 2004) was used as an unsupervised exploratory chemometric tool for the identification of relationships within objects (different groups of water samples collected at the decommissioned mining district), variables and conditions (sampling campaigns performed monthly throughout 2020) (Oliveri et al., 2020). Prior to multivariate analysis, a log-transform was applied to those variables that did not show a normal distribution. Systematic differences between the experimental variables were minimised by applying column autoscaling (j-scaling) to data matrices (Smilde et al., 2004). Multivariate data processing was performed using the CAT (Chemometric Agile Tool) package, based on the R platform (The R Foundation for Statistical Computing, Vienna, Austria) and freely distributed by Gruppo Italiano di Chemiometria (Italy) (Leardi et al., 2019).

3. Results and discussion

3.1. Physico-chemical characterisation and the major ions of waters

The average pH of the investigated water samples ranged between 7.7 and 8.3 (Table 1, Table S1), indicating overall near-neutral to slightly alkaline conditions due to the dissolution of dolostones and limestones, which represent the main lithologies in the area. The average pH of tailings-affected water was closer to neutral (7.7 ± 0.3) than the drainage waters from the mine (avg. 8.3 ± 0.2) and the stream water (avg. 8.2 ± 0.2), suggesting the aquifer has strong pH buffering capacities. The average temperature ranged between 7.6 and 10.9 °C. Tailings-affected water showed lower EC (297 ± 77 μS cm^{-1}) and TDS (Total Dissolved Content) (155 ± 42 mg L^{-1}) values with respect to the mine drainage water, possibly due to longer water-rock interaction and low-flow conditions inside the mine. However, the lowest average TDS value was found in the stream water (avg. 126 ± 29 mg L^{-1}) indicating strong dilution processes promoted by rainfall and a shorter water-rock interaction compared to the mine drainage water in the galleries (226 ± 67 mg L^{-1}).

Generally, reducing conditions were not observed during this study, although Petrini et al. (2016) detected bulk redox potential (ORP) values near to 0 mV within the mine galleries, most likely due to the role of organic oxidisable matter that occurs as intercalations of dark bituminous layers within the carbonate rocks. All the investigated water samples showed positive ORP and relatively high concentrations of dissolved oxygen (DO: 7.3–8.9 mg L^{-1}).

In the Piper diagram (Piper, 1944; Fig. 3), the distribution of the major anions (Cl^-, SO_4^{2-}, HCO_3^-) and cations (Mg^{2+}, Ca^{2+}, Na^+, K^+) (Table 2, Table S1) confirmed the hydrofacies identified in a previous study (Petrini et al., 2016).

Freshwater samples from the stream belonged to the Ca-HCO_3 hydrofacies whereas there is an evident shift to the Ca–Mg–SO_4 hydrofacies for the mine drainage and tailings-affected water samples reflecting higher sulphur availability due to sulphide oxidation (1) or gypsum dissolution (2), initially precipitated as a secondary mineral during limestone neutralisation of the sulphate-rich AMD (Petrini et al., 2016), according to the following Eqs. (1) and (2):

$$FeS_2 + 3.5O_2 + H_2O = Fe^{2+} + 2H^+ + 2SO_4^{2-} \quad (1)$$

$$CaCO_3 + H_2SO_4 + H_2O = CaSO_4 \bullet 2H_2O + CO_2 \quad (2)$$

Very low concentrations of Na^+ and K^+ reflect the scarcity of silicate minerals and the predominance of calcite and dolomite among the main mineral constituents of the host rock. In contrast, high concentrations of Ca^{2+} and Mg^{2+} were observed, especially in water from the mine galleries, testifying to a long residence period and prolonged water-rock interactions. Regarding sulphates, a notable variability was observed within the investigated water samples, generally reaching values >50 mg L^{-1} (Table 2, Table S1). Under certain environmental conditions, especially during rainy periods or spring thaw, the water table inside the tailings impoundments can sufficiently rise to interact and leach inner and slightly altered sulphide-rich tailings beds, leading to high concentrations of dissolved sulphates (max SO_4^{2-} in PZ5: 277 mg L^{-1}; Table S3, Fig. S1). This variability showed that the deepest sector of the tailings beds inside the impoundments are characterised by the lowest sulphur availability, potentially related to the advanced oxidation aging of the deepest tailings in the saturated zone. In contrast, results showed that more surficial tailings can still release sulphur as sulphate, indicating possibly high enough amounts of Fe-sulfides such as pyrite or marcasite that can be oxidised being sources of PTEs.

According to the Ficklin diagram (Plumlee et al., 1999) in Fig. 3, all the waters collected at Raibl fall in the "near-neutral" field confirming strong pH buffering effects as the result of carbonate dissolution processes. The majority of water samples in the area of the tailings impoundments and from the mine drainage system fall into the "high-metal" area whereas all the Rio del Lago and Slizza freshwaters belong to the "low-metal" area. The diagram also highlights the difference between the three groups of water samples in terms of pH. Mine waters were more slightly alkaline and enriched in Ca^{2+} and Mg^{2+}, partially overlapped with more near-neutral and metal-rich tailings-affected waters and less enriched stream waters. Thus, no acid mine drainage (AMD) occurs at the decommissioned mining district of Raibl, which appeared to be characterised by a neutral mine drainage (NMD).

3.2. Potentially toxic trace elements: distribution and behaviour

Despite the notable spatial and temporal variability in the distribution of PTEs, the lowest concentrations were found in the waters of the Rio del Lago stream located upstream from the mine and the tailings impoundments (station: RLM, max concentration: Zn = 2.80 and Tl = 0.06 μg L^{-1}; Table S3). In contrast, the water affected by the presence of tailings showed the highest concentrations and variability of metals in the mining district, especially in the case of Zn, Tl and Pb (Table 3: Zn = 2349 ± 2519, Tl = 38.3 ± 25.5 and Pb = 35.1 ± 17.0 μg L^{-1}; Table S2). Thallium and Pb concentrations are very high if compared to the Italian national regulatory limits for groundwaters (D.Lgs. 152/2006: Tl = 2 μg L^{-1}, Pb = 10 μg L^{-1}). Drainage water from the mine also displayed elevated concentrations of PTEs and appeared to be especially enriched in metalloids such as As and Sb (18.6 ± 27.0 and 2.40 ± 2.03 μg L^{-1}, respectively). Conversely, the tailings-affected waters exhibited concentrations of As and Sb one order of magnitude lower (1.4 ± 0.5 and 0.34 ± 0.20 μg L^{-1}) with respect to the drainage water from the mine. The stream water, although diluted, appeared to be mostly affected by metals, especially in the case of Pb and Tl (16.9 ± 11.1 and 5.0 ± 5.8 μg L^{-1}, respectively), whereas As, Sb and Cd occurred with very low concentrations (< 1 μg L^{-1}). The similar distribution of metals (Zn, Pb, Tl) and Ba as well as the differences with metalloids (As, Sb, Ge) and Cd (Fig. 4) was also confirmed by the 3W-PCA (explained with a variance up to 56.5 %, Fig. 5). Zinc (Zn), which is the most abundant metal of the ore assemblage, was by far the most abundant dissolved trace element in water (Table 3), often being more abundant than common major cations such as K^+ and Na^+ (max Zn = 14,933 μg L^{-1}; Table S3). In addition to Zn, Tl is an element of growing interest due to its high toxicity. The Tl

Table 1
Average physico-chemical parameters measured on the different groups of waters collected at the decommissioned Raibl mining district. ORP: redox potential, EC: Electrical conductivity, TDS: Total dissolved solids, DO: Dissolved oxygen, T: Temperature.

	Mine drainage water (n = 54)	Tailings-affected water (n = 96)	Stream water (n = 26)
pH	8.3 ± 0.2	7.7 ± 0.3	8.2 ± 0.2
ORP (mV)	191 ± 50	176 ± 59	191 ± 51
EC (μS cm^{-1})	446 ± 135	297 ± 77	238 ± 54
TDS (mg L^{-1})	226 ± 67	155 ± 42	126 ± 29
DO (mg L^{-1})	8.9 ± 1.4	7.3 ± 1.0	8.9 ± 1.0
T (°C)	8.6 ± 2.0	9.9 ± 2.7	9.6 ± 3.6

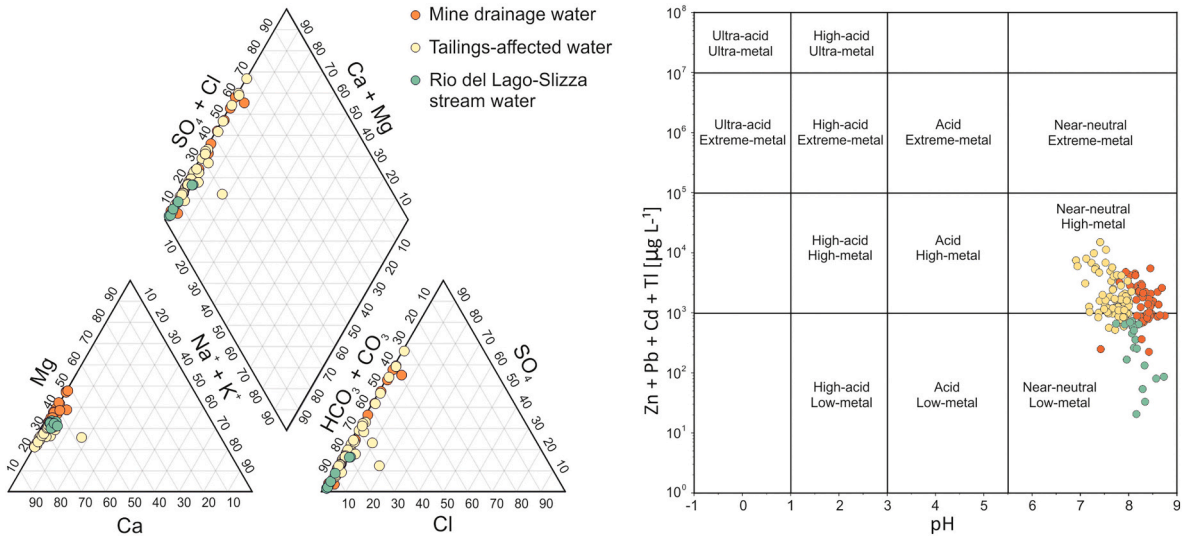

Fig. 3. Piper and modified Ficklin diagrams of the different groups of water collected at the decommissioned Raibl mining district.

Table 2
Average major cation and anion concentrations (mg L^{-1}) in the different groups of water collected at the decommissioned Raibl mining district. Anions were analysed on a subset of data.

	n	Ca^{2+}	Mg^{2+}	Na^{+}	K^{+}	HCO_3^-	SO_4^{2-}	Cl^-	F^-
Mine drainage water	54	67.8 ± 19.1	27.4 ± 10.9	1.06 ± 0.38	1.22 ± 1.98	177 ± 26	88.6 ± 62.5	1.47 ± 1.00	0.14 ± 0.08
Tailings-affected water	96	50.4 ± 14.1	12.2 ± 1.9	1.13 ± 0.25	0.83 ± 2.40	168 ± 10	58.4 ± 67.0	2.37 ± 2.93	0.07 ± 0.03
Stream water	26	40.0 ± 7.5	11.9 ± 2.3	1.36 ± 1.01	0.51 ± 0.52	164 ± 14	12.0 ± 11.7	2.86 ± 2.00	0.04 ± 0.03

Table 3
Average trace element concentrations (µg L^{-1}) in the different groups of water collected at the decommissioned Raibl mining district.

	Mine drainage water (n = 54)	Tailings-affected water (n = 96)	Stream water (n = 26)
Zn	1795 ± 1262	2349 ± 2519	341 ± 256
Tl	16.7 ± 14.1	38.3 ± 25.5	5.0 ± 5.8
Pb	11.5 ± 6.9	35.1 ± 17.0	16.9 ± 11.1
Ba	38.9 ± 17.5	56.2 ± 25.2	28.4 ± 16.3
Cd	1.26 ± 0.89	1.46 ± 2.38	0.28 ± 0.18
As	18.6 ± 27.0	1.4 ± 0.5	0.7 ± 0.3
Sb	2.40 ± 2.03	0.34 ± 0.20	0.16 ± 0.07
Ge	0.68 ± 0.35	0.42 ± 0.45	0.09 ± 0.07
Fe	10.03 ± 8.53	8.07 ± 8.79	6.41 ± 8.33
Mn	0.32 ± 0.20	0.28 ± 0.56	0.33 ± 0.59

concentration range is 0.02–120 µg L^{-1} overall. Maximum concentrations were found in the tailings-affected groundwater, especially at PZ5 (120 µg L^{-1}; Table S3), where extensive interactions between the water table and the saturated tailings beds occurred.

The understanding of PTE behaviour in water systems, especially those affected by mining, is quite complex, since the distinctive geochemical characteristics of different elements strongly govern speciation, mineral-water partitioning as well as PTE mobility and fate. Hereafter, hydrochemical data of dissolved elements are presented together with geochemical modelling results calculated using Visual Minteq (Gustafsson, 2014). The highest concentrations of Zn, Pb and Tl were observed in the near-neutral tailings-affected waters (average pH of 7.7 ± 0.3) where a large amount of metal-bearing waste minerals is present. The dissolution and sorption processes that regulate their mobility are mainly pH dependent (Fig. 6). With respect to release processes affecting Pb, and to a lesser extent Zn, modelling speciation showed that there is a negative correlation between pH and the relative abundance of dissolved ionic Zn^{2+} and Pb^{2+} forms, which is consistent with both field observations (Fig. 6a and b) and the 3 W-PCA output (Fig. 5). However, Pb was present in its ionic form Pb^{+2} only up to 12–13 %, whereas the remaining dissolved fraction was in the carbonate form. Presumably, Pb and to a lesser extent Zn natural attenuation is governed by adsorption processes due to their affinity with Fe-oxyhydroxides (HFO) at pH > 7 (Coup and Swedlund, 2015; Dzombak and Morel, 1990). In addition, the attenuation of Pb does not likely depend on cerussite precipitation (SI $PbCO_3$ < 0), whereas high concentrations of Zn appeared to be buffered by hydrozincite, a hydrated Zn-carbonate (SI $Zn_5(CO_3)_2(OH)_6$ max = 6.85, min = −10.12; Fig. 6c) and less by smithsonite ($ZnCO_3$) precipitation (SI $ZnCO_3$ max = 1.38, min = −2.12). Minimum SI values of Zn carbonates are found in stream water indicating that their potential transport and consequent dissolution to the stream water could be one of the main sources of Zn in water. This is consistent with modelling results and corrosion morphologies of smithsonite found by Miler et al. (2022) at the Mežica Pb-Zn mining area

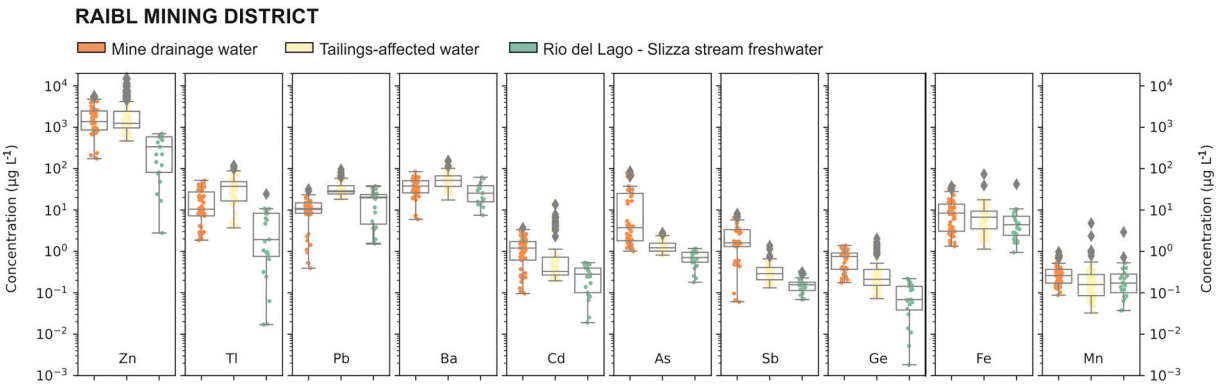

Fig. 4. Boxplot of potentially toxic trace element compositions in the mining district.

in Slovenia, which belongs to the same metallogenic province, indicating that smithsonite can be very soluble in slightly alkaline stream waters. Reasonably hydrozincite could behave similarly to smithsonite.

Although Tl is a trace component in the Raibl tailings, because its concentrations are at least two orders of magnitude lower in comparison to Zn and Pb (Barago et al., 2021), Tl was very abundant in the water matrix. Such high Tl mobility can be explained by two geochemical processes: 1) The modelling results indicate that negligible amounts of poorly mobile species of Tl(III) are expected. On the contrary, Tl should be found mainly in the more mobile Tl(I) form. In detail, the mobile Tl^{+1} ion (> 97 %; Fig. 6b) is expected to prevail among the Tl(I) dissolved species, while the sulphate ($TlSO_4^-$) should occur only to a lesser extent (3 %). 2) Natural attenuation processes of Tl in comparison to other PTEs (As, Pb, Zn) are also expected to be scarce, since Tl removal is not likely to be accomplished by Tl-mineral precipitation, as suggested by modelling results performed in this study, neither by adsorption processes (e.g., onto HFO), which are expected to be weak (Coup and Swedlund, 2015).

Arsenic (As) concentrations were generally low and consistent with previous studies (Petrini et al., 2016), even in the tailings-affected water

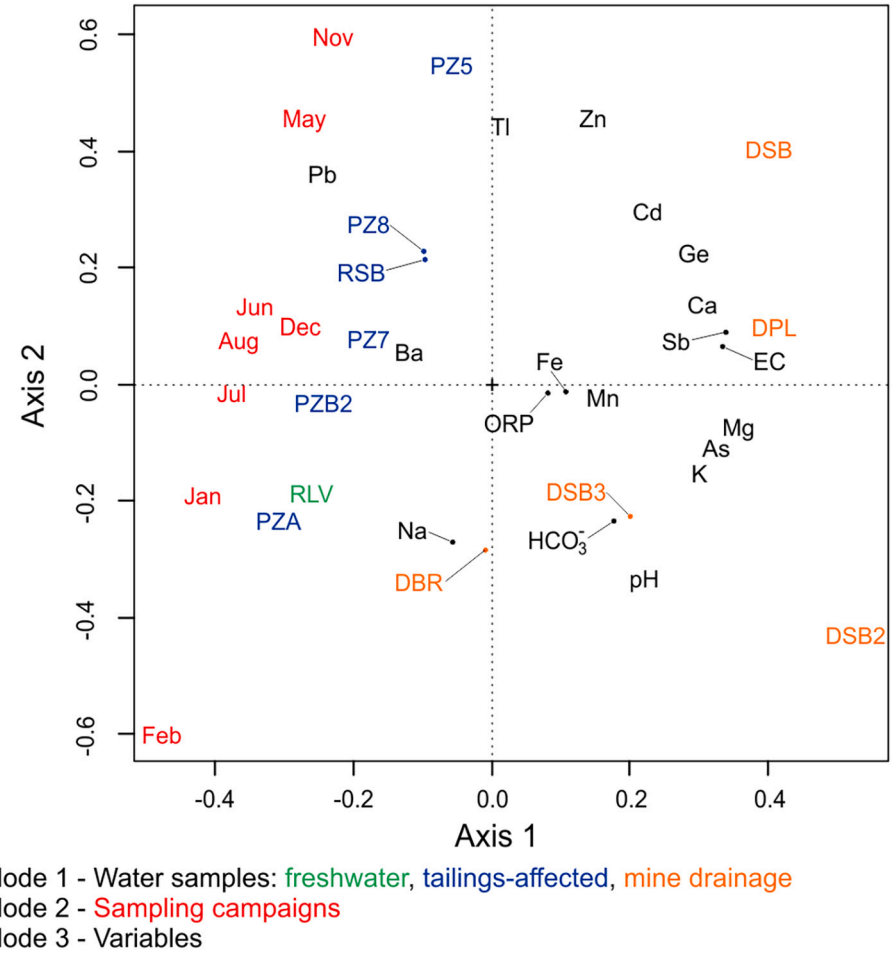

Fig. 5. Plot resuming the results of 3W-PCA performed on different water sampling stations at the Raibl mining district. Months and sampling stations were selected only when all the data were available.

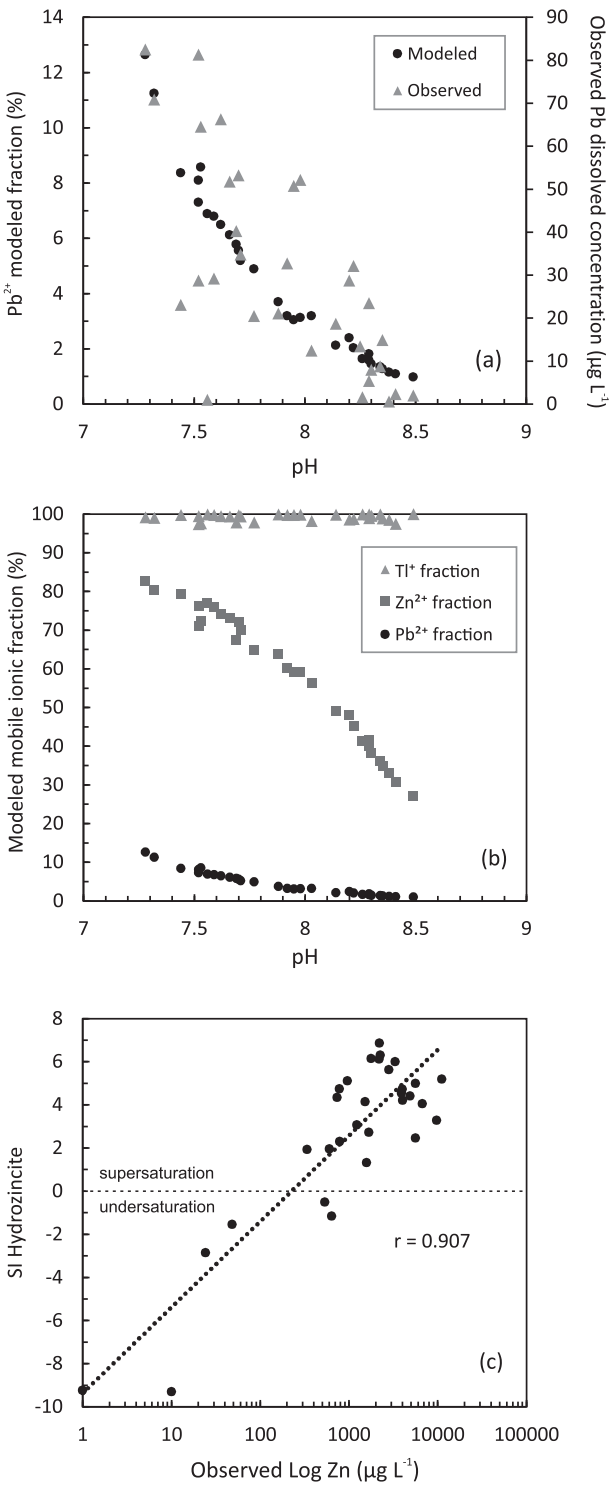

Fig. 6. (a) Observed Pb dissolved concentrations and modelled Pb^{2+} ionic fraction; (b) comparison of modelled ionic and mobile fractions of Tl^{+1}, Pb^{+2} and Zn^{+2}; (c) relation of observed Zn concentrations and hydrozincite saturation index ($Zn_5(CO_3)_2(OH)_6$).

where the PTE-bearing tailings can reach up to almost 1500 mg kg^{-1} of As in the solid phase (Barago et al., 2021). The absence of As can be related to its strong co-precipitation or adsorption on the HFOs as suggested for other similar decommissioned mining sites (Álvarez-Quintana et al., 2020; Cidu et al., 2011). However, high concentrations of As (DSB2: 74.4 ± 7.58 µg L^{-1}; Table S2) were found in the mine drainage water, which also appeared to be enriched in Sb. The occurrence of high concentrations of dissolved As and Sb could be related to relatively high pH values (~8.5) of standing oxygenated water, which induced the desorption of As, and possibly Sb (mainly As(V) and Sb(V) species) from Fe oxide surfaces (Smedley and Kinniburgh, 2002; Leuz et al., 2006). Little is known regarding the hydrogeochemistry of Germanium (Ge). It is believed that Ge distribution resembled that of As and Sb, perhaps indicating that metalloids could be characterised by similar behaviour in this mining environment. However, Ge depletion in the tailings-affected waters may also be related to the depletion of Ge-bearing sphalerite in the flotation tailings, similar to Cd.

3.3. Tailings as a source of Thallium

In Fig. 7, Zn and Tl concentrations are presented together among all the investigated sampling stations. Generally, dissolved Zn reached concentrations two orders of magnitude higher with respect to Tl; such absolute values are consistent with the high Zn availability from the tailings and its generally high mobility. The average Tl/Zn chemical ratio in water upstream from the tailings impoundments, including mine drainage waters, was nearly constant among the stations (Tl:Zn ≃ 1:100, expressed as 1 %). Changes in the Tl/Zn ratio were then observed inside the tailings impoundments. In detail, in the southern upgradient sectors of the impoundments (piezometer: PZA) the interaction between the tailings and the water table remains scarce, explaining the unaltered general Tl/Zn ratio in the corresponding groundwater. Such low interaction is explained by a greater distance between the tailings and the groundwater table, of approximately 4–8 m, in the southern sectors (Barago et al., 2021). Conversely, from PZB2 to the downgradient PZ5, PZ7 and PZ8 groundwaters, the tailings become more saturated as the tailings beds are deeper and the water table is shallower (Fig. 2). This may explain the increase in the Tl concentrations (PZ7 and PZ8: Tl = 43.1 ± 10.3 and 53.6 ± 19.4 µg L^{-1}), together with Tl/Zn ratios (up to 3.4 %). Somewhat similarly the same anomaly was found between Tl and the other main PTEs such as Pb and Cd (Table S2). This positive anomaly of Tl indicates that the tailings represent an active source of this element, and their leaching promotes Tl mobilisation, even 3–4 fold more than other monitored sites in the Raibl district. Such a release of Tl is of concern since a significant amount of dissolved Tl may eventually occur downstream, posing a potential risk for the general quality of the fluvial ecosystem. Although there is no direct evidence that the tailings impoundments represent an active and constant source of contamination affecting the Rio del Lago - Slizza river system, some minor springs of the Rio del Lago, located immediately downgradient with respect to the tailings impoundments and likely fed by the groundwaters below them (RSB), were characterised by very high Tl concentrations (46.8 ± 9.75 µg L^{-1}) and a higher Tl/Zn ratio (2.2 %). This evidence suggests that tailings are responsible for the release of dissolved PTEs with a subsequent contamination of the main stream of the Rio del Lago (RLV: 9.7 ± 5.3 µg L^{-1}; Tl/Zn = 1.5 %). Downstream along the river, Tl concentrations, as well as the other PTEs, were attenuated by dilution as evidenced by a decrease in their concentrations by one order of magnitude (1.01 ± 0.06 µg L^{-1}) at 9 km downstream in the Slizza freshwaters (RSC station; Table S2). However, the geochemical signature was still observable (RSC: Tl/Zn = 1.7 %). As previously discussed, elevated values of Tl/Zn were reasonably related to differences in the attenuation pathways of the different elements. High values of Tl/Zn can be explained by the higher affinity of Tl for the dissolved phase, which was consistent with negligible attenuation pathways. On the other hand, in the case of Zn, its decrease can be attributed to natural attenuation processes such as sorption, precipitation of Zn-bearing secondary minerals such as hydrozincite and pH dependent speciation (Fig. 6a and b) and, consequently, increasing the Tl/Zn ratio.

3.4. Temporal variability of PTE concentrations and total dissolved loads

In general, the temporal variability was characterised by high

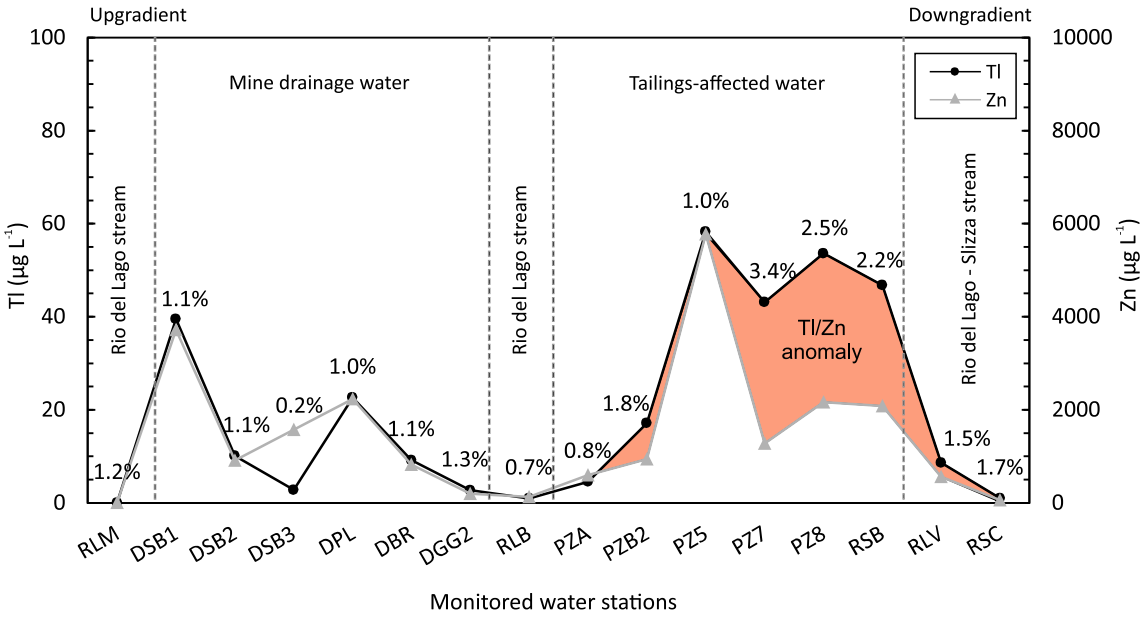

Fig. 7. Zinc and Tl concentrations in the different groups of waters collected upstream and downstream of the decommissioned Raibl mining district along the Rio del Lago Valley. The labels indicate Tl/Zn ratio (%).

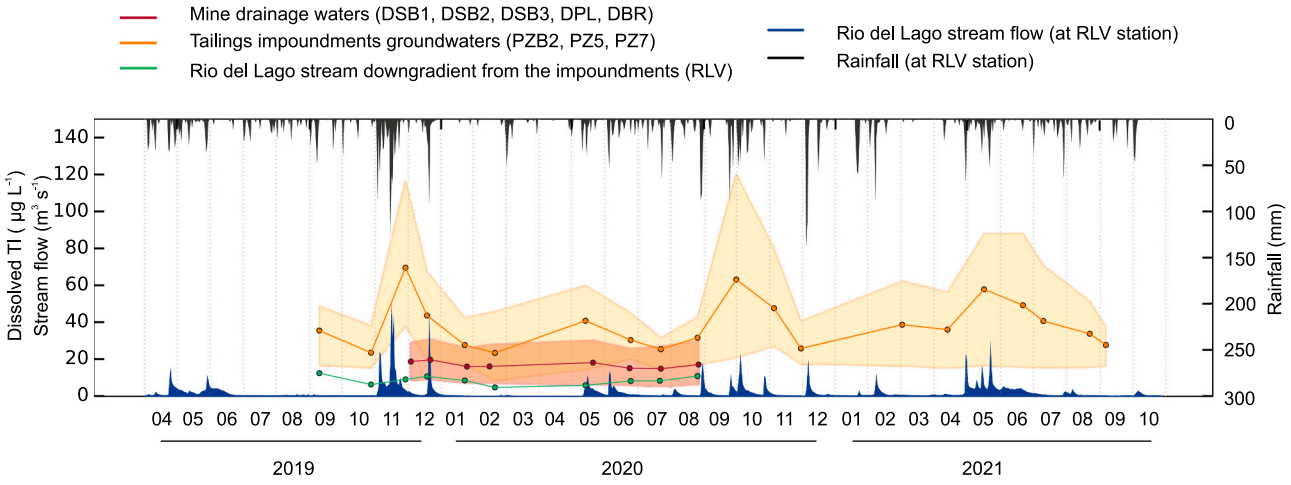

Fig. 8. Time series of dissolved Tl in the different groups of waters collected at the decommissioned Raibl mining district, represented with a 95 % confidence interval. Rainfall and stream flow data were provided by the commissioner station.

concentrations of dissolved Tl (Fig. 8) (and other PTEs, not presented) in the rainy seasons, which corresponded to autumn (November) and spring (May). This seasonal effect, which is responsible for the large standard deviations seen in Table 3 and S2, was also confirmed by the 3W-PCA output, also for Zn and Pb (Fig. 5). The major temporal variations appeared in the groundwaters entrapped in the tailings impoundments, especially when the water table rose as a consequence of intense precipitation and melting snow, which recharged the Rio del Lago stream water (Fig. 8). Such processes caused an extension of the saturated area to less deep and weathered volumes of tailings, with high potential in terms of secondary source of PTEs (Fig. S1). For instance, the minimum PTE concentrations at PZ5 were observed in winter, when snow fall is frequent and the Rio del Lago is in low-flow conditions (February 2020), and in autumn just before the beginning of the rainy season (October 2019) with concentrations ranging from 8.27 to 15.3 µg L^{-1}. In contrast, the maximum concentrations were found at PZ5 during the main rainfalls of the rainy seasons in November 2019 and October 2020 with values of Tl one order of magnitude higher than in the dry season, ranging from 117 to 120 µg L^{-1}.

Since the PTE concentrations in the Rio del Lago River downstream from the tailings impoundments (RLV), appeared moderately constant through the year (Tl: average = 8.65 ± 2.37, max = 12.4 µg L^{-1}), a general increase in the stream flow corresponded to an increase in the total dissolved load (TDL). Considering the average concentration of Tl mentioned above, under low flow conditions (100 L/s), the TDL of Tl was 70 g day^{-1}. In contrast, during high flow events when the Rio del Lago discharge can reach values higher than 50,000 L/s, the TDL transport can reach values higher than 37 kg day^{-1} of Tl, representing an increase of almost three orders of magnitude. In the same low and high flow conditions, the TDL of Zn calculated from the average concentration (563 µg L^{-1}) ranged from 4.8 to 2432 kg day^{-1}. Although the average PTE concentrations and TDL of the Rio del Lago are very low in comparison to other Pb-Zn mining districts characterised by acid drainages, such as the abandoned mining areas in SW Sardinia, Italy (De Giudici et al., 2018; Dore et al., 2020), during such high flow events the TDL of Zn strongly increased reaching values comparable to the extreme values found in the Rio Irvi (Sardinia), which was found to be characterised by a Zn TDL = 2370 kg day^{-1}. This suggests that intense rainfalls

and high flow events, which are not uncommon in the alpine environment, may not only represent a matter of concern for the structural stability of the tailings impoundments but also an environmental hazard. Indeed, very large quantities of dissolved (and particulate) PTEs can be dispersed although their concentrations remain quite constant, and transported over very long distances.

4. Conclusions

Significantly high PTE concentrations persist in the drainage water system of the decommissioned Pb-Zn Raibl mining district despite almost 30 years of flushing after extraction and processing activities shut down. Differences in the geochemical signature were found in different monitored waters: the water affected by the leaching of tailings showed very high concentrations of Zn, Tl and Pb, whereas the waters draining the mine galleries were also enriched in As and, to a lesser extent, Sb. This could be explained by differences in the residence time and higher pH conditions of the water, which can promote the mobility of metalloids such as As due to desorption from HFOs. Anomalous high concentrations of Tl were found in waters affected by post-flotation tailings leaching, with Tl/Zn ratios 3–4 fold higher with respect to mine drainage and riverine waters. This anomaly of Tl was similarly observed with regard to other main PTEs, indicating that tailings are the main source of dissolved Tl in the water at the investigated decommissioned mining district. This is reasonably supported by modelling results since negligible natural attenuation processes are expected for Tl, which appeared to be mainly present in its ionic mobile form Tl(I). In contrast, Zn and Pb concentrations were likely affected by attenuation processes due to sorption on Fe oxy-hydroxides and pH-dependent speciation. Moreover, elevated Zn concentrations were also likely limited by hydrozincite precipitation. Results from this research also reveal that leaching processes involving tailings and the subsequent release and dispersion of PTEs are promoted during periods of intense rainfall and high flow river conditions. During such events the concentrations of metals in the groundwater found in tailings impoundments can be heavily increased by one order of magnitude, whereas the total dissolved load (TDL) in the main stream, the Rio del Lago, can be magnified by three orders of magnitude.

CRediT authorship contribution statement

Nicolò Barago: Investigation, Software, Data curation, Visualization, Writing – original draft. **Elena Pavoni:** Investigation, Software, Writing – review & editing. **Federico Floreani:** Investigation. **Matteo Crosera:** Resources, Validation. **Gianpiero Adami:** Resources, Validation. **Davide Lenaz:** Resources, Supervision. **Stefano Covelli:** Conceptualization, Investigation, Project administration, Supervision, Writing – review & editing.

Declaration of competing interest

The authors declare that they have no known competing financial interests or personal relationships that could have appeared to influence the work reported in this paper.

Data availability

Data will be made available on request.

Acknowledgements

This work was realised under the partnership between the University of Trieste and the Regional Direction for the Environment of Friuli Venezia Giulia (LR 23/2013, art. 4), which provided financial support for the research. We are expressly grateful: to the Deputy Commissioner for the Raibl mining area Guglielmo Berlasso; to Mara Mauri, Flavio Gabrielcig, Sara of the Regional Direction for the Environment of Friuli Venezia Giulia; to Carlo Viola, Andrea Cicogna and Adriano Bortolussi of ARPA FVG and OSMER; to Ilenia Cimenti, Igor Černuta and Manuela C. Codeluppi of the Raibl Mine Museum Center and of the Raibl Mine Museum Center and to Federico Zotta for helping during field sampling and analyses. Karry Close is warmly acknowledged for proofreading the manuscript.

Appendix A. Supplementary data

Supplementary data to this article can be found online at https://doi.org/10.1016/j.gexplo.2022.107129.

References

Acquavita, A., Brandolin, D., Cattaruzza, C., Felluga, A., Maddaleni, P., Meloni, C., Pasquon, M., Predonzani, S., Poli, L., Skert, N., Zanello, A., 2022. Mercury distribution and speciation in historically contaminated soils of the Isonzo River Plain (NE Italy). J. Soils Sediments 22, 79–92. https://doi.org/10.1007/s11368-021-03038-2.

Álvarez-Quintana, J., Álvarez, R., Ordóñez, A., 2020. Arsenic in soils affected by mining: microscopic studies vs. sequential chemical extraction. Int. J. Environ. Res. PublicHealth 17, 8426. https://doi.org/10.3390/ijerph17228426.

APAT, IRSA-CNR, 2003. Metodi analitici per le acque. Volume primo. Manuali e Linee Guida 29/2003.

ARPA FVG-OSMER, GRN. "OMNIA" database. Available online. http://www.meteo.fvg.it/. (Accessed 10 March 2022).

Bačeva, K., Stafilov, T., Šajn, R., Tănăselia, C., Makreski, P., 2014. Distribution of chemical elements in soils and stream sediments in the area of abandoned Sb–As–Tl Allchar mine, Republic of Macedonia. Environ. Res. 133, 77–89. https://doi.org/10.1016/j.envres.2014.03.045.

Barago, N., Floreani, F., Acquavita, A., Esbrí, J.M., Covelli, S., Higueras, P., 2020. Spatial and temporal trends of gaseous elemental mercury over a highly impacted coastal environment (Northern Adriatic, Italy). Atmosphere 11, 935. https://doi.org/10.3390/atmos11090935.

Barago, N., Covelli, S., Mauri, M., Oberti di Valnera, S., Forte, E., 2021. Prediction of trace metal distribution in a tailings impoundment using an integrated geophysical and geochemical approach (Raibl Mine, Pb-Zn Alpine District, Northern Italy). Int. J. Environ. Res. Public Health 18, 1157. https://doi.org/10.3390/ijerph18031157.

Belzile, N., Chen, Y.-W., 2017. Thallium in the environment: a critical review focused on natural waters, soils, sediments and airborne particles. Appl. Geochem. 84, 218–243. https://doi.org/10.1016/j.apgeochem.2017.06.013.

Biagioni, C., D'Orazio, M., Vezzoni, S., Dini, A., Orlandi, P., 2013. Mobilization of Tl-Hg-As-Sb-(Ag, Cu)-Pb sulfosalt melts during low-grade metamorphism in the Alpi Apuane (Tuscany, Italy). Geology 41, 747–750. https://doi.org/10.1130/G34211.1.

Brigo, L., Cerrato, P., 1994. Trace element distribution of Middle-Upper Triassic carbonate-hosted lead-zinc mineralizations: the example of the Raibl Deposit (Eastern Alps, Italy). In: Fontboté, L., Boni, M. (Eds.), Sediment-hosted Zn-Pb Ores. Springer Berlin Heidelberg, Berlin, Heidelberg, pp. 179–197. https://doi.org/10.1007/978-3-662-03054-7_11.

Brigo, L., Kostelka, L., Omenetto, P., Schneider, H.-J., Schroll, E., Schulz, O., Štrucl, I., 1977. Comparative reflections on four Alpine Pb-Zn deposits. In: Klemm, D.D., Schneider, Hans-Jochen (Eds.), Time- And Strata-bound Ore Deposits. SpringerBerlin Heidelberg, Berlin, Heidelberg, pp. 273–293. https://doi.org/10.1007/978-3-642-66806-7_18.

Campanella, B., Colombaioni, L., Benedetti, E., Di Ciaula, A., Ghezzi, L., Onor, M., D'Orazio, M., Giannecchini, R., Petrini, R., Bramanti, E., 2019. Toxicity of thallium at low doses: a review. Int. J. Environ. Res. Public Health 16. https://doi.org/10.3390/ijerph16234732.

Casiot, C., Egal, M., Bruneel, O., Verma, N., Parmentier, M., Elbaz-Poulichet, F., 2011. Predominance of aqueous Tl(I) species in the river system downstream from the abandoned Carnoulès Mine (Southern France). Environ. Sci. Technol. 45, 2056–2064. https://doi.org/10.1021/es102064r.

CCME, 1999. Canadian water quality guidelines or the protection of aquatic life: thallium. In: Canadian Environmental Quality Guidelines. Canadian Council of Ministers of the Environment, Winnipeg.

Cidu, R., Frau, F., Da Pelo, S., 2011. Drainage at abandoned mine sites: natural attenuation of contaminants in different seasons. Mine Water Environ. 30, 113–126. https://doi.org/10.1007/s10230-011-0146-4.

Coup, K.M., Swedlund, P.J., 2015. Demystifying the interfacial aquatic geochemistry of thallium(I): new and old data reveal just a regular cation. Chem. Geol. 398, 97–103. https://doi.org/10.1016/j.chemgeo.2015.02.003.

De Giudici, G., Medas, D., Cidu, R., Lattanzi, P., Podda, F., Frau, F., Rigonat, N., Pusceddu, C., Da Pelo, S., Onnis, P., Marras, P.A., Wanty, R.B., Kimball, B., 2018. Application of hydrologic-tracer techniques to the Casargiu adit and Rio Irvi (SW-Sardinia, Italy): using enhanced natural attenuation to reduce extreme metal loads. Appl. Geochem. 96, 42–54. https://doi.org/10.1016/j.apgeochem.2018.06.004.

Desio, A., Passeri, L.D., Comizzoli, G., Assereto, R., Rulli, A., Gioria, C., Perno, U., 1967. Tarvisio: Foglio 14a 1:100000 - Servizio Geologico d'Italia.

Doglioni, C., 1988. Note sull'evoluzione strutturale della zona di Raibl. Broglio Loriga C Doglioni C Neri C Eds Studi Stratigr. E Strutt. Nell'area Mineraria Raibl Soc. Ital. Min. SpA Unpubl. Rep, 47 pp.

Dore, E., Fancello, D., Rigonat, N., Medas, D., Cidu, R., Da Pelo, S., Frau, F., Lattanzi, P., Marras, P.A., Meneghini, C., Podda, F., Rimondi, V., Runkel, R.L., Kimball, B., Wanty, R.B., De Giudici, G., 2020. Natural attenuation can lead to environmental resilience in mine environment. Appl. Geochem. 117, 104597 https://doi.org/10.1016/j.apgeochem.2020.104597.

Dzombak, D.A., Morel, F.M.M., 1990. Surface Complexation Modeling: Hydrous Ferric Oxide. A Wiley-Interscience publication,Wiley.

Garrido, F., Garcia-Guinea, J., Lopez-Arce, P., Voegelin, A., Göttlicher, J., Mangold, S., Almendros, G., 2020. Thallium and co-genetic trace elements in hydrothermal Fe-Mn deposits of Central Spain. Sci. Total Environ. 717, 137162 https://doi.org/10.1016/j.scitotenv.2020.137162.

George, L.L., Cook, N.J., Ciobanu, C.L., 2016. Partitioning of trace elements in co-crystallized sphalerite–galena–chalcopyrite hydrothermal ores. Ore Geol. Rev. 77, 97–116. https://doi.org/10.1016/j.oregeorev.2016.02.009.

George, L.L., Biagioni, C., Lepore, G.O., Lacalamita, M., Agrosì, G., Capitani, G.C., Bonaccorsi, E., d'Acapito, F., 2019. The speciation of thallium in (Tl, Sb, As)-rich pyrite. Ore Geol. Rev. 107, 364–380. https://doi.org/10.1016/j.oregeorev.2019.02.031.

Ghezzi, L., D'Orazio, M., Doveri, M., Lelli, M., Petrini, R., Giannecchini, R., 2019. Groundwater and potentially toxic elements in a dismissed mining area: thallium contamination of drinking spring water in the Apuan Alps (Tuscany, Italy). J. Geochem. Explor. 197, 84–92. https://doi.org/10.1016/j.gexplo.2018.11.009.

Giani, M., Rampazzo, F., Berto, D., Maggi, C., Mao, A., Horvat, M., Emili, A., Covelli, S., 2012. Bioaccumulation of mercury in reared and wild Ruditapes philippinarum of a Mediterranean lagoon. Estuar. Coast. Shelf Sci. 113, 116–125. https://doi.org/10.1016/j.ecss.2012.05.031.

Gustafsson, J.P., 2009. Visual MINTEQ Version 2.61.

Gustafsson, J.P., 2014. Visual MINTEQ Version 3.1.

Henjes-Kunst, E., Raith, J.G., Boyce, A.J., 2017. Micro-scale sulfur isotope and chemical variations in sphalerite from the Bleiberg Pb-Zn deposit, Eastern Alps,Austria. Ore Geol. Rev. 90, 52–62. https://doi.org/10.1016/j.oregeorev.2017.10.020.

Hudson-Edwards, K.A., Jamieson, H.E., Lottermoser, B.G., 2011. Mine wastes: past, present, future. Elements 7, 375–380. https://doi.org/10.2113/gselements.7.6.375.

Jabłońska-Czapla, M., Nocoń, K., Szopa, S., Łyko, A., 2016. Impact of the Pb and Zn ore mining industry on the pollution of the Biała Przemsza River,Poland. Environ. Monit. Assess. 188 https://doi.org/10.1007/s10661-016-5233-3, 262-262.

Kaplan, D.I., Mattigod, S.V., 1998. Aqueous geochemistry of thallium. In: Nriagu, J.O. (Ed.), Thallium in the Environment. Wiley, New York, pp. 15–29.

Leach, D.L., Taylor, R.D., Fey, D.L., Diehl, S.F., Saltus, R.W., 2010. A Deposit Model for Mississippi Valley-Type Lead-Zinc Ores. Miner. Depos. Models Resour. Assess., U.S. Geological Survey Scientific Investigations Report 2010-5070-A Chapter A, 52 pp.

Leardi, R., Melzi, C., Polotti, G., 2019. CAT (Chemometric Agile Tool). Available online: http://www.gruppochemiometria.it/index.php/software/19-download-the-r-based-chemometric-software. (Accessed 24 January 2022).

Leuz, A.-K., Mönch, H., Johnson, C.A., 2006. Sorption of Sb(III) and Sb(V) to goethite: influence on Sb(III) oxidation and mobilization. Environ. Sci. Technol. 40, 7277–7282. https://doi.org/10.1021/es061284b.

Liu, J., Wang, J., Chen, Y., Xie, X., Qi, J., Lippold, H., Luo, D., Wang, C., Su, L., He, L., Wu, Q., 2016. Thallium transformation and partitioning during Pb–Zn smelting and environmental implications. Environ. Pollut. 212, 77–89. https://doi.org/10.1016/j.envpol.2016.01.046.

Melcher, F., Onuk, P., 2019. Potential of critical high-technology metals in Eastern Alpine base metal sulfide ores. In: BHM Berg- Hüttenmänn. Monatshefte, 164, pp. 71–76. https://doi.org/10.1007/s00501-018-0818-5.

Miler, M., Bavec, Š., Gosar, M., 2022. The environmental impact of historical Pb-Zn mining waste deposits in Slovenia. J. Environ. Manag. 308, 114580 https://doi.org/10.1016/j.jenvman.2022.114580.

Oliveri, P., Malegori, C., Casale, M., 2020. Chemometrics: multivariate analysis of chemical data. In: Pico, Y. (Ed.), Chemical Analysis of Food, 2nd ed. Elsevier, Amsterdam, The Netherlands.

Pavoni, E., Petranich, E., Adami, G., Baracchini, E., Crosera, M., Emili, A., Lenaz, D., Higueras, P., Covelli, S., 2017. Bioaccumulation of thallium and other trace metals in Biscutella laevigata nearby a decommissioned zinc-lead mine (Northeastern Italian Alps). J. Environ. Manag. 186, 214–224. https://doi.org/10.1016/j.jenvman.2016.07.022.

Pavoni, E., Covelli, S., Adami, G., Baracchini, E., Cattelan, R., Crosera, M., Higueras, P., Lenaz, D., Petranich, E., 2018. Mobility and fate of lhallium and other potentially harmful elements in drainage waters from a decommissioned Zn-Pb mine (North-Eastern Italian Alps). J. Geochem. Explor. 188, 1–10. https://doi.org/10.1016/j.gexplo.2018.01.005.

Peter, A.L.J., Viraraghavan, T., 2005. Thallium: a review of public health and environmental concerns. Environ.Int. 9.

Petrini, R., Cidu, R., Slejko, F.F., 2016. Thallium contamination in the Raibl mine site stream drainage system (Eastern Alps, Italy). Mine Water Environ. 35, 55–63. https://doi.org/10.1007/s10230-015-0346-4.

Pimminger, M., Grasserbauer, M., Schroll, E., Cerny, I., 1985. Trace element distribution in sphalerites from Pb-Zn-ore occurrences of the Eastern Alps. In: TMPM Tschermaks Mineral. Petrogr. Mitteilungen, 34, pp. 131–141. https://doi.org/10.1007/BF01081557.

Piper, A.M., 1944. A graphic procedure in the geochemical interpretation of water-analyses. EOS Trans. Am. Geophys. Union 25, 914–928. https://doi.org/10.1029/TR025i006p00914.

Plumlee, G.S., Smith, K.S., Montour, M.R., Ficklin, W.H., Mosier, E.L., 1999. Geologic controls on the composition of natural waters and mine waters draining diverse mineral-deposit types. In: The Environmental Geochemistry of Mineral Deposits, Part B. Case Studies And Research Topics. Society of Economic Geologists, Littleton, CO, pp. 373–432.

Ralph, L., Twiss, M.R., 2002. Comparative toxicity of thallium(I), thallium(III), and cadmium(II) to the unicellular alga Chlorella isolated from Lake Erie. Bull. Environ. Contam. Toxicol. 68, 261–268. https://doi.org/10.1007/s001280247.

Rudnick, R.L., Gao, S., 2003. Composition of the continental crust. In: Treatise On Geochemistry, 3, pp. 1–64, 64.

Sangster, D.F., 1976. Carbonate-hosted lead–zinc deposits. In: Cu, Zn, Pb, And Ag Deposits. Elsevier, pp. 447–456. https://doi.org/10.1016/B978-0-444-41406-9.50013-0.

Schroll, E., 2005. Alpine type Pb-Zn-deposits (APT) hosted by Triassic carbonates. In: Mao, J., Bierlein, F.P. (Eds.), Mineral Deposit Research: Meeting the Global Challenge. SpringerBerlin Heidelberg, Berlin, Heidelberg, pp. 175–178. https://doi.org/10.1007/3-540-27946-6_46.

Schroll, E., Kürzl, H., Weinzierl, O., 1994. Geochemometrical studies applied to the Pb-Zn deposit Bleiberg/Austria. In: Fontboté, L., Boni, M. (Eds.), Sediment-hosted Zn-Pb Ores. SpringerBerlin Heidelberg, Berlin, Heidelberg, pp. 228–245. https://doi.org/10.1007/978-3-662-03054-7_14.

Smedley, P.L., Kinniburgh, D.G., 2002. A review of the source, behaviour and distribution of arsenic in natural waters. Appl. Geochem. 17, 517–568. https://doi.org/10.1016/S0883-2927(02)00018-5.

Smilde, A., Bro, R., Geladi, P., 2004. Multi-way Analysis With Application in the Chemical Science. John Wiley & Sons, Hoboken, NJ, USA. ISBN 0-470-01211-0.

Tatsi, K., Turner, A., Handy, R.D., Shaw, B.J., 2015. The acute toxicity of thallium to freshwater organisms: implications for risk assessment. Sci. Total Environ. 536, 382–390. https://doi.org/10.1016/j.scitotenv.2015.06.069.

Venerandi, I., 1966. Sulla presenza di jordanite nel giacimento di Raibl. In: Atti Symp Int Giac Min Alpi, 1, pp. 243–250.

Viets, J.G., Leach, D.L., Lichte, F.E., Hopkins, R.T., Gent, C.A., Powell, J.W., 1996. Paragenetic and minor- and trace-element studies of Mississippi Valley-type ore deposits of the Silesian-Cracow district,Poland. Pr. Panstwowego Inst. Geol. 154, 36–71.

Vink, B.W., 1993. The behaviour of thallium in the (sub) surface environment in terms of Eh and pH. Chem. Geol. 109, 119–123. https://doi.org/10.1016/0009-2541(93)90065-Q.

Manuscript

Thallium and PTE distribution and mobility in solid matrices at the Zn-Pb Raibl mining site (NE Italy)

Barago N.[a], Pavoni E.[a], Crosera M.[c], Adami G.[c], Floreani F. [a,b], Lenaz D.[a], Covelli S.[a]

[a] Dipartimento di Matematica e Geoscienze, Università di Trieste
[b] Dipartimento di Scienze della Vita, Università di Trieste
[c] Dipartimento di Scienze Chimiche e Farmaceutiche, Università di Trieste

ABSTRACT

The Raibl mine in Friuli Venezia Giulia (Italy) is one of the largest sulfide carbonate-hosted Pb-Zn decommissioned mining districts of the Alps. Large amounts of materials derived from the exploitation and processing of the Tl-rich sulfide ore in open pits, waste rock piles and flotation tailings impoundments are present and contribute to neutral mine drainage (NMD), responsible for the contamination of the main stream by potentially toxic trace elements (PTEs), especially thallium (Tl) which is a very mobile and toxic element. This work examines the relationships between total concentrations and labile fractions of *PTEs by means of a single-step moderate extraction with diluted HCl 0.5 M on 66 samples of different matrices including natural soil, stream sediments and mine wastes. High concentrations of PTEs up to 11.5 % wt. of Zn, 5.0 % wt. of Pb, 908 mg/kg of Tl, 118 mg/kg of Ge in mine wastes indicate that reprocessing mine wastes to obtain elements of economic interest should be evaluated. The geoaccumulation index (I_{geo}) of stream sediments indicate that the Rio del Lago is heavily to extremely contaminated by As, Cd, Pb, Sb, Tl and Zn. The median value (%) of the labile fraction was found in the following order: $Mn \approx Cd > Co > Zn > Ni > Tl > Sb > Cu > Pb > Cr > V \approx As \approx Fe$. Antimony (Sb) was found more mobile than As, although often both were found in the residual fraction. Higher labile fractions of Zn, Tl and Pb were often related to higher total concentrations thus confirming that the most important factors governing the dispersions of dissolved PTEs at the field scale are: high volumes of enriched mining wastes, fine grain size and hydrogeological conditions. Despite of relatively high PTE concentrations in stream sediments, only small labile fractions (< 5 %) of the Tl and Cd total concentration in these sediments may be potentially bioavailable. Although the HCl extraction was found as a valid preliminary approach to evaluate the mobile or extractable fraction of PTEs, the results of the leaching test were not fully comparable with previous analyses of surface and groundwaters in contact with tailings and mining wastes. The moderate extraction performed in this research seems 1) to overestimate Pb mobility and 2) to strongly affect dissolution of secondary Zn carbonate minerals. These results indicate that the HCl partial extraction may inhibit some natural attenuation processes of Pb and Zn availability in dissolved forms such as (co-precipitation) and sorption on Fe oxy-hydroxides (HFOs). Future research should address to more detailed studies to fully understand speciation, mobility and bioavailability of PTEs associated with mine wastes in carbonate buffering environments.*

1 INTRODUCTION

In recent decades we are witnessing an increasing demand for natural resources, driven by demographic and technological development, and now also for the energy, ecological and digital transitions. This need translates into more increased extraction and production of larger volumes of resources from the Earth. However, the occurrence of potentially toxic trace elements (PTEs, such as e.g., As, Cd, Pb, Sb, Tl, Zn) in the environment due to mining activity is a well-known issue around the world, and the knowledge of the geochemical processes is essential to manage both active and dismissed mining sites and to control the dispersion of PTEs reducing risks for ecosystems and human health (e.g., Cidu et al., 2018; Covelli et al., 2007; De Giudici et al., 2019; Gošar et al., 2015; Gosar et al., 2020; Higueras et al., 2006; Hudson-Edwards, 2003; Kasmaeeyazdi et al., 2022; Pavoni et al., 2017; Wang et al., 2017). The purpose of this study is to investigate the mobility of thallium (Tl) and other PTEs in different, from uncontaminated to contaminated, solid matrices in a Pb-Zn Mississippi Valley Type (MVT) decommissioned mining area.

Single-step moderate extraction

Since the biogeochemical and ecotoxicological significance of a given contaminant, mainly trace metal(oid)s, is determined by its specific mobility and speciation characteristics, the evaluation of the labile fraction via (single or sequential) partial extraction may be more appropriate rather than by the total concentration (Kersten, 2002). The key interest is on the determination of the bioavailable metal(oid) concentrations, i.e. those fractions responsible for being potentially bioavailable and then harmful or toxic to biota (Snape et al., 2004). However, the reagents used in the partial extractions are "non-selective" extractants and are insufficient to determine univocally the speciation of the elements of interest (i.e., the mineral/organic phase which hosts or binds the metal(oid)). Many partial extraction procedures are reported in the literature, and diluted HCl moderate extraction is one of the most common extractant used (Adami et al., 1999; Agemian and Chau, 1976; Hotton and Sutherland, 2016; Larner et al., 2006; Malo, 1977; McCready et al., 2003; Snape et al., 2004; Sutherland, 2002; Wang et al., 2017). It is a valuable and cost-effective analytical procedure for determining labile (mobile) phases in trace metal(oid) contamination assessment also because it produces minimal dissolution of crystalline lattices of silicates (Agemian and Chau, 1977, 1976; Larner et al., 2006; Sutherland, 2002). Moreover, Sutherland (2002) and Larner et al. (2006) found strong correlations, in urban soil and road sediments, between the diluted HCl moderate extraction and the sum of the three labile steps of the BCR sequential extraction (Rauret et al., 1999).

Study area and geological setting

The Raibl mine is located at Cave del Predil village, at the NE border of Friuli Venezia Giulia, in the Julian Alps, NE Italy (Figure 1). Near the borders with Slovenia, to the east, and with Austria, to the north, the mining area develops in a mountain area inside and around the Monte Re, where the ore deposit is hosted. The main stream is the Rio del Lago which flows from S to N into the Slizza stream, an affluent of the Gail-Drava-Danube River system flowing into the Black Sea.

Above the sandstones and limestones of the Werfen Formation, the Anisian-Ladinian sequence in the area considered includes four lithostratigraphic units: 1) conglomerates and breccias; 2) shales, sandstones and tuffites; (3) tuffs and ignimbrites; 4) dolomites. The last unit is the so-called "Dolomia Metallifera" which belongs to the Sciliar Formation (Ladinic) and host the Zn-Pb ore deposit. It is a more than 1000 m thick carbonate buildup, intercalated by local carbonatic-tuffaceous formations. The Sciliar Formation is conformably overlain, at Raibl, by the Carnian sediments of the Raibl group (Calcare del Predil, Rio del Lago, Rio Conzen and Tor formations) (Brigo et al., 1977 and references therein).

The zinc and lead mine (Zn-Pb) of Raibl, together with Bleiberg (Austria), Mežica (Slovenia) and Salafossa (Veneto) mines, constituted one of the most important Pb-Zn mining provinces in Europe, on the whole, during the 60s-70s, they produced more than 75 % of the total Pb and Zn of the Alpine area (Brigo et al., 1977). The ore deposit, probably exploited before 1320, year of the first document of mining activity, was the more important ore deposit in the Friuli Venezia Giulia region and was the last to be decommissioned in 1991 (Zucchini, 1998). Nowadays, there are no active metal mines in the region. Although iron (Fe) was mined in ancient times, mainly Zn, Pb, and germanium (Ge) were mined in the last century.

The peak of production occurred in the 60's, with more than 1,000 workers, about 550,000 tons / year of raw ore extracted with a production of Zn concentrate equal to 40,000 – 45,000 tons/year and Pb concentrate equal to about 4,000 – 5,000 tons/year[1], obtained via froth flotation in the mineralurgical plant at Cave del Predil (Figure 1a). Most of the tailings (fine-grained by-product of the froth flotation) were discharged directly into the Rio del Lago before 1976 whereas, from 1976 to 1991, were stored, as slurry, into the tailings impoundments located on the bed of the Rio del Lago, few hundred meters north from Cave del Predil, for an estimated amount of about 4 million tons of tailings and waste rocks, enriched with various elements of potential economic interest (including critical elements such as germanium (Ge)) (European Commission, 2020)) and/or environmental concern (e.g., As, Pb, Sb, Tl) (Barago et al., 2021; Meriggi et al., 2008). A recent work from this research group studied the contamination of water bodies from PTEs at Raibl, mostly due to leaching processes in the tailings impoundments; a remarkable Tl mobility in waters respect to Zn, Pb, As and Sb was found in neutral mine drainage (NMD) conditions (Barago et al., 2023). NMD are waters characterised by near-neutral pH due to the buffering capacity of carbonate lithologies (limestones, dolostones), limiting decrease of pH values caused by sulfide oxidation. NMD is opposite to AMD (acid mine drainages), where pH < 4 can easily found.

[1] Data from the State Archives of Trieste (Archivio di Stato di Trieste)

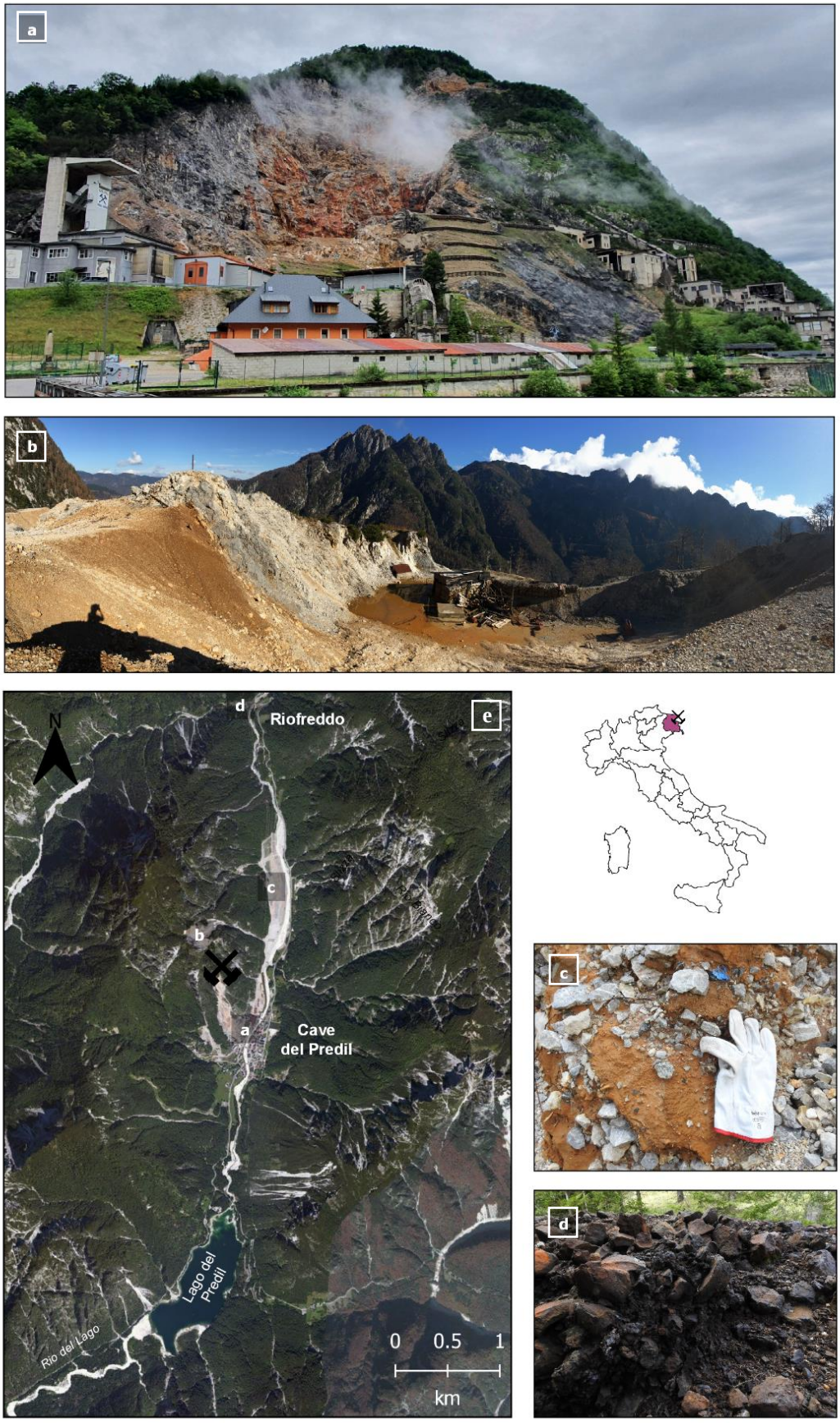

Figure 1 - a) mining village of Cave del Predil - left: “Clara” main shaft; center: main entrance of the mine; right: mineralurgical plant; b) Open pit mine in the ore gossan "Cava Andrea”; c) tailings impoundments and d) slags from the historical lead smelter plant of Rio Freddo stream, a tributary of the main stream, Rio del Lago; e) map of the mining area.

The Pb-Zn ore deposit of Raibl is located southward respect to the “Periadriatic Lineament”, a regional W-E trending fault which divides the Adriatic from the European plate. The deposit is hosted in thick, Ladinian to Lower Carnian, massive dolomitic reefs. Structurally, the Pb-Zn ore deposit is similarly controlled by Triassic to Early Jurassic extensional faults associated with the Pangea breakup in extensional tectonic setting (Doglioni, 1988). The paragenesis is mainly composed by sphalerite (ZnS), galena (PbS) and iron sulfides (mainly pyrite and marcasite, FeS_2). The upper oxidised zone of the ore body, the ore gossan (i.e., the intensely oxidised and weathered exposed rock of the ore deposit), is mainly constituted by Fe oxy-hydroxides (HFOs) secondary minerals derived from weathering of primary sulfides by runoff waters. The lower ore body is characterised by secondary carbonate Zn minerals (e.g. smithsonite: $ZnCO_3$, hydrozincite: $Zn_5(CO_3)_2(OH)_6$) formed by leaching of the sulfide ore body with subsequent precipitation of supergene carbonate minerals in alkaline environment (Di Colbertaldo, 1948). Sulfosalts such as Tl-bearing jordanite ($Pb_{14}As_6S_{23}$) and gratonite ($Pb_9As_4S_{15}$) are rare but are supposed to be present as microphases (Pimminger et al., 1985 and references within). Among gangue minerals, dolomite, calcite, and barite prevail. Among elements of interest at the Raibl site, besides Zn and Pb, there is thallium (Tl), which is an heavy metal that is highly mobile and toxic in freshwater at very low concentrations ranging from a few µg/L to mg/L (Belzile and Chen, 2017; Campanella et al., 2019; Peter and Viraraghavan, 2005; Tatsi et al., 2015) and Ge for which there are important technological applications of this element despite the relatively low annual production and consumption of this semi-metal (Rosenberg, 2009). Thallium (Tl) is hosted in sulfide minerals such as sphalerite (ZnS), especially in the yellow colloform variety, and, possibly with less amount, in galena and pyrite (Melcher and Onuk, 2019; Pimminger et al., 1985; Schroll et al., 1994), but specific studies should be carried out to settle this aspect.

2 MATERIALS AND METHODS

Sampling

The sampling was performed in the period between 2019 and 2021 with the collection of 66 samples in the Raibl mining area. Different types of solids were considered: soil, stream sediment, waste rock, ore gossan sediments, tailings, smelter slags and Zn concentrate (Figure 1). Except for the single sample of Zn concentrate, which was the final product of the mineral treatment in the mineralurgical plant (courtesy of Escuela de Minas, University of Oviedo, Spain), the other samples were collected from the Rio del Lago – Slizza valley, where mining activity has been most developed, at the surface down to a maximum depth of 30 cm. Some soils, near the mine and the village, were sampled in co-operation with ARPA FVG (Environmental Protection Regional Agency – Friuli Venezia Giulia, Italy). The stream sediments were collected in the major stream (Rio del Lago – Slizza) and minor tributaries from upstream of the mining site (Predil Lake) to the border with Austria. Waste rock is coarsely (mm size) crushed low-grade ore and wall rock typically dumped in waste rock piles or used in the area for construction purposes; this type of mine waste is widespread throughout the area. The samples of the ore gossan were collected from the open pit area located at higher altitudes on Mount Re known as "*Cava Andrea*". The samples consist of sedimentary material eroded from outcropping rocks of the ore gossan, which is the upper weathered part of the deposit, composed essentially of limonite derived from the oxidation of sulfides due to weathering (HFOs) (Figure 1b). The material involved is heterometric debris with an extremely heterogeneous grain size distribution, since it is also particularly instable, it could give rise to debris flow events, i.e. mass movement processes, through the steep gully known as "*Canalone Andrea*" orthogonal to Rio del Lago valley (Calligaris et al., 2017). Tailings are the medium-fine-grain waste product of sphalerite and galena concentrate production (Figure 1c), produced by froth flotation cells in the mineralurgical plant (Figure 1a) after milling of the ore and separation of the valuable fraction (Zn and Pb concentrates). The smelter slags of the village of Riofreddo are waste products of a small historical Pb smelter plant, presumably dismantled at the beginning of 20th or at the end of 19th centuries. Today, only some slag crusts on the ground and loose clasts are observable (Figure 1d).

Total digestion

The 66 samples were collected after removal of vegetation or plant litter from the topsoil. In the laboratory, the samples were sieved to 2 mm, ground by an agate mortar and about 250 mg of each sample was solubilised by total digestion in accordance with Method 3052 (US EPA, 1996) using a mixture of inverse *aqua regia* (3:1 = HNO_3 65-69 % : HCl 34-37 %) with HF 47-51 % (VWR Normaton) and H_2O_2 (30 m/v, Merck, only in case of soil samples). Total digestion with HF was chosen for its capability to dissolve refractory minerals such as silicate minerals. A second step of mineralisation was performed by adding suprapure H_3BO_3 6 % (Merck). Blank samples and CRMs were also digested

for each microwave batch to evaluate the quality of the analysis. After digestion, the solutions were diluted up to a volume of 25 mL by adding Milli-Q water and stored at 4 °C until analysis.

Moderate extraction

The determination of the labile and biologically available fractions of PTEs was performed on 61 of 66 samples, by means of a single-step partial extraction using dilute hydrochloric acid (HCl) 0.5 M (Adami et al., 1999 and references therein) similar to other procedures used in literature (Hotton and Sutherland, 2016; Larner et al., 2006; Sutherland, 2002; Wang et al., 2020, 2017). A volume of 20 mL of a 0.5 M solution of HCl were added to about 2.00 g of finely ground sample. In each batch, two analytical blanks were added, consisting solely of the extracting solution. The mixtures were stirred on a magnetic plate at room temperature for 18 hours and then transferred to 50 mL metal free tubes, equalised by weight with Milli-Q deionised water and centrifuged for 15 minutes at 3000 rpm. The solutions obtained were filtered using polypropylene syringe filters (VWR Chemicals, nominal porosity 0.2 μm, suitably conditioned with Milli-Q deionised water and with the extracting solution), brought to a final volume of 25 mL with Milli-Q deionised water and stored in the refrigerator at 4 °C until the analysis. The labile or extractable fraction (%) was calculated applying the formula: extractable concentration (mg/kg) / total concentration (mg/kg), for each element and sample.

Analytical determination

Major and trace elements were determined by means of Inductively Coupled Plasma Mass Spectrometry (ICP-MS, using a NexION 350X equipped with an ESI SC autosampler, Perkin Elmer). In order to avoid and minimise cell-formed polyatomic ion interference, the analysis was performed using Kinetic Energy Discrimination (KED) mode. The instrument was calibrated using standard solutions ranging between 0.5 and 500 μg/L prepared by dilution from multistandard solutions for ICP analyses (Periodic Table MIX1 and MIX2, TraceCERT Sigma-Aldrich). Several aliquots of CRMs were analysed for total concentration to check for accuracy, and allowable recoveries ranging between 81–119 % (PACS-3) and 83–107 % (MESS-4) were obtained. Moreover, potential matrix effects were evaluated by means of laboratory-fortified samples prepared by spiking a standard solution different from that employed for instrument calibration (Multielement quality control standard for ICP, VWR Chemicals) into actual samples. The repeatability of the ICP-MS analysis expressed as RSD was < 3 %. All the analytical results at least 10 times over the LODs were considered.

3 RESULTS

3.1 Total content of PTEs in the solid matrices

In general, the highest concentrations of PTEs (Table 1) were observed nearby Cave del Predil village among the mine entrance, the mineralurgical plant and the tailings impoundments, which are the sites where most of the mine wastes were allocated (Figure 2). However, the results indicate that the PTE-bearing mineralised materials, both processed and unprocessed, are widespread in the whole Cave del Predil area, mainly downstream the mine. In contrast, slags of the historic Riofreddo Pb smelter plant, 3 km north from the mine, although characterised by very high PTE concentrations are strongly limited in few hundred square meters.

The correlations presented in Figure 3 indicate that As, Cd, Ge, Pb, Sb, Tl, Zn and to a lesser extent Fe, Cu belongs to the same geochemical group, the "ore component". Except for Fe, all the metal(loid)s are associated to primary and secondary ore minerals. Whereas Fe, as well as Ni, Mn, V, Cr can be hosted also in silicate minerals of the “lithogenic component”. Cobalt was found not associated to these components.

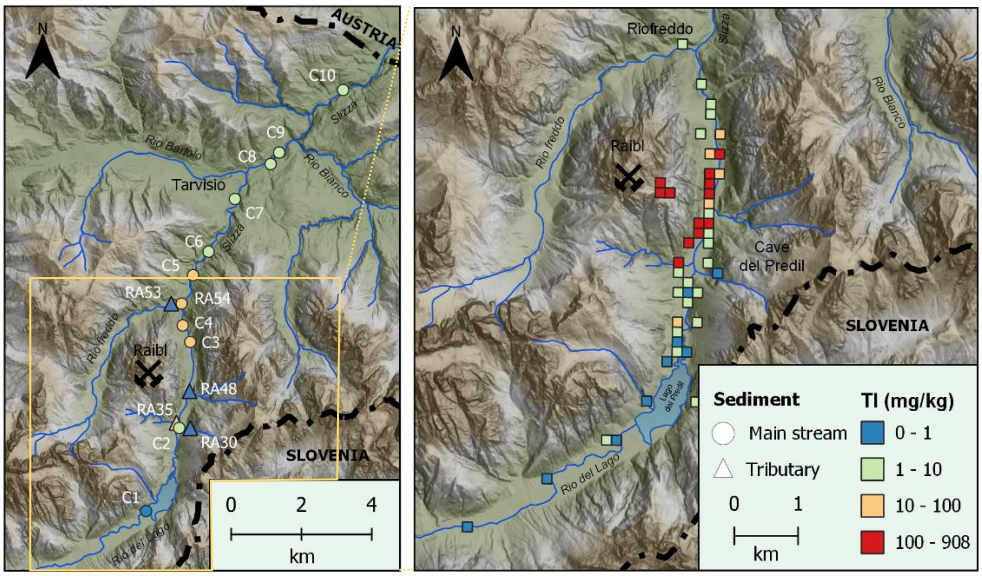

Figure 2 – (left) Total thallium (Tl) content in stream sediments of the main river (circles) and tributaries (triangles) and (right) in soils, ore gossan sediments, waste rock, tailings and smelter slag samples of the Pb-Zn Raibl decommissioned mining site.

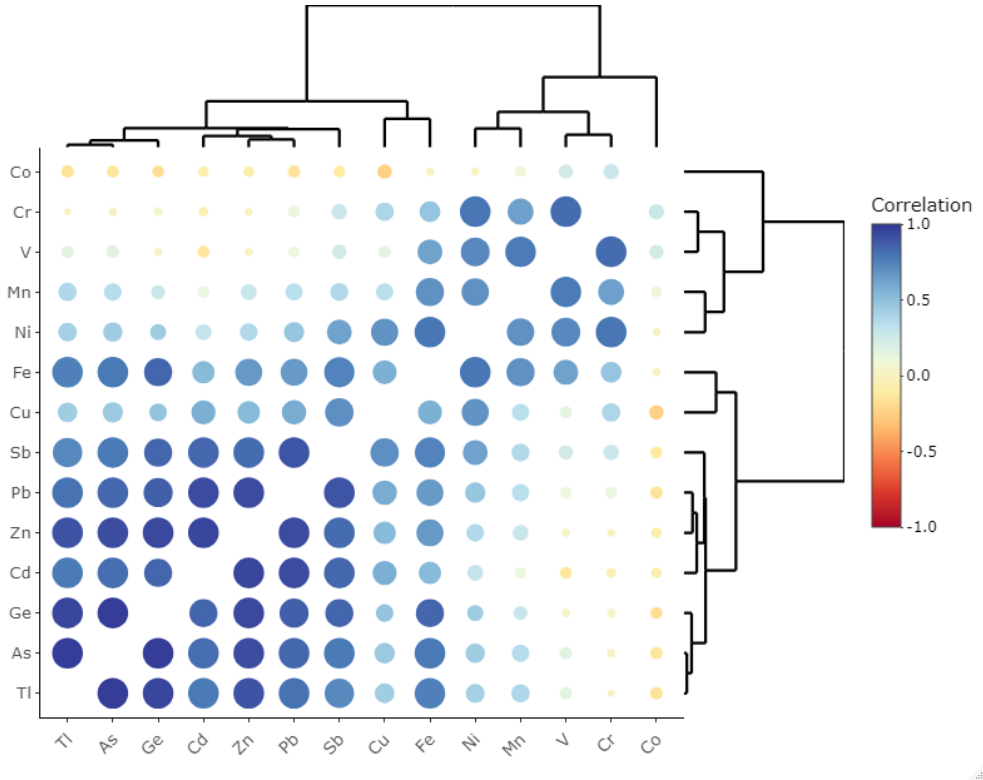

Figure 3 – Pearson correlation heatmap of major and trace elements in all waste rocks, soils and sediments analysed (processed using the heatmaply package; Galili et al., 2018). The colour is a function of the correlation coefficient (r), whereas point size is log function of the p-value.

Table 1 - Average (min-max) of the total concentration in different types of solids in the Raibl Pb-Zn mining site. Concentrations > 100 mg/kg of As, Cd, Ge, Tl and > 1,000 mg/kg of Pb, Zn are highlighted in bold.

Type	Soil	Stream sediment	Ore gossan	Waste rock	Tailings	Smelter slag	Concentrate
mg/kg	Pseudo-natural matrices			Mining waste			Product
N samples	27	16	3	11	6	2	1
As	14.9 (1.27 - 49.0)	48.6 (1.58 - **150**)	**1,044** (197 – **2,693**)	**352** (25.2 - **826**)	**1,643** (**689** – **2,439**)	**1,139** (**148** – **2,129**)	**1,023**
Cd	3.29 (0.24 – 16.0)	6.57 (0.17 - 21.8)	6.60 (1.37 - 16.5)	24.9 (2.11 - **116**)	54.5 (6.57 - **196**)	2.42 (0.82 - 4.01)	**795**
Co	3.21 (0.38 - 13.7)	31.6 (6.73 - 54.8)	1.64 (1.01 - 2.13)	2.12 (0.49 - 8.57)	2.04 (0.30 - 4.90)	85.1 (6.39 - 164)	0.61
Cr	18.8 (3.43 - 45.9)	9.8 (3.56 - 39.3)	10.0 (6.68 - 11.9)	14.8 (3.22 - 59.6)	19.8 (2.07 - 54.9)	18.3 (11.8 - 24.7)	3.56
Cu	12.3 (2.21 - 33.4)	4.80 (0.69 - 11.5)	5.94 (3.96 - 7.36)	28.7 (1.96 - 113)	23.4 (5.65 - 45.0)	618 (308 - 928)	417
Fe	7,977 (418 – 33,370)	6,267 (99 – 19,822)	36,314 (13,278 – 79,630)	18,932 (2,887 – 39,239)	71,950 (24,132 – 117,019)	260,403 (200,669 – 320,138)	11,844
Ge	0.71 (0.16 - 1.45)	1.38 (0.12 - 5.18)	43.7 (5.84 - **118**)	12.7 (2.01 - 29.1)	71.1 (24.4 - **102**)	19.6 (13.7 - 25.5)	**186**
Mn	261 (29.0 – 1,163)	123 (16.6 - 393)	442 (254 - 657)	287 (73.2 - 766)	313 (148 - 477)	2,299 (299 – 4,300)	22.0
Ni	7.29 (1.95 - 14.7)	4.59 (1.00 - 15.2)	9.06 (5.05 - 13.1)	8.76 (1.76 - 20.5)	13.3 (3.44 - 26.0)	11.7 (11.7 - 11.8)	11.9
Pb	814 (8.67 – **4,387**)	622 (6.73 – **2,138**)	**3,692** (229 – **10,599**)	**7,769** (769 – **41,436**)	**15,638** (**1,956** – **50,062**)	**35,580** (**24,778** – **46,381**)	**27,281**
Sb	1.60 (0.09 - 6.04)	1.18 (0.05 - 2.66)	2.68 (1.29 - 5.28)	11.2 (0.36 - 75.0)	14.6 (6.49 - 40.2)	**290** (31.1 - **550**)	46.2
Tl	2.58 (0.11 - 9.01)	10.2 (0.17 - 51.5)	**342** (**195** - **599**)	**143** (5.87 - **609**)	**483** (**150** - **907**)	6.19 (2.97 - 9.41)	**326**
V	26.7 (4.45 - 69.1)	17.2 (4.40 - 50.1)	35.5 (30.0 - 38.4)	24.8 (6.58 - 73.0)	32.8 (7.89 - 65.0)	32.4 (19.4 - 45.4)	1.68
Zn	871 (19.2 – **4,456**)	**2,708** (10.2 – **9,022**)	**17,668** (**1,398** – **49,752**)	**12,584** (**2,247** – **43,957**)	**46,038** (**14,464** – **114,965**)	**43,699** (**8,318** – **79,080**)	**412,620**

Mine wastes

Mine wastes are recognisable in the study area mainly due to morphology, the lack of vegetation, high presence of mineralised clasts and/or red-orange colour of oxidised sulfides in contrast to the white/light grey "lithogenic" / host rock / gangue carbonates. However, sometimes, it is not easy to determine whether the matrix is soil or waste rocks, and the classification may not be entirely objective. Maximum PTE concentrations up to 114,965 mg/kg (11.5 % wt.) of Zn, 50,062 mg/kg (5 % wt.) of Pb, 1,643 mg/kg of As, 908 mg/kg of Tl and 196 mg/kg of Cd were observed in tailings samples (Table 1). In general, PTE concentrations are higher than those reported in a recent study (Barago et al., 2021) which was however focused only on the tailings stored in the main impoundments. The reason could be that tailings older than those previously investigated were sampled. The older tailings are located close to the mineralurgical plant and they could have been produced in earlier times when extraction methods were less efficient. However, mining wastes, in general and especially the less recent ones, still contain elements of potential economic interest such as Zn (up to 11.5 % wt.) or Ge (up to 118 mg/kg). Reprocessing this material should be carefully evaluated not only in order to recover the elements of economic value but also to reduce potential contamination of water resources. About Riofreddo smelter slags, although only a couple of samples (n = 2) were analysed and were found very rich in PTEs (about 20 - 32 % wt. Fe, 2.4 – 4.6 % wt. Pb, 0.8 – 7.9 % wt. Zn, and up to 2,129 mg/kg As, 550 mg/kg Sb and 9.41 mg/kg Tl). Antimony (Sb) is less present in mining wastes than other PTEs (max concentrations up to 75 mg/kg Sb) but its concentration shows the highest value in smelter slags, up to 550 mg/kg, presumably due to the fact that Sb is hosted in galena, and the historical smelter plant produced Pb. However, the plant had small dimensions and reasonably was operative until the end of the 19th century. (Figure 2).

Soils

In general, concentrations of metal(loid)s in soils are orders of magnitude lower than all the other solid matrices with concentrations < 1 mg/kg upstream Cave del Predil village. Specifically, concentrations of Tl, which is the target element in determining the extension of the contamination, range between 0.11 - 9.01 mg/kg Tl with an average of 2.58 mg/kg. Zinc, Pb, Cd, As, Sb, Ge are strongly correlated with Tl (Figure 3) and have a similar spatial distribution (maps not presented). The high variability of the spatial distribution of concentrations mainly depends on: 1) disseminated waste rock piles and waste rocks often mixed with soils 2) the use of waste rock for construction purposes (e.g., roads, service areas) around Cave del Predil and 3) aeolian transport of fine-grain tailings dusts from the top of the impoundments during past spilling operations of the slurry and before they were capped (e.g., Stovern et al., 2015). The locations of the sampling points are not reported for privacy reasons. Results from this study are comparable with those reported by Xiao et al. (2004) in the Guizhou province (China) which found Tl in the 1.5 to 6.9 mg/kg range in undisturbed natural soils but 40 to 124 mg/kg of Tl were observed in soils originating from a Tl-rich sulfide mining area, where Tl bioaccumulation in crops and wild plants occurred posing a threat to the human health.

Zinc concentrate

The only sample of the Zn (sphalerite) concentrate, one of the two market products of the mine was kindly provided by the Escuela de Minas of the University of Oviedo, Spain. As well as an evident Zn abundance (41.2 % wt. Zn) in the Zn concentrate, high impurity of Pb is observed (2.7 % wt.) along with PTEs such as Cd (795 mg/kg), Tl (326 mg/kg) and Ge (186 mg/kg). Except for Zn, compared to the other matrices, Cd is the only element that was found heavily enriched in the Zn concentrate. On average Cd was found more than one order of magnitude lower in tailings, which consist of the waste product of the concentrate production process, than in the concentrate. Indeed, also in a previous investigation focused on the same area (Barago et al., 2021), an average low value of Cd (16 ± 9 mg/kg) was found in tailings impoundments. The relative Cd depletion in tailings, also observed in the chemical compositions of surface and groundwaters in the area (Barago et al., 2023), could be explained by the following factors: 1) natural concentrations of Cd lower than those of Tl; 2) Cd, which is hosted in the main mineral phase sphalerite, has been previously removed by froth flotation and 3) due its mobility in the aqueous phase, Cd might have already been leached from mining residues. In contrast, the Tl concentrations in concentrate and mine wastes are similar or slightly higher in mining wastes. The results indicate that Tl may not have been fully recovered in the final product, thus suggesting that half content or more may have been discarded during the ore processing steps and also considering that the element is also present in pyrite. In relation to what reported above, Tl may be considered an environmental issue of major concern with respect to Cd for surface and groundwaters.

Stream sediments

The highest concentrations of Tl as well as As, Cd, Pb, Sb, Zn in stream sediments are observed in the proximity of the mining site and they slightly decrease downstream. Minimum concentrations were found upstream the mining village and in some lateral tributaries (0.17 – 0.42 mg/kg Tl; Figure 2) of the Rio del Lago stream. Maximum concentrations of Tl, up to 51.5 mg/kg, were found immediately downstream the tailings impoundments and they decrease of one order of magnitude at the border with Austria (4.63 mg/kg Tl) mainly due to dilution of the metal-enriched material with terrigenous supplies from minor tributaries. Such high concentrations are the legacy of hundreds of years of mining waste dumping in the Rio del Lago stream. A similar situation was already highlighted almost 30 years ago by Müller et al. (1994). The authors reported, for the first time, the extent of stream sediment contamination in the Carinthia (Austria) region due to the Pb-Zn at Raibl and Bleiberg mining industries and to ore smelting. It was also stated that similar high Pb contents have not been found in any other European river. In addition, the geochemical signatures of Zn, Pb and Cd from Raibl and Bleiberg could be observed from their sources, in Austria and Italy, respectively, downstream along the whole course of the Gail-Drava River to the border between Austria and Slovenia. However, the lack of a comprehensive no-border study of stream sediments in the Drava River basin focused on the impact of Raibl, Bleiberg and Mežica Pb-Zn mines does not allow to assess the real magnitude of this historical PTE contamination.

Geoaccumulation index (I_{geo}) of stream sediments

The geoaccumulation index or I_{geo} (Müller, 1969) for the stream sediments of the Rio del Lago – Slizza valley (Table 2) was calculated according to the following equation:

$$I_{geo} = log_2\left(\frac{C_n}{1.5B_n}\right).$$

C_n: measured concentration; B_n: geochemical background concentration.

For the background value the C1 sample was collected in the upstream area, in the vicinity of the Predil Lake (Figure 2) and was considered as an uncontaminated sediment. C1 sample is constituted by almost only carbonate rocks, without the influence of the ore deposit and the mining activity. $I_{geo} > 5$ indicating extremely contaminated sediments were found for all the investigated elements (As, Cd, Pb, Sb, Tl and Zn), especially for the main metals Zn and Pb. Extremely contaminated sediments by Tl (and other PTEs) were found downstream the tailings impoundments (C3, C4, RA54), whereas upstream, at the mining village, slightly lower concentrations were found (C2). From the tailings impoundments area to the downstream Slizza stream at the border with Austria (C10) the contamination of PTEs decreases, although sediments remain heavily / extremely contaminated by PTEs. Regarding sediments from the main tributaries, only RA35 shows contamination from PTEs since its sediments derive from open pit mines at Cave del Predil village. The other tributaries do not show contamination from PTEs except for Sb, which background levels could be higher. Also, no increase in contamination (and PTE concentrations) was observed downstream of the confluence with the Rio Freddo stream, where the historic smelter plant was located, therefore the extent of the contamination in stream sediments related to this source may be considered limited.

3.2 Mobility of PTEs

The determination of the total concentrations of trace elements in soil or sediments is often not enough to make any estimate of their potential bioavailability (National Research Council, 2003). For this purpose, the labile or extractable fraction using the cold HCl leaching approach is considered more suitable than total concentration since it represents the "non-residual" fraction related to mobile PTE-bearing phases (Adami et al., 1999; Chester and Voutsinou, 1981; Duzgoren-Aydin et al., 2011; Wang et al., 2017). In general, despite a great variability among different samples, the order of the median mobility observed with a moderate acid extraction with the HCl is: Mn ≈ Cd > Co > Zn > Ni > Tl > Sb > Cu > Pb > Cr > V ≈ As ≈ Fe (Figure 4, Table 3). The median labile fraction of Fe and Cr accounts for < 1 %, except for concentrate and foundry slag, thus indicating that the partial extraction did not affect silicate residual minerals. Conversely, where Fe is not associated with silicates (e.g., smelter slag), the fraction extracted was found to be more relevant (Table 3).

Table 2 - Geoaccumulation index (I_{geo}) (Müller, 1969) for stream sediments of the Rio del Lago - Slizza stream sediments. $I_{geo} > 5$ are highlighted in bold.

Type	Name	As	Cd	Pb	Sb	Tl	Zn
	Concentration (mg/kg)						
	C1 - background	1.58	0.32	6.73	0.05	0.17	15.3
	I_{geo}						
Main stream	C2	4.00	4.02	**6.50**	**5.08**	4.36	**6.96**
Main stream	C3	**5.99**	**5.00**	**7.73**	**5.20**	**7.65**	**8.08**
Main stream	C4	**5.91**	**5.49**	**7.23**	**5.24**	**6.43**	**8.62**
Main stream	RA54	**5.78**	**5.26**	**7.23**	4.97	**6.32**	**8.54**
Main stream	C5	4.79	4.40	**6.65**	4.36	**5.98**	**7.46**
Main stream	C6	2.65	-0.13	2.74	3.65	3.08	3.20
Main stream	C7	4.31	3.53	**5.63**	3.71	**5.01**	**6.75**
Main stream	C8A	3.96	3.34	**5.03**	3.49	4.60	**6.55**
Main stream	C8B	4.76	3.88	**6.04**	4.09	**5.45**	**7.03**
Main stream	C9	3.22	3.37	3.81	3.12	3.24	**6.23**
Main stream	C10	3.69	3.03	4.52	3.33	4.18	**6.20**
Tributaies	RA35	3.46	2.86	**6.44**	4.47	**5.49**	**5.80**
Tributaies	RA30	0.80	-0.95	-0.37	2.58	0.71	-0.43
Tributaies	RA48	-0.21	-1.51	-0.83	1.65	0.41	-0.74
Tributaies	RA53	0.14	-1.07	1.26	1.94	-0.36	-1.17

Value	Class	Pollution quality
$I_{geo} < 0$	1	Uncontaminated
$0 \leq I_{geo} \leq 1$	2	Uncontaminated to moderately contaminated
$1 \leq I_{geo} \leq 2$	3	Moderately contaminated
$2 \leq I_{geo} \leq 3$	4	Moderately contaminated to heavily contaminated
$3 \leq I_{geo} \leq 4$	5	Heavily contaminated
$4 \leq I_{geo} \leq 5$	6	Heavily to extremely contaminated
$I_{geo} \geq 5$	7	Extremely contaminated

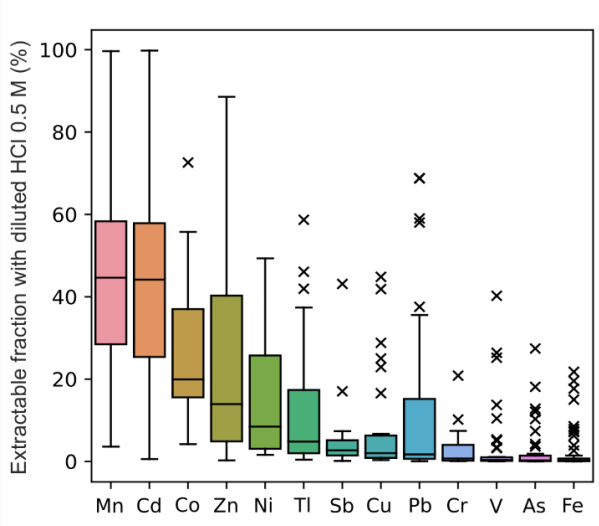

Figure 4 - boxplot of extracted fractions with HCl 0.5 M

.

Table 3 - Average (min-max) of the leached fraction with diluted HCl 0.5 M of each element expressed as percentage (%) of the total concentration in different types of solids matrices. Values > 20 % are highlighted in bold.

Type	Stream sediment	Soil	Ore gossan	Waste rock	Tailings	Smelter slag	Zn Concentrate	Median
	Pseudo-natural matrices			Mining waste			Product	
N samples	11	27	3	11	6	2	1	
As	0.07 (0.03 - 0.10)	2.75 (0.09 - 12.8)	0.03 (< 0.01 - 0.05)	4.20 (< 0.01 - 27.4)	0.01 (< 0.01 - 0.02)	1.01 (0.18 - 1.84)	18.1	0.25
Cd	1.53 (0.55 – 2.58)	**51.4** (20.5 - 99.8)	**53.2** (41.4 - 64.0)	**56.1** (21.0 - 83.8)	**57.6** (43.3 - 75.2)	19.3 (13.6 - 25.0)	13.4	**44.1**
Co	16.3 (11.3 - 19.6)	**21.0** (4.20 - 52.5)	**21.3** (20.1 - 22.7)	**33.9** (11.2 - 55.8)	**40.7** (27.0 - 52.3)	**46.2** (19.8 - 72.6)	**37.7**	19.9
Cr	0.24 (0.24 - 0.24)	1.85 (0.15 - 5.01)	0.10 (0.07 - 0.14)	3.69 (0.16 - 7.40)	0.88 (0.12 - 1.30)	10.2	**20.8**	0.72
Cu	2.67 (0.69 - 6.06)	6.76 (0.34 - 41.9)	1.85 (0.85 - 3.84)	11.2 (0.78 - 44.8)	6.15 (1.04 - 16.6)	14.4 (0.03 - 28.8)	6.67	2.02
Fe	0.43 (0.03 - 3.89)	2.00 (0.05 - 21.8)	0.01 (< 0.01 - 0.02)	2.89 (0.01 - 19.5)	0.12 (< 0.01 - 0.68)	16.3 (15.0 - 17.7)	6.25	0.20
Ge	n.d.	1.62 (1.18 - 2.41)	n.d.	2.05 (0.29 - 7.33)	0.80 (0.35 - 1.63)	9.73 (4.88 - 14.6)	17.1	n.d.
Mn	12.1 (3.58 - 53.7)	**57.0** (20.8 - 99.6)	**30.9** (22.0 - 40.4)	**50.9** (22.4 - 82.4)	**43.9** (27.2 - 66.0)	**34.9** (34.6 - 35.2)	**51.2**	**44.6**
Ni	5.06 (2.49 - 11.5)	8.49 (1.62 - 49.3)	17.6 (10.3 - 26.8)	**23.6** (4.82 - 41.9)	**27.2** (14.6 - 37.5)	**26.6** (25.7 - 27.5)	**26.6**	8.46
Pb	0.06 (0.05 - 0.07)	9.75 (0.18 - 68.8)	5.68 (0.32 - 15.7)	19.5 (0.91 - 59.0)	14.7 (3.05 - 28.4)	**32.0** (28.5 - 35.5)	1.11	1.71
Sb	6.23 (1.26 - 17.0)	2.22 (0.75 - 4.69)	2.24 (1.48 - 3.01)	1.49 (0.55 - 2.33)	0.11	3.88	**43.1**	2.67
Tl	4.08 (1.12 - 8.37)	3.46 (0.43 - 18.0)	**40.3** (29.8 - 58.7)	13.4 (2.04 - 41.9)	**23.2** (2.34 - 46.1)	17.6 (17.3 - 18.0)	17.5	4.80
V	1.14 (0.03 - 3.21)	2.06 (0.06 - 26.4)	0.21 (0.03 - 0.50)	3.53 (0.04 - 25.2)	0.05 (0.02 - 0.10)	13.7 (13.7 - 13.7)	**40.2**	0.35
Zn	0.41 (0.26 - 0.69)	16.8 (0.63 - 88.6)	**28.4** (5.51 - 66.5)	**41.2** (22.3 - 75.6)	**56.8** (45.1 - 77.4)	15.5 (11.2 - 19.8)	16.2	13.9

n.d.: not determined

Median labile fractions less than 1 % were observed for Cr, V, As and Fe according with hydrogeochemical data of the area (Barago et al., 2023); moderate median mobility (1 to 10 % of labile fraction) was observed for Pb, Cu, Sb, Tl and Ni. These results are quite in agreement with hydrogeochemical data for Pb, Tl, Sb and Ni which were found dissolved in the Raibl waters (Barago et al., 2023; Petrini et al., 2016). Higher median mobility (> 10 %) was found for Co and Zn, whereas > 40% values were observed for the most mobile elements: Mn and Cd.

Higher labile fractions of Tl, Zn and Pb were found in mining wastes and ore gossan sediments than in stream sediments or soils. In contrast, elements such as Mn, Cd and Co were found mobile even in soils. With regards to the Tl labile fraction, an increase of up to an order of magnitude was observed in mining wastes and ore gossan sediments rather than soils. In fact, Tl extractable fractions up to 58.7% were found in samples of the ore gossan sediments, up to 41.9% in waste rock and up to 46.1% in tailings. Such values are very high since mining wastes usually show Tl total concentrations in the 100 – 900 mg/kg range.

In the terrestrial environment, the mobility can then induce bioaccumulation processes of Tl in plants, as already found by Fellet et al. (2012) at Raibl. In contrast, lower Tl labile fractions were found in stream sediments and soils. In the stream sediments, the extractable Tl and Cd were less than 5% with a maximum of 8.37% for Tl and 28.8% for Cd. Such values are higher than Zn and Pb (< 1 %), thus indicating that small amounts of Tl and Cd, rather than Pb and Zn may be available for the aquatic compartment, i.e., surface and groundwaters, and finally for bioaccumulation, but further studies focused on the Tl presence in the aquatic trophic chain are needed.

Considering the tailings impoundments as the source of contamination, because the discharge operations of the "clarified" slurry in the Rio del Lago stream occurred near the impoundments, the relationship between the mobile fraction of As, Cd, Pb, Sb, Tl, Zn of stream sediments and the distance from the source, is presented in Figure 5. While As, Pb and Zn are weakly mobile (< 1 %), Cd and Sb showed mobile variable fractions with distance. Interestingly, Tl mobility decrease downstream, starting with an extractable fraction of 8.37 in C3 (near the tailings impoundments), to the lowest values of 2.83% in C10, at the border with Austria. Thus, indicating that both Tl concentration and mobility, and therefore the potential bioavailability decrease by 3 fold with distance. In contrast the highest bioavailability is expected near the mining village.

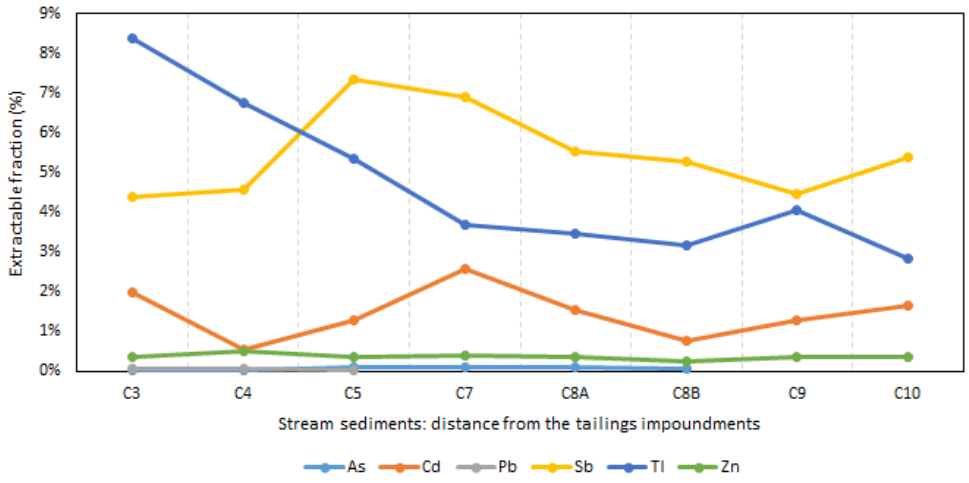

Figure 5 – Relationship between the extractable fraction (%) of stream sediments and distance from the tailings impoundments.

4 DISCUSSION

Total content and mobile fraction

The relation between total content and labile fraction of Pb, Tl, Zn and Cd is complex (Figure 6). In general, the labile fraction of Pb, Tl and Zn roughly increased with total concentration in soils, ore gossan sediments, waste rocks and tailings. These results are in agreement with those found by Svete et al. (2001) and Pavoni et al. (2017) for the Mežica and Salafossa mines, respectively, which belong to the same Eastern Alps Pb-Zn district. However, the results are based on laboratory finely ground samples. However, it is not known how much the natural grain size variability affects the results of the moderate extraction. It is believed that in nature finer samples (i.e. flotation tailings) can release more since they offer more relative surfaces to the extracting solutions or water.

However, such relation found in (Figure 6) do not apply to all matrix types. In fact, this do not apply for smelter slags, and Zn concentrates, which are a more refractory material. Also, Zn and Cd were found not mobile in stream sediments even if present in relatively high concentrations. This may be a consequence of their high solubility in water, since weathering processes probably have already leached stream sediments from Zn and Cd. In contrast, in the other matrices, Cd appears mobile at any concentration indicating great mobility, and perhaps minor residence times in the weathered soils and mine wastes.

Tailings as source of contamination

Barago et al. (2023) reported that tailings are the main source of contamination in the area. In light of the findings of this study, it can be stated that in reality most of the mineralised mining wastes can be a source of Cd, Pb, Tl and Zn in water. In the case of tailings, the release of such PTEs into the aquatic environment may be sought in their total content in addition to particle size and hydrogeological factors. In fact, fine grain materials, such as flotation tailings, offer more surface area for water-sediment interactions, whereas hydrological conditions are related to material saturation level, leaching and transport capacity of waters. In the case of Raibl, tailings impoundments are simultaneously among the most abundant, fine grain and saturated volumes of metal(loid)s (including As and Sb) enriched mining wastes. In contrast, although stream sediments may be characterised by relatively high metal(loid)s concentrations, many of them are scarcely mobile (mobile fraction < 5 or < 1 %; Table 3), thus indicating that stream sediments may not be a significant source of contamination for the fluvial system and PTEs may not be available.

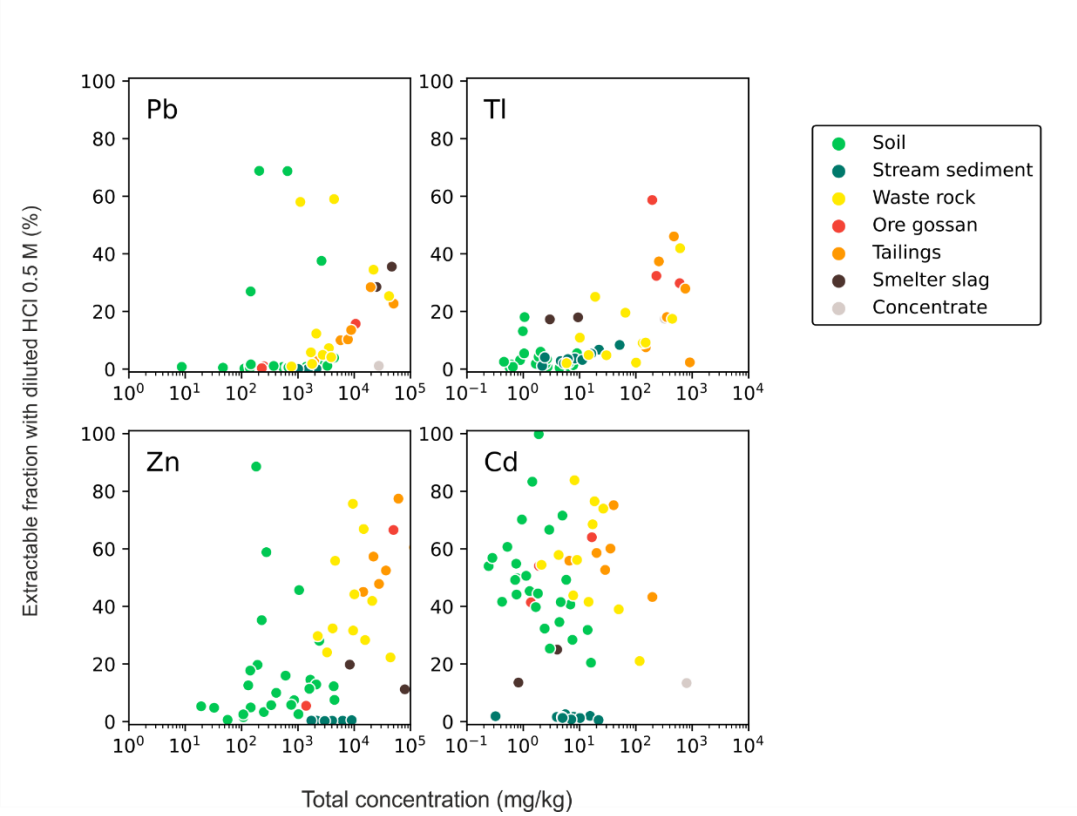

Figure 6 - Relationship between labile fraction obtained with diluted HCl extraction and total content in different types of solid samples.

Geochemical insights

These results confirm the mobility of Cd, Tl, Zn in both moderately acidic and neutral/weakly alkaline environments. On the contrary, the lack of dissolved Cd in the surface waters of Rio del Lago – Slizza stream (Barago et al., 2023, Paper I) could be due to the relative scarcity of this element in mining residues (Table 1) along with its marked mobility, since Cd may have shorter residence times in the environment. Although Sb in absolute terms is less abundant than As, it was noted a greater mobility of Sb compared to As, according to previous studies (Majzlan et al., 2018). Probably As likely remains strongly absorbed onto HFOs (Álvarez-Quintana et al., 2020; Cidu et al., 2011; Oyarzun et al., 2004).

We hypothesize that Zn, Pb, Cd and Tl released during the partial extractions derive from the 1) desorption from Fe secondary minerals (reasonably HFOs) and 2) dissolution of Zn secondary minerals (reasonably Zn carbonates) and

in minor content Pb secondary minerals and Fe sulfides (confirmed in Paper III) as well as sphalerite (ZnS) and galena (PbS) primary sulfide minerals. Sorption to HFOs (Coup and Swedlund, 2015; Wilkin et al., 2007) and precipitation of secondary Zn and in less amount Pb carbonates were hypothesised in the previous work (Barago et al., 2023) and indicated as natural attenuation processes for the release of such metals in the aquatic environment. Thus, the release of these metals during the partial extraction may indicate that the partial extraction inhibited the natural attenuation processes, confirming that they are very important in regulating the dissolved concentrations in waters.

Unexpectedly, Pb was found only slightly less mobile than Tl, which is in contrast with the results obtained from the surface and groundwaters (Barago et al., 2023) where Tl in the dissolved phase was found to be as abundant as Pb, despite Pb concentrations in the solid phase are orders of magnitude higher than Tl. It cannot be excluded that this result may be determined by the more acidic conditions reached during the HCl extraction than the natural ones. This evidence suggests that HCl moderate extraction would overestimate the mobility of Pb compared to leaching process in the natural environment.

Finally, a notable increase in the dissolved Tl/Zn ratio was found in the groundwaters of the tailings impoundments (Barago et al., 2023, Paper I). This Tl anomaly was explained by a greater mobility of Tl compared to Zn and Pb (and other less mobile elements) due to scarce natural attenuation processes of Tl, e.g., (co-)precipitation or sorption on HFOs. However, the moderate extraction applied in this study does not confirm the greater leachability of Tl in tailings compared to Zn and Pb. The discrepancy between the analytical results from water samples collected in field and those obtained from the extraction with HCl 0.5 M are reasonably related to more acid conditions or shorter time of leaching in the laboratory procedure. In fact, laboratory conditions may have dissolved the secondary Zn carbonate minerals (smithsonite or hydrozincite), and/or caused the HFOs to desorb PTEs (Miler and Gosar, 2012; Zuddas and Podda, 2005).

Therefore, the results suggest that the partial extraction with HCl 0.5 M maximised the release of PTEs also inhibiting the natural attenuation mechanisms of some elements such as Zn and Pb. This indirectly supports the hypothesis that, in a carbonate buffering environment, Zn and Pb rather than Tl are subject to natural attenuation processes. Thus, *in-situ* weakly alkaline water conditions and sufficient residence time would allow Tl rather than Zn and Pb to remain in solution.

5 CONCLUSIONS

- The geoaccumulation index (I_{geo}) indicate that the Rio del Lago sediments are heavily to extremely contaminated by As, Cd, Pb, Sb, Tl and Zn. In detail, Tl concentration and mobility decrease with distance from the source.
- A wide range of trace element concentrations was found in the Pb-Zn mining area of Raibl: up to > 100 mg/kg for Tl, Sb, Cd and Ge; > 1,000 mg/kg for As; > 1 % wt. for Pb and > 10 % wt. for Zn. Such high concentrations coupled with volumes of the waste material involved suggest that a potential reprocessing of this material should be evaluated not only to reduce contamination of water resources bu t also to recover elements of economic interest, including critical elements such as Ge.
- The partial extraction with diluted HCl 0.5 M seems a valid approach for a preliminary assessment of the mobility of the elements, although the results are not always comparable with *in-situ* findings. Indeed, the moderate-acid partial extraction overestimated Pb mobility.
- Thallium (Tl) was found less mobile than Zn and Cd from flotation tailings, whereas weak Tl and Cd mobility in stream sediments would indicate their potential bioavailability in the aquatic environment. Among other PTEs, As and Sb were found weakly mobile, however Sb mobility was found higher than As.
- It has been observed that for soils, ore gossan sediments, waste rocks and tailings finely ground samples, the release of Tl, Zn and Pb is roughly related to the total element concentration. However, is expected that in nature finer mine waste release more than the coarse ones. Therefore, a significant release of such PTEs may be expected where there are large volumes of heavily enriched mining residues, fine grain size and under saturated conditions, as in the case of the tailings impoundments.
- Despite relatively high PTE concentrations in stream sediments, most of the PTEs were characterised by very scarce mobility (< 1%) whereas small fractions of Tl and Cd may be potentially bioavailable.

Further research should be addressed to 1) the real extent of the contamination of the Slizza-Gail-Drava river basin: 2) the mobility of PTEs at neutral-weakly alkaline pH, similar to real water conditions: 3) the residual mineral phases after the extraction steps; 4) the PTEs chemistry of secondary minerals product of temporary natural attenuation processes; 5) the potential bioaccumulation of Tl and Cd in the aquatic trophic chain of the contaminated Rio del Lago – Slizza stream.

References

Adami, G., Barbieri, P., Reisenhofer, E., 1999. A Comparison on Five Sediment Decomposition Procedures for Determining Anthropogenic Trace Metal Pollution. Int. J. Environ. Anal. Chem. 75, 251–260. https://doi.org/10.1080/03067319908047314

Agemian, H., Chau, A.S.Y., 1977. A study of different analytical extraction methods for nondetrital heavy metals in aquatic sediments. Arch. Environ. Contam. Toxicol. 6, 69–82. https://doi.org/10.1007/BF02097751

Agemian, H., Chau, A.S.Y., 1976. Evaluation of extraction techniques for the determination of metals in aquatic sediments. Analyst 101, 761–767. https://doi.org/10.1039/AN9760100761

Álvarez-Quintana, J., Álvarez, R., Ordóñez, A., 2020. Arsenic in Soils Affected by Mining: Microscopic Studies vs. Sequential Chemical Extraction. Int. J. Environ. Res. Public. Health 17, 8426. https://doi.org/10.3390/ijerph17228426

Barago, N., Covelli, S., Mauri, M., Oberti di Valnera, S., Forte, E., 2021. Prediction of Trace Metal Distribution in a Tailings Impoundment Using an Integrated Geophysical and Geochemical Approach (Raibl Mine, Pb-Zn Alpine District, Northern Italy). Int. J. Environ. Res. Public. Health 18, 1157. https://doi.org/10.3390/ijerph18031157

Barago, N., Pavoni, E., Floreani, F., Crosera, M., Adami, G., Lenaz, D., Covelli, S., 2023. Hydrogeochemistry of thallium and other potentially toxic elements in neutral mine drainage at the decommissioned PbZn Raibl mine (Eastern Alps, Italy). J. Geochem. Explor. 107129. https://doi.org/10.1016/j.gexplo.2022.107129

Belzile, N., Chen, Y.-W., 2017. Thallium in the environment: A critical review focused on natural waters, soils, sediments and airborne particles. Appl. Geochem. 84, 218–243. https://doi.org/10.1016/j.apgeochem.2017.06.013

Brigo, L., Kostelka, L., Omenetto, P., Schneider, H.-J., Schroll, E., Schulz, O., Štrucl, I., 1977. Comparative Reflections on Four Alpine Pb-Zn Deposits, in: Klemm, D.D., Schneider, Hans-Jochen (Eds.), Time- and Strata-Bound Ore Deposits. Springer Berlin Heidelberg, Berlin, Heidelberg, pp. 273–293. https://doi.org/10.1007/978-3-642-66806-7_18

Calligaris, C., Nicola, G., Casagrande, G., Zini, L., Cucchi, F., 2017. Debris Flow Hazard Assessment (Cave del Predil—NE Italy), in: Mikoš, M., Casagli, N., Yin, Y., Sassa, K. (Eds.), Advancing Culture of Living with Landslides. Springer International Publishing, Cham, pp. 369–376.

Campanella, B., Colombaioni, L., Benedetti, E., Di Ciaula, A., Ghezzi, L., Onor, M., D'Orazio, M., Giannecchini, R., Petrini, R., Bramanti, E., 2019. Toxicity of Thallium at Low Doses: A Review. Int. J. Environ. Res. Public. Health 16. https://doi.org/10.3390/ijerph16234732

Chester, R., Voutsinou, F.G., 1981. The initial assessment of trace metal pollution in coastal sediments. Mar. Pollut. Bull. 12, 84–91. https://doi.org/10.1016/0025-326X(81)90198-3

Cidu, R., Dore, E., Biddau, R., Nordstrom, D.K., 2018. Fate of antimony and arsenic in contaminated waters at the abandoned Su Suergiu mine (Sardinia, Italy). Mine Water Environ. 37, 151–165. https://doi.org/10.1007/s10230-017-0479-8

Cidu, R., Frau, F., Da Pelo, S., 2011. Drainage at Abandoned Mine Sites: Natural Attenuation of Contaminants in Different Seasons. Mine Water Environ. 30, 113–126. https://doi.org/10.1007/s10230-011-0146-4

Coup, K.M., Swedlund, P.J., 2015. Demystifying the interfacial aquatic geochemistry of thallium(I): New and old data reveal just a regular cation. Chem. Geol. 398, 97–103. https://doi.org/10.1016/j.chemgeo.2015.02.003

Covelli, S., Piani, R., Acquavita, A., Predonzani, S., Faganeli, J., 2007. Transport and dispersion of particulate Hg associated with a river plume in coastal Northern Adriatic environments. Mar. Pollut. Bull., Measuring and Managing Changes in Estuaries and Lagoons 55, 436–450. https://doi.org/10.1016/j.marpolbul.2007.09.006

De Giudici, G., Medas, D., Cidu, R., Lattanzi, P., Rigonat, N., Frau, I., Podda, F., Marras, P.A., Dore, E., Frau, F., Rimondi, V., Runkel, R.L., Wanty, R.B., Kimball, B., 2019. Assessment of origin and fate of contaminants along mining-affected Rio Montevecchio (SW Sardinia, Italy): A hydrologic-tracer and environmental mineralogy study. Appl. Geochem. 109, 104420. https://doi.org/10.1016/j.apgeochem.2019.104420

Di Colbertaldo, D., 1948. Il giacimento piombo-zincifero di Raibl in Friuli (Italia). 18a Sessione del Congresso Internazionale di Geologia, Londra.

Doglioni, C., 1988. Note sull'evoluzione strutturale della zona di Raibl. Studi Stratigr. E Strutt. Nell'area Mineraria Raibl Soc. Ital. Min. SpA.

Duzgoren-Aydin, N.S., Avula, B., Willett, K.L., Khan, I.A., 2011. Determination of total and partially extractable solid-bound element concentrations using collision/reaction cell inductively coupled plasma-mass spectrometry and

their significance in environmental studies. Environ. Monit. Assess. 172, 51–66. https://doi.org/10.1007/s10661-010-1317-7

European Commission, 2020. Study on the EU's list of Critical Raw Materials.

Fellet, G., Pošćić, F., Casolo, V., Marchiol, L., 2012. Metallophytes and thallium hyperaccumulation at the former Raibl lead/zinc mining site (Julian Alps, Italy). Plant Biosyst. - Int. J. Deal. Asp. Plant Biol. 146, 1023–1036. https://doi.org/10.1080/11263504.2012.703250

Galili, T., O'Callaghan, A., Sidi, J., Sievert, C., 2018. heatmaply: an R package for creating interactive cluster heatmaps for online publishing. Bioinformatics 34, 1600–1602. https://doi.org/10.1093/bioinformatics/btx657

Gošar, D., Costa, M.R., Ferreira, A., Štrucl, S.F., 2015. Assessment of past and present water quality in closed Mežica Pb-Zn Mine (Slovenia).

Gosar, M., Šajn, R., Miler, M., Burger, A., Bavec, Š., 2020. Overview of existing information on important closed (or in closing phase) and abandoned mining waste sites and related mines in Slovenia. Geologija 63, 221–250. https://doi.org/10.5474/geologija.2020.018

Higueras, P., Oyarzun, R., Lillo, J., Sánchez-Hernández, J.C., Molina, J.A., Esbrí, J.M., Lorenzo, S., 2006. The Almadén district (Spain): Anatomy of one of the world's largest Hg-contaminated sites. Sci. Total Environ. 356, 112–124. https://doi.org/10.1016/j.scitotenv.2005.04.042

Hotton, V.K., Sutherland, R.A., 2016. The legacy of lead (Pb) in fluvial bed sediments of an urban drainage basin, Oahu, Hawaii. Environ. Sci. Pollut. Res. 23, 5495–5506. https://doi.org/10.1007/s11356-015-5777-8

Hudson-Edwards, K.A., 2003. Sources, mineralogy, chemistry and fate ofheavy metal-bearing particles in mining-affected river systems. Mineral. Mag. 67, 205–217. https://doi.org/10.1180/0026461036720095

Kasmaeeyazdi, S., Dinelli, E., Braga, R., 2022. Mapping Co–Cr–Cu and Fe Occurrence in a Legacy Mining Waste Using Geochemistry and Satellite Imagery Analyses. Appl. Sci. 12, 1928. https://doi.org/10.3390/app12041928

Kersten, M., 2002. Speciation of Trace Metals in Sediments, in: Chemical Speciation in the Environment. John Wiley & Sons, Ltd, pp. 301–321. https://doi.org/10.1002/9780470988312.ch11

Larner, B.L., Seen, A.J., Townsend, A.T., 2006. Comparative study of optimised BCR sequential extraction scheme and acid leaching of elements in the certified reference material NIST 2711. Anal. Chim. Acta 556, 444–449. https://doi.org/10.1016/j.aca.2005.09.058

Majzlan, J., Kiefer, S., Herrmann, J., Števko, M., Sejkora, J., Chovan, M., Lánczos, T., Lazarov, M., Gerdes, A., Langenhorst, F., Borčinová Radková, A., Jamieson, H., Milovský, R., 2018. Synergies in elemental mobility during weathering of tetrahedrite [(Cu,Fe,Zn)12(Sb,As)4S13]: Field observations, electron microscopy, isotopes of Cu, C, O, radiometric dating, and water geochemistry. Chem. Geol. 488, 1–20. https://doi.org/10.1016/j.chemgeo.2018.04.021

Malo, B.A., 1977. Partial extraction of metals from aquatic sediments. Environ. Sci. Technol. 11, 277–282. https://doi.org/10.1021/es60126a007

McCready, S., Birch, G.F., Taylor, S.E., 2003. Extraction of heavy metals in Sydney Harbour sediments using 1M HCl and 0.05M EDTA and implications for sediment-quality guidelines. Aust. J. Earth Sci. 50, 249–255. https://doi.org/10.1046/j.1440-0952.2003.00994.x

Melcher, F., Onuk, P., 2019. Potential of Critical High-technology Metals in Eastern Alpine Base Metal Sulfide Ores. BHM Berg- Hüttenmänn. Monatshefte 164, 71–76. https://doi.org/10.1007/s00501-018-0818-5

Meriggi, R., Del Fabbro, M., Blasone, E., Zilli, E., 2008. Dynamic slope stability analysis of mine tailing deposits: The case of Raibl mine. AIP Conf. Proc. 1020, 542–549. https://doi.org/10.1063/1.2963882

Miler, M., Gosar, M., 2012. Characteristics and potential environmental influences of mine waste in the area of the closed Mežica Pb–Zn mine (Slovenia). J. Geochem. Explor. 112, 152–160. https://doi.org/10.1016/j.gexplo.2011.08.012

Müller, G., 1969. Index of geoaccumulation in sediments of the Rhine River. J. Geol. 2, 108–119.

Müller, H.W., Schwaighofer, B., Kalman, W., 1994. Heavy metal contents in river sediments. Water. Air. Soil Pollut. 72, 191–203. https://doi.org/10.1007/BF01257124

National Research Council, 2003. Bioavailability of Contaminants in Soils and Sediments: Processes, Tools, and Applications. National Academies Press, Washington, D.C. https://doi.org/10.17226/10523

Oyarzun, R., Lillo, J., Higueras, P., Oyarzún, J., Maturana, H., 2004. Strong arsenic enrichment in sediments from the Elqui watershed, Northern Chile: industrial (gold mining at El Indio–Tambo district) vs. geologic processes. J. Geochem. Explor. 84, 53–64. https://doi.org/10.1016/j.gexplo.2004.03.002

Pavoni, E., Petranich, E., Adami, G., Baracchini, E., Crosera, M., Emili, A., Lenaz, D., Higueras, P., Covelli, S., 2017. Bioaccumulation of thallium and other trace metals in Biscutella laevigata nearby a decommissioned zinc-lead mine (Northeastern Italian Alps). J. Environ. Manage. 186, 214–224. https://doi.org/10.1016/j.jenvman.2016.07.022

Peter, A.L.J., Viraraghavan, T., 2005. Thallium: a review of public health and environmental concerns. Environ. Int. 9.

Petrini, R., Cidu, R., Slejko, F.F., 2016. Thallium Contamination in the Raibl Mine Site Stream Drainage System (Eastern Alps, Italy). Mine Water Environ. 35, 55–63. https://doi.org/10.1007/s10230-015-0346-4

Pimminger, M., Grasserbauer, M., Schroll, E., Cerny, I., 1985. Trace element distribution in sphalerites from Pb-Zn-ore occurrences of the Eastern Alps. TMPM Tschermaks Mineral. Petrogr. Mitteilungen 34, 131–141. https://doi.org/10.1007/BF01081557

Rauret, G., López-Sánchez, J.F., Sahuquillo, A., Rubio, R., Davidson, C., Ure, A., Quevauviller, P., 1999. Improvement of the BCR three step sequential extraction procedure prior to the certification of new sediment and soil reference materials. J. Environ. Monit. 1, 57–61. https://doi.org/10.1039/A807854H

Rosenberg, E., 2009. Germanium: environmental occurrence, importance and speciation. Rev. Environ. Sci. Biotechnol. 8, 29–57. https://doi.org/10.1007/s11157-008-9143-x

Schroll, E., Kürzl, H., Weinzierl, O., 1994. Geochemometrical Studies Applied to the Pb-Zn Deposit Bleiberg/Austria, in: Fontboté, L., Boni, M. (Eds.), Sediment-Hosted Zn-Pb Ores. Springer Berlin Heidelberg, Berlin, Heidelberg, pp. 228–245. https://doi.org/10.1007/978-3-662-03054-7_14

Snape, I., Scouller, R.C., Stark, S.C., Stark, J., Riddle, M.J., Gore, D.B., 2004. Characterisation of the dilute HCl extraction method for the identification of metal contamination in Antarctic marine sediments. Chemosphere 57, 491–504. https://doi.org/10.1016/j.chemosphere.2004.05.042

Stovern, M., Rine, K.P., Russell, M.R., Félix, O., King, M., Eduardo Sáez, A., Betterton, E.A., 2015. Development of a dust deposition forecasting model for mine tailings impoundments using in situ observations and particle transport simulations. Aeolian Res. 18, 155–167. https://doi.org/10.1016/j.aeolia.2015.07.003

Sutherland, R.A., 2002. Comparison between non-residual Al, Co, Cu, Fe, Mn, Ni, Pb and Zn released by a three-step sequential extraction procedure and a dilute hydrochloric acid leach for soil and road deposited sediment. Appl. Geochem. 17, 353–365. https://doi.org/10.1016/S0883-2927(01)00095-6

Svete, P., Milačič, R., Pihlar, B., 2001. Partitioning of Zn, Pb and Cd in river sediments from a lead and zinc mining area using the BCR three-step sequential extraction procedure. J. Environ. Monit. 3, 586–590. https://doi.org/10.1039/b106311c

Tatsi, K., Turner, A., Handy, R.D., Shaw, B.J., 2015. The acute toxicity of thallium to freshwater organisms: Implications for risk assessment. Sci. Total Environ. 536, 382–390. https://doi.org/10.1016/j.scitotenv.2015.06.069

US EPA, 1996. EPA Method 3052. Microwave assisted acid digestion of siliceous and organically based matrices.

Wang, J., Liu, J., Li, H., Chen, Y., Xiao, T., Song, G., Chen, D., Wang, C., 2017. Uranium and thorium leachability in contaminated stream sediments from a uranium minesite. J. Geochem. Explor. 176, 85–90. https://doi.org/10.1016/j.gexplo.2016.01.008

Wang, J., Zhou, Y., Dong, X., Yin, M., Tsang, D.C.W., Sun, J., Liu, J., Song, G., Liu, Y., 2020. Temporal sedimentary record of thallium pollution in an urban lake: An emerging thallium pollution source from copper metallurgy. Chemosphere 242, 125172. https://doi.org/10.1016/j.chemosphere.2019.125172

Wilkin, R.T., Brady, P.V., Kent, D.B., 2007. Lead. Monitored Natural Attenuation of Inorganic Contaminants in Groundwater, Volume 2 – Assessment for Non-Radionulcides Including Arsenic, Cadmium, Chromium, Copper, Lead, Nickel, Nitrate, Perchlorate, and Selenium. Edited by R.G. Ford, R.T. Wilkin, and R.W. Puls. U.S. Environmental Protection Agency, EPA/600/R-07/140. pgs. 11-20.

Xiao, T., Guha, J., Boyle, D., Liu, C.-Q., Chen, J., 2004. Environmental concerns related to high thallium levels in soils and thallium uptake by plants in southwest Guizhou, China. Sci. Total Environ. 318, 223–244. https://doi.org/10.1016/S0048-9697(03)00448-0

Zucchini, R., 1998. Miniere e mineralizzazioni nella provincia di Udine. Aspetti storici e mineralogici, Edizioni del Museo Friulano di Storia Naturale.

Zuddas, P., Podda, F., 2005. Variations in physico-chemical properties of water associated with bio-precipitation of hydrozincite [Zn5(CO3)2(OH)6] in the waters of Rio Naracauli, Sardinia (Italy). Appl. Geochem. 20, 507–517. https://doi.org/10.1016/j.apgeochem.2004.09.008

Manuscript

Composition of mine tailings: a microanalytical study (Pb-Zn Raibl mine, NE Italy)

Barago N.[1], Covelli S.[1], Turco G.[2], Garcia-Ordiales, E.[3] Lenaz D.[1]

[1] Department of Mathematics and Geoscience, University of Trieste, Trieste, Italy
[2] Clinical Department of Medical, Surgical and Health Sciences, University of Trieste, Trieste, Italy
[3] Mining, Energy, and Materials Engineering School, University of Oviedo, Oviedo, Spain.

PREFACE

The distribution and mobility of potentially toxic elements (PTEs) in the aqueous and solid phases at the Pb-Zn decommissioned Raibl mining site have been investigated and described previously. However, in order to understand the release, the attenuation processes and the partitioning of the contaminants it was necessary to study their speciation. The knowledge about speciation is also essential to evaluate possible future reprocessing of tailings, which would allow the recovery of elements of economic interest and the removal of the main source of contamination. In the previous hydrogeochemical study as well as in the chapter dedicated to the solid phases (Paper II) direct observations of speciation of PTEs were lacking, and only thermodynamic models and literature experiments have been taken into account. Therefore, the composition of the minerals constituting the tailings of the impoundments, which are the main source of contamination in the waters of the Rio del Lago – Slizza River system, was investigated. However, further mineralogical and trace element distribution analyses should be performed to determine the partitioning and speciation of other target elements such as thallium (Tl) and germanium (Ge).

1 MATERIALS AND METHODS

Sampling and granulometric properties

The minerals analyzed come from a single sample of flotation tailings outcropping from below cover materials (Figure 1), after intense rainy events and consequent erosion of the external protective dam, in September 2020 at the Raibl Zn-Pb mining site (RA17, lat. = 46.45486; long. = 13.57420). Tailings are red muds which were produced as waste by the mineralurgical plant, in particular from the froth flotation system, and were discharged in the tailings impoundments as wet slurry from 1976 to 1991. The tailings volumes are protected laterally by waste rock dams and capped at the top by layers made up of waste rock, mud, geotextile and gravel which prevent vertical water infiltration. For a 3D imaging of the tailings impoundments refer to (Barago et al., 2021).

For grain-size analysis on the bulk sample, approximately 15–20 g of the original sample was treated with H_2O_2 (3%) for a minimum of 24 h, to eliminate possible organic matter. Subsequently, the sediment was wet sieved through a 2 mm sieve, to remove coarse rock fragments. The resulting < 2 mm fraction was analyzed, using a laser granulometer (Malvern Mastersizer, 2000).

Preparation of the sample

In the laboratory, the tailings sample (RA17) was wet-sieved and three granulometric fractions were manually separated according to the Wentworth (1922) classification: fine sands: 250 – 125 μm, very fine sands: 125 – 62.5 μm and coarse silt: 62.5 – 31.2 μm. Finer fractions than coarse silt could not be separated due to optical and hand picking limits. The heavy mineral fraction was then collected via density separation using a solution of 1,1,2,2-tetrabromoethane ($C_2H_2Br_4$) with a density of 2.967 kg L^{-1}, used to remove light gangue minerals such as calcite, dolomite, and quartz. Thus, about 150 minerals for each of the three particle size fractions were randomly manually picked, incorporated into a resin in mounts and polished, for a total of 444 minerals investigated.

Figure 1 - portion of flotation tailings outcropping in September 2020.

Microanalyses

Polished surfaces of the heavy minerals were observed by means of a Quanta250 Scanning Electron Microscope (FEI, Oregon, USA), operating in secondary electron detection mode at the Department of Medical Sciences of the University of Trieste. Specimens were mounted on aluminum stubs and subsequently carbon coated (Sputter Coater K550X, Emitech, Quorum Technologies Ltd, UK). The elemental composition of the samples was determined using an EDS probe (Quanta250 FEI with EDAX probe, Hillsboro, OR, USA). The accelerating voltage varied between 10 and 30 kV; both spot size and full frame acquisition were made at a varying time from 5 to 20 s. The electron microprobe (EMPA) model CAMECA SX-100 was used on the same samples analysed via SEM-EDS for the detection of Fe, Pb, S, Zn. Excitation occurred by means of a beam between 15 - 35 kV and detected by means of a WDS spectrometer.

2 RESULTS AND DISCUSSION

Grain size and chemical composition

The bulk sample is a sandy silt (Shepard, 1954). On the basis of the granulometric results, the three fractions from A: 250-125, B: 125-62.5 and C: 62.5-31.2 μm were separated (fine sands, very fine sands and coarse silt, respectively) (Figure 2).

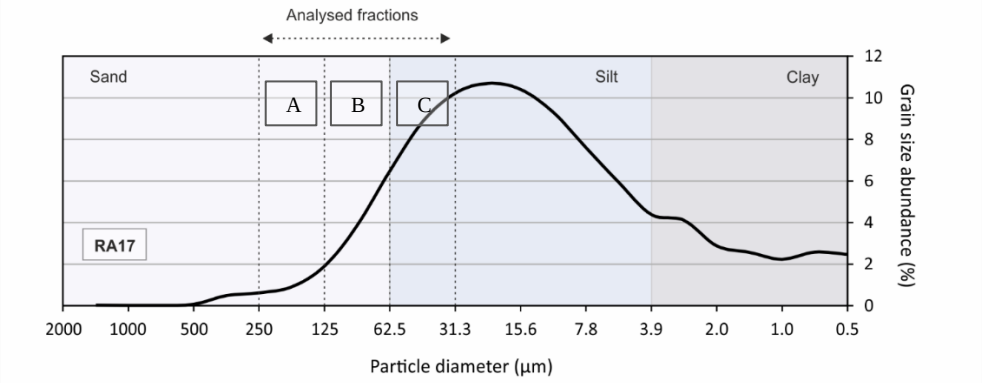

Figure 2 – Grain size distribution of the bulk tailings sample (RA17) (classification of Wentworth, 1922). A, B, C correspond to the analysed fractions.

The chemical composition of the main metal and metal(loid)s (Al, As, Ba, Cd, Co, Cr, Cu, Fe, Ge, Li, Mn, Mo, Ni, Pb, Sb, Sn, Ti, Tl, V, W, Zn, Zr) of sample RA17 determined by means of ICP-MS (described in the Paper II) is presented in Table 1. Except for Ca-Mg which are the main constituents of dolostones and limestones of the "lithogenic" component (i.e., the ore body host rock), the most abundant elements were Fe, Zn, Ba and Pb. The most abundant element was Fe (9.67 % wt.) which is responsible for the reddish coloration of tailings (Figure 1). The second most abundant

element is Zn (3.65 %wt.) followed by Ba (2.03 % wt.) and Pb (0.77 % wt.) which were the main metals extracted. Regarding other trace elements notable associated to the mineralization high concentrations of As (2345 mg/kg), Tl (355 mg/kg), Ge (102 mg/kg), Cd (20.1 mg/kg) and Sb (8.09 mg/kg) were observed.

On the one hand these elevated PTE concentrations in flotation tailings are consistent with previous results from the same area (Barago et al., 2021) and represent a concern for the environment being the main source of contamination of the Rio del Lago – Slizza River system (Barago et al., 2023) due to leaching and dispersion in the environment of PTEs; on the other hand, the high concentrations of Zn and Pb, together with notable concentrations of Ge could be an opportunity for further processing that may be evaluated for the extraction of elements of economic interest thus removing also the source of contamination for the river system. However, to evaluate the possibility of reprocessing, a thorough microanalytical study is necessary because separation techniques (e.g., froth flotation) are mineral-selective, to understand in which phases target elements such as Zn or Ge are hosted.

Table 1 - Chemical composition of the bulk tailings sample (RA17). Data and methods from the Paper II.

Element	**Ba**	**Fe**	**Pb**	**Zn**	**Al**	**As**	**Cd**	**Co**	**Cr**	**Cu**	**Ge**
Unit	%	%	%	%	mg/kg	mg/kg	mg/kg	mg/kg	mg/kg	mg/kg	mg/kg
Concentration	2.03	9.67	0.77	3.65	2797	2345	20.1	2.39	15.2	11.0	102

Element	**Li**	**Mn**	**Mo**	**Ni**	**Sb**	**Sn**	**Ti**	**Tl**	**V**	**W**	**Zr**
Unit	mg/kg	mg/kg	mg/kg	mg/kg	mg/kg	mg/kg	mg/kg	mg/kg	mg/kg	mg/kg	mg/kg
Concentration	3.88	477	33.5	13.8	8.09	0.53	201	355	65.0	0.23	8.45

Microanalyses

On the basis of 416 observations with SEM, EDS and EMPA microanalytical techniques (Table 2), 59 dolomite/calcite minerals (14.2 %) were detected, indicating that the density separation was not completely efficient. Excluding dolomite/calcite, the 70.0 % of the heavy minerals detected were Fe secondary minerals such as Fe oxy-hydroxides (HFOs) or less probable siderite ($FeCO_3$) (Figure 3) and this is in according with the bulk concentration (9.67 % wt. Fe). Unfortunately, since it was not possible to measure carbon due to the carbon coating of the mounts, it has not been possible to distinguish carbonates from oxy-hydroxides. Secondary Fe minerals are reasonably the alteration product of primary Fe sulfides by weathering in ambient condition. In contrast, Fe sulfides (reasonably represented by pyrite or marcasite (FeS_2)) were scarce, with only 2.2 % abundance (8 of 357 minerals) (Figure 4). The FeS_2/HFO ratio is 3.2 %, indicating that more than 95% of primary Fe sulfides could have been weathered. This is in agreement with previous studies (Barago et al., 2023, 2021; Nikonow et al., 2019) since the external layers of the tailings should be the most oxidised and with lower leaching potential. Iron (Fe) sulfides were the only sulfides observed in the investigated sample.

The second most abundant phases were secondary Zn minerals (18.8 % relative abundance, Figure 5) whereas secondary Pb minerals were only 2.0 % (Figure 6). This result is compatible with bulk chemistry (Zn = 3.65 and Pb = 0.77 % wt.). They are reasonably carbonate minerals such as hydrozincite ($Zn_5(CO_3)_2(OH)_6$), smithsonite ($ZnCO_3$) and cerussite ($PbCO_3$). Such minerals are usually found in sites affected by neutral mine drainages (NMD) (Miler and Gosar, 2012; Wilkin et al., 2007; Zuddas and Podda, 2005) and already identified at Raibl (Di Colbertaldo, 1948). NMD occurs in the presence of carbonate lithologies which buffer potential acid conditions of the waters. In AMD (acid mine drainage) context, where the decrease of pH of waters due to sulfides oxidation is not buffered by carbonates, Pb is not stable anymore as carbonate specie [$Pb(CO_3)_2$].

In fact, for pH < 6 it is expected that Pb is stable as sulphate ($PbSO_4$: anglesite) species or as dissolved ion (Pb^{2+}) (Wilkin et al., 2007). The abundance of Zn secondary minerals can indicate that Zn, which is the most abundant element in the aqueous phase in ambient conditions (Barago et al., 2023), could be so abundant to oversaturate the solution and precipitate forming Zn carbonate minerals. This process would be a natural attenuation mechanism for elevated concentrations of dissolved Zn. However, no Zn-Pb primary sulfide minerals such as sphalerite (ZnS) and galena (PbS), which are the main constituents of the ore body, were detected. The absence of ZnS and PbS indicates that most probably froth flotation effectively removed Zn-Pb sulfides and/or less probably that ZnS and PbS may have been weathered and transformed to different mineral phases.

Table 2 – Mineralogical distribution of the tailings sample via SEM-EDS and EMPA analysis

Mineralogy	N° of observations	Fraction (%)
Secondary Fe minerals (Fe oxy-hydroxides)	207	58.0%
Secondary Zn minerals (smithsonite/hydrozincite)	67	18.8%
Secondary Fe minerals Zn-rich	30	8.4%
Baryte	21	5.9%
Secondary Fe minerals Pb-rich	13	3.6%
Fe sulfides (pyrite/marcasite)	8	2.2%
Secondary Pb minerals (cerussite)	7	2.0%
Silicates	4	1.1%
Total Secondary Fe minerals	250	70.0%
Total	357	100%

The third most abundant mineral species is baryte ($BaSO_4$) (5.9 % relative abundance) which is a heavy gangue mineral that was not recovered during froth flotation thus it was discarded in tailings, as also confirmed by bulk chemistry (2.03 % wt. Ba). It is known for the Raibl and other Pb-Zn carbonate-hosted deposit that Tl appears to be preferentially hosted in colloform ZnS, and likely to a lesser extent in PbS and Fe sulfides (Brigo and Cerrato, 1994; Melcher and Onuk, 2019; Schroll et al., 1994). In this context, if the sulfides are scarce in the investigated tailings sample, an open question is in which phase Tl and Ge, and PTEs in general are hosted.

Interestingly, secondary Fe minerals very rich in Pb-Zn (Pb, Zn > 10 % wt.) were observed (Figure 7) with concentrations apparently up to 20% wt. of Pb and up to 40% wt. in the case of Zn. Although the occurrence of mixed nanophases cannot be excluded, such high concentrations indicate that HFO sorption, both on the surface and in the mineral lattice, is an effective process regulating Pb-Zn mobility (Coup and Swedlund, 2015). Although both Pb and Zn were found to be associated to HFOs and in Zn and Pb secondary minerals, Zn was found more abundant in its secondary phases (more often than Pb). In contrast, Pb was found to be more associated with Fe than with secondary Pb minerals. Thus, indicating that although Pb-Zn can precipitate and be absorbed, apparently Zn prefers to precipitate in secondary phases whereas Pb prefers to associate with Fe.

About PTEs, no primary As, Cd, Ge, Sb, Tl minerals were detected by EDS analyses indicating that their concentrations and the physico-chemical conditions may promote the formation of As-Cd-Ge-Sb-Tl minerals in ambient conditions, thus indicating that those elements are hosted in other minerals. It would be interesting to study finer grain-size fractions to investigate differences from a mineralogical and chemical point of view.

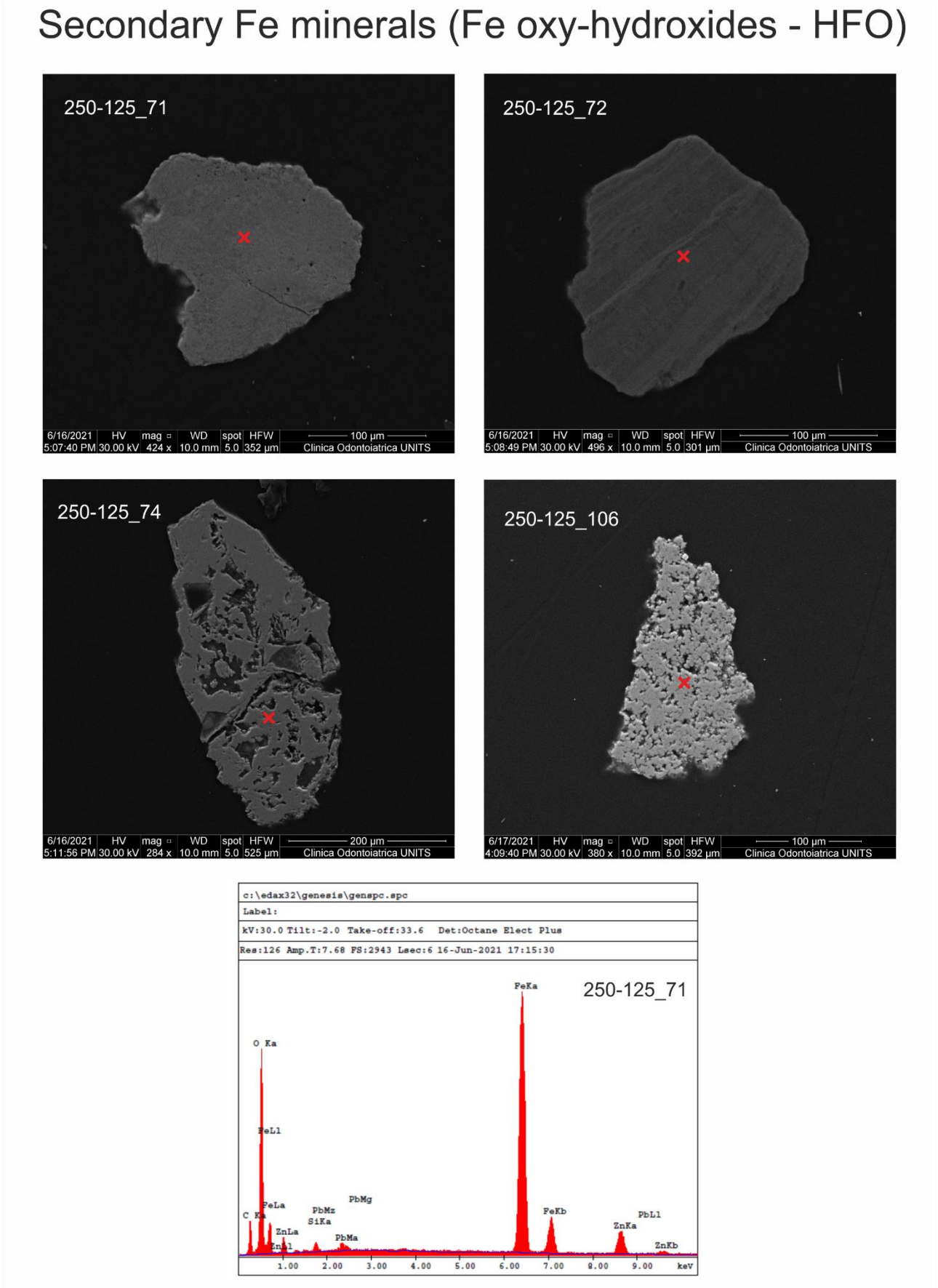

Figure 3 – SEM images with EDS analysis on secondary Fe minerals. Red crosses indicate EMPA analysis spots.

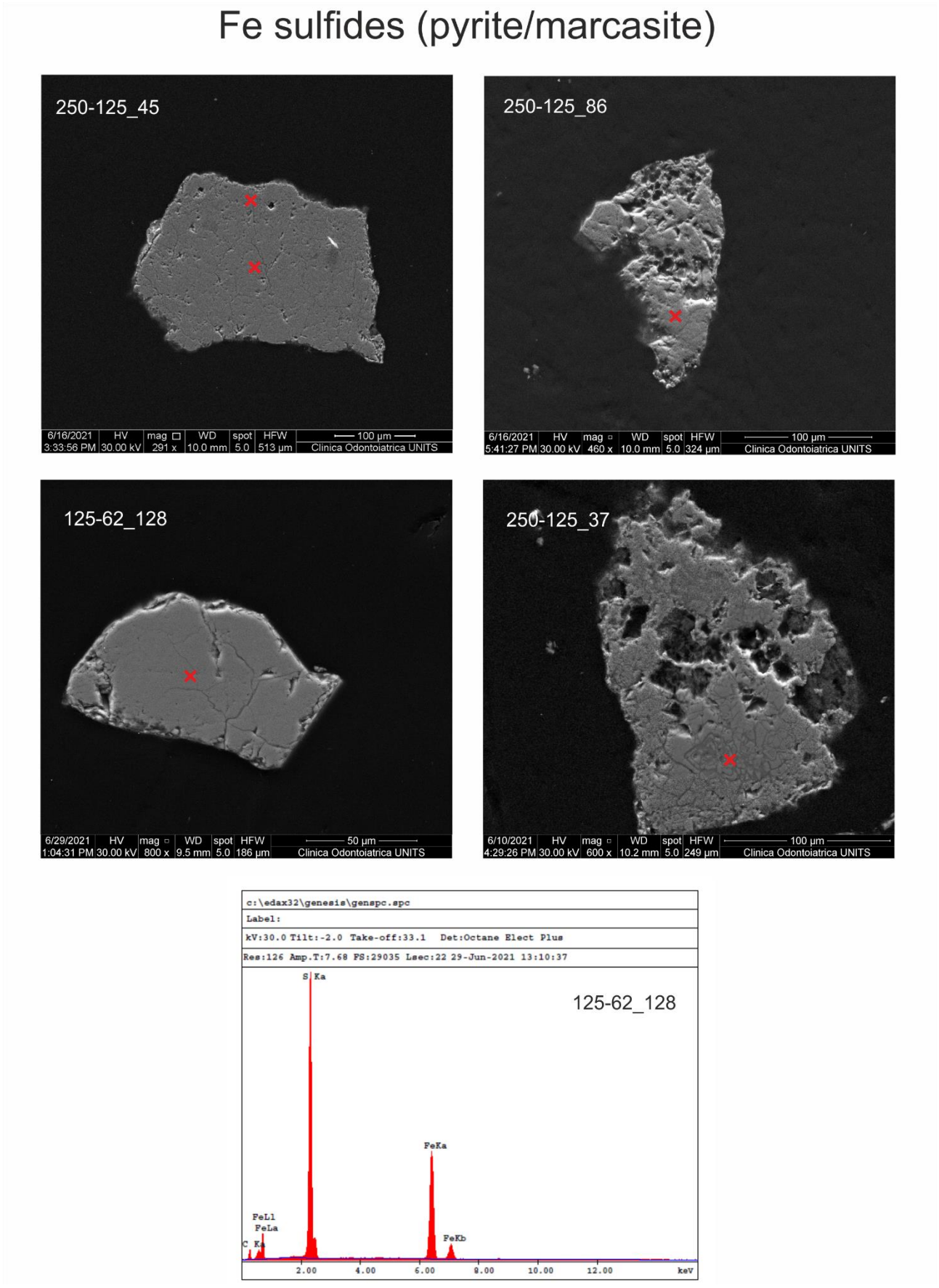

Figure 4 – SEM images with EDS analysis on Fe sulfide minerals. Red crosses indicate EMPA analysis spots.

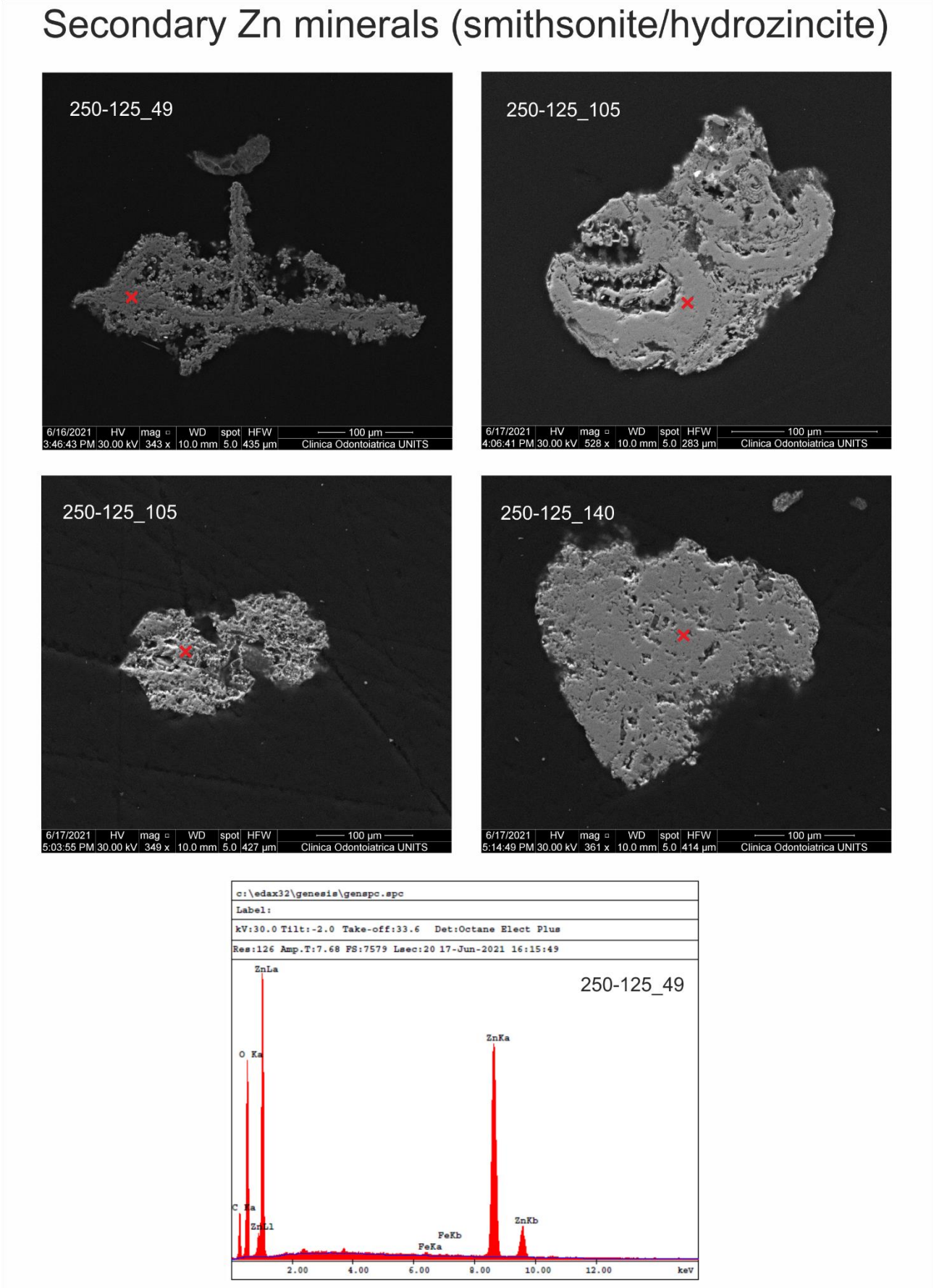

Figure 5 – SEM images with EDS analysis on secondary Zn minerals. Red crosses indicate EMPA analysis spots.

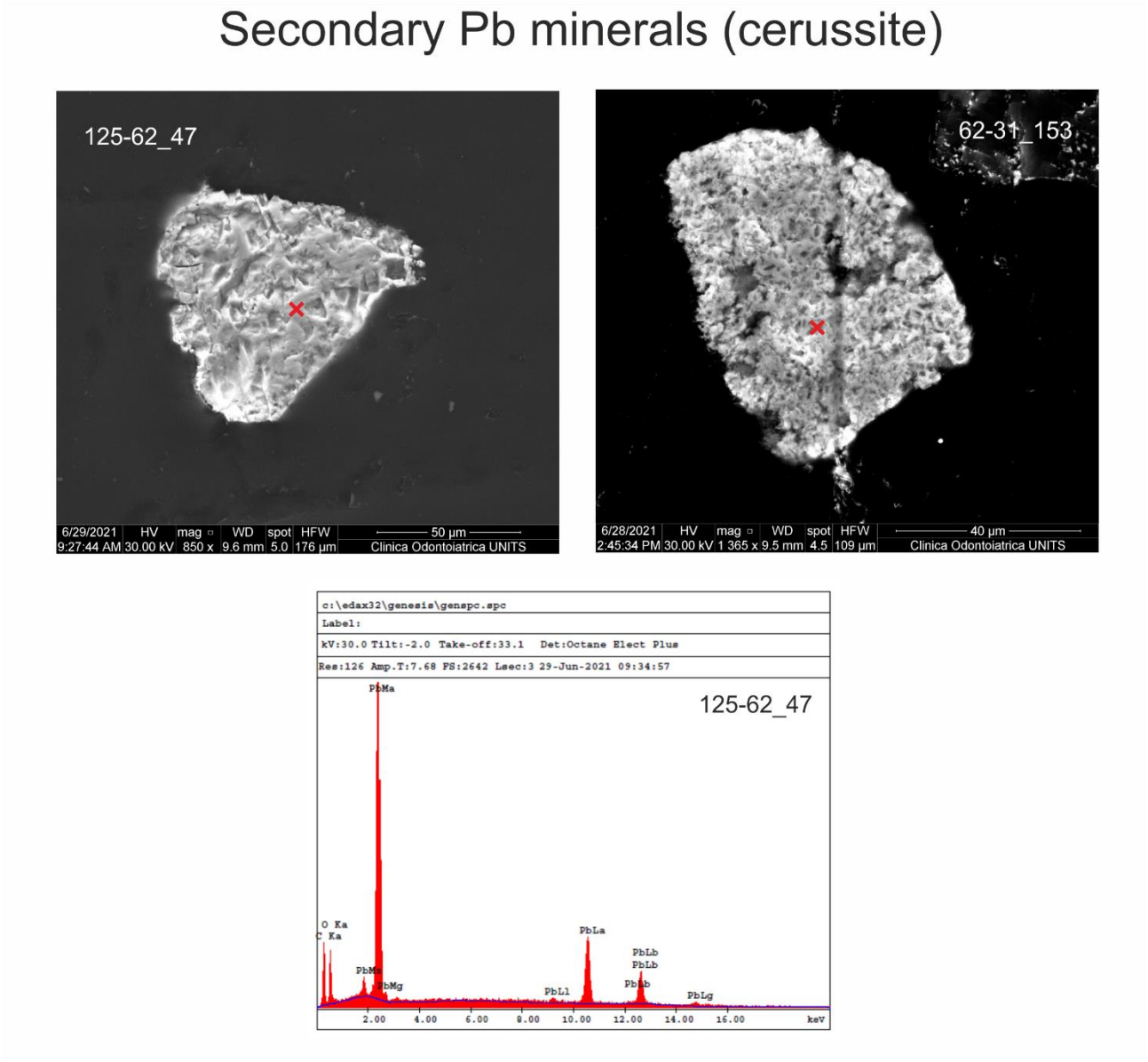

Figure 6 – SEM images with EDS analysis on secondary Pb minerals. Red crosses indicate EMPA analysis spots.

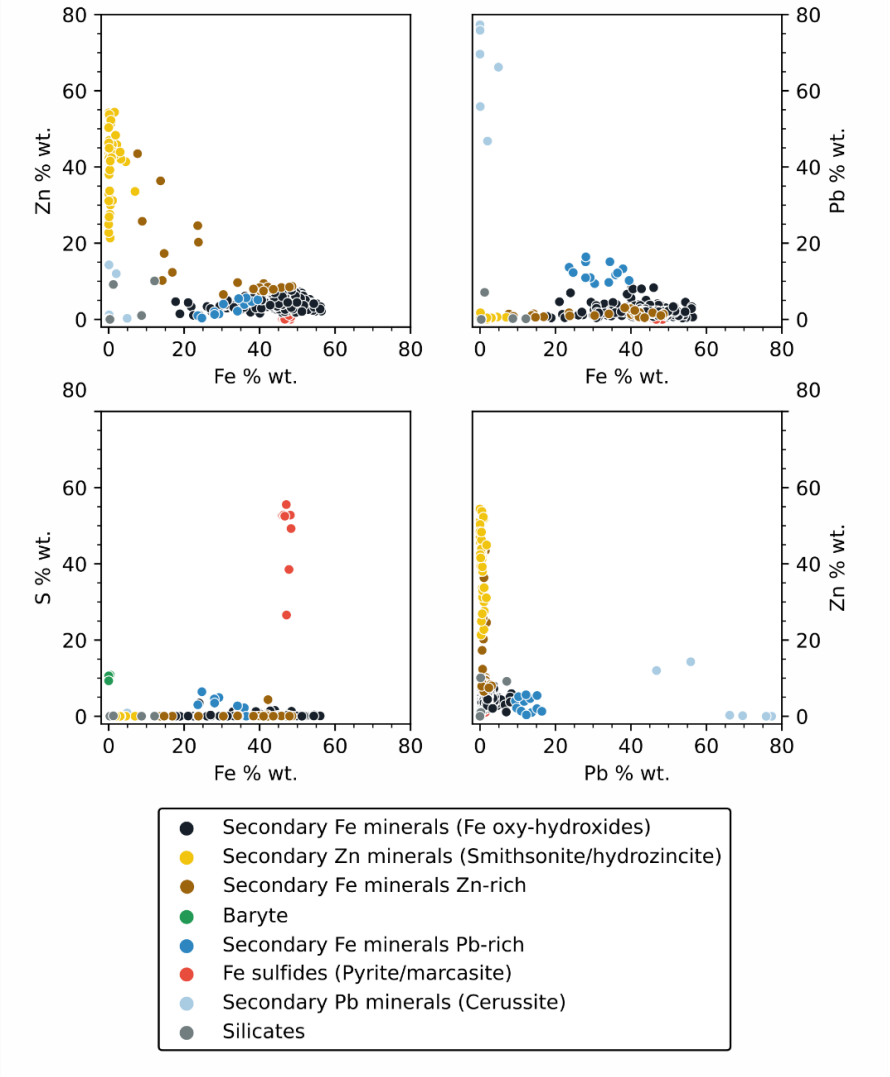

Figure 7 – Scatterplots of different elements in single spot analysis via EMPA

3 CONCLUSIONS

In this study, the compositional analyses of 444 minerals in a tailings sample collected from the external layers of the Raibl tailings impoundments by means of SEM, EDS and EMPA analyses are presented.

- The scarce amount of pyrite/marcasite (2.2 %) (and totally absence of sphalerite, ZnS, and galena, PbS) in the heavy mineral fraction and the high abundance of secondary Fe minerals (Fe oxy-hydroxides) (70.0 %) indicate that the tailings of outer layers of impoundments are strongly weathered and constituted mainly by strongly oxidised Fe minerals.
- Sorption onto HFO is an effective natural attenuation process for Pb and Zn. Lead was found more sorbed onto HFOs than Zn.
- Zinc can be removed from solution during the precipitation of (reasonably) Zn carbonate such as smithsonite and hydrozincite.
- Regarding PTEs, no minerals with As-Cd-Ge-Sb-Tl as major element were found indicating that those elements are hosted in other phases.

Unfortunately, further mineralogical (Raman) and trace element (LA-ICP-MS) analysis are missing, and further studies must be performed to detect the PTEs partitioning and speciation. This knowledge is fundamental on the one hand to understand the processes of release and attenuation of PTEs (Tl, Zn, Pb, As), on the other to evaluate potential steps of reprocessing of tailings, which would allow a recovery of elements of economic interest (Ge, Zn, Pb) and at the same time the removal of the main source of contamination for the Rio del Lago - Slizza River system.

References

Barago, N., Covelli, S., Mauri, M., Oberti di Valnera, S., Forte, E., 2021. Prediction of Trace Metal Distribution in a Tailings Impoundment Using an Integrated Geophysical and Geochemical Approach (Raibl Mine, Pb-Zn Alpine District, Northern Italy). Int. J. Environ. Res. Public. Health 18, 1157. https://doi.org/10.3390/ijerph18031157

Barago, N., Pavoni, E., Floreani, F., Crosera, M., Adami, G., Lenaz, D., Covelli, S., 2023. Hydrogeochemistry of thallium and other potentially toxic elements in neutral mine drainage at the decommissioned Pb-Zn Raibl mine (Eastern Alps, Italy). J. Geochem. Explor. 245, 107129. https://doi.org/10.1016/j.gexplo.2022.107129

Brigo, L., Cerrato, P., 1994. Trace Element Distribution of Middle-Upper Triassic Carbonate-Hosted Lead-Zinc Mineralizations: The Example of the Raibl Deposit (Eastern Alps, Italy), in: Fontboté, L., Boni, M. (Eds.), Sediment-Hosted Zn-Pb Ores. Springer Berlin Heidelberg, Berlin, Heidelberg, pp. 179–197. https://doi.org/10.1007/978-3-662-03054-7_11

Coup, K.M., Swedlund, P.J., 2015. Demystifying the interfacial aquatic geochemistry of thallium(I): New and old data reveal just a regular cation. Chem. Geol. 398, 97–103. https://doi.org/10.1016/j.chemgeo.2015.02.003

Di Colbertaldo, D., 1948. Il giacimento piombo-zincifero di Raibl in Friuli (Italia). 18a Sessione del Congresso Internazionale di Geologia, Londra.

Melcher, F., Onuk, P., 2019. Potential of Critical High-technology Metals in Eastern Alpine Base Metal Sulfide Ores. BHM Berg- Hüttenmänn. Monatshefte 164, 71–76. https://doi.org/10.1007/s00501-018-0818-5

Miler, M., Gosar, M., 2012. Characteristics and potential environmental influences of mine waste in the area of the closed Mežica Pb–Zn mine (Slovenia). J. Geochem. Explor. 112, 152–160. https://doi.org/10.1016/j.gexplo.2011.08.012

Nikonow, W., Rammlmair, D., Furche, M., 2019. A multidisciplinary approach considering geochemical reorganization and internal structure of tailings impoundments for metal exploration. Appl. Geochem. 104, 51–59. https://doi.org/10.1016/j.apgeochem.2019.03.014

Schroll, E., Kürzl, H., Weinzierl, O., 1994. Geochemometrical Studies Applied to the Pb-Zn Deposit Bleiberg/Austria, in: Fontboté, L., Boni, M. (Eds.), Sediment-Hosted Zn-Pb Ores. Springer Berlin Heidelberg, Berlin, Heidelberg, pp. 228–245. https://doi.org/10.1007/978-3-662-03054-7_14

Shepard, F.P., 1954. Nomenclature Based on Sand-Silt-Clay Ratios. J. Sediment. Petrol. 24, 151–158.

Wentworth, K., 1922. A Scale of Grade and Class Terms for Clastic Sediments. Journal of Geology, Vol. 30, No. 5, pp. 377-392. doi:10.1086/622910.

Wilkin, R.T., Brady, P.V., Kent, D.B., 2007. Lead. Monitored Natural Attenuation of Inorganic Contaminants in Groundwater, Volume 2 – Assessment for Non-Radionulcides Including Arsenic, Cadmium, Chromium, Copper, Lead, Nickel, Nitrate, Perchlorate, and Selenium. Edited by R.G. Ford, R.T. Wilkin, and R.W. Puls. U.S. Environmental Protection Agency, EPA/600/R-07/140. pgs. 11-20.

Zuddas, P., Podda, F., 2005. Variations in physico-chemical properties of water associated with bio-precipitation of hydrozincite [Zn5(CO3)2(OH)6] in the waters of Rio Naracauli, Sardinia (Italy). Appl. Geochem. 20, 507–517. https://doi.org/10.1016/j.apgeochem.2004.09.008

Manuscript

Environmental impact of potentially toxic elements on soils, sediments, waters and air nearby an abandoned Hg-rich fahlore mine (Mt. Avanza, Carnic Alps, NE Italy)

Nicolò Barago[1,*], Cristiano Mastroianni[1], Elena Pavoni[1], Federico Floreani[1], Filippo Parisi[1], Davide Lenaz[1], Stefano Covelli[1]

[1] Dipartimento di Matematica e Geoscienze, Università di Trieste, Via Weiss 2, 34128, Trieste, Italy
* Corresponding author.
Keywords: tetrahedrite-tennantite, contamination, potentially toxic trace elements, Gaseous Elemental Mercury (GEM), decommissioned mines, mercury (Hg), antimony (Sb), arsenic (As)
Journal: Environmental Science and Pollution Research (Springer); accepted for publication.

ABSTRACT

The decommissioned fahlore Cu-Sb(-Ag) mine at Mt. Avanza (Carnic Alps, Italy) is a rare example of exploited ore deposits, as the tetrahedrite ($Cu_6[Cu_4(Fe,Zn)_2]Sb_4S_{13}$) is the main ore mineral found. This multi-compartmental geochemical characterisation approach provides one of the first case studies regarding the geochemical behaviour and fate of Hg, Sb, As, Cu and other elements in solid and water matrices, and of Hg in the atmosphere in an environment affected by the mining activity of a fahlore ore deposit. Elevated concentrations of the elements (Cu, Sb, As, Pb, Zn, Hg) associated with both (Zn-Hg)-tetrahedrite and to other minor ore minerals in mine wastes, soils and stream sediments were observed. Concentrations in stream sediments greatly decreased with increasing distance from the mining area and the I_{geo} index values testify the highest levels of contamination inside the mine area. Thallium and Ge were associated with the "lithogenic component" and not to sulfosalt/sulfide minerals. Although mine drainage water often slightly exceeded the national regulatory limits for Sb and As, with Sb being more mobile than As, the relatively low dissolved concentrations indicate a moderate stability of the tetrahedrite. The fate of Hg at the investigated fahlore mining district appeared similar to cinnabar mining sites around the world. Weak solubility but the potential evasion of Gaseous Elemental Mercury (GEM) into the atmosphere also appear to be characteristics of Hg in fahlore ores. Although GEM concentrations are such that they do not present a pressing concern, real-time field surveys allowed for the easy identification of Hg sources, proving to be an effective, suitable high-resolution indirect approach for optimising soil sampling surveys and detecting mine wastes and mine adits.

1 INTRODUCTION

The spread of potentially toxic elements (PTEs) in environmental compartments has often been closely associated with the mining industry, in particular with the extraction and processing of a variety of metal(loid)-bearing sulfide minerals (e.g., Higueras et al. 2006). Similar to mining districts that are still in operation, decommissioned mines may remain a potential source of PTEs which may be released into the environment for decades or even centuries. The recovery of metal(loid)s from ores involves extraction, crushing, milling and different separation processes, e.g., roasting in the case of Hg or froth flotation in the case of Zn and Pb. In the vicinity of ore dressing and smelting plants, the release of contaminated waste in solid and liquid forms, leaching of PTEs from mine waste (Barago et al. 2023), or the escape of fumes containing metal(loid)s vapour and dust (Kotnik et al. 2005) following the dry and wet deposition of the element may be responsible for widespread contamination of the environment (Gosar and Teršič 2012). Additionally, eroded mine waste particles can be mechanically removed by flood events and accumulated in riverbank deposits downstream from the mine (Gosar et al. 1997), representing a secondary source of contamination even at considerable distances from mining sites.

Mercury (Hg), antimony (Sb) and arsenic (As) are often considered priority contaminants due to their potentially toxic effects (DFG 1994; US EPA 1999; UNEP 2019). Centuries of anthropogenic activities, such as mining and burning fossil fuels, have contributed and still contribute in large part to a significant increase in the total amount of Hg and Sb emissions into the environment (Smichowski 2008; Selin 2009). In fact, only a small fraction (< 5%) of these

emissions are associated with primary geogenic sources (i.e., volcanoes, geothermal activities) and weathering of naturally enriched rocks and soils (Hinkley et al. 1999; Shotyk et al. 2004; Driscoll et al. 2013), whereas the remaining portion is imputed to primary anthropogenic inputs and secondary re-emissions (Driscoll et al. 2013; UNEP 2019).

However, different PTEs are characterised by different behaviour and fate, and consequently mobility and bioavailability. Some PTE-bearing sulfides such as cinnabar (HgS), being resistant to normal oxidation and physical-chemical alteration processes, are extremely insoluble in water and can enter the hydrogeochemical cycle through abiotic transport pathways mainly in the form of mechanically degraded solid particles (Biester et al. 2000; Covelli et al. 2007) rather than in the dissolved phase (Gray et al. 2004; Li et al. 2012). In some cases, such as world-class Hg mine sites (e.g., Almadén, Idrija, Monte Amiata) (Esbrí et al. 2010), riverine water draining the mining districts can also be enriched in Hg in dissolved phases (Kocman et al. 2011). However, since Hg is a generally poorly soluble metal, it is more often associated with suspended particulate matter (Baptista-Salazar et al. 2017), colloidal fraction (Lowry et al. 2004) and stream sediments (Gosar et al. 1997). The element dispersion in the entire river basin downstream from the mining area (e.g., Chiarantini et al. 2016; Hines et al. 2000; Garcia-Ordiales et al. 2017, 2019; Gray et al. 2014, 2015) is the result of runoff or drainage of mine waste, including the most active ones, calcines produced during roasting of the ore (Rytuba 2000). Mercury in particular, being a volatile element, can be released to the atmosphere in Gaseous Elemental Mercury (GEM) form from surfaces where Hg can already be present in the substrate as native Hg, as a primary mineral, together with the sulfide (cinnabar, HgS) (Higueras et al. 2012; Loredo et al., 2007), or as a by-product of ore processing (Gray et al., 2010; Kotnik et al. 2005). Moreover, the evasion of GEM usually derives from the reduction of Hg^{2+} forms to Hg^0 through both abiotic and biotic pathways mainly controlled by solar radiation, and air and soil temperatures (Choi and Holsen 2009; Wang et al. 2005). The primary control over GEM evasion into the atmosphere is exerted by the presence of volatile Hg compounds and their Hg concentrations in the substrate. Hence, high volumes of Hg-bearing minerals in Hg mining areas usually lead to the notable stimulation of Hg emission (Agnan et al., 2016). Furthermore, sunlight and heat promote Hg volatilisation (Carmona et al. 2013)

Arsenic and Sb are metalloids and are either associated often together in sulfide ores or related to anthropogenic sources (Filella et al. 2002a). The common primary sulfide minerals of As include arsenopyrite (FeAsS), orpiment (As_2S_3), and realgar (AsS); of Sb is stibnite (Sb_2S_3). The predominant forms of As and Sb in nature are the +3 and +5 oxidation states, mainly found in reducing and oxidising environments, respectively. Geochemical triggers to As mobilisation in waters may be different such as 1) desorption at high pH under oxic conditions and 2) reducing environment (Hounslow 1980; Smedley and Kinniburgh 2002). However, in near-neutral to slightly alkaline environments As may not be mobile (Barago et al. 2023), in contrast, Sb appears to be more mobile respect to As (Majzlan et al. 2018).

In addition to cinnabar, which is the most widespread Hg-bearing mineral, and therefore the most commercially exploited for the production of elemental Hg all over the world, there are about twenty minerals in nature, mainly sulfur compounds in association with Zn, Fe and other metals, containing variable amounts of Hg. Mercury is found as a native metal only in small quantities. Fahlore minerals from the tetrahedrite-tennantite group, which are Cu-Sb and Cu-As sulfosalts, respectively, are abundant in many types of deposits (Ciobanu et al. 2005; Apopei et al. 2016; Lyubimtseva et al. 2019). They have recently been of interest to the scientific community for their high compositional variability and historic importance for Cu and Ag extraction and, rarely, other trace elements (Hg, Bi, Te, Cd, Pb, Se) (Johnson et al. 1986; Sack and Ebel 1993; Karup-Møller and Makovicky 2003). Although the tetrahedrite mineral group has already been recognised as a contamination source of As and Sb (Borčinová Radková et al. 2017) along with Hg in some cases, very little is known about what is left over from the extraction activity of fahlore mineralisations.

The occurrence of potential toxic elements (PTEs), with a particular focus on mercury (Hg) and other PTEs, such as arsenic (As) and antimony (Sb), in several environmental matrices from active and decommissioned mining sites characterised by “non-traditional” (e.g., cinnabar, stibnite) ore deposits represent an issue of environmental concern. A growing number of recent and on-going studies have examined the characteristics of (Cu, Sb, As)-rich minerals from the tetrahedrite-tennantite group as source of contaminants, the geochemical behaviour of PTEs at such mining sites and the subsequent environmental issues related to PTE mobility (e.g., Higueras et al. 2012; Borčinová Radková et al. 2017; Majzlan et al. 2018). However, little information is currently available regarding the role of such minerals in terms of the release of PTEs into riverine water and the atmosphere. New studies can provide more information with which to establish cause-and-effect linkages among the geological attributes and the environmental behaviour, further developing geoenvironmental models for fahlore ore deposits (Plumlee et al., 1999; Seal II and Foley, 2002).

The main purposes of this research aim at assessing the environmental impact and PTE behaviour in soils, stream sediments, mine drainage and surface waters as well as air around one of the historical Cu-Sb fahlore ore deposits in Europe, which is a rare example of exploited ore deposit as the tetrahedrite is the main ore mineral found.

2 MATERIALS AND METHODS

2.1 Geological setting

The carbonate-hosted stratabound fahlore ore deposit of Mt. Avanza (Brigo et al. 2001) belongs to the Palaeocarnic Devonian-Lower Carboniferous (Dinantian) metallogenic province, whose mineralisation is bound to a palaeorelief of Devonian limestones transgressively overlain by Lower Carboniferous to Lower Permian clastic sediments in the Palaeocarnic Chain (Spalletta et al. 2021, and references therein, Fig. 1). It is thought that they are genetically associated with metal-bearing hydrothermal fluids linked to the Middle Carboniferous magmatic event (Brigo et al. 1988). The mineralisation crops out for 100 km in the Carnic Alps (Italy and Austria) and 50 km in the Karawanken (Slovenia) to the east, evidence of a regional event. The province is highly variable, being characterised by copper-dominant fahlore (tetrahedrite), base metal sulfides, barite and fluorite, with predominating Hg-Cu in the west, Zn-Sb-Cu and Zn alone in the centre, and Ba in the east of the Palaeocarnic Chain (Brigo et al. 1988, 2001).

The Palaeocarnic Chain, which is the northernmost east-west oriented sector of the Friuli Venezia Giulia Region consists of a sequence characterised, from W to E, by metamorphic rocks of the greenschist facies to mainly sedimentary rocks overlying the crystalline basement (Brime et al. 2008), with the oldest units belonging to the Ordovician. The area is directly south of the dextral transpressive Gail Line, which is part of the Periadriatic Fault system delineating the boundary between the European and Adriatic plates (Doglioni 1988; Schmid et al. 1989; Handy et al. 2015).

The fahlore Cu-Sb(-Ag) Mt. Avanza mineralisation is hosted in a sub-vertical south-dipping tectonic contact between the Devonian limestones which are represented by the Mt. Avanza and Mt. Navastolt reliefs, and deformed low grade metasedimentary rocks, the age of which are still subject to debate (Carboniferous or Ordovician) (Di Colbertaldo 1960; Feruglio 1966; Spalletta et al. 1981; Venturini et al. 2001; Venturini 2006). Such low grade metamorphic metasedimentary rocks (phyllites) alternating with quartzite beds, possibly belong to the Val Visdende and Fleons Formations (Ordovician) mixed with scanty tectonic slices of low grade metamorphic turbidites of the Hochwipfel Formations (Carboniferous) (Venturini et al. 2001). At the foot of the Mt. Avanza mining area, Permian red sandstones from the Val Gardena Formation Permian crop out, whereas in the area surrounding the Avanza Valley, Permian gypsums and dolostones pertaining to the Bellerophon Formation are reported.

The paragenesis is constituted by sulfosalts and sulfides where massive and microcrystalline tetrahedrite is the most abundant mineral phase with minor galena. Limited occurrence of sphalerite is reported together with rare to very rare pyrite, chalcopyrite and cinnabar (Bortolozzi et al. 2015; Ciriotti et al. 2006; Di Colbertaldo 1960; Dondi et al. 1995; Feruglio 1966; Pirri 1977). The chemical composition of tetrahedrite was found to be variable and generally enriched in Zn and/or Hg, with Hg contents ranging from 1.48 to 8.66 wt. %. (Table 1; Casari, 1996).

The tetrahedrite group has recently been defined as represented by five different series on the basis of the constituents (Biagioni et al. 2020a). Tetrahedrite is a complex sulfosalt with a general formula $Cu_6[Cu_4(Fe,Zn)_2]Sb_4S_{13}$ which can host many minor components in its lattice structure (such as As, Ag, Hg, Cd, Mn, Bi, Te, Se). In particular, Hg can be present in variable amounts, and when the Hg-content is extremely high in tetrahedrite (up to 22.70 wt. %) it can be referred to tetrahedrite-(Hg), by using the general formula: $Cu_6(Cu_4Hg_2)Sb_4S_{13}$ (Biagioni et al. 2020b). Tetrahedrite with variable Hg content can be found in several kinds of deposits around the world: 1) cinnabar deposits, 2) Hg-Sb deposits, 3) Hg tetrahedrite-tennantite deposits, and 4) low-Hg tetrahedrites in Sb-W, Pb-Ag and Au deposits (Mozgova et al. 1979).

Casari (1996) reported that two types of tetrahedrite were found at Mt. Avanza: a Hg-rich and a Zn-rich member. The tetrahedrite specimen with the highest concentrations of Hg are represented by the following compositional formula:

$$(Cu_{9.91}Ag_{0.06}Fe_{0.13}Zn_{1.24}Hg_{0.55})_{11.89}(Sb_{3.17}As_{0.92})_{4.09}S_{13.02}$$

In different horizons mixed varieties of tetrahedrite-tennantite with a Sb:As ratio of 1:1 can occasionally be found. Copper carbonates secondary minerals are very frequent (e.g., azurite, malachite, covellite), due to the contact with carbonate water, in association with secondary Sb-minerals (so-called “antimony ochre”) and minor Fe-oxy-hydroxides and Pb secondary carbonate minerals (cerussite). The presence of Sb or As supergene minerals generally may depends on the amount of tetrahedrite or subordinates tennantite phases, respectively, that has undergone alteration (Dondi et al., 1995). Such Sb-bearing secondary minerals possibly belong to the Roméite group (Bortolozzi et al. 2015). The main non-metallic and gangue minerals are baryte and quartz, followed by calcite and dolomite (Feruglio 1966).

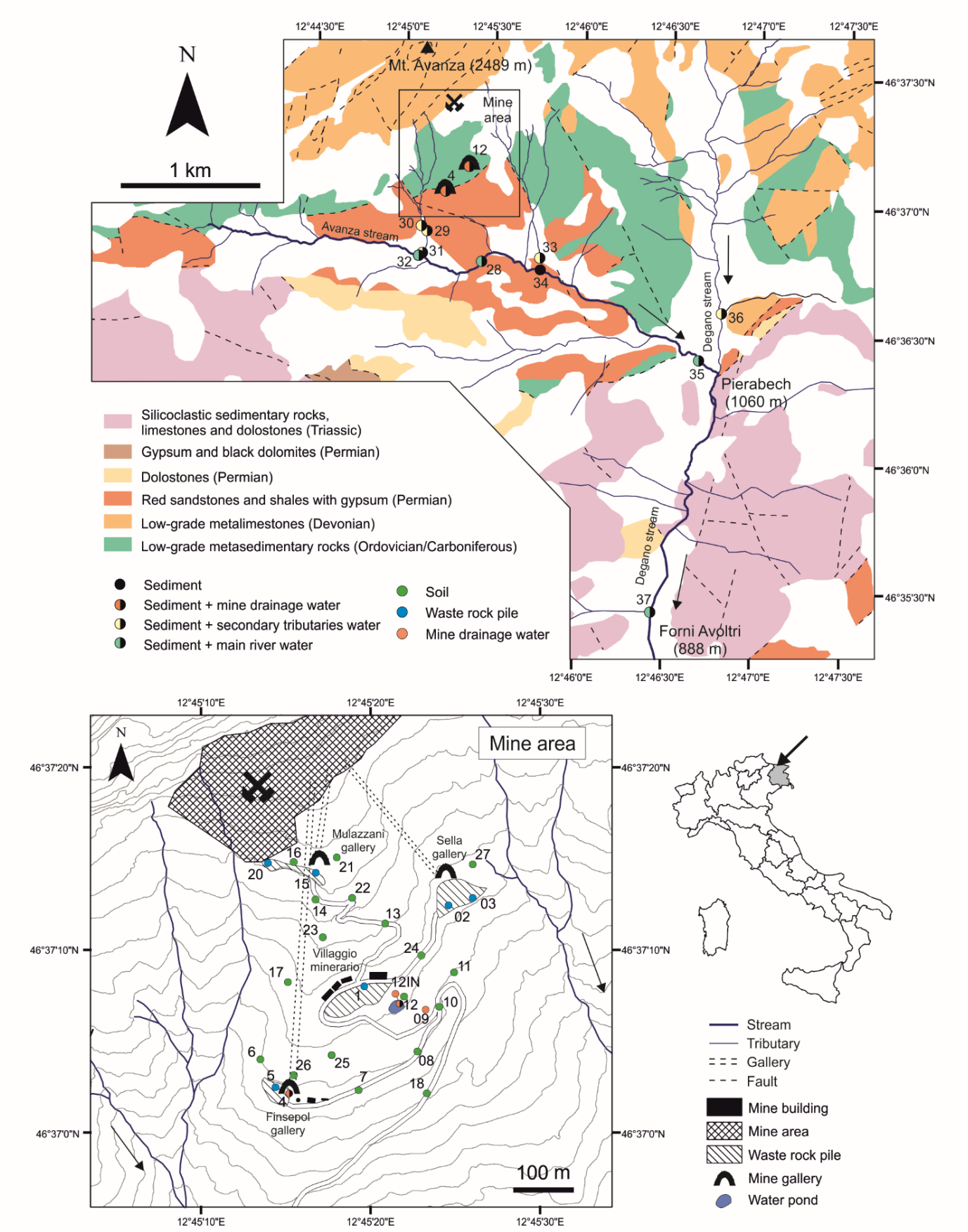

Fig. 1 Geological sketch of the Mt. Avanza mining district with location of the sampling sites. Geological units from Venturini et al. (2001).

Table 1 Electron microprobe analyses of tetrahedrite from Mt. Avanza (wt. %) (Casari 1996)

	Cu	Ag	Hg	Fe	Zn	Sb	As	S
Average	37.57	0.20	4.26	0.37	5.62	23.88	3.69	24.90
Min	35.52	0.10	1.48	0.09	4.01	20.46	1.50	23.62
Max	39.43	0.29	8.66	1.01	6.97	27.91	5.66	25.74

Due to the sub-vertical distribution of the mineralisation, mine galleries have been realised over the years at different levels to reach the mineralised tectonic contact. The following galleries from N to S can be found: Bauer (1861 m a.s.l.), O'Conor (1815 m a.s.l.), Mulazzani (1780 m a.s.l.), Q. Sella (1686 m a.s.l.) and Finsepol (1640 m a.s.l.) (Fig. 1).

2.2 Study Area

The study area is located between 900 and 1800 m a.s.l., in the Avanza Valley (Fig. 2d) (Carnic Alps, Friuli Venezia Giulia, Italy) near the village of Forni Avoltri, on the border with Austria and the Region of Veneto. The landscape is characterised by an Alpine mountainous environment which is morphologically controlled by past glacial and present fluvial erosion and covered by coniferous forest.

Fig. 2 (a) Outcrop of alteration supergene minerals related to the tetrahedrite Cu-Sb-(Ag) mineralisation "Pietra Verde", (b) mining village of the Mt. Avanza mine ("Villaggio minerario"), (c) Finsepol gallery, (d) Avanza valley and Avanza stream.

The Cu-Sb-(Ag) Mt. Avanza mine was an important Cu ore deposits in the Eastern Alps during the 19th century (Feruglio 1966) and is historically important as it might have been active since the European Bronze Age (Artioli et al. 2020). A comprehensive review of the history of the Mt. Avanza mining site is reported in Zucchini (1998). The first document mentioning the mine dates back to 778 AD. The mine was in operation intermittently until 1952, when extraction definitively ended. The last phase of mineral exploration began in 1975, as evidenced by the realisation of the "Finsepol gallery" (Fig. 2c) and the largest waste rock pile near the mining village "Villaggio Minerario" (Fig. 2b), but no recovery of Cu-Ag followed, and exploration permanently halted in 1995. The area has been abandoned since then.

Until the end of the 19th century, metals were recovered using roasting processes in Pierabech, near the village of Forni Avoltri (Fig. 1), while a flotation plant was operating for a couple of years during World War II (Feruglio 1966).

2.3 Sampling strategy

Sampling campaigns in the Mt. Avanza decommissioned mining district were performed in June, September, October and November 2021. Solid (ore-bearing rocks, soils, mine wastes, sediments), and water (mine drainages, main river and secondary tributaries) samples were collected, whereas atmospheric GEM was monitored in the field.

After removing organic debris (e.g., roots, leaves), almost 1 kg of a composite sample of the most surficial layer (0-10 cm) of soils and mine waste piles was collected at each selected site (Fig. 2). Sediments were collected immediately downstream from the mine drainages (MA4 and MA12 sites) and along the main stream (Rio Avanza) and its tributaries. Ore-bearing rocks of > 5 cm in diameter and characterised by noticeable ore minerals were collected in the mine site near the main waste piles.

The physico-chemical parameters of water (temperature, pH, redox potential (ORP), electrical conductivity (EC), dissolved oxygen (DO) and total dissolved solids (TDS)) were measured *in situ* using a portable probe (Hanna HI98194). All the collected water samples and field blanks prepared with ultrapure water were preventively filtered *in situ* (syringe filters Millipore Millex HA, 0.45 µm) and separated in different aliquots for distinct chemical analysis. Water aliquots for PTE and major cation analytical determinations were stored in HDPE vessels and acidified with ultrapure HNO_3 (1% v/v, HNO_3 67-69% v/v VWR), whereas water aliquots for Hg determination were collected in borosilicate glass containers and immediately oxidised with bromine chloride (BrCl, 0.5% v/v).

2.4 Chemical elemental analysis of the solid matrix

Solid samples were first air-dried in the laboratory at a temperature of 25°C to minimise the loss of Hg due to its easy volatilisation. Then, each dried sample was sieved at 2 mm and finely ground in tungsten carbide mills.

For the determination of major and trace elements, with the exception of Hg, aliquots were acid-digested in PTFE vessels through a total dissolution in a closed microwave system (Multiwave PRO, Anton Paar) using inverse *aqua regia* (HNO_3 67-69% v/v and HCl 34-37% v/v, VWR, 3:1), HF (47-51% v/v, VWR), and H_2O_2 (30% w/v) according to US EPA method 3052 (US EPA 1996). Blanks were prepared for each microwave batch to check the analytical performance. The samples were subjected to two heating steps for mineralisation and boric acid (H_3BO_3, 6%) was added in the second step to buffer HF excesses. The obtained solutions were diluted up to a final volume of 25 mL by adding Milli-Q water and filtered through syringe filters (Millipore Millex HA, 0.45 µm) before analytical determinations. Concentrations of major and trace elements were determined via Inductively Coupled Plasma – Mass Spectrometry (ICP-MS, NexION 350X equipped with an ESI SC autosampler, PerkinElmer) using the Kinetic Energy Discrimination (KED) mode to avoid and minimise cell-formed polyatomic ion interference. The calibration of the instrument was performed via the analysis of standard solutions prepared by dilution (ranging between 0.5 and 500 µg/L) from two multistandard solutions (Periodic Table MIX 1 e MIX 2 for ICP, TraceCERT Sigma-Aldrich) and acidified with HNO_3 (1% v/v). Moreover, certified reference material (PACS-3 Marine Sediment Certified Reference Material, NRCC, Canada) was digested in the same batch as the solid samples to assess the accuracy of the analysis. Acceptable recoveries were obtained varying between 80 and 109 % and the precision of the analysis expressed as RSD% was < 3%.

Total Hg (THg) was determined using a Direct Mercury Analyzer (DMA-80 Milestone), in accordance with EPA method 7473 (US EPA 1998). Each sample was analysed in triplicate and the quality of the analysis was evaluated using a Certified Reference Material (PACS-3 Marine Sediment CRM, NRCC, Canada). The relative standard deviation of at least three determinations was < 2%.

2.5 Mineralogical determinations of the solid matrix

Manually separated ore minerals (n = 8) from rock fragments sampled on the waste rock piles were grounded with an agate mortar and analysed by means of the powder XRD technique using a STOE D500 (Siemens, Monaco, Germany) diffractometer with Cu Kα radiation (λ=1.5418Å), monochromatised by a secondary flat graphite crystal. The scanning angle ranged from 5° to 90° of 2θ, steps were of 0.005° of 2θ, and the counting time was of 6 s/step. The current used was 20 mA and the voltage 40 kV. The "Match!" software version 3.14 as well as the reference patterns calculated from the COD (Crystallography Open Database) database were used for phase identification.

2.6 Chemical analysis of the water matrix

The concentrations of major cations (Ca^{2+}, Mg^{2+}, Na^{+} and K^{+}) in water samples were determined via Inductively Coupled Plasma – Optical Emission Spectrometry (ICP-OES) using an Optima 8000 Spectrometer (Perkin Elmer, USA) equipped with a S10 Autosampler. Instrument calibration was performed using standard solutions (ranging between 0.1 and 100 mg/L) prepared by dilution from a multistandard solution (Periodic Table MIX 5 for ICP, TraceCERT Sigma-Aldrich) and acidified with HNO_3 (1%, v/v). The precision of the analysis expressed as RSD% was <5%. The analytical determination of major anions (F^{-}, Cl^{-}, NO^{3-}, SO_4^{2-}) was performed via Ion Chromatography (IC, Dionex IonPac™ AS9-HC, Thermo Scientific™). The instrument was calibrated using 7 standard solutions (ranging between 0.1 and 100 mg/L) prepared by dilution from multistandard solutions (Anion multi-element standard I and Anion multi-element standard II, Merck). Each standard was analysed in triplicate. Moreover, three aliquots of the company's calibration solutions (Dionex Seven Anion Retention Time Standard Concentration, Thermo Scientific™) were analysed for quality control. With regard to CO_3^{2-} and HCO^{3-}, the determination was made using potentiometric titration using 0.01N HCl (APAT and IRSA-CNR 2003).

The analytical determination of trace elements was performed via Inductively Coupled Plasma Mass Spectrometry (ICP-MS, NexION 360x equipped with an ESI SC autosampler, Perkin Elmer), using the KED mode and scandium (Sc), yttrium (Y) and holmium (Ho) were used as internal standards in order to evaluate and chek for potential matrix effects. For the analysis of the water matrix, the instrument was calibrated using 5 standard solutions (ranging between 0.5 and 10 µg/L) prepared by dilution of two multistandard solutions (Periodic Table MIX 1 and Periodic Table MIX 2 for ICP, TraceCERT Sigma-Aldrich) and acidified with HNO_3 (1%, v/v). The precision of the analysis expressed as RSD% was <3%.

Dissolved Hg in water samples was determined by Cold Vapor-Atomic Fluorescence Spectrophotometry coupled with a gold trap pre-concentration system (CV-AFS Mercur, Analytic Jena), according to EPA method 1631e (US EPA 2002). Before the analytical determination, a pre-reduction using NH_2OH-HCl (250 µL/100 mL sample) was performed until the yellow colour disappeared, followed by a reduction with $SnCl_2$ (2% v/v in HCl 2% v/v). The instrument was calibrated using standard solutions (ranging between 1 and 50 ng/L) prepared by diluting a Hg standard solution (mercury standard solution, Merck) and acidified with BrCl (0.5%, v/v). The precision of the analysis expressed as RSD% was < 3%.

2.7 On-site monitoring of Gaseous Elemental Mercury (GEM)

Measurements of gaseous elemental mercury (GEM) were conducted by means of a Lumex RA-915M Hg portable analyser during a single survey in October 2021. The instrument is an atomic absorption spectrometer (AAS) with Zeeman background correction and high frequency modulation of light polarization that provides both high sensitivity and minimal interference (Sholupov and Ganeyev 1995). The accuracy of the method is 20% and the dynamic range is 2-25,000 ng/m^3. Values below the limit of detection (LOD = 2 ng/m^3) were treated with the medium bound approach thus set to 50% of the LOD (US EPA 2000). Data were acquired continuously with an integration time of 10 s as average values of concentrations observed every 1 s and stored in instrument datalogger. Baseline checks were performed at the beginning and at the end of measurement session and constantly each 15 minutes during sampling. Monitoring was performed by car along all the access roads from Pierabech to the mine village at a constant speed of 5-10 km/h and on foot in the mining area, focusing on spatial distribution of GEM around possible point sources (e.g. mine wastes, gallery entrances). GPS coordinates were acquired in parallel with the measurements. For sampling by car, the inlet of the instrument was connected to a 1-m long PVC tube mounted outside a side window of the vehicle. Spatial distribution of GEM concentration was assessed with QGIS software and graphically represented using inverse distance weighting (IDW) interpolation.

3 RESULTS AND DISCUSSION

3.1 The mine area

The concentrations of PTEs in soils, mine wastes and sediments were largely variable, from few to thousands of mg/kg, but never exceeding 1%. In detail, the maximum concentrations in the mining district found were: Cu = 4019 mg/kg, Sb = 1049 mg/kg, Pb = 1216 mg/kg, Zn = 1204 mg/kg, As = 654 mg/kg and Hg = 473 mg/kg, demonstrating that ore-bearing minerals were diffused in the area as a result of mining (Table 2, Table S1).

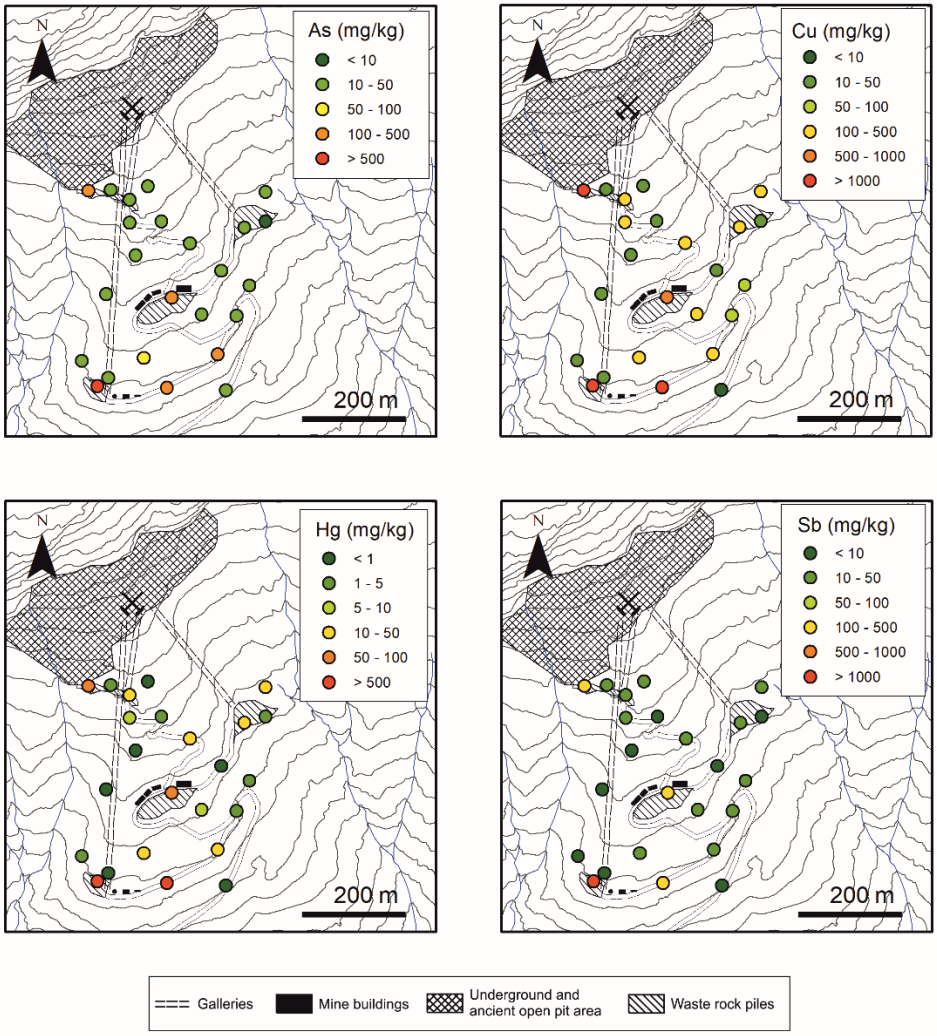

Fig. 3 Distribution of As, Cu, Hg and Sb concentrations in the surficial soils and waste rock piles of the Mt. Avanza mining area.

While maximum concentrations were associated with waste rock piles, also the soils around these waste deposits were also heavily enriched in PTEs (Fig. 3). Elevated concentrations (e.g., 132 mg/kg of Hg or 1557 mg/kg of Cu) can indeed be found in surficial soils due to the extensive use of by-product gravel and sands for the construction of the main access roads and mine infrastructure. However, great variability occurred depending on mining operations and the natural distribution of the different elements.

Table 2 Summary of the concentrations (min-max) of the main metals and metalloids in the environmental matrices.

	Type (n samples)	As	Cu	Hg	Sb	Pb	Zn
		mg/kg	*mg/kg*	*mg/kg*	*mg/kg*	*mg/kg*	*mg/kg*
Solid	Waste rock pile (6)	8.20-654	31.3-4019	1.42-473	5.00-1049	19.4-397	20.3-553
	Soil (18)	12.1-162	10.1-1557	0.21-132	2.74-153	26.4-1216	62.0-1204
	Sediment (12)	12.9-212	14.0-242	0.04-9.15	1.64-28.0	14.7-78.8	57.1-171
		µg/L	*µg/L*	*ng/L*	*µg/L*	*µg/L*	*µg/L*
Water	Mine drainage (11)	0.87-14.8	0.29-8.28	2.41-13.2	4.33-20.3	< LOD-1.02	< LOD-11.0
	Tributaries (5)	0.18-3.89	0.12-0.41	1.81-10.2	0.19-1.59	< LOD	< LOD-1.90
	Main river (5)	0.60-2.98	<LOD-1.08	1.17-6.49	0.30-1.16	< LOD-0.72	< LOD-4.30
				ng/m^3			
Gas	Mine area (1222)	n.d.	n.d.	< LOD-25.4	n.d.	n.d.	n.d.
	Avanza valley [a] (344)	n.d.	n.d.	< LOD-13.7	n.d.	n.d.	n.d.
	Rural area [b] (134)	n.d.	n.d.	< LOD-4.50	n.d.	n.d.	n.d.

[a] Between the mine and the downstream rural area
[b] The villages of Pierabech and Forni Avoltri (Fig. 1)

Although the concentrations of metal(loid)s in soils and waste rocks are in the same order of magnitude, Pb-Zn distribution can be discordant with respect to that Cu-Sb-Hg-As, indicating that the source of metal(loid)s (i.e., the ore minerals of the mineralised veins) was heterogeneous and composed of multiple minerals. The Cu-Sb-Hg-As group can be clearly attributed to the Hg-rich tetrahedrite and lesser extent to tennantite minerals, whereas Pb-Zn can be related also to galena (PbS) and sphalerite (ZnS) sulphides which are less abundant. The correlation plot of Fig. 4 represents the Pearson correlation matrix with cluster analysis on $\log_{10}$ transformed data of all the trace elements analysed on waste rocks, soils and sediments.

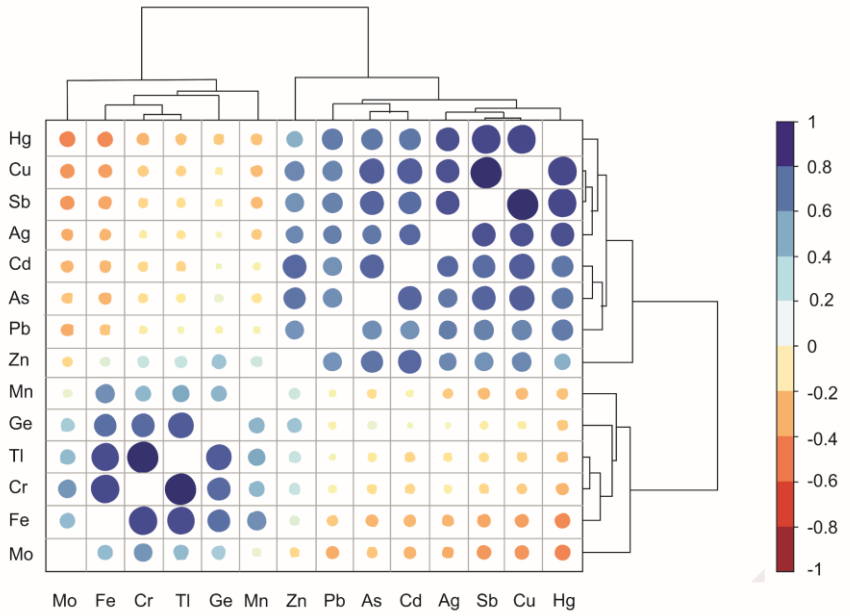

Fig. 4 Pearson correlation heatmap of major and trace elements in all waste rocks, soils and sediments analysed (processed using the heatmaply package; Galili et al. 2018). The colour is a function of the correlation coefficient (r), whereas point size is log function of the p-value.

Two groups of elements are identifiable based on linear correlation and cluster analysis of major and trace components. The "metallogenic component" consists of the chalcophile elements: Cu-Sb-Hg-Ag-Zn-Pb-As-Cd which are metals and metalloids associated with mineralisation. In contrast, the "lithogenic component" is constituted by elements such as Mo-Fe-Cr-Tl-Ge-Mn, associated with the host rocks and adjacent lithologies such as limestones, metasediments and red sandstones (Fig. 1). Cluster analysis confirms tight relationships among Cu, Sb, Ag and Zn thus reflecting the abundant distribution of (Hg, Zn)-rich tetrahedrite. Conversely, the Pb-As-Cd association might be related to As-Cd rich galena as yet unreported mineral phases. Zinc was included within the metallogenic component, but its occurrence as a common minor constituent of the upper continental crust (Rudnick and Gao 2003) placed it between the metallogenic and lithogenic components. Among the second group of elements, the most correlated are Cr, Fe, Tl and Ge, which unlikely were present in the ore-bearing minerals. Interestingly, Tl and Ge behave like siderophile elements in the Mt. Avanza mining site although they can be usually found as chalcophile elements in many sulfide ore deposits (Barago et al. 2021; Leach et al. 2010; Pavoni et al. 2017). In fact, since Tl has ionic radius and charge (+1) similar to the alkali metals such as potassium (K), it is reasonably hosted in K-bearing mica minerals of the Carboniferous/Ordovician mica schist formation (Peter and Viraraghavan 2005). Whereas most of Ge is reasonably dispersed through silicate minerals due to the substitution of Ge^{4+} with the geochemically similar Si^{4+} (Rosenberg 2009).

Four mineral phases have clearly been identified via XRD powder diffraction performed on manually separated specimens (n=8): tetrahedrite, dolomite, calcite, and quartz. The patterns are presented in Fig. 5. In tetrahedrite there could be several substitutions of cations including Hg, Ag, Zn and Fe. All these substitutions affected the cell edges of the tetrahedrite according to the general formula by Johnson et al. (1987):

$$a\,(\text{Å}) = 10.379 + 0.082(\text{Ag}) - 0.01(\text{Ag2}) - 0.009(Cu^{*}) + 0.066(\text{Hg}) - 0.038(\text{As}) + 0.144(\text{Bi})$$

where Cu* = 2.0 – (Fe + Zn + Hg + Cd) and the coefficient of the Hg term was corrected according to Di Benedetto et al. (2002). Hall (1972) found a cell edge equal to 10.3191 ± 0.0005 Å for pure synthetic tetrahedrite. Biagioni et al. (2020a) found a cell edge value of 10.4725 ± 0.0001 to 10.5057 ± 0.0008 Å for specimens of tetrahedrite-(Hg) with a chemical content of Hg in the range 15-20 wt.%. Biagioni et al. (2020b) found a value of 10.3798 ± 0.0008 Å for a tetrahedrite-(Zn). Considering the chemical analyses of tetrahedrite from Mt. Avanza (Casari et al. 1996) where the average Hg content was 4.26 wt. %, and Zn was about 5.62, the cell edge found here was equal to 10.3929 ± 0.0001 Å confirmed these data being higher than that of tetrahedrite-(Zn) and in the middle between that of the synthetic tetrahedrite and the tetrahedrite-(Hg) specimens. Quartz, calcite and dolomite were identified in variable amounts and were gangue constituents as indicated by Feruglio (1966).

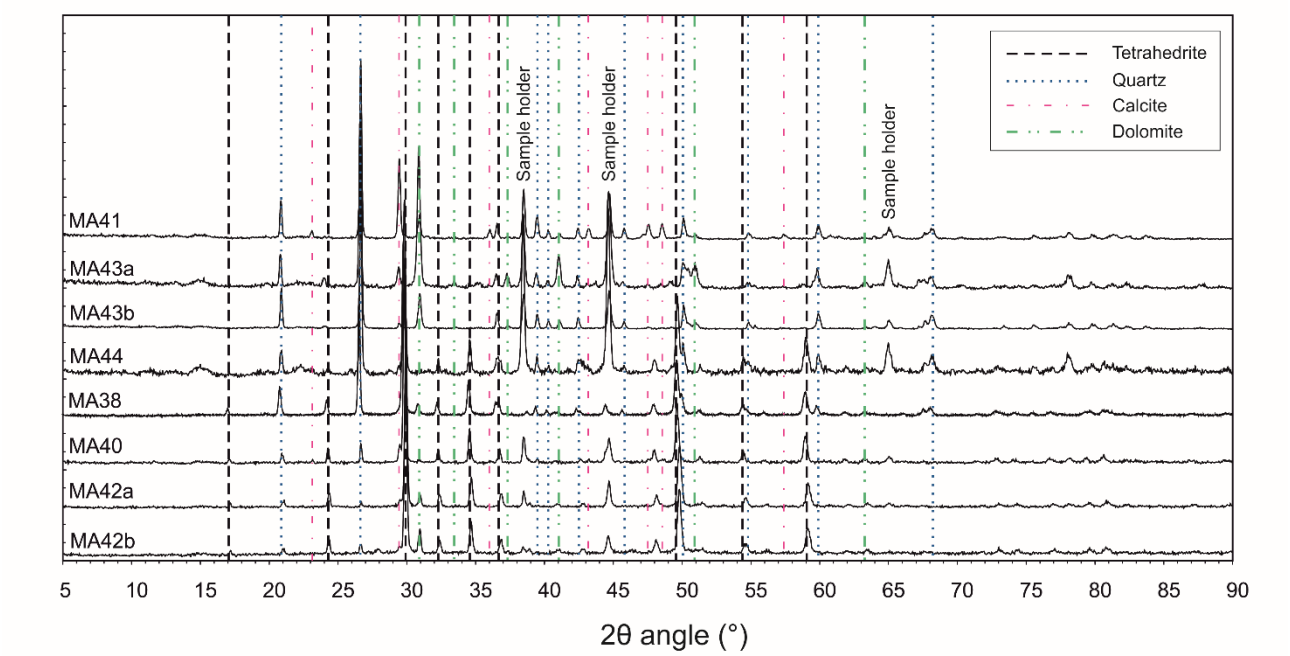

Fig. 5 X-ray powder diffractograms (XRD) of the manually separated minerals.

3.2 Sediment quality

With respect to sediments, the variability of metal(loid) concentrations was strictly related to the distance from the mining district, decreasing "exponentially" moving away from the source of contamination (Fig. 6). Maximum concentrations were 212 mg/kg As (MA04) and 242 mg/kg Cu, 9.15 mg/kg Hg and 28.0 mg/kg Sb for MA12 sample (Tab. S1) as a consequence of the extraction activity and transport of sediments from the mine to the external area.

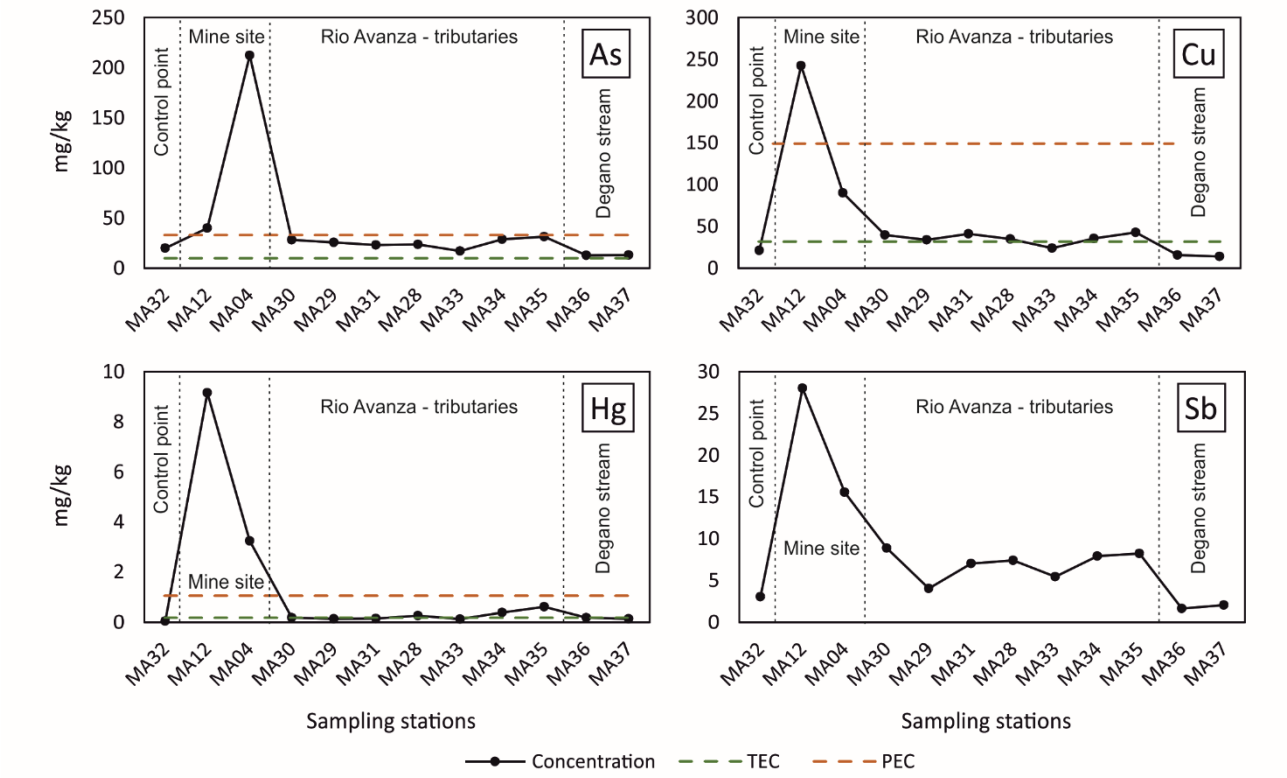

Fig. 6 Concentrations of As, Cu, Hg and Sb of stream sediments collected at the historic mining district of Mt. Avanza. Threshold Effect Concentration (TEC) and Probable Effect Concentrations (PEC) from (MacDonald et al. 2000).

The contamination assessment was provided by means of the geoaccumulation index (I_{geo}) (Müller 1969), calculated according to the following equation:

$$I_{geo} = log_2\left(\frac{C_n}{1.5B_n}\right)$$

C_n: measured element concentration; B_n: background element concentration.

The MA32 sample was chosen as the control point (Garcia-Ordiales et al. 2017) and B_n, since it was collected in the Rio Avanza upstream the confluence of the tributaries (Figure 2). The I_{geo} values (Table 3) between 2 and 3, indicating moderately contaminated sediments, were found for As, Cu and Sb in the mine area. However, sediments extremely contaminated by Hg (I_{geo} > 5) were found in the mine area, as well as moderately to heavily contaminated sediments (I_{geo} = 2 - 3) were found in the Rio Avanza stream. Downstream sediments (e.g. MA37), far from the source, are characterised by lower I_{geo} values, thus indicating that the environmental impact is restricted to the area surrounding the mine site, whereas it is very low on the drainage basin. It is reasonable to think that the volumes extracted and processed were relatively small and decades of flushing have diluted element concentrations in the stream sediments. In fact, the overall legacy impact of the mining activity at Mt. Avanza is very low compared to other areas where hundreds or thousands of mg/kg of PTEs in stream sediments were also found at tens of kilometers from large and historical mine sites (Müller et al. 1994, Covelli et al., 2001; Garcia-Ordiales et al. 2017).

Table 3 Geoaccumulation index (Igeo) (Müller 1969) for stream sediments of the Rio del Lago - Slizza stream sediments. Igeo > 5 are highlighted in bold. MA32 was selected as "control sample".

Type	Name	As	Cd	Cr	Cu	Fe	Ge	Hg	Mn	Mo	Ni	Pb	Sb	Tl	Zn
	Concentration (mg/kg)														
	MA32	19.8	0.15	62.3	21.2	36890	1.84	0.04	525	1.22	32.0	21.9	3.06	0.74	86.3
	I_{geo}														
Mine area	MA12	-0.1	1.4	-1.1	**2.9**	-1.3	-1.2	**7.3**	-1.2	-2.1	-1.0	1.1	**2.9**	-1.1	0.0
Mine area	MA04	**2.8**	0.9	-0.7	1.5	-0.9	-0.4	**5.8**	-0.7	-0.5	-0.3	0.9	1.8	-0.6	0.3
Main stream	MA28	-0.3	1.0	-0.1	0.1	-0.1	-0.6	**2.2**	-0.4	-0.5	-0.2	-0.2	0.7	-0.6	0.2
Main stream	MA34	0.0	1.2	-0.1	0.2	-0.3	0.0	**2.7**	-0.6	-0.7	-0.3	0.4	0.8	-0.3	0.1
Main stream	MA35	0.1	1.5	-0.2	0.4	-0.3	-0.7	**3.4**	-0.2	-0.1	-0.4	0.7	0.8	-0.4	0.1
Main stream	MA37	-1.2	-1.2	-0.9	-1.2	-0.2	-0.4	1.1	-1.3	-0.6	-1.1	-1.1	-1.2	-1.2	-1.2
Tributaries	MA30	-0.1	1.4	0.1	0.3	-0.5	-0.8	1.6	-0.6	-0.9	0.0	0.1	1.0	-0.3	0.4
Tributaries	MA29	-0.2	-0.5	-0.6	0.1	-0.4	-0.6	1.1	-0.6	-1.6	-0.7	0.0	-0.2	-0.1	-0.1
Tributaries	MA31	-0.4	1.1	-0.1	0.4	-0.5	-0.6	1.3	-0.7	-0.8	-0.2	0.8	0.6	-0.6	0.2
Tributaries	MA33	-0.8	-1.0	-0.6	-0.4	-1.3	-0.9	1.0	-0.7	-0.9	-0.6	-0.4	0.2	-0.7	-0.5
Tributaries	MA36	-1.2	-0.9	-0.8	-1.0	-1.4	-0.9	1.6	-1.1	-0.5	-0.5	-1.2	-1.5	-1.1	-1.1

Value	Class	Pollution quality
Igeo < 0	1	Uncontaminated
$0 < I_{geo} \leq 1$	2	Uncontaminated to moderately contaminated
$1 < I_{geo} \leq 2$	3	Moderately contaminated
$2 < I_{geo} \leq 3$	4	Moderately to heavily contaminated
$3 < I_{geo} \leq 4$	5	Heavily contaminated
$4 < I_{geo} \leq 5$	6	Heavily to extremely contaminated
$5 < I_{geo} \leq 6$	7	Extremely contaminated

PTE concentrations in sediments were compared with Sediment Quality Guidelines (SQG) for metal toxicity in freshwater ecosystems. TEC (threshold effect concentration) and PEC (probable effect concentration) are used to identify the concentration ranges of chemicals associated with sediment toxicity and biological effects in sediment-dwelling organisms (MacDonald et al. 2000). Moreover, they provide a preliminary basis for assessing sediment quality conditions in freshwater ecosystems, being PEC correlated to the incidence of toxicity. Our data indicate that in the mining area, PTE concentrations are always above the PEC value, attesting that a probable adverse effect may frequently occur, whereas most of the stream sediments from the Rio Avanza stream are between TEC and PEC, thus suggesting that adverse effects may occasionally occur. Speciation analyses on sediment samples, especially considering the bioavailable fraction, could be of help in depicting the real impact on the aquatic biota in the drainage basin affected by the past mining activities.

3.3 Hydrogeochemistry and transport of dissolved metal(loid)s

The investigated water samples showed overall near-neutral to slightly alkaline conditions (7.52 – 8.78; Table S2). Average pH value of 8.0 ± 0.4 was found in the mine drainage water, whereas surface water collected from the Rio Avanza stream and its secondary tributaries showed slightly more alkaline conditions (pH = 8.4 ± 0.1). This indicates the natural pH buffering capacities following dissolution of limestones, which is one of the main lithologies outcropping in the investigated area, as also confirmed by HCO_3^- concentrations ranging overall between 132 and 221 mg/L.

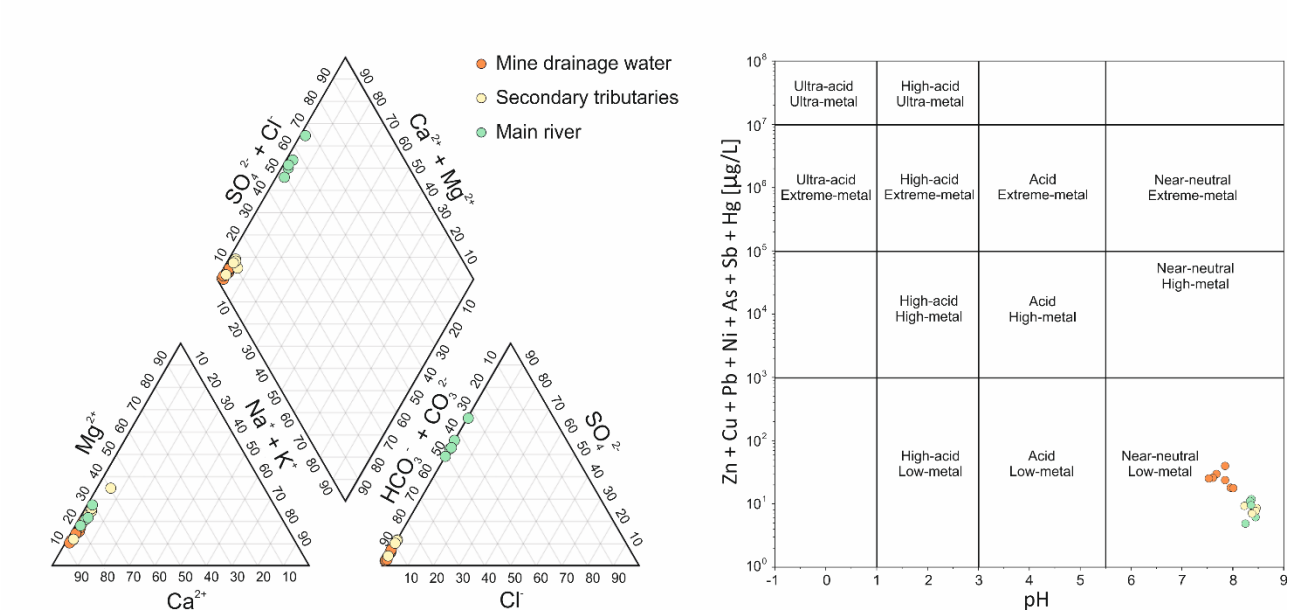

Fig. 7 Piper (left) and Ficklin (right) diagrams of the different groups of water collected at the decommissioned mining district of Mt. Avanza.

Similar to other decommissioned mining districts characterised by carbonate host rock (Hiller et al. 2013; Petrini et al. 2016; Pavoni et al. 2018), the waters draining the decommissioned mining district of Mt. Avanza belong to neutral mine drainage (NMD) and no evidence of acid mine drainage (AMD) was observed, although AMD is quite commonly observed in areas affected by the mining of sulfides (Aguilar-Carrillo et al. 2022; D'Orazio et al. 2017; De Giudici et al. 2019; Li et al. 2020; Perotti et al. 2018; Zhou et al. 2017). Among the different sampling campaigns, the mine drainage water showed relatively constant EC (175 ± 40 µS cm^{-1}) and TDS (92.5 ± 18.8 mg/L) values, which were found to be lower with respect to those observed in the Rio Avanza stream water samples (EC = 538 ± 223 µS cm^{-1}, TDS = 304 ± 93 mg/L) most likely due to the dissolution of gypsum lithologies and resuspension events related to maintenance and up-keep on the slopes upstream from the sampling stations along the Rio Avanza stream basin. Oxidative conditions (mean 270 ± 70 mV) and relatively elevated concentrations of dissolved oxygen (mean 7.4 ± 0.5 mg/L) were observed in all the investigated water samples.

According to the Piper diagram (Piper 1944), the waters mostly belong to the calcium-bicarbonate hydrochemical facies as the result of carbonate rock dissolution (Fig. 7, left). Conversely, calcium-sulfate was identified as the dominant hydrochemical facies in the case of the Rio Avanza stream water, most likely due to weathering of Permian gypsum lithologies outcropping along the stream basin (Fig. 2). Indeed, the SO_4^{2-} concentration was found to be notably higher in the Rio Avanza main stream (mean 198 ± 71 mg/L) rather than in its secondary tributaries (mean 13.6 ± 4.6 mg/L) as well as in the mine drainage water (mean 6.7 ± 2.9 mg/L). Moreover, the content of SO_4^{2-} still remained elevated in the Degano stream water collected downstream from the confluence with the Rio Avanza stream (196 mg/L at site MA37) and notably higher than that observed upstream (14.2 mg/L at site MA36).

The relatively low concentration of SO_4^{2-} in the mine drainage water suggests that sulfide oxidation did not significantly contribute, although quite a significant correlation was observed between SO_4^{2-} and dissolved PTEs potentially released following sulfide oxidation in the mine drainage water, excluding site MA04 (Sb: r=0.903, N=8, 0.001<P<0.01; As: r=0.828, N=8, 0.001<P<0.01; Cu: r=0.639, N=8, P<0.05)

In keeping with the Ficklin diagram (Plumlee et al. 1999), all the investigated water samples were classified as "near-neutral, low-metal" water (Fig. 7, right) thus confirming 1) the role of carbonate dissolution which resulted in natural pH buffering effects, 2) the moderate stability of primary and secondary ore-bearing minerals and 3) the limited extent of the impact of mining activities on water composition. However, stream water from the main stream and its secondary tributaries clearly differed from the mine drainage water samples which showed a slightly higher PTE content in the Ficklin diagram, indicating that a geochemical signature from the Mt. Avanza mining district can be observed.

Regarding the occurrence of dissolved PTEs, relatively low concentrations were observed (Table S2) and a general dilution effect occurred by moving downstream from the mining district (Fig. 8). The same dilution effect was observed for sediments and was especially evident in the case of Cu, Sb and Hg. In the case of water, the dilution of

PTEs was notable only for Cu, Sb and As which were more abundant in the mine drainage water samples (maximum concentrations: Cu 8.28 µg/L at sampling station MA12IN, Sb = 20.3 µg/L at sampling station MA09 and As = 14.8 µg/L at the sampling station MA04) and decreasing downstream, thus suggesting water-rock interaction processes involving the main mineralisation at Mt. Avanza (Fig. 8). Moreover, the Rio Avanza water collected upstream from the mining district showed concentrations of one order of magnitude lower (site MA32: Cu = 0.18 µg/L, Sb = 0.30 µg/L and As = 1.02 µg/L).

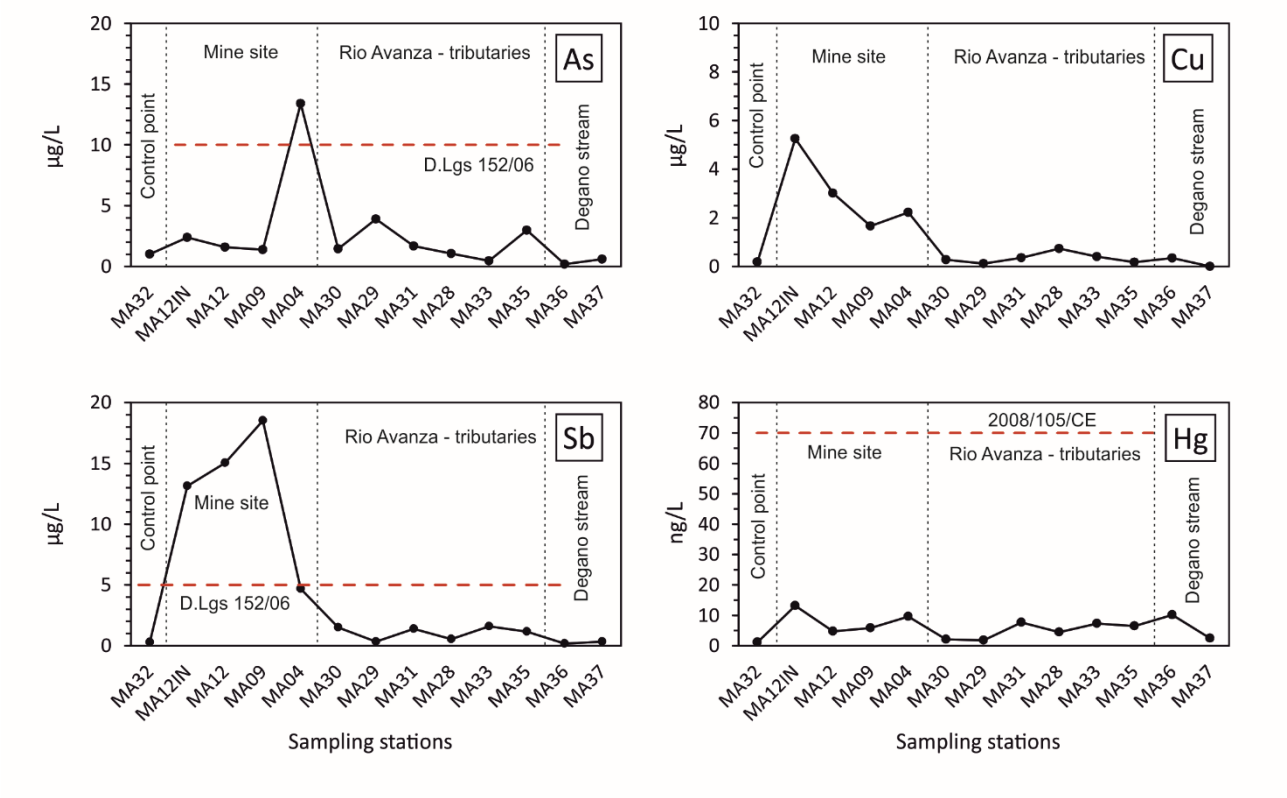

Fig. 8 Concentrations of As, Cu, Hg and Sb in water collected at the historic mining district of Mt. Avanza. D.Lgs. 152/06: Italian reference legislation for groundwater quality. 2008/105/CE European water quality standard.

Conversely, dissolved Hg was found to be notably less abundant (ranging between 1.17 and 13.2 ng/L) and marked differences were not observed among all the water samples (Fig. 2), indicating that there was not a significant release of dissolved Hg in the water basin. Moreover, Hg concentrations were always below the European maximum allowable concentration of 70 ng/L in surface waters (European Directive 2008/105/CE). Comparatively, the neutral waters of the world-class cinnabar Idrija mining district can reach concentrations of dissolved Hg more than one order of magnitude higher (up to 359 ng/L; Baptista-Salazar et al. 2017). Although Hg is abundant in tetrahedrite minerals (Table 1) and in the analysed solid fraction (maximum concentration of 476 mg/kg at site MA05), this evidence suggests that Hg may be not easily released in solution following mineral weathering (Fu et al. 2010).

Contrary to what was expected as the result of tetrahedrite and tennantite oxidation resulting in the release of Sb and As in solution (Borčinová Radková et al. 2017; Hiller et al. 2013), As behaved differently in terms of mobility with respect to Sb under oxidising conditions (Hiller et al. 2012). Indeed, according to Majzlan et al. (2018), Sb is generally more mobile and easily released during weathering of tetrahedrite-rich mining waste than As (50% and 10% of release for Sb and As, respectively) which is commonly involved in attenuation processes as the result of adsorption/precipitation of Fe oxyhydroxides (Casiot et al. 2007; Hiller et al. 2012). However, although Fe oxyhydroxides (HFO) may play a crucial role in regulating the mobility of both As and Sb (Herath et al. 2017; Ritchie et al. 2013 and references therein), this did not appeared to be a dominant process in the investigated area where 1) a small amount of primary Fe sulfides were reported, and subsequently secondary HFOs are present and 2) absence of correlation between As-Sb and Fe in the solid matrix, whereas the latter showed slightly constant concentration in all the investigated stream sediments (3.68 ± 1.00 %). According to Craw et al. (2004), in the absence of attenuation processes mediated by Fe oxy-hydroxides, Sb may be readily leached from mine tailings and deposits and dispersed in the surrounding environment. In contrast, some natural attenuation process of Sb could act in the Mt. Avanza district.

The formation of the so-called “antimony ochre” is related to Sb secondary minerals in the form of coatings which are a product of alteration from tetrahedrite minerals. Such supergene minerals could be constituted by oxide minerals from the Roméite group ($A_2B_2X_6Y$ formula in which Sb^{5+} predominated in the B-site) (Álvarez-Ayuso 2021; Lopes et al. 2021; Borčinová Radková et al. 2017; Bortolozzi et al. 2015). It is less likely but not impossible that the attenuation could be also helped by the formation of Fe antimonates such as tripuhyite ($FeSbO_4$) (Berlepsch et al. 2003). Such attenuation processes could limit the release of Sb in water being interesting potential natural attenuation processes that should be more thoroughly investigated in the future.

In this study, the Sb/As ratio in water clearly decreased by moving downstream from the mining district (5.09 – 18.3 at the mining district to values <1 downstream) and the mine drainage water generally showed low As content (mean 1.42 ± 0.84 µg/L) as well as both stream water collected from the main stream (mean 1.35 ± 0.94 µg/L) and its secondary tributaries (1.53 ± 1.46 µg/L). Antimony (Sb) appeared to be more mobile in the aquatic environment since it can be more easily desorbed and released with respect to As from tetrahedrite-bearing rocks of the mine drainage system in most of the mine drainage waters (Fu et al. 2010; Hiller et al. 2012) (Fig. 9), most likely due to the fact that Sb adsorption notably decreases with increasing pH (Filella et al. 2002b; Leuz et al. 2006; Martínez-Lladó et al. 2008).

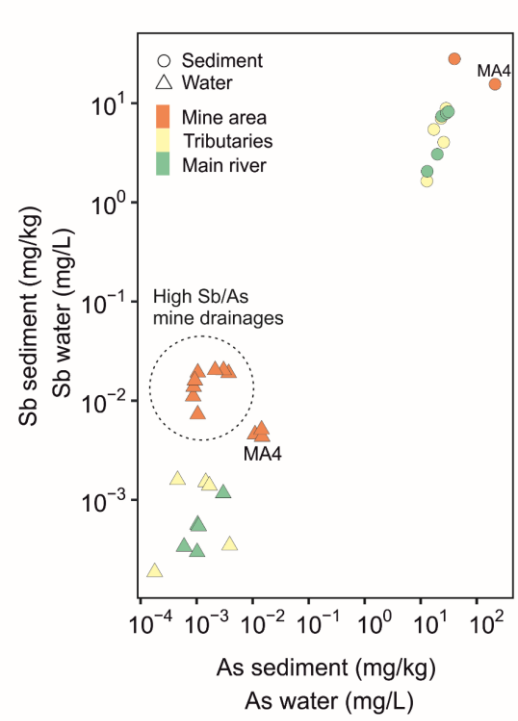

Fig. 9 Correlation between Sb and As in water and sediments collected from the Mt. Avanza mining district.

Regarding the general water quality, due to a lack of proper national guidelines concerning water draining mineral deposits, the results from this research may only be compared to the Italian regulatory threshold limits for contaminated groundwaters (Italian D.Lgs. 152/2006 according to EU Directive 2000/60/EC and 2008/105/CE) highlighting a persistent Sb or As exceeding of the limit values (5 and 10 µg/L, respectively) in almost all the mine drainage water (Fig. 8). This is especially evident in the case of Sb since non-contaminated water usually shows concentrations below 1 µg/L (Filella et al. 2002a).

3.4 Gaseous Elemental Mercury (GEM) occurrence in the mining district

The GEM concentrations recorded during the field survey within the Mt. Avanza mining site were relatively low, ranging between values below the instrumental LOD (2 ng/m^3) up to a maximum of 25.4 ng/m^3 (Table 2), with a mean GEM concentration of 4.78 ± 3.61 ng/m^3. These values were slightly higher than the estimated natural background of atmospheric GEM for the Northern Hemisphere (1.5 - 1.7 ng/m^3, Sprovieri et al. 2010) and not far from those recorded during a year-long monitoring at the remote site of Col Margherita, located ~75 km WSW from our study area in the North-Eastern Italian Alps (mean 3.14 ± 1.29 ng/m^3; Vardè et al. 2022). Moreover, similar peak values of atmospheric GEM (up to 48.5 ng/m^3) were reported for the other Hg impacted coastal, lagoonal areas and alluvial

plains of the Friuli Venezia Giulia region (Acquavita et al., 2022; Barago et al., 2020; Floreani et al., 2020), which suffered extended contamination due to the transport by the Isonzo River of Hg-enriched material from the Idrija cinnabar mine, located ~100 km upstream these locations (Acquavita et al. 2022; Covelli et al. 2001, 2007). Overall, in the surroundings of the mining district, peaks of GEM concentrations higher than 15 ng/m^3 were observed above the abandoned waste rock piles and along the roads where Hg-rich material was used for construction of the various facilities (Fig. 10).

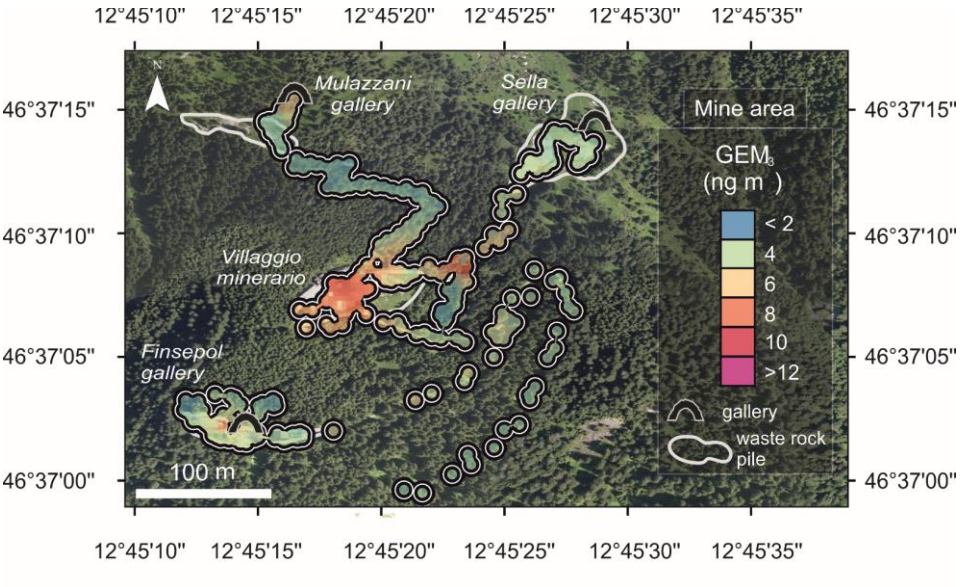

Fig. 10 Detail of the spatial distribution of atmospheric GEM concentration at the Mt. Avanza mining site.

The spatial distribution of GEM in the study area roughly corresponded to that of Hg concentrations in soils and waste rock piles (Fig. 3), supporting the hypothesis of emission from the Hg-rich substrate. As observed at other former Hg-mining sites, abandoned wastes and contaminated soils can represent relevant sources of this metal into the atmosphere even for decades after mining and metallurgical activities have ceased (e.g., Floreani et al., 2023; Higueras et al. 2013; Loredo et al. 2007; Nacht et al. 2004; Yan et al. 2019).

The highest mean GEM concentrations (9.47 ± 4.16 ng/m^3) were indeed observed at the waste rock pile by "Villaggio Minerario" (Fig. 2b and 9), characterised by high Hg concentration in the substrate (up to 56.9 mg/kg). Moreover, these measurements were taken during the period of maximum irradiation, at midday, when the enhanced formation of GEM through photoreduction and a following evasion is expected (Dalziel and Tordon 2014; Fantozzi et al. 2013; Floreani et al., 2023; Kotnik et al. 2005) also considering the lack of vegetation cover on the waste rock piles (Loredo et al. 2007). Reduced GEM emission due to a more extended vegetation cover above the residues could therefore explain the lower GEM concentration recorded at the waste rock pile near the "Finsepol" gallery, despite a higher average Hg content in the substrate than in the "Villaggio Minerario" area. As observed in other field studies (e.g. Coolbaugh et al. 2002; Floreani et al., 2023), vegetation significantly reduces GEM release from enriched substrates compared to bare areas: this effect can be attributed to the reduction of solar radiation reaching the surface, which decreases the GEM generation rate through photo-reduction (Liu et al. 2014). Moreover, lower GEM emission under canopy shading may also be related to lower soil temperatures, which limit the diffusion of GEM to the atmosphere and can affect the rates of microbial reactions involved in Hg reduction (Mazur et al. 2014; Yuan et al. 2019).

Lower GEM values were found at a waste rock pile near the entrance of the "Sella" gallery, characterised by lower Hg concentration in the substrate (up to 13.3 mg/kg) possibly due to the burial of residues containing tetrahedrite, which reduced the amount of Hg in surface layers available for evasion in gaseous form. Remediation of Hg-rich wastes by covering with inert material, soil and vegetation has proven to be effective at significantly reducing GEM concentrations in the air, as previously reported for the Almadén (Spain) and Tongren (China) Hg-mining districts (Higueras et al. 2013; Yan et al. 2019).

Slight increases in GEM concentrations from background levels (up to ~10 ng/m^3) were observed near the entrances of the "Finsepol" and "Mulazzani" mine galleries, likely due to the occurrence of Hg in mineral phases similar to that observed by Higueras et al. (2012) in the Potosì mining area (Bolivia), where the occurrence of

tetrahedrite was reported. The values of GEM in the air observed in that area were similar to those found in this study at Mt. Avanza, although concentrations from hundreds to thousands of ng/m^3 are frequently reported in sites characterised by notably elevated Hg contents in substrates, such as near larger former Hg mines and cinnabar roasting plants (e.g. Ao et al. 2017; Fornasaro et al. 2022; Higueras et al. 2013; Kocman et al. 2011).

Far from the above-described point sources, GEM concentrations dropped to values similar to the natural background within distances of ~100 m, likely due to efficient atmospheric dilution in the mixing layer under the sunny weather conditions which occurred during sampling (Cabassi et al. 2017). Similar spatial patterns characterised by sharp decreases in GEM within few hundreds of meters from the emission source, independently from its absolute importance, were also observed at world-class Hg-mining districts such as Almadén (Esbrí et al. 2020, Llanos et al. 2010) and Mt. Amiata (Vaselli et al. 2013) confirming the importance of atmospheric dilution processes in regulating GEM dispersion. Indeed, GEM concentration observed in nearby Forni Avoltri and Pierabech rural areas, were relatively low due to dilution processes, (mean 2.20 ± 0.76 ng/m^3, max = 4.50 ng/m^3, Table 2) even though in the past such villages were the sites of roasting plants and furnaces. Moreover, as forest ecosystems can serve as net sinks for atmospheric Hg (Yuan et al. 2019), GEM spatial spreading could also be limited through canopy scavenging by local coniferous vegetation thanks to stomatal uptake and depositions through litterfall and throughfall (Wright et al. 2016). Several studies reported higher total Hg depositions in coniferous rather than deciduous forests (Blackwell and Driscoll 2015; Demers et al. 2007; Witt et al. 2009): this, coupled with reduced emissions from the forest floor generally observed in these ecosystems (Agnan et al. 2016) can result in the notable accumulation of Hg in soils (Blackwell and Driscoll 2015; Richardson and Friedland 2015). Further research is needed to assess GEM levels, especially in summer, under conditions of high irradiation and temperatures more conducive for Hg release, and thus to quantify the role of the gaseous exchanges in controlling the atmospheric Hg pool at the Mt. Avanza district.

4 CONCLUSIONS

The geochemical signature of the past mining activity at the fahlore Cu-Sb(-Ag) Mt. Avanza ore deposit was evidenced by notable concentrations of the elements associated with the (Hg-Zn)-rich tetrahedrite in mine wastes, soils and stream sediments (max: Cu = 4019 mg/kg, Sb = 1049 mg/kg, Pb = 1216 mg/kg, Zn = 1204 mg/kg, As = 654 mg/kg and Hg = 473 mg/kg). Results from this research suggest that extraction activities as well as the by-products employed in the constructions of roads and mine facilities contribute to a heterogeneous distribution of PTE concentrations in the soil matrix. Conversely, notable amounts of PTEs in the stream sediments appeared to be restricted to the mining area as shown by the general decrease in the PTE concentrations with increasing distance from the source area. This was confirmed by the I_{geo} index values which were found to be significantly high inside the mine area. Interestingly, thallium (Tl) and germanium (Ge) are associated with the "lithogenic components" substituting K and Si in silicate minerals, respectively, and are not associated to the ore-bearing minerals like in many other base metal ore deposits (e.g., carbonate-hosted Pb-Zn ores).

Regarding solid-water interactions, the water draining the mining district belonged to a "Neutral Mine Drainage" (NMD) as the result of pH buffering effects due to dissolution of the Devonian carbonate host rocks, promoting the release of Sb, which was found to be generally more mobile than As in solution. Although mine drainages often exceeded the national regulatory limits for Sb and As, relatively low dissolved concentrations of the main metal(loid)s were observed, suggesting the moderate stability of the tetrahedrite and other minor ore-bearing minerals as well as the occurrence of natural attenuation processes along the river system, most likely due to dilution, (co-)precipitation and potential sorption processes.

Surprisingly, the geochemical behaviour of Hg in the fahlore site appeared similar to cinnabar deposits investigated around the world. Indeed, dissolved Hg concentrations were generally very low compared to other metal(loid)s such as As, Cu and Sb, testifying to the weak solubility of this element which remained partitioned in the crystalline structures. However, similar to other cinnabar mining sites, the Hg-rich ore-bearing substrate was identified as a potential source of Hg into the atmosphere and real-time measurements of GEM were confirmed as a suitable preliminary tool to identify mine wastes and Hg contaminated solid environmental matrices.

Acknowledgments: The authors are very grateful to Roberto Zucchini and Giuseppe Muscio of the "Museo Friulano di Storia Naturale" for their help and their broad knowledge about the mining activity in FVG, to Carlo Corradini for his valuable help regarding the geological setting and to the Forni Avoltri Forestry Corp for their help programming the field activities. A special thanks to Sara Oberti di Valnera of the Regional Geogical Survey of Friuli Venezia Giulia for supporting the research. The authors are also very grateful to Karry Close for proofreading.
Author contributions: Sampling was performed by Nicolò Barago, Cristiano Mastroianni, Stefano Covelli. Chemical analyses and data processing was performed by Nicolò Barago, Cristiano Mastroianni, Elena Pavoni, Federico Floreani, Filippo Parisi, Davide Lenaz. The first draft of the manuscript was written by Nicolò Barago, Cristiano Mastroianni, Elena Pavoni, Federico Floreani and Stefano Covelli. All authors have contributed and agreed to the published version of the manuscript.
Funding: This work was partially realised under the partnership between the University of Trieste and the Regional Direction for the Environment of Friuli Venezia Giulia (LR 23/2013, art. 4), which provided financial support.
Competing interests: The authors declare no competing interests.
Ethical approval: Not applicable.
Consent to participate: Not applicable.
Consent to publish: Not applicable.
Availability of data and materials: Data available on request from the authors.

References

Acquavita A, Brandolin D, Cattaruzza C, et al (2022) Mercury distribution and speciation in historically contaminated soils of the Isonzo River Plain (NE Italy). J Soils Sediments 22:79–92. https://doi.org/10.1007/s11368-021-03038-2

Agnan Y, Le Dantec T, Moore CW, et al (2016) New Constraints on Terrestrial Surface–Atmosphere Fluxes of Gaseous Elemental Mercury Using a Global Database. Environ Sci Technol 50:507–524. https://doi.org/10.1021/acs.est.5b04013

Aguilar-Carrillo J, Velázquez A, Gutiérrez EJ, Reyes-Domínguez IA (2022) Partitioning and mobility of arsenic (As) and lead (Pb) in an ancient Pb–Zn mine in central Mexico: Role of amorphous ferric arsenate. Appl Geochem 136:105172. https://doi.org/10.1016/j.apgeochem.2021.105172

Álvarez-Ayuso E (2021) Stabilization and encapsulation of arsenic-/antimony-bearing mine waste: Overview and outlook of existing techniques. Crit Rev Environ Sci Technol 1–33. https://doi.org/10.1080/10643389.2021.1944588

Ao M, Meng B, Sapkota A, et al (2017) The influence of atmospheric Hg on Hg contaminations in rice and paddy soil in the Xunyang Hg mining district, China. Acta Geochim 36:181–189. https://doi.org/10.1007/s11631-017-0142-x

APAT, IRSA-CNR (2003) Metodi analitici per le acque. Volume primo. Manuali e Linee Guida 29/2003.

Apopei AI, Damian G, Buzgar N, Buzatu A (2016) Mineralogy and geochemistry of Pb–Sb/As-sulfosalts from Coranda-Hondol ore deposit (Romania) — Conditions of telluride deposition. Ore Geol Rev 72:857–873. https://doi.org/10.1016/j.oregeorev.2015.09.014

Artioli G, Canovaro C, Nimis P, Angelini I (2020) LIA of Prehistoric Metals in the Central Mediterranean Area: A Review. Archaeometry 62:53–85. https://doi.org/10.1111/arcm.12542

Baptista-Salazar C, Richard J-H, Horf M, et al (2017) Grain-size dependence of mercury speciation in river suspended matter, sediments and soils in a mercury mining area at varying hydrological conditions. Appl Geochem 81:132–142. https://doi.org/10.1016/j.apgeochem.2017.04.006

Barago N, Floreani F, Acquavita A, et al (2020) Spatial and Temporal Trends of Gaseous Elemental Mercury over a Highly Impacted Coastal Environment (Northern Adriatic, Italy). Atmosphere 11:935. https://doi.org/10.3390/atmos11090935

Barago N, Covelli S, Mauri M, et al (2021) Prediction of Trace Metal Distribution in a Tailings Impoundment Using an Integrated Geophysical and Geochemical Approach (Raibl Mine, Pb-Zn Alpine District, Northern Italy). Int J Environ Res Public Health 18:1157. https://doi.org/10.3390/ijerph18031157

Barago N, Pavoni E, Floreani F, et al (2023) Hydrogeochemistry of thallium and other potentially toxic elements in neutral mine drainage at the decommissioned Pb-Zn Raibl mine (Eastern Alps, Italy). J Geochem Explor 245:107129. https://doi.org/10.1016/j.gexplo.2022.107129

Berlepsch P, Armbruster T, Brugger J, et al (2003) Tripuhyite, FeSbO4, revisited. Mineral Mag 67:31–46. https://doi.org/10.1180/0026461036710082

Biagioni C, George LL, Cook NJ, et al (2020a) The tetrahedrite group: Nomenclature and classification. Am Mineral 105:109–122. https://doi.org/10.2138/am-2020-7128

Biagioni C, Sejkora J, Musetti S, et al (2020b) Tetrahedrite-(Hg), a new 'old' member of the tetrahedrite group. Mineral Mag 84:584–592. https://doi.org/10.1180/mgm.2020.36

Biester H, Gosar M, Covelli S (2000) Mercury Speciation in Sediments Affected by Dumped Mining Residues in the Drainage Area of the Idrija Mercury Mine, Slovenia. Environ Sci Technol 34:3330–3336. https://doi.org/10.1021/es991334v

Blackwell BD, Driscoll CT (2015) Deposition of Mercury in Forests along a Montane Elevation Gradient. Environ Sci Technol 49:5363–5370. https://doi.org/10.1021/es505928w

Borčinová Radková A, Jamieson H, Lalinská-Voleková B, et al (2017) Mineralogical controls on antimony and arsenic mobility during tetrahedrite-tennantite weathering at historic mine sites Špania Dolina-Piesky and Ľubietová-Svätodušná, Slovakia. Am Mineral 102:1091–1100. https://doi.org/10.2138/am-2017-5616

Bortolozzi G, Ciriotti ME, Bittarello E, Möckel S (2015) Monte Avanza, Forni Avoltri, Carnia (Udine, Friuli-Venezia Giulia): conferme e nuovi ritrovamenti. Micro 13:2–39

Brigo L, Camana G, Rodeghiero F, Potenza R (2001) Carbonate-hosted siliceous crust type mineralization of Carnic Alps (Italy-Austria). Ore Geol Rev 17:199–214

Brigo L, Dulski P, Möller P, et al (1988) Strata-Bound Mineralizations in the Carnic Alps/Italy. In: Boissonnas J, Omenetto P (eds) Mineral Deposits within the European Community. Springer Berlin Heidelberg, Berlin, Heidelberg, pp 485–498

Brime C, Perri MC, Pondrelli M, et al (2008) Polyphase metamorphism in the eastern Carnic Alps (N Italy–S Austria): clay minerals and conodont Colour Alteration Index evidence. Int J Earth Sci 97:1213–1229. https://doi.org/10.1007/s00531-007-0218-7

Cabassi J, Tassi F, Venturi S, et al (2017) A new approach for the measurement of gaseous elemental mercury (GEM) and H 2 S in air from anthropogenic and natural sources: Examples from Mt. Amiata (Siena, Central Italy) and Solfatara Crater (Campi Flegrei, Southern Italy). J Geochem Explor 175:48–58. https://doi.org/10.1016/j.gexplo.2016.12.017

Carmona M, Llanos W, Higueras P, Kocman D (2013) Mercury emissions in equilibrium: a novel approach for the quantification of mercury emissions from contaminated soils. Anal Methods 5:2793. https://doi.org/10.1039/c3ay25700b

Casari L (1996) Tetrahedrite-tennantite series in the Carnic chain (Eastern Alps, Italy). Neues Jahrb Mineral-Monatshefte 193–200

Casiot C, Ujevic M, Munoz M, et al (2007) Antimony and arsenic mobility in a creek draining an antimony mine abandoned 85 years ago (upper Orb basin, France). Appl Geochem 22:788–798. https://doi.org/10.1016/j.apgeochem.2006.11.007

Chiarantini L, Benvenuti M, Beutel M, et al (2016) Mercury and Arsenic in Stream Sediments and Surface Waters of the Orcia River Basin, Southern Tuscany, Italy. Water Air Soil Pollut 227:408. https://doi.org/10.1007/s11270-016-3110-x

Choi H-D, Holsen TM (2009) Gaseous mercury emissions from unsterilized and sterilized soils: The effect of temperature and UV radiation. Environ Pollut 157:1673–1678. https://doi.org/10.1016/j.envpol.2008.12.014

Ciobanu CL, Cook NJ, Capraru N, et al (2005) Mineral assemblages from the vein salband at Sacarimb, Golden Quadrilateral, Romania: I. Sulphides and sulphosalts. Bulg Acad Sci Geochem Mineral Petrol 43:47–55

Ciriotti ME, Möckel S, Blaß G, Bortolozzi G (2006) Cualstibite: ritrovamenti italiani. Micro 19–24

Coolbaugh M, Gustin M, Rytuba J (2002) Annual emissions of mercury to the atmosphere from natural sources in Nevada and California. Environ Geol 42:338–349. https://doi.org/10.1007/s00254-002-0557-4

Covelli S, Faganeli J, Horvat M, Brambati A (2001) Mercury contamination of coastal sediments as the result of long-term cinnabar mining activity (Gulf of Trieste, northern Adriatic sea). Appl Geochem 16:541–558. https://doi.org/10.1016/S0883-2927(00)00042-1

Covelli S, Piani R, Acquavita A, et al (2007) Transport and dispersion of particulate Hg associated with a river plume in coastal Northern Adriatic environments. Mar Pollut Bull 55:436–450. https://doi.org/10.1016/j.marpolbul.2007.09.006

Craw D, Wilson N, Ashley P m. (2004) Geochemical controls on the environmental mobility of Sb and As at mesothermal antimony and gold deposits. Appl Earth Sci 113:3–10. https://doi.org/10.1179/037174504225004538

Dalziel J, Tordon R (2014) Gaseous mercury flux measurements from two mine tailing sites in the Seal Harbour area of Nova Scotia. Geochem Explor Environ Anal 14:17. https://doi.org/10.1144/geochem2011-112

De Giudici G, Medas D, Cidu R, et al (2019) Assessment of origin and fate of contaminants along mining-affected Rio Montevecchio (SW Sardinia, Italy): A hydrologic-tracer and environmental mineralogy study. Appl Geochem 109:104420. https://doi.org/10.1016/j.apgeochem.2019.104420

Demers JD, Driscoll CT, Fahey TJ, Yavitt JB (2007) Mercury cycling in litter and soil in different forest types in the Adirondack region, New York, USA. Ecol Appl 17:1341–1351. https://doi.org/10.1890/06-1697.1

DFG (1994) Deutsche Forschungsgemeinschaft. Analysis of Hazardous Substances in Biological Materials, VCH, Weinheim, p. 51.

Di Benedetto F, Bernardini GP, Borrini D, et al (2002) Crystal chemistry of tetrahedrite solid-solution: EPR and magnetic investigations. Can Mineral 40:837–847. https://doi.org/10.2113/gscanmin.40.3.837

Di Colbertaldo D (1960) Le risorse di minerali metallici in Friuli. Ind Mineraria 559–569

Doglioni C (1988) Examples of strike-slip tectonics on platform-basin margins. Tectonophysics 156:293–302. https://doi.org/10.1016/0040-1951(88)90066-2

Dondi M, Palenzona A, Puggioli G (1995) La miniera di Monte Avanza, Forni Avoltri (UD). Riv Mineral Ital 2:125–136

D'Orazio M, Biagioni C, Dini A, Vezzoni S (2017) Thallium-rich pyrite ores from the Apuan Alps, Tuscany, Italy:constraints for their origin and environmental concerns. Miner Deposita 52:687–707. https://doi.org/10.1007/s00126-016-0697-1

Driscoll CT, Mason RP, Chan HM, et al (2013) Mercury as a Global Pollutant: Sources, Pathways, and Effects. Environ Sci Technol 47:4967–4983. https://doi.org/10.1021/es305071v

Esbrí JM, Higueras PL, Martínez-Coronado A, Naharro R (2020) 4D dispersion of total gaseous mercury derived from a mining source: identification of criteria to assess risks related to high concentrations of atmospheric mercury. Atmospheric Chem Phys 20:12995–13010. https://doi.org/10.5194/acp-20-12995-2020

Esbrí JM, Bernaus A, Ávila M, et al (2010) XANES speciation of mercury in three mining districts – Almadén, Asturias (Spain), Idria (Slovenia). J Synchrotron Radiat 17:179–186. https://doi.org/10.1107/S0909049510001925

Fantozzi L, Ferrara R, Dini F, et al (2013) Study on the reduction of atmospheric mercury emissions from mine waste enriched soils through native grass cover in the Mt. Amiata region of Italy. Environ Res 125:69–74. https://doi.org/10.1016/j.envres.2013.02.004

Feruglio G (1966) Il giacimento cuprifero del Monte Avanza in Carnia. Symp Internazionale Sui Giacimenti Minerari Delle Alpi Mendola Trento Italia

Filella M, Belzile N, Chen Y-W (2002a) Antimony in the environment: a review focused on natural waters I. Occurrence. Earth-Sci Rev 57:125–176

Filella M, Belzile N, Chen Y-W (2002b) Antimony in the environment: a review focused on natural waters II. Relevant solution chemistry. Earth-Sci Rev 59:265–285

Floreani F, Barago N, Acquavita A, et al (2020) Spatial Distribution and Biomonitoring of Atmospheric Mercury Concentrations over a Contaminated Coastal Lagoon (Northern Adriatic, Italy). Atmosphere 11:1280. https://doi.org/10.3390/atmos11121280

Floreani F, Zappella V, Faganeli J, et al (2023) Gaseous mercury evasion from bare and grass-covered soils contaminated by mining and ore roasting (Isonzo River alluvial plain, Northeastern Italy). Environ Pollut 318:120921. https://doi.org/10.1016/j.envpol.2022.120921

Fornasaro S, Morelli G, Rimondi V, et al (2022) Mercury distribution around the Siele Hg mine (Mt. Amiata district, Italy) twenty years after reclamation: Spatial and temporal variability in soil, stream sediments, and air. J Geochem Explor 232:106886. https://doi.org/10.1016/j.gexplo.2021.106886

Fu Z, Wu F, Amarasiriwardena D, et al (2010) Antimony, arsenic and mercury in the aquatic environment and fish in a large antimony mining area in Hunan, China. Sci Total Environ 408:3403–3410. https://doi.org/10.1016/j.scitotenv.2010.04.031

Galili T, O'Callaghan A, Sidi J, Sievert C (2018) heatmaply: an R package for creating interactive cluster heatmaps for online publishing. Bioinformatics 34:1600–1602. https://doi.org/10.1093/bioinformatics/btx657

Garcia-Ordiales E, Cienfuegos P, Roqueñí N, et al (2019) Historical accumulation of potentially toxic trace elements resulting from mining activities in estuarine salt marshes sediments of the Asturias coastline (northern Spain). Environ Sci Pollut Res 26:3115–3128. https://doi.org/10.1007/s11356-017-0449-5

Garcia-Ordiales E, Loredo J, Covelli S, et al (2017) Trace metal pollution in freshwater sediments of the world's largest mercury mining district: sources, spatial distribution, and environmental implications. J Soils Sediments 17:1893–1904. https://doi.org/10.1007/s11368-016-1503-5

Gosar M, Pirc S, Bidovec M (1997) Mercury in the Idrijca River sediments as a reflection of mining and smelting activities of the Idrija mercury mine. J Geochem Explor 58:125–131. https://doi.org/10.1016/S0375-6742(96)00064-7

Gosar M, Teršič T (2012) Environmental geochemistry studies in the area of Idrija mercury mine, Slovenia. Environ Geochem Health 34:27–41. https://doi.org/10.1007/s10653-011-9410-6

Gray JE, Hines ME, Higueras PL, et al (2004) Mercury Speciation and Microbial Transformations in Mine Wastes, Stream Sediments, and Surface Waters at the Almadén Mining District, Spain. Environ Sci Technol 38:4285–4292. https://doi.org/10.1021/es040359d

Gray JE, Rimondi V, Costagliola P, et al (2014) Long-distance transport of Hg, Sb, and As from a mined area, conversion of Hg to methyl-Hg, and uptake of Hg by fish on the Tiber River basin, west-central Italy. Environ Geochem Health 36:145–157. https://doi.org/10.1007/s10653-013-9525-z

Gray JE, Theodorakos PM, Fey DL, Krabbenhoft DP (2015) Mercury concentrations and distribution in soil, water, mine waste leachates, and air in and around mercury mines in the Big Bend region, Texas, USA. Environ Geochem Health 37:35–48. https://doi.org/10.1007/s10653-014-9628-1

Hall AJ (1972) Substitution of Cu by Zn, Fe and Ag in synthetic tetrahedrite, Cu12Sb4S13. Bull Minéralogie 95:583–594. https://doi.org/10.3406/bulmi.1972.6736

Handy MR, Ustaszewski K, Kissling E (2015) Reconstructing the Alps–Carpathians–Dinarides as a key to understanding switches in subduction polarity, slab gaps and surface motion. Int J Earth Sci 104:1–26. https://doi.org/10.1007/s00531-014-1060-3

Herath I, Vithanage M, Bundschuh J (2017) Antimony as a global dilemma: Geochemistry, mobility, fate and transport. Environ Pollut 223:545–559. https://doi.org/10.1016/j.envpol.2017.01.057

Higueras P, Esbrí JM, Oyarzun R, et al (2013) Industrial and natural sources of gaseous elemental mercury in the Almadén district (Spain): An updated report on this issue after the ceasing of mining and metallurgical activities in 2003 and major land reclamation works. Environ Res 125:197–208. https://doi.org/10.1016/j.envres.2012.10.011

Higueras P, Llanos W, García ME, et al (2012) Mercury vapor emissions from the Ingenios in Potosí (Bolivia). J Geochem Explor 116–117:1–7. https://doi.org/10.1016/j.gexplo.2011.05.004

Higueras P, Oyarzun R, Lillo J, et al (2006) The Almadén district (Spain): Anatomy of one of the world's largest Hg-contaminated sites. Sci Total Environ 356:112–124. https://doi.org/10.1016/j.scitotenv.2005.04.042

Hiller E, Lalinská B, Chovan M, et al (2012) Arsenic and antimony contamination of waters, stream sediments and soils in the vicinity of abandoned antimony mines in the Western Carpathians, Slovakia. Appl Geochem 27:598–614. https://doi.org/10.1016/j.apgeochem.2011.12.005

Hiller E, Petrák M, Tóth R, et al (2013) Geochemical and mineralogical characterization of a neutral, low-sulfide/high-carbonate tailings impoundment, Markušovce, eastern Slovakia. Environ Sci Pollut Res 20:7627–7642. https://doi.org/10.1007/s11356-013-1581-5

Hines ME, Horvat M, Faganeli J, et al (2000) Mercury Biogeochemistry in the Idrija River, Slovenia, from above the Mine into the Gulf of Trieste. Environ Res 83:129–139. https://doi.org/10.1006/enrs.2000.4052

Hinkley TK, Lamothe PJ, Wilson SA, et al (1999) Metal emissions from Kilauea, and a suggested revision of the estimated worldwide metal output by quiescent degassing of volcanoes. Earth Planet Sci Lett 170:315–325. https://doi.org/10.1016/S0012-821X(99)00103-X

Hounslow AW (1980) Ground-water geochemistry: arsenic in landfills. Ground Water 18:331–333

Johnson NE, Craig JR, Rimstidt JD (1987) Effect of substitutions on the cell dimension of tetrahedrite. Can Mineral 25:237–244

Johnson NE, Craig JR, Rimstidt JD (1986) Compositional trends in tetrahedrite. Can Mineral 24:385–397

Karup-Møller S, Makovicky E (2003) Exploratory studies of element substitutions in synthetic tetrahedrite. Part V.Mercurian tetrahedrite. Neues Jahrb Für Mineral - Abh 179:73–83. https://doi.org/10.1127/0077-7757/2003/0179-0073

Kocman D, Kanduč T, Ogrinc N, Horvat M (2011) Distribution and partitioning of mercury in a river catchment impacted by former mercury mining activity. Biogeochemistry 104:183–201. https://doi.org/10.1007/s10533-010-9495-5

Kotnik J, Horvat M, Dizdarevic T (2005) Current and past mercury distribution in air over the Idrija Hg mine region, Slovenia. Atmos Environ 39:7570–7579. https://doi.org/10.1016/j.atmosenv.2005.06.061

Leach DL, Taylor RD, Fey DL, et al (2010) A Deposit Model for Mississippi Valley-Type Lead-Zinc Ores. Miner Depos Models Resour Assess Chapter A:52 p.

Leuz A-K, Mönch H, Johnson CA (2006) Sorption of Sb(III) and Sb(V) to Goethite: Influence on Sb(III) Oxidation and Mobilization. Environ Sci Technol 40:7277–7282. https://doi.org/10.1021/es061284b

Li C, Hao C, Zhang W, Gui H (2020) High Antimony Source and Geochemical Behaviorsin Mine Drainage Water in China's LargestAntimony Mine. Pol J Environ Stud 29:3663–3673. https://doi.org/10.15244/pjoes/114970

Li P, Feng X, Qiu G, et al (2012) Mercury pollution in Wuchuan mercury mining area, Guizhou, Southwestern China: The impacts from large scale and artisanal mercury mining. Environ Int 42:59–66. https://doi.org/10.1016/j.envint.2011.04.008

Liu F, Cheng H, Yang K, et al (2014) Characteristics and influencing factors of mercury exchange flux between soil and air in Guangzhou City. J Geochem Explor 139:115–121. https://doi.org/10.1016/j.gexplo.2013.09.005

Llanos W, Higueras P, Oyarzun R, et al (2010) The MERSADE (European Union) project: Testing procedures and environmental impact for the safe storage of liquid mercury in the Almadén district, Spain. Sci Total Environ 408:4901–4905. https://doi.org/10.1016/j.scitotenv.2010.05.026

Lopes G, Atencio D, Ellena J, Andrade M (2021) Roméite-Group Minerals Review: New Crystal Chemical and Raman Data of Fluorcalcioroméite and Hydroxycalcioroméite. Minerals 11:1409. https://doi.org/10.3390/min11121409

Loredo J, Soto J, Álvarez R, Ordóñez A (2007) Atmospheric Monitoring at Abandoned Mercury Mine Sites in Asturias (NW Spain). Environ Monit Assess 130:201–214. https://doi.org/10.1007/s10661-006-9389-0

Lowry GV, Shaw S, Kim CS, et al (2004) Macroscopic and Microscopic Observations of Particle-Facilitated Mercury Transport from New Idria and Sulphur Bank Mercury Mine Tailings. Environ Sci Technol 38:5101–5111. https://doi.org/10.1021/es034636c

Lyubimtseva NG, Bortnikov NS, Borisovsky SE (2019) Coexisting Bournonite–Seligmannite and Tennantite–Tetrahedrite Solid Solutions of the Darasun Gold Deposit, Eastern Transbaikalia, Russia: Estimation of the Mineral Formation Temperature. Geol Ore Depos 61:274–291. https://doi.org/10.1134/S1075701519030061

MacDonald DD, Ingersoll CG, Berger TA (2000) Development and Evaluation of Consensus-Based Sediment Quality Guidelines for Freshwater Ecosystems. Arch Environ Contam Toxicol 39:20–31. https://doi.org/10.1007/s002440010075

Majzlan J, Kiefer S, Herrmann J, et al (2018) Synergies in elemental mobility during weathering of tetrahedrite [(Cu,Fe,Zn)12(Sb,As)4S13]: Field observations, electron microscopy, isotopes of Cu, C, O, radiometric dating, and water geochemistry. Chem Geol 488:1–20. https://doi.org/10.1016/j.chemgeo.2018.04.021

Martínez-Lladó X, de Pablo J, Giménez J, et al (2008) Sorption of Antimony (V) onto Synthetic Goethite in Carbonate Medium. Solvent Extr Ion Exch 26:289–300. https://doi.org/10.1080/07366290802053637

Mazur M, Mitchell CPJ, Eckley CS, et al (2014) Gaseous mercury fluxes from forest soils in response to forest harvesting intensity: A field manipulation experiment. Sci Total Environ 496:678–687. https://doi.org/10.1016/j.scitotenv.2014.06.058

Mozgova NN, Tsepin AI, Ozerova NN, et al (1979) Mercuriferous grey copper ores. [in Russian]. Zap Vsesoyuznogo Mineral Obshchestva 108:437–452

Müller G (1969) Index of geoaccumulation in sediments of the Rhine River. J Geol 2:108–119

Müller HW, Schwaighofer B, Kalman W (1994) Heavy metal contents in river sediments. Water Air Soil Pollut 72:191–203. https://doi.org/10.1007/BF01257124

Nacht DM, Gustin MS, Engle MA, et al (2004) Atmospheric Mercury Emissions and Speciation at the Sulphur Bank Mercury Mine Superfund Site, Northern California. Environ Sci Technol 38:1977–1983. https://doi.org/10.1021/es0304244

Pavoni E, Covelli S, Adami G, et al (2018) Mobility and fate of Thallium and other potentially harmful elements in drainage waters from a decommissioned Zn-Pb mine (North-Eastern Italian Alps). J Geochem Explor 188:1–10. https://doi.org/10.1016/j.gexplo.2018.01.005

Pavoni E, Petranich E, Adami G, et al (2017) Bioaccumulation of thallium and other trace metals in Biscutella laevigata nearby a decommissioned zinc-lead mine (Northeastern Italian Alps). J Environ Manage 186:214–224. https://doi.org/10.1016/j.jenvman.2016.07.022

Perotti M, Petrini R, D'Orazio M, et al (2018) Thallium and Other Potentially Toxic Elements in the Baccatoio Stream Catchment (Northern Tuscany, Italy) Receiving Drainages from Abandoned Mines. Mine Water Environ 37:431–441. https://doi.org/10.1007/s10230-017-0485-x

Peter ALJ, Viraraghavan T (2005) Thallium: a review of public health and environmental concerns. Environ Int 9

Petrini R, Cidu R, Slejko FF (2016) Thallium Contamination in the Raibl Mine Site Stream Drainage System (Eastern Alps, Italy). Mine Water Environ 35:55–63. https://doi.org/10.1007/s10230-015-0346-4

Piper AM (1944) A graphic procedure in the geochemical interpretation of water-analyses. Eos Trans Am Geophys Union 25:914–928. https://doi.org/10.1029/TR025i006p00914

Pirri IV (1977) Le paragenesi a Zn, Cu, Pb, Sb, Hg, Ni, As, fluorite, barite nel Devonico della Catena Carnica. Rendiconti Soc Ital Mineral E Petrol 33 (2):821–844

Plumlee GS, Smith KS, Montour MR, et al (1999) Geologic controls on the composition of natural waters and mine waters draining diverse mineral-deposit types. In: The Environmental Geochemistry of Mineral Deposits, Part B. Case Studies and Research Topics. Society of Economic Geologists, Littleton, CO, pp 373–432

Richardson JB, Friedland AJ (2015) Mercury in coniferous and deciduous upland forests in northern New England, USA: implications of climate change. Biogeosciences 12:6737–6749. https://doi.org/10.5194/bg-12-6737-2015

Ritchie VJ, Ilgen AG, Mueller SH, et al (2013) Mobility and chemical fate of antimony and arsenic in historic mining environments of the Kantishna Hills district, Denali National Park and Preserve, Alaska. Chem Geol 335:172–188. https://doi.org/10.1016/j.chemgeo.2012.10.016

Rosenberg E (2009) Germanium: environmental occurrence, importance and speciation. Rev Environ Sci Biotechnol 8:29–57. https://doi.org/10.1007/s11157-008-9143-x

Rudnick RL, Gao S (2003) Composition of the Continental Crust. Treatise On Geochemistry. 3, 1-64. 64

Rytuba J (2000) Mercury mine drainage and processes that control its environmental impact. Sci Total Environ 260:57–71. https://doi.org/10.1016/S0048-9697(00)00541-6

Sack RO, Ebel DS (1993) As-Sb Exchange Energies in Tetrahedrite-Tennantite Fahlores and Bournonite-Seligmannite Solid Solutions. Mineral Mag 57:635–642. https://doi.org/10.1180/minmag.1993.057.389.07

Schmid SM, Aebli HR, Heller F, Zingg A (1989) The role of the Periadriatic Line in the tectonic evolution of the Alps. Geol Soc Lond Spec Publ 45:153–171. https://doi.org/10.1144/GSL.SP.1989.045.01.08

Seal II RR, Foley NK (2002) Progress on geoenvironmental models for selected mineral deposit types. U.S. Geological Survey Open-File Report 02-195.

Selin NE (2009) Global Biogeochemical Cycling of Mercury: A Review. Annu Rev Environ Resour 34:43–63. https://doi.org/10.1146/annurev.environ.051308.084314

Sholupov SE, Ganeyev AA (1995) Zeeman atomic absorption spectrometry using high frequency modulated light polarization. Spectrochim Acta Part B At Spectrosc 50:1227–1236. https://doi.org/10.1016/0584-8547(95)01316-7

Shotyk W, Krachler M, Chen B (2004) Antimony in recent, ombrotrophic peat from Switzerland and Scotland: Comparison with natural background values (5,320 to 8,020 14 C yr BP) and implications for the global atmospheric Sb cycle. Glob Biogeochem Cycles 18. https://doi.org/10.1029/2003GB002113

Smedley PL, Kinniburgh DG (2002) A review of the source, behaviour and distribution of arsenic in natural waters. Appl Geochem 17:517–568. https://doi.org/10.1016/S0883-2927(02)00018-5

Smichowski P (2008) Antimony in the environment as a global pollutant: A review on analytical methodologies for its determination in atmospheric aerosols. Talanta 75:2–14. https://doi.org/10.1016/j.talanta.2007.11.005

Spalletta C, Corradini C, Feist R, et al (2021) The Devonian–Carboniferous boundary in the Carnic Alps (Austria and Italy). Palaeobiodiversity Palaeoenvironments 101:487–505. https://doi.org/10.1007/s12549-019-00413-3

Spalletta C, Vai GB, Venturini C (1981) Controllo ambientale e stratigrafico delle mineralizzazioni in calcari devono-dinantiani delle Alpi Carniche. Mem Soc Geol It 22:101–110

Sprovieri F, Pirrone N, Ebinghaus R, et al (2010) A review of worldwide atmospheric mercury measurements. Atmospheric Chem Phys 10:8245–8265. https://doi.org/10.5194/acp-10-8245-2010

UNEP (2019) Global Mercury Assessment 2018. UN Environment Programme, Geneva. https://www.unep.org/resources/publication/global-mercury-assessment-2018

US EPA (1996) EPA Method 3052. Microwave assisted acid digestion of siliceous and organically based matrices.

US EPA (1998) EPA Method 7473 (SW-846) Mercury in solids and solutions by thermal decomposition, amalgamation, and atomic absorption spectrophotometry.

US EPA (1999) Integrated Risk Information System (IRIS) on Antimony, National Center for Environmental Assessment, Office of Research and Development, Washington, DC.

US EPA (2002) EPA Method 1631, Revision E: Mercury in Water by Oxidation, Purge and Trap, and Cold Vapor Atomic Fluorescence Spectrometry.

US EPA (2000) Guidance for Data Quality Assessment: Practical Methods for Data Analysis EPA QA/G-9 QA00 UPDATE; EPA/600/R-96/084.

Vardè M, Barbante C, Barbaro E, et al (2022) Characterization of atmospheric total gaseous mercury at a remote high-elevation site (Col Margherita Observatory, 2543 m a.s.l.) in the Italian Alps. Atmos Environ 271:118917. https://doi.org/10.1016/j.atmosenv.2021.118917

Vaselli O, Higueras P, Nisi B, et al (2013) Distribution of gaseous Hg in the Mercury mining district of Mt. Amiata (Central Italy): A geochemical survey prior the reclamation project. Environ Res 125:179–187. https://doi.org/10.1016/j.envres.2012.12.010

Venturini C (2006) Evoluzione geologica delle Alpi Carniche. Ed Mus Friul Storia Nat - Comune Udine 48:208

Venturini C, Pondrelli M, Fontana C, et al (2001) Carta geologica delle Alpi Carniche - Geological map of the Carnic Alps, scala 1:25.000 (Western sheet: Sappada - M. Dimon).

Wang S, Feng X, Qiu G, et al (2005) Mercury emission to atmosphere from Lanmuchang Hg–Tl mining area, Southwestern Guizhou, China. 7th Int Conf Mercury Glob Pollut 39:7459–7473. https://doi.org/10.1016/j.atmosenv.2005.06.062

Witt EL, Kolka RK, Nater EA, Wickman TR (2009) Influence of the Forest Canopy on Total and Methyl Mercury Deposition in the Boreal Forest. Water Air Soil Pollut 199:3–11. https://doi.org/10.1007/s11270-008-9854-1

Wright LP, Zhang L, Marsik FJ (2016) Overview of mercury dry deposition, litterfall, and throughfall studies. Atmospheric Chem Phys 16:13399–13416. https://doi.org/10.5194/acp-16-13399-2016

Yan J, Wang C, Wang Z, et al (2019) Mercury concentration and speciation in mine wastes in Tongren mercury mining area, southwest China and environmental effects. Appl Geochem 106:112–119. https://doi.org/10.1016/j.apgeochem.2019.05.008

Yuan W, Wang X, Lin C-J, et al (2019) Process factors driving dynamic exchange of elemental mercury vapor over soil in broadleaf forest ecosystems. Atmos Environ 219:117047. https://doi.org/10.1016/j.atmosenv.2019.117047

Zhou J, Nyirenda MT, Xie L, et al (2017) Mine waste acidic potential and distribution of antimony and arsenic in waters of the Xikuangshan mine, China. Appl Geochem 77:52–61. https://doi.org/10.1016/j.apgeochem.2016.04.010

Zucchini R (1998) Miniere e mineralizzazioni nella provincia di Udine. Aspetti storici e mineralogici

Supplementary Material

Table S1 Minimum and maximum values of concentration of the main major and trace elements of mine waste, soil samples in the Mt. Avanza mine area, and sediments sampled in the mine area and downstream in the Avanza-Degano valley.

Parameter	Unit	Waste rock pile (n = 6)	Soil (n = 18)	Sediment (n = 12)
Ag	mg/kg	0.15 - 14.1	<LOD - 5.54	<LOD - 0.65
As	mg/kg	8.20 - 654	12.1 - 162	12.9 - 212
Cd	mg/kg	0.17 - 6.19	0.06 - 2.03	0.10 - 0.65
Cr	mg/kg	6.91 - 88.0	25.0 - 95.1	49.0 - 102
Cu	mg/kg	31.3 - 4019	10.13 - 1556.8	13.97 - 242
Ge	mg/kg	0.20 - 2.26	0.84 - 1.75	1.20 - 2.83
Fe	mg/kg	3248 - 36895	8042 - 39296	20816 - 49918
Hg	mg/kg	1.42 - 473	0.21 - 132	0.04 - 9.15
Mn	mg/kg	138 - 689	185 - 1227	247 - 667
Mo	mg/kg	<LOD - 1.33	0.44 - 1.45	0.59 - 1.69
Pb	mg/kg	19.4 - 397	26.4 - 1216	14.7 - 78.8
Sn	mg/kg	<LOD - 3.92	<LOD - 3.71	<LOD
Sb	mg/kg	5.00 - 1049	2.74 - 153	1.64 - 28.0
Tl	mg/kg	0.09 - 1.07	0.31 - 0.95	0.50 - 1.04
Zn	mg/kg	20.3 - 553	62.0 - 309	57.1 - 171

Table S2 Minimum and maximum values of physico-chemical parameters (pH, T, ORP, EC, TDS, DO), major ions (Ca^{2+}, Mg^{2+}, Na^{+}, K^{+}, F^{-}, Cl^{-}, NO_3^{-}, SO_4^{2-}, CO_3^{2-}, HCO_3^{-}) and trace elements (Ba, As, Cu, Fe, Mn, Mo, Pb, Zn, Sb, Hg) in mine drainage waters, Rio Avanza stream water and other surface water representative of minor tributaries and the Degano stream, sampled upstream and downstream its confluence with the Rio Avanza stream.

Parameter	Unit	Mine drainage water (n = 11)	Main river (n = 5)	Secondary tributaries (n = 5)
pH		7.52 - 8.78	8.24 - 8.44	8.22 - 8.46
T	°C	4.96 - 6.50	5.66 - 7.68	6.34 - 8.18
ORP	mV	74.0 - 303	72.0 - 301	287 - 294
EC	µS cm^{-1}	114 - 227	262 - 864	176 - 226
TDS	mg/L	54.0 - 113	213 - 432	88.0 - 113
DO	mg/L	5.61 - 12.3	6.64 - 8.20	6.67 - 8.08
Ca^{2+}	mg/L	36.9 - 42.4	82.3 - 197	34.1 - 42.8
Mg^{2+}	mg/L	2.65 - 6.49	14.0 - 26.1	3.25 - 11.7
Na^{+}	mg/L	0.49 - 1.07	2.85 - 4.65	0.85 - 2.68
K^{+}	mg/L	0.42 - 0.66	0.99 - 1.17	0.46 - 1.26
F^{-}	mg/L	0.01 - 0.10	0.02 - 0.29	0.03 - 0.05
Cl^{-}	mg/L	0.13 - 0.65	0.46 - 2.15	0.22 - 0.37
NO_3^{-}	mg/L	0.37 - 1.25	2.01 - 2.97	1.04 - 4.29
SO_4^{2-}	mg/L	2.44 - 10.2	124 - 316	5.40 - 16.2
CO_3^{2-}	mg/L	<LOD	<LOD - 10.8	<LOD - 12.0
HCO_3^{-}	mg/L	148 - 171	143 - 221	132 - 178
Ba	mg/L	0.04 - 0.10	0.05 - 0.10	<LOD - 0.28
As	µg/L	0.87 - 14.8	0.60 - 2.98	0.18 - 3.89
Cu	µg/L	0.29 - 8.28	<LOD - 1.08	0.12 - 0.41
Fe	µg/L	4.16 - 14.1	10.5 - 27.5	3.66 - 5.42
Mn	µg/L	0.11 - 2.78	0.27 - 1.62	0.15 - 0.37
Mo	µg/L	<LOD - 0.47	0.58 - 6.70	<LOD - 0.96
Pb	µg/L	<LOD - 1.02	<LOD - 0.72	<LOD
Zn	µg/L	<LOD - 11.0	<LOD - 4.30	<LOD - 1.90
Sb	µg/L	4.33 - 20.3	0.30 - 1.16	0.19 - 1.59
Hg	ng/L	2.41 - 13.2	1.17 - 6.49	1.81 - 10.2

applied sciences

MDPI

Article

Portable X-ray Fluorescence (pXRF) as a Tool for Environmental Characterisation and Management of Mining Wastes: Benefits and Limits

Nicolò Barago [1,*], Elena Pavoni [1], Federico Floreani [1,2], Matteo Crosera [3], Gianpiero Adami [3], Davide Lenaz [1], Francesca Larese Filon [4] and Stefano Covelli [1]

[1] Dipartimento di Matematica e Geoscienze, Università di Trieste, 34128 Trieste, Italy
[2] Dipartimento di Scienze della Vita, Università di Trieste, 34127 Trieste, Italy
[3] Dipartimento di Scienze Chimiche e Farmaceutiche, Università di Trieste, 34127 Trieste, Italy
[4] Dipartimento Universitario Clinico di Scienze Mediche Chirurgiche e della Salute, Università di Trieste, 34129 Trieste, Italy
* Correspondence: nicolo.barago@phd.units.it

Abstract: Portable X-ray fluorescence (pXRF) is one of the main geochemical techniques employed in multi-elemental analysis screening for contaminated sites management. As the confidence of pXRF analyses are matrix-specific, efforts are made to provide studies of pXRF quality on different geochemical datasets, focusing on less investigated elements such as mercury (Hg) and antimony (Sb), to help both new and experienced users. The analysis of environmental solid samples from two decommissioned mining sites in NE Italy, characterised by Pb-Zn and (Hg-rich) Cu-Sb ore deposits, were prepared with two different protocols and compared with traditional destructive analyses. Sample composition was found strictly dependent to the occurrence of false positives and overestimation at low concentrations. In contrast, milling the sample did not produce major variations in the overall quality. Lead (Pb), Sb, and Zn reached the definitive data quality in at least one of the two datasets. Consequently, as far as a thorough QA/QC protocol is followed, pXRF can rapidly produce chemical data that is as accurate as that produced by destructive standard laboratory techniques, thus allowing to identify potential sources of contamination that could be reprocessed for the extraction of valuable elements and mitigating the dispersion of contaminants and ecological or health risks.

Keywords: portable X-ray fluorescence (pXRF); validation; mining wastes; contamination; sample preparation

Citation: Barago, N.; Pavoni, E.; Floreani, F.; Crosera, M.; Adami, G.; Lenaz, D.; Larese Filon, F.; Covelli, S. Portable X-ray Fluorescence (pXRF) as a Tool for Environmental Characterisation and Management of Mining Wastes: Benefits and Limits. *Appl. Sci.* **2022**, *12*, 12189. https://doi.org/10.3390/app122312189

Academic Editor: Abdeltif Amrane

Received: 14 November 2022
Accepted: 24 November 2022
Published: 28 November 2022

1. Introduction

Portable X-ray fluorescence (pXRF) is widely accepted as geochemical in situ or laboratory instrumentation in several scientific and industrial fields such as mining exploration, environmental characterisation of contaminated sites for remediation, waste management, or archaeometry. It is a non-destructive, rapid, simultaneous multi-element analytical technique for solid sample analysis. Since it can be used in situ or in the laboratory for the analysis of unprepared or lab-prepared samples, it provides a cost- and time-saving alternative solution compared to the more accurate and expensive standard laboratory analytical procedures (e.g., Inductively Coupled Plasma Atomic Emission and Mass Spectrometry—ICP-AES and ICP-MS; [1–4]). Moreover, pXRF allows for the rapid collection of a considerable amount of data, facilitating geostatistical approaches and decision making. Even showing a relatively elevated analytical uncertainty, as long as a quality assurance/quality control (QA/QC) for pXRF measurement is followed, the confidence level of the decisions made onsite will actually be higher than with a small number of laboratory-prepared samples and fewer geochemical data [5]. Thanks to its compact size and weight, pXRF can also be used in

remote regions, providing cost-effective technology for real-time data, especially when immediate action is needed as a result of environmental disasters [6].

The description of the technique and its applications have been reported in several studies and reviews [5,7,8]. Portable XRF offers many advantages and few disadvantages compared to conventional laboratory analysis of environmental samples. Sensitivity to trace element variations is one of the strong points of pXRF. However, there are possible pitfalls when a new pXRF instrument is employed, and it is worth focusing on the possible errors that occur during pXRF analyses since these instruments can be easily used by any operator.

The limit of detection (LOD) varies with different analysers and measurement time. Overall, the best instruments are capable of a LOD in the 5 to 100 mg/kg range for elements with an atomic number (Z) between 19 (K) and 68 (Pb). Hence, pXRF is not suitable for analysing very low concentrations although the sensitivity can vary among different analytes. For most of the elements of environmental concern, pXRF may not be capable of discriminating values above or below national regulatory threshold levels (e.g., in soils, for public, private, and residential use, the limit for Hg is fixed at 1 mg/kg according to Italian Legislative Decree 152/2006 [9]). However, this technique is particularly useful in the detection of samples with "anomalous" high concentrations with respect to background levels or weakly impacted environmental areas. Based on pXRF analysis on large datasets, a subset of samples can be selected for further analyses such as, for instance, mineralogical, compositional, or related to the speciation of potentially toxic elements (PTEs). Otherwise, old mining wastes with exceptional high metal concentrations can be identified for potential reprocessing. Thus, the extraction of valuable elements would be followed by the mitigation of dispersion of the contaminant and ecological or health risks. However, to achieve the best overall results, pXRF data should be validated using conventional laboratory-based spectrometric techniques, and geochemical expertise is required for the reliable interpretation of pXRF data. This is especially important since pXRF can over- or underestimate concentrations as well as detect false positives, with varying levels of accuracy for different elements.

The handling of the sample prior to pXRF analysis greatly affects the accuracy of the technique. Variations in soil moisture, particle size, heterogeneity, and density directly affect the accuracy of the results. For instance, Laiho and Perämäki [10] found that sample preparation could lead to more significant errors than the use of different pXRF instruments. When the sample preparation procedure is the same as the laboratory standard procedures, and the sample is sieved, dried, milled, and homogenised ("lab-prepared samples"), pXRF can provide accurate results comparable to destructive standard laboratory analyses (e.g., ICP-OES, ICP-MS), hereafter referred to as "laboratory analyses" [5,6,11]. However, the standard procedure can be so time-consuming that pXRF analysis on lab-prepared samples may not be cost-effective, as the gain in accuracy is followed by a reduction in the geochemical dataset.

The last issue affecting pXRF analyses is related to interferences and matrix effects. Interferences among elements can be produced by overlaps of the characteristic X-ray emission lines. Matrix effects appear as either X-ray absorption or enhancement phenomena, which can affect the determination of a single analyte. In the absence of a clear bias with any possibility to correct the output (e.g., adjusting the calibration slope of the linear regression), those errors may not be corrected. However, those effects can occur particularly in sites characterised by a uncommon geochemical composition, such as metal-bearing mineralised rocks or geological materials affected by mining, where trace elements that normally occur in the environment in the ppm or ppb range can reach notably higher concentrations, up to wt.%, with a variability of several orders of magnitude [12].

Mining exploration and industrial use of common and uncommon elements (e.g., precious metals, rare-earth elements—REEs) have increased in recent years due to an exponentially growing demand. As a result, there is still substantial concern regarding the subsequent risk of dispersion into the environment of those elements known for their high toxicity, such as mercury (Hg) or antimony (Sb). In the last decades, many studies [7,11,13–17] have

reported the performance of pXRF instruments based on QA/QC validation procedures using certified reference materials (CRMs), blank samples, and/or traditional laboratory analyses on site-specific samples, studying different groups of elements in various matrices. Moreover, pXRF analyses of soil, lato sensu, samples are usually performed on common elements such as base metal(loid)s (e.g., As, Cu, Fe, Mn, Pb, Zn), whereas, curiously, highly toxic elements such as Hg and Sb have not been considered or have not been found in concentrations high enough and were detected in a small number of studies, e.g., [18,19]. Thus, the main purpose of this research was to evaluate the advantages and disadvantages of the use of pXRF on samples collected from two different decommissioned mining areas in Italy characterised by Pb-Zn and (Hg-rich) Cu-Sb ore deposits found to have very low to very high concentrations of As, Cu, Hg, Pb, Sb, and Zn. In order to reach this objective, a validation with traditional laboratory analyses considering various metal(loid)s was performed on a large geochemical dataset, including samples of soils, stream sediments, and mining wastes. Moreover, this research may provide insights as to how analytical determinations using pXRF can be influenced by (1) different spectral interferences and matrix effects at Pb-Zn and Cu-Sb mining sites, (2) low concentrations, and (3) heterogeneity and sample preparation.

2. Materials and Methods

2.1. Sampling Strategy and Sample Preparation

A total of 95 discrete samples of soils, stream sediments, mine wastes, and flotation tailings from two decommissioned mining sites in the Friuli Venezia Giulia Region (north-eastern Italy) were collected and analysed by means of pXRF, ICP-MS, and DMA-80 for As, Cr, Cu, Fe, Hg, Mn, Pb, Sb, and Zn determination. The two mining sites are the carbonate-hosted "Alpine-type"/"Mississippi-Valley-type" (MVT) Pb-Zn Raibl mine [20–23] and the Mt. Avanza "fahlore-type" Cu-Sb(-Ag) tetrahedrite mine [24,25]. The Pb-Zn Raibl site (46.442772° N, 13.568707° E) is a base metal hydrothermal ore deposit hosted in a Triassic massive dolomitic reef, characterised by a mineralogical assemblage where sphalerite (ZnS), galena (PbS), and pyrite/marcasite (FeS_2) are the dominant constituents. The host rocks generally show a dominant carbonate composition. The main lithology is Triassic dolostone with a limited presence of shales, sandstones, tuffs, and ignimbrites [26]. At the Cu-Sb(-Ag) Mt. Avanza site (46.618780° N, 12.755281° E), the ore is composed of a (Zn-Hg)-rich variety of tetrahedrite, a complex Cu-Sb sulfosalt hosted in Palaeozoic rocks with a more pronounced silicate composition. The ore veins are located at the tectonic interface between the metamorphic Devonian limestones and Carboniferous, siliciclastic metapelites [24].

From each original sample, two aliquots of 0.5–1 kg were collected. Rock and plant fragments were removed, and the aliquots were manually pre-homogenised in situ. Once in the laboratory, the samples were dried in the open air to prevent Hg volatilisation and sieved using a 2.0 mm sieve. The first aliquot was heterogeneous and prepared via a "fast lab-preparation" mode similar to the "intrusive-unprepared" mode reported by the U.S. EPA [11], with a very similar approach to the GTK procedure described by Laiho and Perämäki [10] for sampling preparation. This "fast lab-preparation" mode simply consists of drying and sieving the sample using a 2.0 mm sieve and placing it into a pXRF sample cup. This procedure is a good compromise in terms of time if compared to the in situ mode ("point-and-shoot"), during which the analyser probe is placed in direct contact with the soil surface for a real-time measurement. The only differences between the procedure followed in this study and the GTK are represented by the use of 5 g of the sample placed in sample cups with a window X-ray film (Kapton) instead of plastic bags and a counting time of 60 s (three beams with different keV of 20 s each) instead of 120 s. The second aliquot of each sample was treated following a "lab-type preparation" [5], which is the "intrusive mode" described by the U.S. EPA [11], consisting of a time-consuming procedure in which 5 g of the sample were dried, milled in a tungsten carbide (WC) mill or an agate mortar, and homogenised into a fine powder.

2.2. Analytical Determinations by Means of Portable X-ray Fluorescence (pXRF)

In this research, an Olympus Vanta C Series with a 4 W Ag anode X-ray tube (VCA) and a silicon drift detector was used. The VCA has an excitation source ranging from 8 to 50 keV and is capable of detecting elements from magnesium (Mg) to uranium (U). As is the case with many pXRF instruments, there are various factory methods available, each with different calibrations. The "soil" method is more suited for trace concentrations, whereas the "geochem" method is more accurate at higher concentrations. Both methods were used to determine as many elements as possible with the best data quality [27] without moving the analyser between two measurements [5]. In this study, pXRF data > 1 wt.% were selected from the geochem method, whereas values < 1 wt.% were determined using the soil method. Both methods used three beams set to 20 s each, with a total of 1 min for analysis, replicated three times. Although the payback for longer analyses would be lower LODs, a reasonable measurement time was selected to maintain the analysis fast enough to characterise a large number of samples. The accuracy was evaluated by means of certified reference materials (CRMs; "PACS-3" and "MESS-4", Marine Sediment, NRCC, Whitehorse, YT, Canada), which were analysed in the same batch of samples using both methods.

2.3. Confirmatory Analyses: Inductively Coupled Plasma-Mass Spectrometry (ICP-MS) and Direct Mercury Analyser (DMA-80)

As a confirmatory analysis for the determination of metals (Cu, Fe, Mn, Pb, Zn) and metalloids (As, Sb) except for Hg, 250 mg of "lab-prepared" samples were acid-digested in PTFE vessels through a total acid dissolution in a closed microwave system (Multiwave PRO, Anton Paar) using two heating steps. In the first mineralisation step, inverse aqua regia (3:1, HNO_3 67–69% and hydrochloric acid HCl 34–37%; hydrofluoric acid (HF, 47–51%, VWR Normatom), suprapure H_2O_2 (30%, Merck, only in the case of soil samples), and U.S. EPA method 3052 [28] were used. In the second step, boric acid (suprapure H_3BO_3 6%, Merck) was added to buffer the excess HF. Blank samples and CRMs were also digested for each microwave batch to evaluate the quality of the analysis. After mineralisation, the solutions were diluted up to a volume of 25 mL by adding Milli-Q water and stored at 4 °C until analysis. Total digestion with HF was chosen for its capability to dissolve refractory minerals such as silicate minerals.

Major and trace elements were determined by means of ICP-MS (NexION 350x equipped with an ESI SC autosampler, Perkin Elmer). In order to avoid and minimise cell-formed polyatomic ion interference, the analysis was performed using Kinetic Energy Discrimination (KED) mode. The instrument was calibrated via an analysis of standard solutions ranging between 0.5 and 500 µg/L prepared by dilution from multistandard solutions for ICP analyses (Periodic Table MIX1 and MIX2, TraceCERT Sigma-Aldrich). Several aliquots of CRMs were analysed to check for accuracy, and allowable recoveries ranging between 70–119% (PACS-3) and 83–107% (MESS-4) were obtained. Except for Cu in PACS-3 CRM, ICP-MS produced 106 of 112 results (94.6%) within the 80–120% recovery acceptance range for all analytes and replicates in the two CRMs. Moreover, potential matrix effects were evaluated by means of laboratory-fortified samples prepared by spiking a standard solution different from that employed for instrument calibration (Multielement quality control standard for ICP, VWR Chemicals) into actual samples. The repeatability of the ICP-MS analysis expressed as RSD% was <3%.

Total Hg in powders was determined using a Direct Mercury Analyzer (DMA-80, Milestone, Sorisole, Italy) atomic absorption spectrophotometer, according to EPA method 7473 [29]. The LOD was calculated as 3 times the standard deviation of 10 blanks and divided by the slope of the calibration curve was 0.004 mg/kg. Regarding accuracy, acceptable recoveries were obtained using certified reference material (PACS-3), ranging between 100 and 105%.

All ICP-MS and DMA-80 analytical results were at least 10 times over the LODs. Data below such threshold were not considered in the statistical analysis. A summary of the accuracy of both methods is reported in Table S1.

2.4. Statistical Analysis

Data were processed in Python, with SciPy as the main package used for statistical analysis. Accuracy was determined by "recovery" calculated with ((pXRF value/CRM value) × 100), while repeatability, which is indicated as precision in the U.S. EPA report [11], was determined by RSD% as ((standard deviation/mean) × 100) on replicates for each analyte and technique. For further statistical analysis and data quality levels for pXRF results, the U.S. EPA [11] procedure was followed according to the majority of recent studies, e.g., [13,24,25,30]. Comparability of pXRF with confirmatory data (ICP-MS and DMA-80) was assessed using linear regression statistics, where optimal correlations were found with a coefficient of determination $r^2 = 1$, slope equal to 1, and intercept with the y-axis equal to 0. Since a wide range in concentrations can be associated with a wide range in variance, to provide a correlation that was equally influenced by both high and low values, all data were $\log_{10}$ transformed according to the U.S. EPA method [11], providing equal weight in the square regression analysis to both small and large values. A Z-test was used to test the statistical similarity between the slope regression and an ideal slope = 1 and between the y-intercept of the regression function and an ideal y-intercept = 0. Furthermore, the *t*-test was also carried out on $\log_{10}$-transformed data to evaluate if the two datasets, respectively, obtained by means of pXRF and the confirmatory data for each element and sample treatment procedure belong to the same population, implying that any significant difference between the two analytical techniques occurred. *t*-Test, slope and y-intercept z-tests are successful for *p*-value > 0.05. Lower values of *p*-value imply significant differences between sample populations or from the ideal slope and y-intercept and vice versa. According to criteria established by the U.S. EPA [11], 3 levels of pXRF data quality can be defined: the definitive level is considered the highest level of quality, quantitative screening level data provide the quantification although it may be relatively imprecise, whereas qualitative screening level data indicate the presence or absence of elements of interest but do not provide reliable concentration estimates (Table 1).

Table 1. US EPA Criteria for establishing data quality [11].

Data Quality Level	Statistical Parameter
Definitive	r^2 = 0.85 to 1.0. The repeatability (RSD%) must be less than or equal to 10%, and inferential statistics indicate the two data sets are statistically similar.
Quantitative screening	r^2 = 0.70 to 1.0. The RSD% must be less than 20%, but the inferential statistics indicate that the data sets are statistically different.
Qualitative screening	r^2 = less than 0.70. The RSD% is greater than 20%. The data must have less than a 10 percent false-negative rate.

Lastly, a "site-specific accuracy" was calculated ((pXRF concentration/ICP-MS or DMA-80 concentration) × 100) and used to highlight method detection limits (MDLs) and concentration effect issues for the analysis of pXRF [11]. The MDL is defined as a threshold below which the analytes exhibit a region where there is no longer a linear relationship.

3. Results

3.1. Accuracy and Repeatability: pXRF vs. Certified Reference Materials (CRMs)

Accuracy refers to the degree to which a measured value for a sample agrees with a reference of true value for a CRM. An acceptable range of 80–120% of recovery with respect to the certified value was used to evaluate accuracy and two CRMs (PACS-3 and MESS-4) were analysed via pXRF for this purpose (Table 2). Except for Hg and Sb, which were not detected by pXRF, acceptable recoveries were obtained for Cr, Fe, Mn, Pb, and Zn. In the case of Cu, accuracy was acceptable only in the PACS-3, which has higher concentrations of Cu, and As was not acceptable in either, with the better recoveries on the MESS-4 than in the PACS-3 most likely due to interferences related to the relatively higher concentration of Pb in PACS-3. Repeatability expressed as RSD% was <10% for

all the analytes, with the lone exception of Pb in the MESS-4, which showed a slightly higher value (13%). In the case of As, the accuracy was lower in PACS-3, which has a higher Pb content (As mean recovery = 164% with Pb concentration = 188 mg/kg) than in MESS-4, which, conversely, has a concentration of Pb one order of magnitude lower (As mean recovery = 121% and Pb = 21.5 mg/kg) because the As-K and Pb-L X-ray overlaps can be so severe that the resolution may not be enough to discriminate between the two elements [7], and the identification of As may be compromised. In fact, when the Pb:As ratio exceeds 10:1, As is not efficiently detected by means of pXRF [31].

Table 2. QA/QC of pXRF data from CRMs. Data presented in bold are out of the acceptable quality range.

Element	CRM Value (mg/kg)		Mean Accuracy—Recovery (%)		Mean Repeatability—RSD (%)	
	PACS-3	MESS-4	PACS-3	MESS-4	PACS-3	MESS-4
As	30.3	21.7	**164%**	**121%**	3.9%	6.1%
Cr	90.6	94.3	120%	106%	7.4%	4.1%
Cu	356	32.9	104%	**160%**	3.5%	2.4%
Fe	41060	37900	107%	102%	0.6%	1.4%
Hg	2.98	0.09	n.d.	n.d.	n.d.	n.d.
Mn	432	298	107%	103%	3.7%	3.4%
Pb	188	21.5	93%	93%	3.4%	**13.0%**
Sb	14.7	1.07	n.d.	n.d.	n.d.	n.d.
Zn	376	147	109%	102%	2.0%	3.3%

3.2. Validation Assessment: pXRF vs. ICP-MS and DMA-80

The comparability is determined by the degree to which the pXRF concentration of an element in a sample matches the concentration value obtained with the confirmatory analysis via reference methods. The comparability is assessed by the statistical equivalence of pXRF and ICP-MS (and DMA-80 for Hg) $\log_{10}$-transformed data and acceptable repeatability (RSD%) as described by the U.S. EPA [11], which indicates that pXRF results can reach definitive-, quantitative-screening-, or qualitative-screening-level criteria.

The first step in the evaluation of the quality of the pXRF analysis was performed under optimal sample preparation conditions ("lab-prepared" samples), where samples were finely ground and prepared in the same manner as samples for traditional laboratory analysis. The comparability between pXRF and confirmatory analysis on site-specific samples (soils, stream sediments, and mine wastes) are shown in the log-log plot in Figure 1 and in the statistical summary shown in Table 3.

The quality of pXRF analytical determination is variable among elements and matrices, in agreement to previous studies [13,27,32]. In general, a good comparability was found in both datasets for major elements as base metals (Table 3), according to previous investigations reporting significant correlations between digested samples through reference methods and pXRF for base metals [16,33]. In general, deviations from reference data may be due to uncertainties deriving from both pXRF and/or ICP-MS/DMA-80 analytical procedures, as demonstrated by the variability of the recovery for the different techniques (Table S1). Lead (Pb) was found to be the most accurate pXRF analyte and was the only element that reached the definitive data quality in both datasets among the nine elements investigated. Such high quality was the result of excellent comparability with ICP-MS analysis in a very wide concentration range, from 5 mg/kg to around 40,000 mg/kg (4 wt.%). Definitive quality levels were also obtained in the case of Zn in the Pb-Zn matrix and in the case of Sb in the Cu-Sb matrix. In addition, As, Fe, and Mn reached quantitative screening levels in both matrices, whereas Cu and Hg met the quantitative screening level only in the Cu-Sb-rich matrix due to the highest content of such metals in the host rocks and in the ore minerals [25,34].

In the case of As, results from pXRF were found to be slightly less correlated to ICP-MS results for the Pb-Zn site most likely due to the fact that As determination is affected by

high Pb concentrations. The same issue was observed for the CRM analysis. Hence, for the Pb-Zn site, a better As determination was obtained by ICP-MS, e.g., [25], although statistics indicated that As could still be identified via pXRF at the quantitative screening level.

Chromium (Cr) and Hg (Table 3) reached low to very low concentrations in the Pb-Zn carbonate matrix. Their peaks were incorrectly interpreted by the factory calibration producing meaningless data (Figure 1). In the Pb-Zn site, Hg was in the 0.03–0.12 mg/kg interval according to the analysis performed by means of DMA-80, whereas the pXRF output was 33–280 mg/kg. The occurrence of false positives for Hg from pXRF is known to occur [18], and they can be removed after manual observation of the spectra. However, in the Cu-Sb site, Hg (up to 473 mg/kg—"quantitative") determination was better than Cr (up to 182 mg/kg—"qualitative").

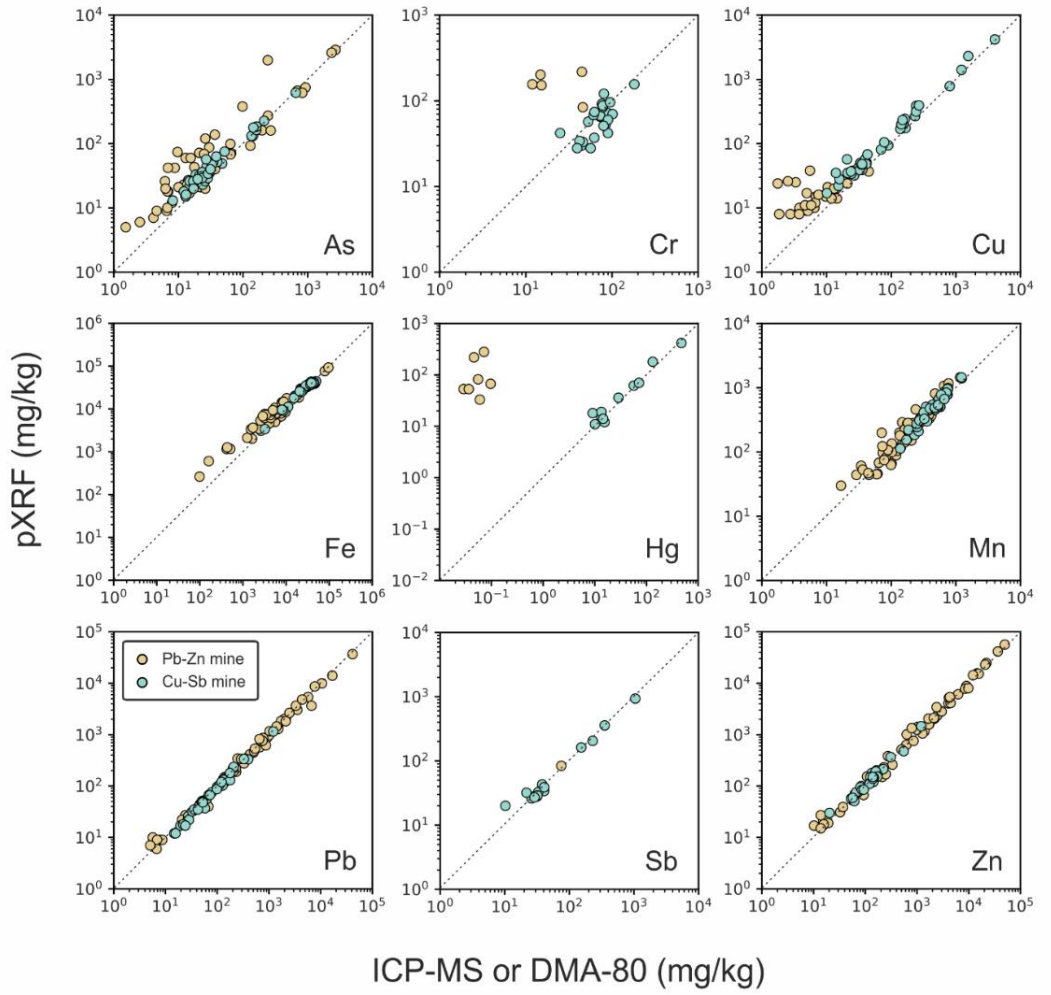

Figure 1. Comparison between pXRF and standard laboratory analyses (ICP-MS and DMA-80 for Hg) in "lab-prepared" samples (powders) of two datasets from Pb-Zn and Cu-Sb mining sites, marked using different colours.

Table 3. Statistical summary of comparability on "lab-prepared" samples (powders). Linear regression and *t*-test performed on log_{10}-transformed data. n, number of data; Y-int, Y-intercept.

Matrix Type	Element	Data Quality [a]	n	Concentration Range ICP-MS—DMA	Concentration Range pXRF	RSD%	r^2	*t*-Test	Slope z-Test	Y-Int z-Test
				(mg/kg)	(mg/kg)				*p*-Value	
Cu-Sb	As	Quantitative	37	8.20–654	13–1057	7%	0.963 *	0.000	0.527	0.185
	Cr	Qualitative	25	6.91–182	28–156	12%	0.523 *	0.021	0.721	0.720
	Cu	Quantitative	37	10.1–4019	17–7739	8%	0.979 *	0.000	0.641	0.201
	Fe	Quantitative	37	3248–49,918	3405–44,504	1%	0.970 *	0.000	0.731	0.410
	Hg	Quantitative	11	0.04–473	11–720	14%	0.959 *	0.127	0.802	0.637
	Mn	Quantitative	37	138–1227	113–1452	3%	0.929 *	0.004	0.605	0.458
	Pb	Definitive	37	14.7–1216	12–1156	6%	0.988 *	0.760	0.770	0.524
	Sb	Definitive	15	1.64–1049	20–1627	9%	0.970 *	0.576	0.704	0.589
	Zn	Quantitative	37	20.3–1204	30–1462	4%	0.969 *	0.007	0.849	0.709
Pb-Zn	As	Quantitative	52	0.91–2693	5–2886	10%	0.856 *	0.000	0.383	0.051
	Cr	Qualitative	5	2.04–50.0	84–218	7%	0.100	0.007	0.035	0.000
	Cu	Qualitative	34	0.69–45.0	8–50	16%	0.358 *	0.000	0.024	0.001
	Fe	Quantitative	53	99–96,674	263–92,931	1%	0.952 *	0.000	0.201	0.003
	Hg	Qualitative	7	0.03–0.12	33–280	11%	0.050	0.000	0.537	0.017
	Mn	Quantitative	57	16.6–1239	30–1449	7%	0.895 *	0.003	0.917	0.747
	Pb	Definitive	58	5.05–41,436	6–36,853	5%	0.993 *	0.370	0.789	0.718
	Sb	Qualitative	2	0.05–75.0	21–84	-	-	-	-	-
	Zn	Definitive	58	10.2–49,752	15–56,400	4%	0.992 *	0.053	0.887	0.711

[a] Data quality levels are defined by [11]. * Significant for $p < 0.001$. Different colours identify the three data quality levels.

3.3. Low Concentration Effect

Results from this research indicate that the reliability of the pXRF analysis decreased at low concentrations for some elements, thus resulting in an overestimation, as in the case of As, Cu, and Fe. The results of the comparison considering "lab-prepared" samples from the two mining sites between confirmatory analyses (ICP-MS/DMA-80) and errors that are represented with a percent "site-specific accuracy" (pXRF analyte concentration/reference concentration × 100) are presented in Figure 2.

The field-based MDL was variable considering different elements. Regarding the pXRF analysis, acceptable results were obtained at concentrations of Fe > 10,000 mg/kg, As > 100 mg/kg, and Cu > 30 mg/kg, respectively. Below such MDLs, site-specific recoveries showed a non-linear increase, which started approximately from 120–130%, reaching almost 500% at very low concentrations. Method detection limits (MDLs) and overestimation observed in this research were consistent with previous studies reporting similar MDLs [11]. Especially for such elements, MDLs were found to be several orders of magnitude higher than the LOD indicated by the instrument documentation (LOD: Fe = 10 mg/kg, As = 1 mg/kg, Cu = 3 mg/kg, with a measurement time of 120 s/beam, against 20 s/beam of this study). The discrepancy is due to differences in counting time and to disparities in the developer's definition of MDLs [11].

The concentration effect for Cu and Fe was mostly found in the Pb-Zn samples most likely due to a lower geogenic abundance of these two elements with respect to the other investigated site. Indeed, the geological matrices of the Cu-Sb site are constituted by higher background levels of Cu and Fe, and subsequently, such elements can be better determined by pXRF. The main reasons for the higher background in the Cu-Sb site are (1) dominance of silicate minerals in the host rock, which are in general characterised by higher concentrations in various elements, including Fe, with respect to carbonates (dolomite, calcite), which are the major mineralogical constituent of wall rocks and gangue in the Pb-Zn site, and (2) the natural enrichment, as in the case of Cu, related to the high and disseminated occurrence of Cu-bearing tetrahedrite minerals and possibly to the presence of a halo, which is the product of diffusion of trace elements related to the ore deposit during

its emplacement or weathering. A similar concentration effect was also observed for the CRMs. The accuracy of the analysis in the case of Cu was found to be low in MESS-4, where Cu is <100 mg/kg (accuracy = 158–164% and Cu concentration = 32.9 mg/kg), whereas the opposite was observed in PACS-3, where Cu is >100 mg/kg (accuracy = 111–135% with Cu concentration = 372 mg/kg). Analytical issues in As determination in the Pb-Zn samples appeared to be influenced by both concentration effects and interferences with Pb, as described previously. However, interference caused by high concentrations of Pb appeared to be weaker as concentrations increased.

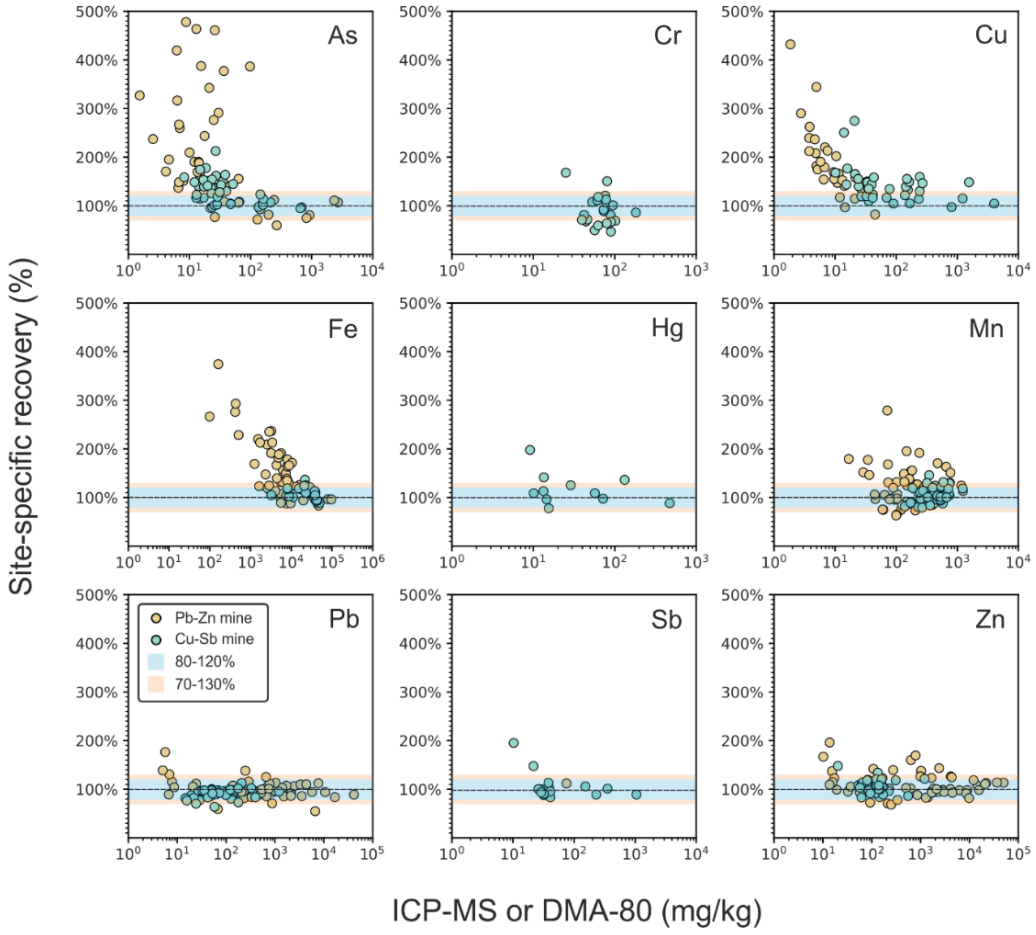

Figure 2. Concentration effect on pXRF data: site-specific recovery versus confirmatory analyses in "lab-prepared" samples (powders) of two datasets from a Pb-Zn and Cu-Sb mining sites, marked with different colours. Possible acceptance ranges are depicted in blue and yellow.

3.4. Effect of Sample Treatment

In order to evaluate the quality of the pXRF analysis, an additional QA/QC test was adopted in this study involving the potential influence of heterogeneity in samples prepared with a fast preparation procedure. The analytical procedure for pXRF analysis was not changed between "fast lab-prepared" aliquots (only dried and sieved <2 mm) and "lab-prepared" samples, as described previously. The results are presented in Figure 3 and Table S2.

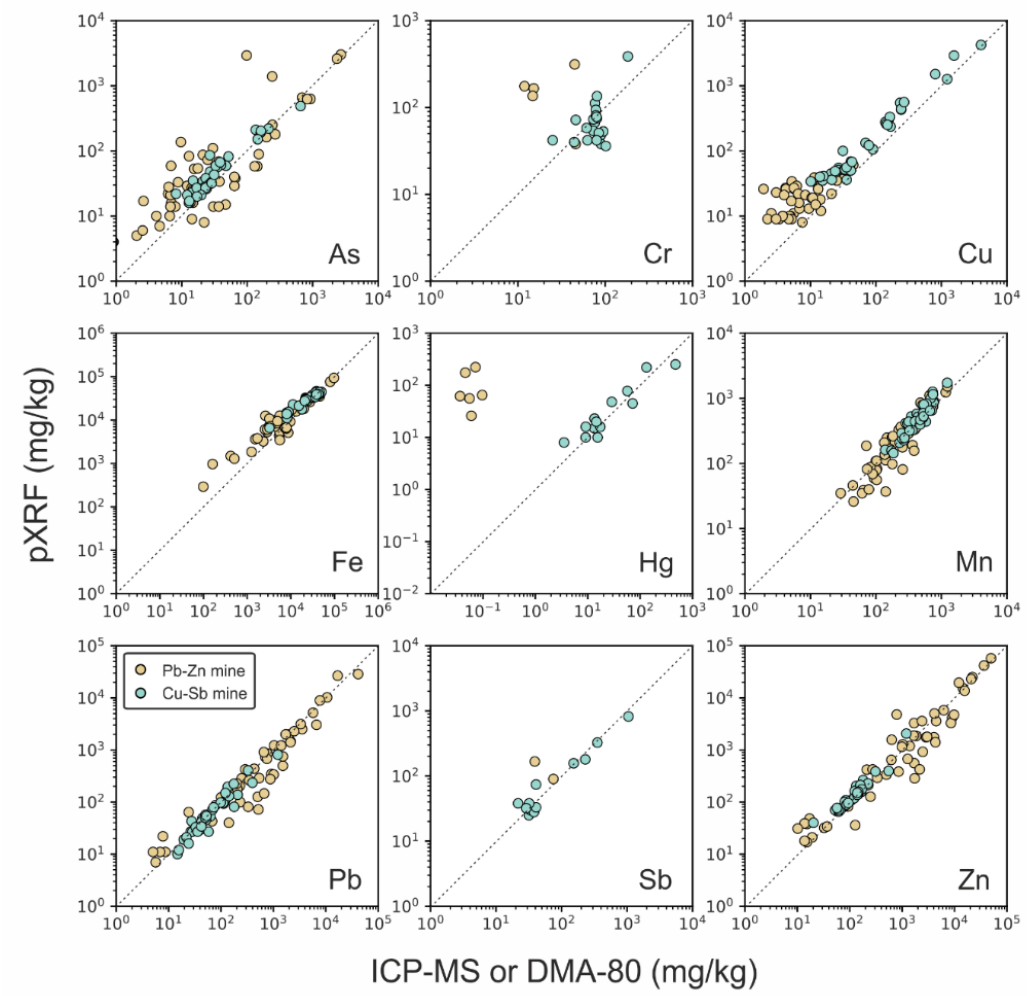

Figure 3. Comparison between pXRF and confirmatory data (ICP-MS and DMA) in "fast lab-prepared" samples (only dried and sieved < 2 mm) of two datasets from a Pb-Zn and Cu-Sb mining sites, marked with different colours.

In general, the scatterplots regarding "fast lab-prepared" aliquots (Figure 3) are similar to those reported for the "lab-prepared" aliquots (Figure 1). Most of the elements that were significantly correlated during the first validation step also maintained significant correlations for unground samples ($p < 0.001$). Those correlations were still robust, and the repeatability did not suffer heterogeneity as long as the sample was not displaced between each pXRF replicate analysis. For the data quality classification adopted [11], there were hardly any substantial upgrades or downgrades between the comparability of homogenised "lab-prepared" and "fast lab-prepared" heterogeneous samples.

However, some differences were observed. Indeed, the pXRF analysis of heterogeneous samples produced data that are slightly less correlated, more scattered, and less accurate. A moderate improvement in the pXRF data quality was observed; therefore, laboratory milling operations of field samples should be evaluated on the basis of the data quality desired.

4. Conclusions

In areas close to mining operations, the preliminary use of pXRF may be able to easily identify the location of the mining wastes characterized by the highest metal or metalloid concentrations, exploring even the occurrence of elements of potential economic interest. Conversely, users may encounter unreliable results when pXRF data are not validated, especially when dealing with low concentrations. Care must be taken regarding the concentration effects

since the absence or occurrence of very low concentrations can be interpreted by pXRF as higher background levels and also regarding actual LODs, which may be higher than those indicated by the factory producer due to different operating conditions.

In this study, the overall analytical quality was found to be mainly influenced by the composition of samples due to interferences, matrix effects, and low concentrations more than the heterogeneity of the sample. Although milling is a highly time-consuming procedure, the sample preparation should be carefully defined according to the desired data quality. However, the loss in comparability due to "fast lab-prepared" samples was negligible in comparison to compositional differences. A summary of the results is presented:

- Lead (Pb), zinc (Zn), and manganese (Mn): the determination of these base metals by pXRF was often found to be successful (from quantitative to definitive quality levels), and no notable analytical issues related to interferences or concentration effects were observed;
- Arsenic (As): the element met the "quantitative" quality level in both datasets. However, better comparability is found in sites where Pb is not dominant, and As concentrations are elevated enough due to As-K and Pb-L X-ray overlaps, which reduce the accuracy of As determination, so that the traditional laboratory analysis may be preferential. A concentration effect was observed leading to a decrease in comparability for As < 100 mg/kg;
- Chromium (Cr): the metal showed moderate comparability between the two analytical approaches in the Cu-Sb matrix, characterised by relatively higher Cr concentrations and occurrence of false positives by using pXRF in the carbonate-hosted Pb-Zn samples that should be removed by the user via manual spectral interpretation. Overall, Cr never exceeded the "qualitative" level when determined via pXRF;
- Copper (Cu): comparability of pXRF with ICP-MS results was strongly dependent on the element concentration and acceptable for Cu > 100 mg/kg, whereas below such values, Cu concentrations detected via pXRF were false;
- Iron (Fe): similar to Cu, its detectability by pXRF was strongly dependent on the concentration. Comparability between the two analytical approaches was found to be optimal for values >10,000 mg/kg, which are common in many (but not all) natural samples;
- Mercury (Hg) and antimony (Sb): these trace elements were found quantitatively determined by pXRF only when occurring with concentrations > 10–20 mg/kg. Conversely, when the real sample concentrations were below such values, as in the case of Hg, pXRF produced false-positive results, which should be manually removed by the user via spectral interpretation. Unfortunately, this result reveals a serious limitation in using pXRF, as the operator may be precluded from detecting low concentrations of Hg in soils that exceed those threshold levels specified by national regulations that define the use of uncontaminated soil. This is the case with the Italian legislation, for instance, where the highest threshold level, defined by major land use, i.e., for commercial and industrial purposes, is fixed at 5 mg kg^{-1}, whereas for public, private, and residential use, it is 1 mg kg^{-1} (Italian Legislative Decree 152/06 [9]).

Overall, pXRF is a rapid and inexpensive technique, useful for preliminary quantification of element concentrations in contaminated solid matrices (e.g., soil, sediment, mining waste) without complex sample preparations followed by destructive standard laboratory analyses (e.g., ICP-OES, ICP-MS, DMA-80) and in a relatively short time interval. However, this study has shown that analytical results obtained using pXRF cannot be accepted outright, and they must be carefully evaluated, as interpretations should also take into consideration an initial accurate QA/QC protocol in addition to the skill and experience of the operator.

Supplementary Materials: The following supporting information can be downloaded at: https://www.mdpi.com/article/10.3390/app122312189/s1; Table S1: Comparison of the accuracy of ICP-MS, DMA-80 and pXRF analysis; Table S2: Linear regression and *t*-test carried out on log_{10}-transformed data.

Author Contributions: Conceptualization, N.B. and S.C.; data curation, N.B.; formal analysis, N.B., E.P. and F.F.; investigation, N.B., E.P., F.F. and M.C.; resources, M.C., G.A., F.L.F. and S.C.; software, N.B.; supervision, D.L. and S.C.; validation, M.C. and G.A.; visualization, N.B.; writing—original draft, N.B.; writing—review and editing, N.B., E.P., F.F., M.C., G.A., D.L., F.L.F. and S.C. All authors have read and agreed to the published version of the manuscript.

Funding: This research received no external funding.

Institutional Review Board Statement: Not applicable.

Informed Consent Statement: Not applicable.

Data Availability Statement: Data available on request from the authors.

Acknowledgments: The authors are grateful to Samuel Princi, Cristiano Mastroianni, Rossana de Faveri, Michele Relevant, and Josipa Repanić for their help with the data collection. Karry Close is warmly acknowledged for proofreading the manuscript.

Conflicts of Interest: The authors declare no conflict of interest.

Abbreviations

CRM, certified reference material; DMA-80, Direct Mercury Analyser; ICP-AES, inductively coupled plasma atomic emission spectroscopy; ICP-MS, inductively coupled plasma mass spectroscopy; LOD, limit of detection; MDL, method detection limit; PTE, potentially toxic element; pXRF, portable X-ray fluorescence; QA/QC, quality assurance/quality control; RSD, relative standard deviation.

References

1. Crosera, M.; Baracchini, E.; Prenesti, E.; Giacomello, A.; Callegher, B.; Oliveri, P.; Adami, G. Elemental Characterization of Surface and Bulk of Copper-Based Coins from the Byzantine-Period by Means of Spectroscopic Techniques. *Microchem. J.* **2019**, *147*, 422–428. [CrossRef]
2. Pavoni, E.; Crosera, M.; Petranich, E.; Faganeli, J.; Klun, K.; Oliveri, P.; Covelli, S.; Adami, G. Distribution, Mobility and Fate of Trace Elements in an Estuarine System Under Anthropogenic Pressure: The Case of the Karstic Timavo River (Northern Adriatic Sea, Italy). *Estuaries Coasts* **2021**, *44*, 1831–1847. [CrossRef]
3. Pavoni, E.; Crosera, M.; Petranich, E.; Adami, G.; Faganeli, J.; Covelli, S. Partitioning and Mixing Behaviour of Trace Elements at the Isonzo/Soča River Mouth (Gulf of Trieste, Northern Adriatic Sea). *Mar. Chem.* **2020**, *223*, 103800. [CrossRef]
4. Sibilia, M.; Stani, C.; Gigli, L.; Pollastri, S.; Migliori, A.; D'Amico, F.; Schmid, C.; Licen, S.; Crosera, M.; Adami, G.; et al. A Multidisciplinary Study Unveils the Nature of a Roman Ink of the I Century AD. *Sci. Rep.* **2021**, *11*, 7231. [CrossRef] [PubMed]
5. Lemière, B. A Review of PXRF (Field Portable X-ray Fluorescence) Applications for Applied Geochemistry. *J. Geochem. Explor.* **2018**, *188*, 350–363. [CrossRef]
6. Higueras, P.; Oyarzun, R.; Iraizoz, J.M.; Lorenzo, S.; Esbrí, J.M.; Martínez-Coronado, A. Low-Cost Geochemical Surveys for Environmental Studies in Developing Countries: Testing a Field Portable XRF Instrument under Quasi-Realistic Conditions. *J. Geochem. Explor.* **2012**, *113*, 3–12. [CrossRef]
7. Kalnicky, D.J.; Singhvi, R. Field Portable XRF Analysis of Environmental Samples. *J. Hazard. Mater.* **2001**, *83*, 93–122. [CrossRef]
8. Horta, A.; Malone, B.; Stockmann, U.; Minasny, B.; Bishop, T.F.A.; McBratney, A.B.; Pallasser, R.; Pozza, L. Potential of Integrated Field Spectroscopy and Spatial Analysis for Enhanced Assessment of Soil Contamination: A Prospective Review. *Geoderma* **2015**, *241–242*, 180–209. [CrossRef]
9. Lgs, D. Decreto Legislativo n. 152 "Norme in Materia Ambientale". 88 Gazzetta Ufficiale Repubblica Italiana. 152/06, 14 April 2006.
10. Laiho, J.V.; Perämäki, P. Evaluation of Portable X-ray Fluorescence (PXRF) Sample Preparation Methods. *Spec. Pap.-Geol. Surv. Finl.* **2005**, *38*, 73.
11. *US EPA Environmental Technology Verification Report, Field Portable X-ray Fluorescence Analyzer*; Metorex X-MET 920-P; United States Environmental Protection Agency: Washington, DC, USA, 1998; EPA/600/R-97/146.
12. Pavoni, E.; Petranich, E.; Adami, G.; Baracchini, E.; Crosera, M.; Emili, A.; Lenaz, D.; Higueras, P.; Covelli, S. Bioaccumulation of Thallium and Other Trace Metals in Biscutella Laevigata Nearby a Decommissioned Zinc-Lead Mine (Northeastern Italian Alps). *J. Environ. Manag.* **2017**, *186*, 214–224. [CrossRef]
13. Hall, G.E.M.; Bonham-Carter, G.F.; Buchar, A. Evaluation of Portable X-ray Fluorescence (PXRF) in Exploration and Mining: Phase 1, Control Reference Materials. *Geochem. Explor. Environ. Anal.* **2014**, *14*, 99–123. [CrossRef]
14. Knight, R.D.; Kjarsgaard, B.A.; Russell, H.A.J. An Analytical Protocol for Determining the Elemental Chemistry of Quaternary Sediments Using a Portable X-ray Fluorescence Spectrometer. *Appl. Geochem.* **2021**, *131*, 105026. [CrossRef]
15. Migaszewski, Z.; Gałuszka, A.; Dołęgowska, S. The Use of FPXRF in the Determinations of Selected Trace Elements in Historic Mining Soils in the Holy Cross Mts., South-Central Poland. *Geol. Q.* **2015**, *59*, 248–256. [CrossRef]

16. Rouillon, M.; Taylor, M.P. Can Field Portable X-ray Fluorescence (PXRF) Produce High Quality Data for Application in Environmental Contamination Research? *Environ. Pollut. Barking Essex 1987* **2016**, *214*, 255–264. [CrossRef] [PubMed]
17. Rincheval, M.; Cohen, D.R.; Hemmings, F.A. Biogeochemical Mapping of Metal Contamination from Mine Tailings Using Field-Portable XRF. *Sci. Total Environ.* **2019**, *662*, 404–413. [CrossRef] [PubMed]
18. Spearman, S.; Bartrem, C.; Sharshenova, A.; Salymbekova, K.; Isirailov, M.; Gaynazarov, S.; Gilmanov, R.; von Lindern, I.; von Braun, M.; Möller, G. Comparison of X-ray Fluorescence (XRF) and Atomic Absorption Spectrometry (AAS) Results for an Environmental Assessment at a Mercury Site in Kyrgyzstan. *Appl. Sci.* **2022**, *12*, 1943. [CrossRef]
19. Lemière, B.; Melleton, J.; Auger, P.; Derycke, V.; Gloaguen, E.; Bouat, L.; Mikšová, D.; Filzmoser, P.; Middleton, M. PXRF Measurements on Soil Samples for the Exploration of an Antimony Deposit: Example from the Vendean Antimony District (France). *Minerals* **2020**, *10*, 724. [CrossRef]
20. Brigo, L.; Cerrato, P. Trace Element Distribution of Middle-Upper Triassic Carbonate-Hosted Lead-Zinc Mineralizations: The Example of the Raibl Deposit (Eastern Alps, Italy). In *Sediment-Hosted Zn-Pb Ores*; Fontboté, L., Boni, M., Eds.; Springer: Berlin/Heidelberg, Germany, 1994; pp. 179–197. ISBN 978-3-662-03054-7.
21. Barago, N.; Covelli, S.; Mauri, M.; Oberti di Valnera, S.; Forte, E. Prediction of Trace Metal Distribution in a Tailings Impoundment Using an Integrated Geophysical and Geochemical Approach (Raibl Mine, Pb-Zn Alpine District, Northern Italy). *Int. J. Environ. Res. Public. Health* **2021**, *18*, 1157. [CrossRef]
22. Henjes-Kunst, E.; Raith, J.G.; Boyce, A.J. Micro-Scale Sulfur Isotope and Chemical Variations in Sphalerite from the Bleiberg Pb-Zn Deposit, Eastern Alps, Austria. *Ore Geol. Rev.* **2017**, *90*, 52–62. [CrossRef]
23. Giorno, M.; Barale, L.; Bertok, C.; Frenzel, M.; Looser, N.; Guillong, M.; Bernasconi, S.M.; Martire, L. Sulfide-Associated Hydrothermal Dolomite and Calcite Reveal a Shallow Burial Depth for Alpine-Type Zn-(Pb) Deposits. *Geology* **2022**, *50*, 853–858. [CrossRef]
24. Brigo, L.; Dulski, P.; Möller, P.; Schneider, H.-J.; Wolter, R. Strata-Bound Mineralizations in the Carnic Alps/Italy. In *Mineral Deposits within the European Community*; Boissonnas, J., Omenetto, P., Eds.; Springer: Berlin/Heidelberg, Germany, 1988; pp. 485–498, ISBN 978-3-642-51860-7.
25. Brigo, L.; Camana, G.; Rodeghiero, F.; Potenza, R. Carbonate-Hosted Siliceous Crust Type Mineralization of Carnic Alps (Italy-Austria). *Ore Geol. Rev.* **2001**, *17*, 199–214. [CrossRef]
26. Brigo, L.; Kostelka, L.; Omenetto, P.; Schneider, H.-J.; Schroll, E.; Schulz, O.; Štrucl, I. Comparative Reflections on Four Alpine Pb-Zn Deposits. In *Time- and Strata-Bound Ore Deposits*; Klemm, D.D., Schneider, H.-J., Eds.; Springer: Berlin/Heidelberg, Germany, 1977; pp. 273–293, ISBN 978-3-642-66808-1.
27. Ross, P.-S.; Bourke, A.; Fresia, B. Improving Lithological Discrimination in Exploration Drill-Cores Using Portable X-ray Fluorescence Measurements: (1) Testing Three Olympus Innov-X Analysers on Unprepared Cores. *Geochem. Explor. Environ. Anal.* **2014**, *14*, 171–185. [CrossRef]
28. *US EPA Method 3052*; Microwave Assisted Acid Digestion of Siliceous and Organically Based Matrices; United States Environmental Protection Agency: Washington, DC, USA, 1996.
29. *US EPA Method 7473 (SW-846)*; Mercury in Solids and Solutions by Thermal Decomposition, Amalgamation, and Atomic Absorption Spectrophotometry; United States Environmental Protection Agency: Washington, DC, USA, 1998.
30. Al-Musawi, M.; Kaczmarek, S. A New Carbonate-Specific Quantification Procedure for Determining Elemental Concentrations from Portable Energy-Dispersive X-ray Fluorescence (PXRF) Data. *Appl. Geochem.* **2020**, *113*, 104491. [CrossRef]
31. *US EPA Method 6200*; Field Portable X-ray Fluorescence Spectrometry for the Determination of Elemental Concentrations in Soils and Sediment; United States Environmental Protection Agency: Washington, DC, USA, 2007.
32. Durance, P.; Jowitt, S.M.; Bush, K. An Assessment of Portable X-ray Fluorescence Spectroscopy in Mineral Exploration, Kurnalpi Terrane, Eastern Goldfields Superterrane, Western Australia. *Appl. Earth Sci.* **2014**, *123*, 150–163. [CrossRef]
33. Sarala, P. Comparison of Different Portable XRF Methods for Determining till Geochemistry. *Geochem. Explor. Environ. Anal.* **2016**, *16*, 181–192. [CrossRef]
34. Casari, L. Tetrahedrite-Tennantite Series in the Carnic Chain (Eastern Alps, Italy). *N. Jb. Miner. Mh.* **1996**, *5*, 193–200.

APPENDICES

Appendix A: data from the Zn-Pb Raibl mining site

Table A.1 - Chemical-physical parameters and concentrations of the major ions of waters in the Zn-Pb Raibl decommissioned mining site (Paper I).

Name	**Date**	**Type**	**Water level**	**Depth water**	**pH**	**ORP**	**T**	**EC**	**DO**	**Sat. O_2**	**TDS**	**Ca^{2+}**	**Mg^{2+}**	**Na^{+}**	**K^{+}**	**F^{-}**	**Cl^{-}**	**NO_3^{-}**	**SO_4^{2-}**	**HCO_3^{-}**	**CO_3^{2-}**
			m a.s.l.	*m*		*mV*	*°C*	*µS/cm*	*mg/L*	*%*	*mg/L*	mg/L	mg/L	mg/L	mg/L	mg/L	mg/L	mg/L	mg/L	mg/L	mg/L
DSB1	13/07/2021	Mine drainage water			8.3	126	7.9	611	8.3	78.4	306	84.8	35.0	0.90						162	7.2
DSB1	27/08/2020	Mine drainage water			8.1	225	9.5	611	6.5	61.3	305	105	37.6	0.69	0.59					155	
DSB1	23/07/2020	Mine drainage water			8.0	199	8.8	597	9.1	87.6	299	97.5	37.1	0.65	0.58					166	
DSB1	24/06/2020	Mine drainage water			8.1	252	8.2	547	9.5	92.8	284	91.5	33.0	0.61	0.59					164	
DSB1	21/05/2020	Mine drainage water			7.8	292	9.7	591	9.4	91.4	296	81.9	29.8	0.58	0.55	0.18			171	186	
DSB1	15/02/2020	Mine drainage water			8.3	186	7.4	601				89.5	34.4	0.65	0.62					171	
DSB1	25/01/2020	Mine drainage water			8.5	188	7.6	689				108	37.8	0.77	0.80					153	
DSB1	22/12/2019	Mine drainage water			8.2	179	7.7	309				49.5	18.0	0.58	0.64	0.11			89.9	155	
DSB1	04/12/2019	Mine drainage water			7.8	193	7.5	520				79.6	30.4	0.71	0.87					151	
DSB1	03/11/2019	Mine drainage water			7.9	198	8.5	565	9.6	81.7		98.3	34.6	0.78	0.68					164	
DSB1	02/07/2018	Mine drainage water			8.7	218	8.1	625	11.4	95.2		80.4	35.1	0.65	0.44	0.17	0.73	0.65	178	167	
DSB2	13/07/2021	Mine drainage water			8.4	110	7.7	599	8.1	76.6	300	81.5	45.4	1.41	2.24					220	7.2
DSB2	27/08/2020	Mine drainage water			8.5	200	8.5	548	5.8	50.8	274	80.4	45.4	1.16	0.96					234	
DSB2	23/07/2020	Mine drainage water			8.5	178	8.2	549	8.6	81.6	274	78.8	44.6	1.02	0.83					195	14.4
DSB2	24/06/2020	Mine drainage water			8.4	226	8.4	549	9.0	84.4	275	77.5	42.3	0.98	0.78					237	
DSB2	21/05/2020	Mine drainage water			8.4	266	8.5	548	9.7	92.8	274	76.4	41.6	1.03	0.94	0.26			118	212	8.4
DSB2	15/02/2020	Mine drainage water			8.5	145	7.0	600				76.6	42.0	1.07	0.84					210	9.6
DSB2	25/01/2020	Mine drainage water			8.7	173	7.1	593				78.6	43.8	1.04	0.79					223	7.2
DSB2	22/12/2019	Mine drainage water			8.4	184	7.5	488				68.5	36.8	1.16	0.89	0.25	1.43		201	208	10.2
DSB2	04/12/2019	Mine drainage water			8.4	185	7.2	496				67.1	37.0	1.26	0.96					190	15.6
DSB3	13/07/2021	Mine drainage water			8.4	119	7.5	394	8.5	79.9	197	58.8	22.9	1.42	3.04					178	7.2
DSB3	27/08/2020	Mine drainage water			8.5	204	7.8	420	5.6	50.0	210	69.5	25.3	1.39	1.33					190	
DSB3	23/07/2020	Mine drainage water			8.5	180	8.1	409	8.7	81.6	205	68.2	23.8	1.30	1.18					182	7.2
DSB3	24/06/2020	Mine drainage water			8.4	230	8.1	415	8.7	81.8	208	68.9	23.7	1.22	1.28					201	
DSB3	21/05/2020	Mine drainage water			8.4	280	7.7	394	9.5	88.2	197	65.4	21.5	1.11	1.20	0.23			82.0	193	
DSB3	15/02/2020	Mine drainage water			8.5	146	7.1	425				65.2	22.6	1.29	1.17					184	6.0
DSB3	25/01/2020	Mine drainage water			8.6	177	6.8	428				62.9	23.3	1.21	1.14					188	8.4
DSB3	22/12/2019	Mine drainage water			8.3	95	7.9	270				53.7	14.2	0.82	1.06	0.15	1.10		71.9	147	6.6

Name	Date	Type	Water level	Depth water	pH	ORP	T	EC	DO	Sat. O_2	TDS	Ca^{2+}	Mg^{2+}	Na^{+}	K^{+}	F^{-}	Cl^{-}	NO_3^{-}	SO_4^{2-}	HCO_3^{-}	CO_3^{2-}
			m a.s.l.	*m*		*mV*	*°C*	*µS/cm*	*mg/L*	*%*	*mg/L*	mg/L	mg/L	mg/L	mg/L	mg/L	mg/L	mg/L	mg/L	mg/L	mg/L
DSB3	04/12/2019	Mine drainage water			8.2	186	7.4	380				63.4	19.5	1.35	1.68					162	9.6
DPL	13/07/2021	Mine drainage water			8.3	111	11.6	580	9.1	90.6	290	81.6	36.1	0.97	0.83					178	10.8
DPL	25/08/2020	Mine drainage water			8.2	227	11.8	548	8.6	88.3	274	87.4	36.8	1.06	0.91					193	
DPL	22/07/2020	Mine drainage water			8.2	173	12.5	536	8.4	87.0	268	83.5	36.3	0.98	0.87					171	9.6
DPL	24/06/2020	Mine drainage water			8.2	208	14.3	503	7.9	85.2	252	85.1	33.8	0.92	0.90					201	
DPL	21/05/2020	Mine drainage water			8.0	262	13.2	520	8.3	87.6	260	84.2	33.2	0.88	0.86				142	165	7.2
DPL	15/02/2020	Mine drainage water			8.5	134	5.4	579				79.9	34.9	0.90	0.77					187	6.0
DPL	25/01/2020	Mine drainage water			8.6	150	6.0	571				79.7	34.5	1.53	0.87					192	3.6
DPL	22/12/2019	Mine drainage water			8.2	180	6.7	306				51.2	16.6	0.51	0.55	0.11			97.2	137	
DPL	04/12/2019	Mine drainage water			8.3	196	3.9	494				77.1	29.0	1.10	1.25					170	
DPL	28/10/2019	Mine drainage water			8.3	283	8.7	479	9.4	80.7		74.9	33.8	2.56	1.15					206	
DPL	02/07/2018	Mine drainage water			8.8	162	9.9	410	11.0	97.7		50.9	22.0	0.96	0.40	0.04	0.94	1.43	63.2	111	
DGG2	13/07/2021	Mine drainage water			8.4	106	10.8	231	8.5	86.6	116	40.1	12.1	0.64	4.34	0.05	3.68	1.70	5.40	157	8.4
DGG2	24/06/2021	Mine drainage water					10.6	253	10.3	102.0	127	40.2	11.7	0.58	0.39					159	8.4
DGG2	15/04/2021	Mine drainage water			7.4	222	5.9	278	7.8	70.8	139	42.1	11.6	0.46	0.30					181	
DGG2	30/11/2020	Mine drainage water					4.1	250	11.3	96.3	125	38.0	11.2	0.44	0.29				5.61	171	
PZA	26/08/2020	Tailings-affected water	876.29	25.06	7.9	112	14.6	240	6.6	72.4	120	42.9	12.4	1.00	0.33					170	
PZA	23/07/2020	Tailings-affected water	876.19	25.16	7.9	100	14.3	237	7.1	77.1	118	41.0	11.8	0.98	0.31					164	
PZA	25/06/2020	Tailings-affected water	876.81	24.54	7.9	235	10.6	232	7.9	78.3	116	41.2	11.4	0.95	0.31					173	
PZA	14/05/2020	Tailings-affected water	877.27	24.08	7.8	268	12.4	239	7.3	75.8	120	42.2	11.5	0.99	0.29					172	
PZA	20/02/2020	Tailings-affected water	874.16	27.19	7.9	123	7.1	257				40.9	10.5	0.97	0.34					166	
PZA	23/01/2020	Tailings-affected water	875.65	25.70	8.0	158	7.2	275				42.7	11.3	1.13	0.46					171	
PZA	19/12/2019	Tailings-affected water	876.84	24.51	7.6	206	8.3	202				38.9	10.3	1.17	0.27		1.04		15.1	161	
PZA	29/11/2019	Tailings-affected water	877.22	24.13	7.9	89	8.8	224				41.5	11.5	1.60	0.49					162	
PZA	10/09/2019	Tailings-affected water	876.23	25.12																	
PZA	22/11/2018	Tailings-affected water	876.71	24.64	7.7	165	8.0	253	8.1	67.6		39.0	10.6	1.81		0.04		2.07	15.1	110	
PZB2	09/09/2021	Tailings-affected water	874.86	24.93	7.9	95	13.3	232	6.0	64.5		41.3	11.5	1.01	0.34					171	
PZB2	25/08/2021	Tailings-affected water	875.44	24.35	7.9	114	10.1	366	7.3	73.8	184	39.4	11.5	0.95	0.33					157	
PZB2	13/07/2021	Tailings-affected water	875.70	24.09	8.0	128	11.1	254	7.4	72.3	127	41.0	11.4	1.28	3.00					155	

Name	Date	Type	Water level	Depth water	pH	ORP	T	EC	DO	Sat. O_2	TDS	Ca^{2+}	Mg^{2+}	Na^{+}	K^{+}	F^{-}	Cl^{-}	NO_3^{-}	SO_4^{2-}	HCO_3^{-}	CO_3^{2-}
			m a.s.l.	*m*		*mV*	*°C*	*µS/cm*	*mg/L*	*%*	*mg/L*	mg/L	mg/L	mg/L	mg/L	mg/L	mg/L	mg/L	mg/L	mg/L	mg/L
PZB2	24/06/2021	Tailings-affected water	875.99	23.80			11.9	269	6.9	77.9		41.5	11.9	1.19	0.41					161	
PZB2	19/05/2021	Tailings-affected water	876.21	23.58	7.5	158	8.3	288	6.4	61.2	144	47.2	12.7	1.25	0.37					168	
PZB2	15/04/2021	Tailings-affected water	875.75	24.04	7.2	223	8.4	289	6.5	61.7	145	44.0	12.1	1.36	0.34					172	
PZB2	04/03/2021	Tailings-affected water	875.70	24.09	7.4	262	6.8	278	8.2	75.1	139	42.5	11.4	1.16	0.15					171	
PZB2	30/11/2020	Tailings-affected water	874.74	25.05	7.4	237	7.4	276	8.0	72.2	138	41.9	11.2	0.92	0.14		1.06		17.6	176	
PZB2	05/11/2020	Tailings-affected water	875.70	24.09	7.7	201	7.7	273	7.2	70.2	136	42.5	11.4	1.02	0.13		1.04		24.5	173	
PZB2	08/10/2020	Tailings-affected water	876.09	23.70																	
PZB2	01/10/2020	Tailings-affected water	875.89	23.90	7.9	97	12.4	273	8.0	84.0	137	42.6	11.7	1.04	0.16		1.05		25.1	170	
PZB2	26/08/2020	Tailings-affected water	875.41	24.38	7.8	101	13.3	256	6.9	72.7	128	46.5	12.8	1.01	0.33					188	
PZB2	23/07/2020	Tailings-affected water	875.33	24.46	7.8	109	13.1	247	7.2	76.1	124	43.2	12.4	0.99	0.31					165	
PZB2	25/06/2020	Tailings-affected water	875.81	23.98	7.8	277	10.2	251	7.8	76.6	126	44.1	12.1	0.96	0.31					168	
PZB2	14/05/2020	Tailings-affected water	876.18	23.61	7.8	236	10.6	302	8.1	80.0	151	51.2	13.6	1.08	0.33					178	
PZB2	20/02/2020	Tailings-affected water	873.91	25.88	7.8	116	7.9	263				40.4	10.9	0.98	0.34					167	
PZB2	23/01/2020	Tailings-affected water	874.98	24.81	8.0	158	8.5	268	9.4	77.6		42.3	11.8	1.10	0.43					167	
PZB2	19/12/2019	Tailings-affected water	875.83	23.96	7.6	200	8.6	225	9.0	85.0		43.0	12.1	1.24	0.40					172	
PZB2	29/11/2019	Tailings-affected water	876.10	23.69	7.7	97	8.9	278				48.8	12.7	1.22	0.40					165	
PZB2	28/10/2019	Tailings-affected water	874.21	25.58	8.0	280	10.4	231	9.8	90.5		41.1	11.7	1.27	0.43					161	
PZB2	10/09/2019	Tailings-affected water	875.46	24.33	7.9	135	12.2	415	9.8	90.5		41.7	11.6	1.46	0.58					170	
PZB2	22/11/2018	Tailings-affected water	875.81	23.98	7.6	166	8.4	245	7.6	64.2		43.1	11.6	1.21		0.06		2.23	23.5	129	
PZ5	09/09/2021	Tailings-affected water	871.89	22.42	7.8	106	14.4	193	6.3	62.8		39.5	10.4	0.98	0.36					166	
PZ5	25/08/2021	Tailings-affected water	872.26	22.05	7.9	120	8.4	296	7.3	71.5	148	49.3	11.4	1.06	0.58					153	
PZ5	13/07/2021	Tailings-affected water	872.46	21.85	7.8	137	13.5	232	7.0	75.1	116	43.8	9.64	0.85	0.38					151	
PZ5	24/06/2021	Tailings-affected water	872.71	21.60			13.5	325	5.7	62.8	163	54.5	10.2	0.93	0.37					157	
PZ5	19/05/2021	Tailings-affected water	872.91	21.40	7.1	193	8.0	438	6.1	57.2	219	78.6	12.8	1.18	0.42					159	
PZ5	15/04/2021	Tailings-affected water	872.51	21.80	6.9	222	6.9	355	6.9	62.3	177	59.6	11.6	1.32	0.36					176	
PZ5	04/03/2021	Tailings-affected water	872.47	21.84	6.9	315	6.1	403	8.0	71.6	202	66.8	11.5	1.43	0.35					162	
PZ5	30/11/2020	Tailings-affected water	871.82	22.49	7.1		7.1	244	8.3	73.4	122	37.2	9.64	0.83	0.10		1.76		9.38	168	
PZ5	05/11/2020	Tailings-affected water	872.47	21.84	7.2	217	7.2	366	7.0	68.2	183	63.3	10.8	0.91	0.23				81.0	164	
PZ5	08/10/2020	Tailings-affected water	872.81	21.50																	

Name	Date	Type	Water level	Depth water	pH	ORP	T	EC	DO	Sat. O_2	TDS	Ca^{2+}	Mg^{2+}	Na^{+}	K^{+}	F^{-}	Cl^{-}	NO_3^{-}	SO_4^{2-}	HCO_3^{-}	CO_3^{2-}
			m a.s.l.	*m*		*mV*	*°C*	*µS/cm*	*mg/L*	*%*	*mg/L*	mg/L	mg/L	mg/L	mg/L	mg/L	mg/L	mg/L	mg/L	mg/L	mg/L
PZ5	01/10/2020	Tailings-affected water	872.62	21.69	7.4	213	13.8	710	5.7	62.0	355	130.7	21.5	1.41	0.41	0.13	1.61		277	178	
PZ5	26/08/2020	Tailings-affected water	872.27	22.04	7.6	114	16.0	287	6.4	71.8	143	51.7	12.3	0.98	0.36		1.53		35.5	167	
PZ5	23/07/2020	Tailings-affected water	872.21	22.10	7.7	132	14.6	252	6.5	72.2	126	43.4	11.2	0.96	0.37		1.42		19.3	162	
PZ5	25/06/2020	Tailings-affected water	872.58	21.73	7.7	272	10.5	275	7.5	73.9	137	50.9	11.2	0.90	0.39		1.15		39.0	164	
PZ5	14/05/2020	Tailings-affected water	872.89	21.42	7.5	237	11.6	513	7.6	78.0	257	92.6	19.0	1.09	0.39		1.54		191	165	
PZ5	20/02/2020	Tailings-affected water	871.29	23.02	7.9	121	6.5	234				34.6	10.5	0.95	0.31		1.30		5.34	164	
PZ5	23/01/2020	Tailings-affected water	871.98	22.33	8.0	160	6.8	238				38.6	9.69	0.94	0.32		2.18		10.3	159	
PZ5	19/12/2019	Tailings-affected water	872.61	21.70	7.3	205	8.1	281				53.6	11.1	1.17	0.38		2.19		64.5	165	
PZ5	29/11/2019	Tailings-affected water	872.83	21.48	7.3	110	9.4	433				83.7	15.4	1.13	0.54		1.06		62.0	165	
PZ5	28/10/2019	Tailings-affected water	871.51	22.80	8.0	280	10.6	226				39.1	11.5	1.18	0.34		1.98		12.3	176	
PZ5	10/09/2019	Tailings-affected water	872.37	21.94	7.5	146	12.7	550	6.9	73.8		77.1	18.6	1.64	0.72		2.06		201	176	
PZ5	22/11/2018	Tailings-affected water	872.66	21.65	7.3	167	8.9	281	7.3	62.4		52.1	10.3	1.32		0.06		2.08	50.4	160	
PZ7	09/09/2021	Tailings-affected water	870.72	16.83	7.9	112	11.5	228	4.6	56.4		44.2	11.9	1.07	0.45					171	
PZ7	25/08/2021	Tailings-affected water	870.95	16.60	7.8	124	13.4	312	7.5	79.1	156	43.9	11.7	1.04	0.45					162	
PZ7	13/07/2021	Tailings-affected water	871.08	16.47	7.9	147	12.9	253	7.0	70.7	126	44.6	11.7	1.09	0.68					160	
PZ7	24/06/2021	Tailings-affected water	871.29	16.26			15.4	302	6.6	72.9	151	47.9	12.1	1.19	0.45					163	
PZ7	19/05/2021	Tailings-affected water	871.45	16.10	8.0	189	8.4	349	5.0	47.8	175	53.7	13.1	1.24	0.44					168	
PZ7	15/04/2021	Tailings-affected water	871.09	16.46	7.2	186	7.6	293	6.2	57.4	146	48.0	11.9	1.19	0.37					171	
PZ7	04/03/2021	Tailings-affected water	871.06	16.49	7.5	259	6.6	362	7.5	68.2	182	46.7	11.5	1.08	0.24					170	
PZ7	30/11/2020	Tailings-affected water	870.68	16.87	7.5	219	7.5	315	7.8	69.4	158	44.0	11.5	0.96	0.17		1.19		29.8	171	
PZ7	05/11/2020	Tailings-affected water	871.09	16.46	7.5	162	7.5	300	7.0	66.9	150	49.5	12.1	0.92	0.16		1.07		39.9	173	
PZ7	08/10/2020	Tailings-affected water	871.39	16.16																	
PZ7	01/10/2020	Tailings-affected water	871.23	16.32	7.8	92	12.2	328	4.9	49.9	164	54.0	13.6	1.11	0.24		1.19		56.5	175	
PZ7	26/08/2020	Tailings-affected water	870.93	16.62	7.8	106	13.2	271	7.2	76.2	135	48.7	13.5	1.00	0.33					170	
PZ7	23/07/2020	Tailings-affected water	870.89	16.66	7.8	119	13.4	260	7.1	74.6	130	46.3	12.2	0.98	0.32					170	
PZ7	25/06/2020	Tailings-affected water	871.15	16.40	7.9	251	9.4	265	7.0	67.6	132	50.2	12.7	0.92	0.31					168	
PZ7	14/05/2020	Tailings-affected water	871.45	16.10	7.9	235	11.3	359	7.9	79.0	180	62.9	15.1	1.08	0.40					171	
PZ7	20/02/2020	Tailings-affected water	870.35	17.20	7.7	129	7.5	284				45.8	11.2	0.98	0.41					166	
PZ7	23/01/2020	Tailings-affected water	870.76	16.79	7.9	152	7.2	296				47.7	12.1	0.97	0.38					176	

Name	Date	Type	Water level	Depth water	pH	ORP	T	EC	DO	Sat. O_2	TDS	Ca^{2+}	Mg^{2+}	Na^{+}	K^{+}	F^{-}	Cl^{-}	NO_3^{-}	SO_4^{2-}	HCO_3^{-}	CO_3^{2-}
			m a.s.l.	*m*		*mV*	*°C*	*µS/cm*	*mg/L*	*%*	*mg/L*	mg/L	mg/L	mg/L	mg/L	mg/L	mg/L	mg/L	mg/L	mg/L	mg/L
PZ7	19/12/2019	Tailings-affected water	871.18	16.37	7.6	195	8.6	255	8.5	80.2		47.8	12.2	1.10	0.36					179	
PZ7	29/11/2019	Tailings-affected water	871.39	16.16	7.6	130	8.2	339				63.2	14.7	1.12	0.54					178	
PZ7	28/10/2019	Tailings-affected water	870.50	17.05	7.9	280	9.2	243				43.8	12.0	1.16	0.35					177	
PZ7	10/09/2019	Tailings-affected water	871.04	16.51	7.8	108	10.4	352	8.1	82.4		49.9	12.6	1.79	0.74					178	
PZ7	22/11/2018	Tailings-affected water	871.26	16.29	7.4	168	7.7	297	8.3	69.8		55.5	12.7	1.85		0.06		3.33	48.1	149	
PZ7	25/09/2018	Tailings-affected water	870.95	16.60																	
PZ8	26/08/2020	Tailings-affected water	872.79	16.41	7.6	131	13.9	335	6.0	64.0	168	66.1	13.2	0.93	0.38					179	
PZ8	23/07/2020	Tailings-affected water	872.77	16.43	7.7	145	12.5	298	6.4	66.4	149	56.2	12.5	0.94	0.35					177	
PZ8	14/05/2020	Tailings-affected water	873.23	15.97	8.0	202	10.3	263	7.4	73.2	132	45.5	11.7	0.96	0.31					171	
PZ8	20/02/2020	Tailings-affected water	872.29	16.91	7.7	125	7.1	271				44.1	10.8	0.90	0.34					172	
PZ8	23/01/2020	Tailings-affected water	872.66	16.54	7.9	173	6.4	297				51.3	11.9	1.01	0.38					170	
PZ8	19/12/2019	Tailings-affected water	873.02	16.18	7.5	194	8.6	237				46.3	11.2	1.15	0.32		1.04		34.8	178	
PZ8	29/11/2019	Tailings-affected water	873.22	15.98	7.4	136	8.4	414				84.3	13.6	0.92	0.52					179	
PZ8	28/10/2019	Tailings-affected water	872.45	16.75	7.9	288	9.8	240	8.4	73.3		44.6	11.6	1.12	0.32					175	
PZ8	10/09/2019	Tailings-affected water	872.87	16.33	7.8	120	12.3	304	8.6	80.1		44.2	11.3	1.38	0.50					178	
PZ8	22/11/2018	Tailings-affected water	873.11	16.09	7.5	173	8.5	282	8.3	71.0		52.3	11.5	1.20	2.96	0.06	2.12	1.86	40.3	164	
RLM	25/06/2020	Stream water			8.5	168	11.6	209	8.1	82.2	105	35.0	11.2	0.65	0.21		1.17		1.69	160	
RLM	21/05/2020	Stream water			8.3	219	9.8	206	9.3	91.3	103										
RLM	14/05/2020	Stream water			8.3	279	12.7	215			109	35.1	10.4	0.75	0.24		1.58		1.97	160	
RLM	22/11/2018	Stream water			7.9	171	7.2	187	9.4	79.0		32.9	9.65	1.03	1.04	0.01	4.51	1.67	1.24	134	
RLB	25/08/2020	Stream water			8.1	283	13.0	224	9.4	99.1	112	39.3	11.9	1.04	0.34					162	
RLB	22/07/2020	Stream water			8.2	134	16.3	230	7.5	84.5	115	37.6	11.7	0.87	0.29					166	
RLB	24/06/2020	Stream water			8.0	198	15.0	354	8.3	90.2	176	37.5	11.0	0.98	0.34					159	
RLB	21/05/2020	Stream water			8.3	208	10.7	210	9.7	96.8	105	36.1	10.6	0.81	0.23		1.20		2.29	162	
RLB	22/12/2019	Stream water			8.3	160	3.8	171				30.4	9.42	0.91	0.26		1.30		2.86	152	
RLB	04/12/2019	Stream water			8.3	177	6.4	185				32.4	10.2	1.04	0.24					161	
RSB	26/08/2020	Tailings-affected water			7.9	228	9.2	292			146	52.7	13.8	1.04	0.36					168	
RSB	22/07/2020	Tailings-affected water			8.0	157	13.0	284	7.5	78.6	142	48.5	12.5	0.99	0.33					168	

Name	Date	Type	Water level	Depth water	pH	ORP	T	EC	DO	Sat. O_2	TDS	Ca^{2+}	Mg^{2+}	Na^{+}	K^{+}	F^{-}	Cl^{-}	NO_3^{-}	SO_4^{2-}	HCO_3^{-}	CO_3^{2-}
			m a.s.l.	*m*		*mV*	*°C*	*µS/cm*	*mg/L*	*%*	*mg/L*	mg/L	mg/L	mg/L	mg/L	mg/L	mg/L	mg/L	mg/L	mg/L	mg/L
RSB	25/06/2020	Tailings-affected water			7.9	258	9.3	276	7.5	72.1	138	49.8	13.0	0.99	0.33					171	
RSB	14/05/2020	Tailings-affected water			7.7	213	12.1	457	6.8	70.7	228	83.8	18.1	1.11	0.45		1.11		166	179	
RSB	20/02/2020	Tailings-affected water			7.8	125	5.1	273				44.9	10.8	0.93	0.36					172	
RSB	23/01/2020	Tailings-affected water			8.1	177	4.7	318				52.8	12.3	0.98	0.40					171	
RSB	19/12/2019	Tailings-affected water			7.7	202	7.7	241				49.0	12.2	1.13	0.36				40.3	175	
RSB	04/12/2019	Tailings-affected water			7.6	188	6.2	323													
RSB	29/11/2019	Tailings-affected water			7.7	277	7.7	350				63.5	15.3	1.16	0.43					175	
RSB	28/10/2019	Tailings-affected water			8.0	270	9.5	254	8.2	71.7		45.1	12.2	2.48	0.45					172	
RLV	26/08/2020	Stream water			8.1	213	10.8	239			119	42.6	13.0	1.00	0.31					166	
RLV	22/07/2020	Stream water			8.1	139	12.3	228	7.6	78.1	114	39.1	11.9	0.93	0.28					166	
RLV	25/06/2020	Stream water			8.1	242	10.4	222	7.8	77.2	111	40.4	11.5	0.88	0.27					166	
RLV	14/05/2020	Stream water			8.1	185	12.1	226	7.9	82.0	113	37.9	11.3	0.89	0.26		1.29		6.86	164	
RLV	20/02/2020	Stream water			8.1	122	5.4	233				36.1	10.6	0.94	0.30					167	
RLV	23/01/2020	Stream water			8.2	151	5.0	250				38.4	11.4	0.97	0.30					168	
RLV	19/12/2019	Stream water			7.9	186	7.3	186	10.2	93.3		37.8	11.1	1.09	0.27		1.36		13.7	178	
RLV	04/12/2019	Stream water			8.1	192	6.7	213													
RLV	29/11/2019	Stream water			8.1	271	7.3	216				41.1	11.2	1.03	0.26					164	
RLV	28/10/2019	Stream water			8.1	280	9.4	206	8.5	73.7		36.9	11.1	1.16	0.32					176	
RLV	10/09/2019	Stream water			8.0	111	11.8	286	9.8	89.3		38.6	11.4	1.51	0.54					166	
RLV	22/11/2018	Stream water			7.7	163	7.9	233	8.8	73.4		42.0	11.3	1.28	2.03	0.05	2.77	1.87	17.1	154	
RSC	25/08/2020	Stream water			8.7	230	11.8	337	10.9	107.8	169	58.1	18.2	3.83	0.67		4.94		30.7	149	20.4
RSC	22/07/2020	Stream water			8.6	134	15.6	366	8.6	92.9	183	57.3	17.2	3.32	0.57		4.40		30.9	167	13.2
RSC	22/11/2018	Stream water			8.2	159	6.3	327	10.2	82.1		56.5	16.5	4.40	2.09	0.05	6.90	2.49	22.5	211	

Table A.2 – Trace element concentration of waters in the Zn-Pb Raibl decommissioned mining site (Paper I).

Name	Date	Type	As	Ba	Cd	Cu	Fe	Ge	Mn	Pb	Sb	Tl	Zn
			µg/L	µg/L	µg/L	µg/L	µg/L	µg/L	µg/L	µg/L	µg/L	µg/L	µg/L
DSB1	13/07/2021	Mine drainage water	4.65	27.6	1.63	0.91	17.2	0.91	0.26	19.6	4.74	37.3	2789
DSB1	27/08/2020	Mine drainage water	4.20		3.37	0.53	10.6	1.28	0.16	16.8	7.27	41.8	4511
DSB1	23/07/2020	Mine drainage water	3.65		2.45	0.57	4.39	1.09	0.15	15.3	6.58	38.4	4191
DSB1	24/06/2020	Mine drainage water	3.45	5.94	2.68	0.49	1.33	1.14	0.10	15.3	5.79	37.2	4184
DSB1	21/05/2020	Mine drainage water	4.28	7.49	2.55		3.89	1.13	0.24	20.4	5.48	41.8	3994
DSB1	15/02/2020	Mine drainage water	4.05	7.13	1.75		5.16	1.05	0.15	19.3	5.49	39.0	3014
DSB1	25/01/2020	Mine drainage water	3.03		3.03		9.72	1.26	0.41	12.3	6.82	36.3	5484
DSB1	22/12/2019	Mine drainage water	3.87	40.8	1.62		18.4	1.35	0.40	32.0	2.68	31.1	2259
DSB1	04/12/2019	Mine drainage water	2.67	26.8	1.87		9.45	1.23	0.14	19.9	3.47	36.3	3192
DSB1	03/11/2019	Mine drainage water	3.92	19.8	3.69		15.4	1.39	0.22	14.9	8.18	52.2	4765
DSB1	02/07/2018	Mine drainage water	5.43		2.16	0.89	2.44		0.17	21.3		43.3	2508
DSB2	13/07/2021	Mine drainage water	86.6	46.5	1.26	1.11	32.4	0.84	0.98	2.64	1.56	11.0	994
DSB2	27/08/2020	Mine drainage water	80.1	21.3	0.98	0.86	11.6	0.92	0.19	1.10	1.56	10.7	966
DSB2	23/07/2020	Mine drainage water	64.5	20.8	0.63	0.59	2.31	0.78	0.13	0.53	1.38	9.03	940
DSB2	24/06/2020	Mine drainage water	64.2	27.0	0.61	0.50	3.02	0.76	0.16	0.39	1.31	8.70	944
DSB2	21/05/2020	Mine drainage water	68.3	26.1	0.83		3.54	0.82	0.15	0.51	1.40	9.83	963
DSB2	15/02/2020	Mine drainage water	76.9	23.7	0.89		6.20	0.86	0.24	0.95	1.52	10.3	890
DSB2	25/01/2020	Mine drainage water	77.8	17.7	0.90		14.8	0.87	0.52	1.81	1.54	10.4	909
DSB2	22/12/2019	Mine drainage water	78.9	39.5	0.69		23.1	0.92	0.36	2.29	1.62	10.7	784
DSB2	04/12/2019	Mine drainage water	72.6	39.4	0.69		28.1	0.91	0.39	1.43	1.56	10.3	823
DSB3	13/07/2021	Mine drainage water	2.38	84.9	1.20	1.14	37.9	0.27	0.67	16.0	1.75	2.94	1369
DSB3	27/08/2020	Mine drainage water	1.45	63.6	1.32	1.25	11.1	0.27	0.35	13.4	1.69	2.56	1540
DSB3	23/07/2020	Mine drainage water	1.27	62.3	0.94	0.67	3.04	0.24	0.19	10.8	1.38	1.87	1380
DSB3	24/06/2020	Mine drainage water	1.13	66.0	1.21	0.52	1.82	0.22	0.18	12.5	1.38	2.17	1676
DSB3	21/05/2020	Mine drainage water	1.22	57.8	1.52		2.66	0.23	0.16	14.8	1.32	1.99	2215
DSB3	15/02/2020	Mine drainage water	1.50	64.8	1.02		7.78	0.27	0.50	14.7	1.66	2.57	1256
DSB3	25/01/2020	Mine drainage water	1.64	57.2	1.11		17.4	0.28	0.81	16.0	1.76	2.94	1353
DSB3	22/12/2019	Mine drainage water	1.81	45.9	1.76		15.6	0.38	0.30	23.4	1.60	3.84	1777

Name	Date	Type	As	Ba	Cd	Cu	Fe	Ge	Mn	Pb	Sb	Tl	Zn
			µg/L	µg/L	µg/L	µg/L	µg/L	µg/L	µg/L	µg/L	µg/L	µg/L	µg/L
DSB3	04/12/2019	Mine drainage water	1.91	62.6	1.66		11.3	0.30	0.32	14.9	1.67	4.13	1628
DPL	13/07/2021	Mine drainage water	31.6	43.9	1.59	0.59	31.3	0.81	0.69	12.9	3.35	22.8	2091
DPL	25/08/2020	Mine drainage water	29.7	25.7	2.09	0.54	9.56	0.86	0.31	9.12	3.84	21.9	2620
DPL	22/07/2020	Mine drainage water	25.1	25.6	1.42	0.56	1.50	0.69	0.26	7.83	3.01	17.6	2359
DPL	24/06/2020	Mine drainage water	21.4	29.9	1.69	0.54	3.06	0.71	0.24	9.33	3.13	19.9	2786
DPL	21/05/2020	Mine drainage water	16.4	29.4	1.92		2.69	0.75	0.23		2.89	28.9	2814
DPL	15/02/2020	Mine drainage water	30.7	23.4	1.44		3.62	0.81	0.17	10.6	3.39	20.2	2065
DPL	25/01/2020	Mine drainage water	25.4	19.5	1.43		12.2	0.80	0.43	12.3	3.38	21.1	2206
DPL	22/12/2019	Mine drainage water	4.12	48.7	2.52		11.5	0.69	0.26	28.7	1.40	37.5	2201
DPL	04/12/2019	Mine drainage water	14.2	39.9	1.92		14.5	0.93	0.74	12.9	2.93	30.4	2729
DPL	28/10/2019	Mine drainage water	37.5	46.8	1.59		8.94	0.85	0.20	8.48	3.48	17.3	1852
DPL	02/07/2018	Mine drainage water	16.5		0.74	1.96	22.8		0.80	7.79		11.3	866
DGG2	13/07/2021	Mine drainage water	1.15	56.5	0.13	2.90	9.13	0.19	0.32	9.19	0.10	2.79	211
DGG2	24/06/2021	Mine drainage water	1.02	53.4	0.10	0.94	8.11	0.18	0.13	8.48	0.06	2.29	175
DGG2	15/04/2021	Mine drainage water	1.19	59.1	0.11	0.40	7.22	0.25	0.09	9.56	0.07	2.96	238
DGG2	30/11/2020	Mine drainage water	1.28	53.4	0.13	1.30	14.9	0.21	0.13	10.3		2.78	183
PZA	26/08/2020	Tailings-affected water	0.99	29.4	0.27	0.68	4.90	0.11	0.03	28.8	0.18	5.05	595
PZA	23/07/2020	Tailings-affected water	0.81	26.6	0.22	0.76	1.66	0.09	0.06	23.8	0.17	4.12	579
PZA	25/06/2020	Tailings-affected water	0.88	31.1	0.22	1.07	1.71	0.08	0.10	22.8	0.15	3.72	599
PZA	14/05/2020	Tailings-affected water	0.83	32.7	0.24		1.93	0.07	0.06	24.4	0.13	3.73	653
PZA	20/02/2020	Tailings-affected water	0.86	32.2	0.27		2.49	0.08	0.06	25.5	0.15	4.16	732
PZA	23/01/2020	Tailings-affected water	0.82	27.3	0.26		2.69	0.09	0.19	26.7	0.18	4.27	664
PZA	19/12/2019	Tailings-affected water	0.96	49.5	0.29		6.16	0.09	0.09	29.1	0.18	4.51	535
PZA	29/11/2019	Tailings-affected water	1.07	58.2	0.32		7.25	0.10	0.21	33.1	0.19	5.06	559
PZA	10/09/2019	Tailings-affected water											
PZA	22/11/2018	Tailings-affected water	1.25		0.38	1.92	73.7		2.36	38.0		6.35	468
PZB2	09/09/2021	Tailings-affected water	0.87	50.1	0.29	0.86	6.86	0.13	0.08	26.7	0.17	16.2	815
PZB2	25/08/2021	Tailings-affected water	0.83	49.0	0.26	0.66	6.00	0.12	0.06	25.0	0.16	15.5	819
PZB2	13/07/2021	Tailings-affected water	1.17	49.9	0.34	1.67	6.11	0.13	0.19	22.4	0.21	15.5	949

Name	Date	Type	As	Ba	Cd	Cu	Fe	Ge	Mn	Pb	Sb	Tl	Zn
			µg/L	µg/L	µg/L	µg/L	µg/L	µg/L	µg/L	µg/L	µg/L	µg/L	µg/L
PZB2	24/06/2021	Tailings-affected water	0.81	50.8	0.29	2.21	8.47	0.13	0.12	25.8	0.17	15.6	958
PZB2	19/05/2021	Tailings-affected water	0.83	55.4	0.34	2.13	7.45	0.15	0.08	28.6	0.19	16.5	1121
PZB2	15/04/2021	Tailings-affected water	0.82	53.1	0.31	0.80	14.6	0.13	0.93	26.8	0.20	15.1	1000
PZB2	04/03/2021	Tailings-affected water	0.92	51.0	0.37	0.66	5.15	0.15	0.08	28.7	0.19	16.3	971
PZB2	30/11/2020	Tailings-affected water	1.02	52.2	0.32	0.86	15.5	0.15	0.15	29.4	0.21	17.3	809
PZB2	05/11/2020	Tailings-affected water	1.00	54.7	0.35	1.75	7.21	0.18	0.16	30.6	0.25	18.4	936
PZB2	08/10/2020	Tailings-affected water											
PZB2	01/10/2020	Tailings-affected water	0.99	55.3	0.39	1.16	7.25	0.19	0.18	29.8	0.36	20.7	995
PZB2	26/08/2020	Tailings-affected water	1.02	30.4	0.32	0.81	5.70	0.16	0.06	30.0	0.21	16.8	973
PZB2	23/07/2020	Tailings-affected water	0.82	26.2	0.24	0.63	2.27	0.12	0.06	24.4	0.17	14.3	918
PZB2	25/06/2020	Tailings-affected water	0.82	32.8	0.26	1.11	3.12	0.13	0.09	24.2	0.17	13.8	1029
PZB2	14/05/2020	Tailings-affected water	0.83	39.5	0.30		2.16	0.14	0.07	27.3	0.17	14.3	1216
PZB2	20/02/2020	Tailings-affected water	1.02	28.6	0.25		3.91	0.14	0.13	25.5	0.19	16.1	845
PZB2	23/01/2020	Tailings-affected water	0.89	26.5	0.29		2.84	0.15	0.12	28.4	0.20	16.7	937
PZB2	19/12/2019	Tailings-affected water	0.99	51.6	0.36		6.94	0.20	0.22	31.3	0.24	19.7	940
PZB2	29/11/2019	Tailings-affected water	0.94	59.0	0.41		5.75	0.23	0.04	34.2	0.23	22.2	1155
PZB2	28/10/2019	Tailings-affected water	1.05	47.7	0.29		11.3	0.15	0.16	30.2	0.42	17.0	685
PZB2	10/09/2019	Tailings-affected water	1.04	47.0	0.31		8.52	0.14	0.41	28.5	0.27	16.5	753
PZB2	22/11/2018	Tailings-affected water	0.94		0.46	0.83	6.69		0.20	37.6		25.4	984
PZ5	09/09/2021	Tailings-affected water	2.60	89.3	3.32	1.32	6.46	0.91	0.09	55.7	0.34	29.5	2783
PZ5	25/08/2021	Tailings-affected water	2.41	98.2	4.24	8.55	10.5	1.14	0.32	56.4	0.42	51.3	4111
PZ5	13/07/2021	Tailings-affected water	2.18	68.8	3.95	1.53	17.4	1.34	4.81	55.9	0.41	70.7	4180
PZ5	24/06/2021	Tailings-affected water	2.04	66.9	4.90	1.52	11.3	1.45	0.14	58.6	0.42	88.0	5743
PZ5	19/05/2021	Tailings-affected water	1.99	77.1	6.36	3.90	11.9	1.40	0.24	63.5	0.41	106	7912
PZ5	15/04/2021	Tailings-affected water	2.09	74.6	5.01	1.61	9.90	0.95	0.17	61.3	0.33	56.3	5913
PZ5	04/03/2021	Tailings-affected water	2.11	77.3	6.52	2.01	9.39	1.19	0.40	61.6	0.42	62.3	7415
PZ5	30/11/2020	Tailings-affected water	2.61	75.7	3.60	1.36	14.5	0.86	0.10	55.8	0.34	19.6	3034
PZ5	05/11/2020	Tailings-affected water	2.31	79.5	6.54	3.08	9.77	1.61	0.97	69.4	0.49	79.8	6712
PZ5	08/10/2020	Tailings-affected water											
PZ5	01/10/2020	Tailings-affected water	2.12	148	13.6	2.16	15.4	2.05	0.79	96.3	0.58	120	14933

Name	Date	Type	As	Ba	Cd	Cu	Fe	Ge	Mn	Pb	Sb	Tl	Zn
			µg/L	µg/L	µg/L	µg/L	µg/L	µg/L	µg/L	µg/L	µg/L	µg/L	µg/L
PZ5	26/08/2020	Tailings-affected water	2.56	69.0	4.58	1.54	9.43	1.23	0.08	66.2	0.42	42.8	4878
PZ5	23/07/2020	Tailings-affected water	2.14	61.3	3.33	1.42	2.97	0.98	0.10	53.2	0.34	31.4	3915
PZ5	25/06/2020	Tailings-affected water	1.93	72.5	3.99	2.28	5.83	1.05	0.25	51.7	0.37	45.0	5637
PZ5	14/05/2020	Tailings-affected water	1.76	116	6.77		3.53	0.92	0.07	64.5	0.31	59.9	11181
PZ5	20/02/2020	Tailings-affected water	1.33	17.5	0.78		4.00	0.20	0.16	21.0	0.16	8.27	789
PZ5	23/01/2020	Tailings-affected water	2.34	48.2	3.22		2.17	0.82	0.07	52.1	0.33	23.8	3320
PZ5	19/12/2019	Tailings-affected water	2.24	83.3	5.52		6.53	1.37	0.21	70.8	0.45	67.3	5614
PZ5	29/11/2019	Tailings-affected water	2.11	102	7.78		10.2	1.69	0.33	82.4	0.49	117	9727
PZ5	28/10/2019	Tailings-affected water	2.83	80.4	2.30		14.3	0.52	0.34	50.7	0.37	15.3	1523
PZ5	10/09/2019	Tailings-affected water	2.41	157	7.04		9.76	1.12	0.32	81.3	0.49	48.7	6741
PZ5	22/11/2018	Tailings-affected water	2.24		5.34	2.15	7.07		0.17	70.1		80.1	5243
PZ7	09/09/2021	Tailings-affected water	1.14	56.1	0.23	1.55	7.64	0.18	0.23	19.9	0.23	37.3	1084
PZ7	25/08/2021	Tailings-affected water	1.13	52.2	0.22	1.96	7.02	0.17	0.13	18.7	0.23	34.3	1077
PZ7	13/07/2021	Tailings-affected water	1.12	47.5	0.23	1.64	10.4	0.17	0.12	19.3	0.23	35.7	1126
PZ7	24/06/2021	Tailings-affected water	1.07	45.2	0.27	1.68	10.7	0.17	0.17	21.0	0.23	43.9	1300
PZ7	19/05/2021	Tailings-affected water	1.09	52.4	0.34	1.72	17.1	0.20	0.33	21.5	0.28	50.5	1574
PZ7	15/04/2021	Tailings-affected water	1.08	48.1	0.26	1.87	8.51	0.19	0.10	20.8	0.33	36.6	1239
PZ7	04/03/2021	Tailings-affected water	1.26	46.3	0.26	1.27	6.35	0.21	0.30	19.7	0.28	37.4	1197
PZ7	30/11/2020	Tailings-affected water	1.28	47.0	0.27	1.31	16.7	0.20	0.28	21.6	0.28	40.5	1119
PZ7	05/11/2020	Tailings-affected water	1.30	50.4	0.31	1.28	7.05	0.23	0.09	22.3	0.29	44.6	1322
PZ7	08/10/2020	Tailings-affected water											
PZ7	01/10/2020	Tailings-affected water	1.21	57.9	0.38	1.84	6.71	0.23	0.11	22.5	0.32	48.4	1481
PZ7	26/08/2020	Tailings-affected water	1.34	28.4	0.24	0.89	5.60	0.19	0.07	21.3	0.27	35.2	1134
PZ7	23/07/2020	Tailings-affected water	1.10	28.7	0.20	0.92	1.84	0.16	0.06	18.5	0.22	30.4	1066
PZ7	25/06/2020	Tailings-affected water	1.07	31.5	0.21	1.20	1.36	0.17	0.09	18.2	0.23	32.3	1194
PZ7	14/05/2020	Tailings-affected water	1.06	46.9	0.33		2.50	0.21	0.07	22.7	0.27	48.1	1858
PZ7	20/02/2020	Tailings-affected water	1.33	30.1	0.29		3.51	0.20	0.17	23.5	0.27	45.7	1193
PZ7	23/01/2020	Tailings-affected water	1.18	25.1	0.26		2.30	0.21	0.05	21.6	0.27	42.5	1248
PZ7	19/12/2019	Tailings-affected water	1.29	52.1	0.30		8.65	0.23	0.23	25.6	0.30	43.9	1163
PZ7	29/11/2019	Tailings-affected water	1.21	64.2	0.41		7.59	0.28	0.10	27.7	0.31	69.9	1816

Name	Date	Type	As	Ba	Cd	Cu	Fe	Ge	Mn	Pb	Sb	Tl	Zn
			µg/L	µg/L	µg/L	µg/L	µg/L	µg/L	µg/L	µg/L	µg/L	µg/L	µg/L
PZ7	28/10/2019	Tailings-affected water	1.41	55.1	0.27		17.7	0.21	0.32	24.6	0.33	38.1	948
PZ7	10/09/2019	Tailings-affected water	1.32	61.0	0.32		7.07	0.22	0.33	25.2	0.30	41.2	1166
PZ7	22/11/2018	Tailings-affected water	1.22		0.38	0.98	2.79		0.24	28.8		69.0	1552
PZ7	25/09/2018	Tailings-affected water											
PZ8	26/08/2020	Tailings-affected water	1.40	48.1	0.38	5.68	6.61	0.37	0.50	32.0	1.13	72.2	3333
PZ8	23/07/2020	Tailings-affected water	1.35	60.2	0.28	3.79	2.27	0.25	0.30	26.1	0.74	50.7	2478
PZ8	14/05/2020	Tailings-affected water	1.44	61.9	0.21		2.27	0.19	0.15	22.9	0.53	35.3	1459
PZ8	20/02/2020	Tailings-affected water	1.55	68.6	0.22		3.00	0.22	0.18	24.4	0.63	41.9	1629
PZ8	23/01/2020	Tailings-affected water	1.57	49.2	0.28		2.99	0.27	0.27	27.0	0.78	49.4	2057
PZ8	19/12/2019	Tailings-affected water	1.42	57.3	0.28		8.08	0.24	0.36	28.7	0.66	43.6	1587
PZ8	29/11/2019	Tailings-affected water	1.30	67.1	0.60		8.24	0.45	1.05	40.8	1.37	97.0	4644
PZ8	28/10/2019	Tailings-affected water	1.64	80.2	0.26		5.28	0.25	0.15	28.6	0.63	40.8	1279
PZ8	10/09/2019	Tailings-affected water	1.60	91.5	0.24		8.18	0.23	0.34	27.5	0.62	38.6	1246
PZ8	22/11/2018	Tailings-affected water	1.69		0.32	4.22	5.15		0.56	36.3		66.5	1946
RLM	25/06/2020	Stream water	0.26		0.03	0.68	3.70	0.01	0.17	1.95	0.07	0.06	
RLM	21/05/2020	Stream water											
RLM	14/05/2020	Stream water	0.18		0.02		1.96	0.00	0.15	1.55	0.07	0.02	
RLM	22/11/2018	Stream water					4.40		0.39	3.67		0.02	3
RLB	25/08/2020	Stream water	0.72	15.8	0.28	0.91	4.69	0.07	0.12	37.7	0.32	1.94	223
RLB	22/07/2020	Stream water	0.62	13.8	0.25	0.64	1.61	0.06	0.06	33.0	0.16	1.75	220
RLB	24/06/2020	Stream water	0.54	11.7	0.17	0.92	5.67	0.04	0.22	21.1	0.15	0.87	144
RLB	21/05/2020	Stream water	0.39		0.08		2.80	0.01	0.12	8.74	0.09	0.32	24
RLB	22/12/2019	Stream water	0.23	7.49	0.07		9.06	0.01	0.25	5.32	0.09	0.24	48
RLB	04/12/2019	Stream water	0.45	18.1	0.14		4.78	0.03	0.14	11.5	0.13	0.65	121
RSB	26/08/2020	Tailings-affected water	1.35	32.0	0.66	1.20	16.1	0.32	0.14	30.7	0.32	47.6	1917
RSB	22/07/2020	Tailings-affected water	1.23	29.9	0.54	0.87	1.14	0.29	0.06	28.3	0.28	43.0	1741
RSB	25/06/2020	Tailings-affected water	1.18	36.5	0.55	1.17	1.81	0.27	0.08	27.8	0.27	41.4	1852
RSB	14/05/2020	Tailings-affected water	1.27	112	1.14		3.74	0.44	0.27	40.2	0.40	69.1	4036

Name	Date	Type	As	Ba	Cd	Cu	Fe	Ge	Mn	Pb	Sb	Tl	Zn
			µg/L	µg/L	µg/L	µg/L	µg/L	µg/L	µg/L	µg/L	µg/L	µg/L	µg/L
RSB	20/02/2020	Tailings-affected water	1.18	35.7	0.47		4.36	0.30	0.19	27.0	0.29	36.5	1639
RSB	23/01/2020	Tailings-affected water	1.14	35.3	0.64		3.57	0.36	0.08	28.1	0.32	52.9	2229
RSB	19/12/2019	Tailings-affected water	1.22	56.8	0.67		7.31	0.33	0.10	34.7	0.30	42.9	1675
RSB	04/12/2019	Tailings-affected water											
RSB	29/11/2019	Tailings-affected water	1.24	69.0	0.87		39.4	0.33	0.31	39.5	0.31	48.4	2390
RSB	28/10/2019	Tailings-affected water	1.39	58.1	0.45		7.55	0.31	0.09	28.5	0.46	39.3	1259
RLV	26/08/2020	Stream water	1.12	33.8	0.54	0.95	10.6	0.20	0.22	25.1	0.22	10.8	698
RLV	22/07/2020	Stream water	0.94	29.6	0.39	0.69	0.95	0.15	0.04	20.3	0.17	8.27	571
RLV	25/06/2020	Stream water	0.96	33.4	0.39	1.18	1.81	0.14	0.15	22.3	0.18	8.13	586
RLV	14/05/2020	Stream water	0.58	13.5	0.25		9.09	0.07	2.95	18.6	0.13	5.82	338
RLV	20/02/2020	Stream water	0.94	40.1	0.33		2.36	0.11	0.08	18.9	0.14	4.68	433
RLV	23/01/2020	Stream water	0.94	25.6	0.37		2.53	0.14	0.08	20.1	0.17	8.45	624
RLV	19/12/2019	Stream water	1.10	46.4	0.49		7.35	0.16	0.08	32.7	0.20	10.6	605
RLV	04/12/2019	Stream water											
RLV	29/11/2019	Stream water	0.83	38.8	0.40		42.1	0.12	0.18	23.0	0.16	9.03	554
RLV	28/10/2019	Stream water	1.03	57.4	0.47		6.82	0.18	0.04	21.1	0.23	6.28	487
RLV	10/09/2019	Stream water	1.06	62.0	0.53		10.4	0.22	0.30	24.5	0.28	24.5	667
RLV	22/11/2018	Stream water	1.18		0.50		3.46		0.27	27.6		10.6	632
RSC	25/08/2020	Stream water	0.67	19.3	0.10	0.93	6.61	0.06	0.53	3.71	0.12	1.06	81
RSC	22/07/2020	Stream water	0.57	16.0	0.09	0.50	1.63	0.05	0.72	3.43	0.10	0.95	76
RSC	22/11/2018	Stream water	0.71				2.88		0.40	3.85		0.96	17

Table A.3 – Chemical composition of solids in the Zn-Pb Raibl decommissioned mining site (Paper II).

TOTAL CONCENTRATION		**As**	**Cd**	**Co**	**Cr**	**Cu**	**Fe**	**Ge**	**Mn**	**Ni**	**Pb**	**Sb**	**Tl**	**V**	**Zn**
Name	**Type**	*mg/kg*	*mg/kg*	*mg/kg*	*mg/kg*	*mg/kg*	*mg/kg*	*mg/kg*	*mg/kg*	*mg/kg*	*mg/kg*	*mg/kg*	*mg/kg*	*mg/kg*	*mg/kg*
RACONC	Zn concentrate	1023	795	0.61	3.56	417	11844	186	22.0	11.9	27281	46.2	326	1.68	412620
RA10	Ore gossan	243	1.90	2.13	11.5	6.49	16033	7.18	417	9.09	248	1.47	231	38.1	1854
RA11	Ore gossan	197	1.37	1.01	6.68	3.96	13278	5.84	254	5.05	229	1.29	195	30.0	1398
RA12	Ore gossan	2693	16.5	1.76	11.9	7.36	79630	118	657	13.1	10599	5.28	599	38.4	49752
RA52	Smelter slag	2129	4.01	6.39	11.8	308	200669	25.5	299	11.7	46381	550	9.41	19.4	8318
RASL	Smelter slag	148	0.82	164	24.7	928	320138	13.7	4300	11.8	24778	31.1	2.97	45.4	79080
RA20	Soil	8.81	1.89	1.60	15.4	19.5	5507	0.63	35.9	7.52	653	1.78	1.06	18.5	182
RA21	Soil	11.7	1.45	2.91	18.3	14.6	6759	0.33	208	8.01	371	1.03	1.04	27.7	192
RA22	Soil	15.6	2.90	3.13	26.1	16.6	6786	0.57	240	11.3	770	1.65	2.49	30.9	604
RA23	Soil	7.06	1.88	1.29	14.2	16.1	3438	0.33	51.4	7.26	145	1.25	0.98	16.5	276
RA27	Soil	24.8	4.96	2.57	20.8	17.8	8912	0.92	228	8.48	2625	3.96	2.64	31.4	1049
RA29	Soil	5.38	1.83	0.90	9.08	9.57	2280	0.31	80.4	4.21	261	0.74	1.87	9.82	412
RA30	Soil	6.72	0.28	8.85	40.7	13.6	20882	0.99	378	13.4	40.2	1.62	0.60	63.4	72
RA44	Soil	7.01	0.52	0.71	3.43	3.38	1127	0.16	144	2.09	29.7	0.20	2.03	4.45	142
RA45	Soil	49.0	4.63	1.48	10.0	11.9	4796	1.45	167	5.46	646	0.96	9.01	13.6	1598
RA46	Soil	15.6	2.40	6.00	32.9	15.5	15891	1.16	454	11.8	681	1.75	4.00	59.1	761
RA47	Soil	10.2	0.42	8.36	45.8	16.7	21675	1.00	514	14.7	68.7	1.40	3.05	69.1	107
S161 10-30	Soil	1.27	0.24	0.38	3.63	2.21	418	n.d.	29.0	1.95	8.67	0.09	0.11	**5.92**	19.2
S163 10-30	Soil	2.53	0.75	0.74	6.64	3.76	1256	n.d.	59.7	2.76	46.7	0.25	0.22	**8.21**	32.6
S165 10-30	Soil	6.58	1.30	1.39	11.8	4.96	2348	n.d.	103	4.83	117	0.45	0.62	**14.5**	249
S167 10-30	Soil	12.1	0.77	4.10	21.2	21.6	10808	n.d.	151	9.95	132	1.44	0.59	**32.7**	145
S168 10-30	Soil	6.93	0.72	5.18	22.3	9.47	11254	n.d.	296	7.90	112	1.40	0.58	**34.2**	108
S169 10-30	Soil	14.2	1.67	1.20	32.1	6.81	2551	n.d.	45.4	5.11	139	1.06	0.88	**29.3**	335
S170 10-30	Soil	7.95	0.76	2.13	13.0	3.81	4429	n.d.	164	5.15	141	0.78	0.66	**20.8**	56.5
S171 10-30	Soil	6.74	1.13	1.00	6.57	2.76	1533	n.d.	78.1	2.97	146	0.52	0.46	**9.22**	132
S172 10-30	Soil	15.6	0.95	13.7	45.9	14.2	33370	n.d.	747	13.2	206	2.76	1.67	**68.5**	228
S173 10-30	Soil	29.9	16.0	2.44	16.6	21.0	6244	n.d.	316	8.07	2491	2.63	6.35	**20.5**	4456
S175 10-30	Soil	13.6	4.39	3.08	19.6	9.69	7373	n.d.	362	6.93	537	1.54	2.75	**29.6**	856

TOTAL CONCENTRATION		As	Cd	Co	Cr	Cu	Fe	Ge	Mn	Ni	Pb	Sb	Tl	V	Zn
Name	**Type**	*mg/kg*	*mg/kg*	*mg/kg*	*mg/kg*	*mg/kg*	*mg/kg*	*mg/kg*	*mg/kg*	*mg/kg*	*mg/kg*	*mg/kg*	*mg/kg*	*mg/kg*	*mg/kg*
S176 10-30	Soil	21.0	6.88	1.81	8.84	13.1	5595	n.d.	222	4.35	1717	1.68	4.60	**15.2**	2391
S177 10-30	Soil	15.5	2.96	1.67	8.51	5.77	4803	n.d.	164	3.54	774	1.01	4.42	**14.8**	1022
S179 10-30	Soil	24.9	5.81	3.81	21.8	33.4	8395	n.d.	1163	11.2	1410	2.07	7.76	**25.8**	1664
S180 10-30	Soil	36.6	13.9	2.49	16.2	14.5	8105	n.d.	374	7.97	3329	3.10	6.45	**22.2**	4322
S182	Soil	26.0	7.48	3.78	16.2	9.72	8856	n.d.	279	6.86	4387	6.04	2.71	**25.1**	2116
C01	Stream sediment	1.58	0.32	24.4	3.59	0.69	99	n.d.	16.6	1.00	6.73	0.05	0.17	4.40	15.3
C02	Stream sediment	37.7	7.82	29.0	4.70	1.92	2617	n.d.	64.6	2.53	914	2.37	5.27	7.41	2856
C03	Stream sediment	150	15.4	25.4	9.17	10.6	8396	n.d.	104	4.52	2138	2.58	51.5	14.2	6232
C04	Stream sediment	142	21.8	26.5	4.20	5.20	6948	n.d.	74.1	2.71	1516	2.66	22.1	8.75	9022
C05	Stream sediment	65.6	10.2	25.3	6.21	5.63	5401	n.d.	94.3	2.89	1012	1.44	16.2	13.5	4060
C06	Stream sediment	14.9	0.44	6.73	39.3	11.5	19822	n.d.	393	15.2	67.5	0.88	2.17	50.1	212
C07	Stream sediment	46.8	5.59	36.7	8.84	6.17	5579	n.d.	120	3.84	501	0.92	8.25	16.0	2472
C08A	Stream sediment	36.8	4.91	48.6	11.3	4.22	7798	n.d.	141	4.60	330	0.79	6.19	20.0	2161
C08B	Stream sediment	63.9	7.12	54.8	13.7	5.60	9642	n.d.	150	5.34	666	1.20	11.2	21.5	2996
C09	Stream sediment	22.0	4.99	34.1	8.39	3.00	5581	n.d.	125	3.05	141	0.61	2.42	15.0	1731
C10	Stream sediment	30.4	3.95	35.6	10.2	4.19	6781	n.d.	141	4.82	232	0.70	4.63	18.2	1693
RA30	Stream sediment	4.11	0.25	n.d.	9.05	3.34	4071	0.18	102	n.d.	7.80	0.42	0.42	n.d.	17.1
RA35	Stream sediment	26.0	3.52	n.d.	13.4	5.54	7554	1.26	206	n.d.	874	1.55	11.5	n.d.	1277
RA48	Stream sediment	2.05	0.17	n.d.	6.48	2.53	2858	0.16	99.7	n.d.	5.67	0.22	0.34	n.d.	13.8
RA53	Stream sediment	2.61	0.23	n.d.	3.56	1.76	1634	0.12	61.5	n.d.	24.2	0.27	0.20	n.d.	10.2
RA54	Stream sediment	130	18.5	n.d.	4.11	4.94	5492	5.18	82.4	n.d.	1517	2.20	20.4	n.d.	8557
RA13	Tailings	689	6.57	1.68	9.09	5.65	24132	n.d.	404	8.33	1956		256	41.5	14464
RA16	Tailings	925	35.4	0.30	2.07	45.0	45660	24.4	148	3.44	5722	6.49	150	7.89	21925
RA17	Tailings	2345	20.1	2.39	15.2	11.0	96674	102	477	13.8	7733	8.09	355	65.0	36537
RA37	Tailings	2284	40.2	4.90	54.9	16.9	117019	92.4	419	26.0	19542	11.0	754	42.0	60824
RA38	Tailings	1175	28.5	1.00	11.6	30.3	47824	44.1	205	12.3	8812	7.43	474	22.2	27516
RA39	Tailings	2439	196	1.97	26.1	31.7	100392	92.7	228	15.7	50062	40.2	907	18.2	114965
RA18	Waste rock	826	14.5	0.57	4.58	8.35	37900	29.1	176	6.16	3541	3.89	442	19.0	15590
RA28	Waste rock	25.2	7.73	2.64	14.1	48.2	5032	2.01	404	9.17	1787	4.00	5.87	17.1	3289

TOTAL CONCENTRATION		**As**	**Cd**	**Co**	**Cr**	**Cu**	**Fe**	**Ge**	**Mn**	**Ni**	**Pb**	**Sb**	**Tl**	**V**	**Zn**
Name	**Type**	*mg/kg*	*mg/kg*	*mg/kg*	*mg/kg*	*mg/kg*	*mg/kg*	*mg/kg*	*mg/kg*	*mg/kg*	*mg/kg*	*mg/kg*	*mg/kg*	*mg/kg*	*mg/kg*
RA34	Waste rock	516	117	1.99	12.1	14.3	20181	21.9	176	11.1	21962	19.8	101	37.3	43957
RA36	Waste rock	359	8.14	8.57	59.6	27.9	39239	14.3	766	20.5	4380	3.00	132	73.0	9462
RA40	Waste rock	355	26.4	0.71	9.11	113	14960	10.1	131	6.06	2755	4.67	65.1	10.6	14692
RA41	Waste rock	668	4.25	0.66	7.37	6.78	33335	19.0	243	6.43	1704	2.04	609	31.0	9566
RA42	Waste rock	650	17.1	2.14	16.7	46.2	33188	11.3	555	12.8	3903	5.32	149	26.4	10056
RA43	Waste rock	68.7	2.11	0.81	4.29	3.58	3055	2.86	151	3.13	769	0.36	10.1	6.58	2247
RA51	Waste rock	97.4	18.4	1.94	17.3	32.2	8068	3.52	240	10.0	1106	2.45	19.0	19.4	4586
S178 10-30	Waste rock	63.7	9.02	0.49	3.22	1.96	2887	n.d.	73.2	1.76	2119	2.85	14.5	**7.27**	4138
S181 10-30	Waste rock	241	49.6	2.76	14.8	13.9	10403	n.d.	240	9.17	41436	75.0	30.0	**24.7**	20837

Table A.4 – Extracted concentration of solids after a diluted HCl 0.5 M partial extraction in the Zn-Pb Raibl decommissioned mining site (Paper II).

EXTRACTED CONCENTRATION		**As**	**Cd**	**Co**	**Cr**	**Cu**	**Fe**	**Ge**	**Mn**	**Ni**	**Pb**	**Sb**	**Tl**	**V**	**Zn**
Name	**Type**	*mg/kg*	*mg/kg*	*mg/kg*	*mg/kg*	*mg/kg*	*mg/kg*	*mg/kg*	*mg/kg*	*mg/kg*	*mg/kg*	*mg/kg*	*mg/kg*	*mg/kg*	*mg/kg*
RACONC	Zn concentrate	185	107	0.23	0.74	27.8	740	31.8	11.2	3.16	304	19.9	57.0	0.68	67009
RA10	Ore gossan	0.07	1.03	0.45	0.01	0.06	2.93	n.d.	168	1.42	2.44	0.02	74.7	0.04	246
RA11	Ore gossan	0.09	0.57	0.20	0.01	0.03	2.85	n.d.	76.7	0.52	0.74	0.04	114	0.15	77.0
RA12	Ore gossan	0.05	10.6	0.40	0.01	0.28	2.20	n.d.	144	3.50	1666	< LOD	179	0.01	33108
RA52	Smelter slag	39.2	1.00	1.26	1.20	88.6	30116	3.72	103.3	3.00	16488	21.3	1.69	2.66	1647
RASL	Smelter slag	0.27	0.11	119	< LOD	0.30	56607	0.67	1515	3.24	7070	< LOD	0.51	< LOD	8875
RA20	Soil	1.06	1.88	0.84	0.48	8.18	1199	0.02	19.6	3.71	449	< LOD	0.19	4.89	161
RA21	Soil	< LOD	1.21	0.68	< LOD	0.30	15.7	< LOD	202	0.25	3.99	< LOD	0.06	0.25	37.9
RA22	Soil	0.24	1.93	0.63	< LOD	< LOD	14.6	< LOD	198	0.31	6.16	< LOD	0.04	0.13	96.6
RA23	Soil	0.52	1.88	0.61	0.71	0.64	293	< LOD	43.1	2.03	39.1	< LOD	0.13	0.83	162
RA27	Soil	3.17	3.55	1.22	0.89	0.90	653	0.01	227	2.08	986	0.03	0.09	1.66	479
RA29	Soil	0.55	0.81	0.14	< LOD	< LOD	10.3	< LOD	57.3	< LOD	< LOD	< LOD	0.08	0.07	41.3
RA30	Soil	< LOD	0.16	3.25	< LOD	< LOD	17.3	< LOD	261	1.51	< LOD	< LOD	< LOD	0.04	< LOD
RA44	Soil	< LOD	0.32	0.04	< LOD	< LOD	11.7	< LOD	40.8	< LOD	< LOD	< LOD	0.12	0.05	25.3
RA45	Soil	< LOD	1.92	0.25	< LOD	< LOD	12.4	0.02	83.8	< LOD	3.80	< LOD	0.49	0.06	182
RA46	Soil	< LOD	0.78	1.09	< LOD	< LOD	11.3	< LOD	265	0.32	3.96	< LOD	< LOD	0.06	44.4
RA47	Soil	< LOD	0.18	1.33	< LOD	< LOD	11.2	< LOD	236	0.96	< LOD	< LOD	< LOD	0.04	2.71
S161 10-30	Soil	0.05	0.13	0.08	< LOD	< LOD	11.0	n.d.	16.3	0.09	0.07	< LOD	< LOD	0.20	1.02
S163 10-30	Soil	0.04	0.41	0.10	< LOD	< LOD	10.5	n.d.	37.5	0.06	0.23	< LOD	< LOD	0.08	1.57
S165 10-30	Soil	0.05	0.59	0.17	< LOD	0.07	10.4	n.d.	64.8	0.08	0.32	< LOD	0.01	0.08	8.34
S167 10-30	Soil	0.03	0.38	0.61	< LOD	0.13	11.5	n.d.	77.2	0.23	0.59	< LOD	0.01	0.06	7.15
S168 10-30	Soil	0.03	0.35	0.82	< LOD	< LOD	13.2	n.d.	187	0.21	0.20	< LOD	0.00	0.04	1.68
S169 10-30	Soil	0.09	0.66	0.27	0.05	< LOD	10.9	n.d.	25.2	0.12	1.66	0.02	0.03	0.11	19.3
S170 10-30	Soil	0.03	0.34	0.14	< LOD	< LOD	9.37	n.d.	55.7	0.13	0.38	< LOD	0.01	0.05	0.36
S171 10-30	Soil	0.04	0.57	0.16	< LOD	< LOD	9.45	n.d.	36.2	0.08	2.36	0.02	0.01	0.05	16.6
S172 10-30	Soil	0.57	0.66	6.84	1.41	3.25	2373	n.d.	479	2.75	142	0.03	0.03	3.66	80.3
S173 10-30	Soil	0.11	3.26	0.41	0.03	0.10	14.5	n.d.	177	0.26	40.3	< LOD	0.06	0.07	337
S175 10-30	Soil	0.02	1.52	0.13	0.04	0.08	8.98	n.d.	75.5	0.18	3.84	0.04	0.02	0.04	63.8

EXTRACTED CONCENTRATION		As	Cd	Co	Cr	Cu	Fe	Ge	Mn	Ni	Pb	Sb	Tl	V	Zn
Name	**Type**	*mg/kg*	*mg/kg*	*mg/kg*	*mg/kg*	*mg/kg*	*mg/kg*	*mg/kg*	*mg/kg*	*mg/kg*	*mg/kg*	*mg/kg*	*mg/kg*	*mg/kg*	*mg/kg*
S176 10-30	Soil	0.11	2.80	0.38	< LOD	0.09	26.3	n.d.	123	0.34	95.2	0.06	0.04	0.05	671
S177 10-30	Soil	0.03	0.75	0.19	0.04	< LOD	9.84	n.d.	71.0	0.32	1.88	< LOD	0.02	0.03	26.6
S179 10-30	Soil	0.08	2.86	0.26	< LOD	0.11	11.3	n.d.	393	0.30	11.5	< LOD	0.11	0.05	242
S180 10-30	Soil	0.03	4.43	0.24	< LOD	< LOD	9.23	n.d.	125	0.19	37.4	0.05	0.14	0.03	531
S182	Soil	0.05	2.12	0.94	0.03	0.08	16.5	n.d.	162	0.42	171	< LOD	0.02	< LOD	274
C01	Stream sediment	< LOD	0.01	4.49	< LOD	< LOD	3.84	n.d.	0.59	0.12	< LOD	0.01	< LOD	0.14	< LOD
C02	Stream sediment	0.03	0.13	5.53	< LOD	0.12	4.85	n.d.	5.74	0.16	0.61	0.15	0.10	< LOD	19.7
C03	Stream sediment	0.06	0.31	3.35	< LOD	0.11	4.54	n.d.	8.86	0.16	1.29	0.11	4.31	< LOD	22.0
C04	Stream sediment	0.05	0.12	5.20	< LOD	< LOD	4.49	n.d.	4.39	0.12	1.11	0.12	1.49	< LOD	46.9
C05	Stream sediment	0.06	0.13	4.49	0.01	0.16	5.67	n.d.	9.04	0.15	0.47	0.11	0.87	0.03	14.1
C06	Stream sediment	< LOD	0.13	n.d.	< LOD	0.08	6.49	n.d.	211	< LOD	< LOD	0.01	0.02	0.01	< LOD
C07	Stream sediment	0.04	0.14	4.14	< LOD	< LOD	5.32	n.d.	10.6	0.21	< LOD	0.06	0.31	< LOD	9.67
C08A	Stream sediment	0.04	0.08	7.89	< LOD	< LOD	4.81	n.d.	13.4	0.15	< LOD	0.04	0.22	< LOD	7.94
C08B	Stream sediment	0.04	0.05	6.52	< LOD	< LOD	4.73	n.d.	11.1	0.13	< LOD	0.06	0.36	< LOD	7.66
C09	Stream sediment	< LOD	0.06	6.05	< LOD	< LOD	4.74	n.d.	9.08	0.15	< LOD	0.03	0.10	< LOD	6.56
C10	Stream sediment	< LOD	0.07	6.21	< LOD	< LOD	5.14	n.d.	13.6	0.15	< LOD	0.04	0.13	< LOD	6.02
RA30	Stream sediment	n.d.	n.d.	n.d.	n.d.	n.d.	n.d.	n.d.	n.d.	n.d.	n.d.	n.d.	n.d.	n.d.	n.d.
RA35	Stream sediment	n.d.	n.d.	n.d.	n.d.	n.d.	n.d.	n.d.	n.d.	n.d.	n.d.	n.d.	n.d.	n.d.	n.d.
RA48	Stream sediment	n.d.	n.d.	n.d.	n.d.	n.d.	n.d.	n.d.	n.d.	n.d.	n.d.	n.d.	n.d.	n.d.	n.d.
RA53	Stream sediment	n.d.	n.d.	n.d.	n.d.	n.d.	n.d.	n.d.	n.d.	n.d.	n.d.	n.d.	n.d.	n.d.	n.d.
RA54	Stream sediment	n.d.	n.d.	n.d.	n.d.	n.d.	n.d.	n.d.	n.d.	n.d.	n.d.	n.d.	n.d.	n.d.	n.d.
RA13	Tailings	0.05	3.67	0.59	0.11	0.09	3.99	n.d.	165	2.09	59.7	< LOD	95.7	0.02	6519
RA16	Tailings	0.02	21.3	0.14	0.03	2.07	2.86	n.d.	40.1	0.95	574	< LOD	11.4	0.01	12565
RA17	Tailings	0.15	11.7	0.94	0.02	1.83	2.74	n.d.	194	3.57	795	< LOD	64.1	0.01	19172
RA37	Tailings	< LOD	30.2	1.32	< LOD	1.14	31.6	0.39	214	3.80	5559	< LOD	211	< LOD	47084
RA38	Tailings	< LOD	15.0	0.44	< LOD	1.94	7.97	0.16	77.1	4.00	1195	< LOD	218.1	< LOD	13157
RA39	Tailings	0.38	84.9	1.03	< LOD	0.33	679	1.51	151	5.9	11378	0.04	21.2	< LOD	69535
RA18	Waste rock	0.03	6.02	0.26	0.01	0.26	4.74	n.d.	57.0	1.32	257	< LOD	77.2	0.01	4417
RA28	Waste rock	1.07	3.39	0.38	< LOD	0.38	11.4	0.04	261	0.44	32.1	0.05	0.12	0.18	791

EXTRACTED CONCENTRATION		As	Cd	Co	Cr	Cu	Fe	Ge	Mn	Ni	Pb	Sb	Tl	V	Zn
Name	**Type**	*mg/kg*	*mg/kg*	*mg/kg*	*mg/kg*	*mg/kg*	*mg/kg*	*mg/kg*	*mg/kg*	*mg/kg*	*mg/kg*	*mg/kg*	*mg/kg*	*mg/kg*	*mg/kg*
RA34	Waste rock	0.48	24.5	0.79	< LOD	< LOD	144	0.58	102	3.4	7576	0.46	2.27	0.03	9805
RA36	Waste rock	3.58	6.82	4.42	3.68	12.5	3088	0.18	625	5.3	2585	0.04	12.0	7.6	7157
RA40	Waste rock	< LOD	19.5	0.33	< LOD	2.22	8.94	0.74	37.4	2.54	136	0.07	12.7	0.03	9826
RA41	Waste rock	< LOD	2.46	0.13	< LOD	< LOD	7.60	0.10	54.4	0.84	99	< LOD	255	0.04	3026
RA42	Waste rock	3.77	11.7	0.66	< LOD	0.45	286	0.03	416	1.49	161	0.03	13.7	0.14	4445
RA43	Waste rock	< LOD	1.15	0.09	< LOD	< LOD	11.8	0.05	44.7	< LOD	7.0	< LOD	1.10	0.04	668
RA51	Waste rock	26.7	14.1	1.08	1.28	8.1	1576	0.01	197	3.21	642	< LOD	4.76	4.89	2561
S178 10-30	Waste rock	0.02	5.07	0.15	< LOD	< LOD	20.9	n.d.	32.7	0.32	261	0.07	0.71	0.02	1340
S181 10-30	Waste rock	0.64	19.3	0.77	0.15	0.25	145	n.d.	99.2	3.38	10494	0.76	1.44	0.03	8734

Table A.5 – Labile or extractable fraction of solids after a diluted HCl 0.5 M partial extraction in the Zn-Pb Raibl decommissioned mining site (Paper II).

LABILE FRACTION		**As**	**Cd**	**Co**	**Cr**	**Cu**	**Fe**	**Ge**	**Mn**	**Ni**	**Pb**	**Sb**	**Tl**	**V**	**Zn**
Name	**Type**	*%*	*%*	*%*	*%*	*%*	*%*	*%*	*%*	*%*	*%*	*%*	*%*	*%*	*%*
RACONC	Zn concentrate	18.1%	13.4%	37.7%	20.8%	6.67%	6.25%	17.1%	51.2%	26.6%	1.11%	43.1%	17.5%	40.2%	16.2%
RA10	Ore gossan	0.03%	54.1%	21.1%	0.07%	0.86%	0.02%	n.d.	40.4%	15.7%	0.98%	1.48%	32.4%	0.09%	13.3%
RA11	Ore gossan	0.05%	41.4%	20.1%	0.14%	0.85%	0.02%	n.d.	30.2%	10.3%	0.32%	3.01%	58.7%	0.50%	5.51%
RA12	Ore gossan	0.00%	64.0%	22.7%	0.08%	3.84%	0.00%	n.d.	22.0%	26.8%	15.7%	< LOD	29.8%	0.03%	66.5%
RA52	Smelter slag	1.84%	25.0%	19.8%	10.2%	28.8%	15.0%	14.6%	34.6%	25.7%	35.5%	3.88%	18.0%	13.7%	19.8%
RASL	Smelter slag	0.18%	13.6%	72.6%	< LOD	0.03%	17.7%	4.88%	35.2%	27.5%	28.5%	< LOD	17.3%	< LOD	11.2%
RA20	Soil	12.1%	99.7%	52.5%	3.13%	41.9%	21.8%	2.41%	54.7%	49.3%	68.7%	< LOD	18.0%	26.4%	88.6%
RA21	Soil	< LOD	83.3%	23.4%	< LOD	2.07%	0.23%	< LOD	96.9%	3.06%	1.07%	< LOD	5.43%	0.89%	19.7%
RA22	Soil	1.52%	66.6%	20.1%	< LOD	< LOD	0.22%	< LOD	82.5%	2.79%	0.80%	< LOD	1.78%	0.42%	16.0%
RA23	Soil	7.37%	99.8%	47.8%	5.01%	4.00%	8.53%	< LOD	83.9%	28.0%	27.0%	< LOD	13.2%	5.01%	58.8%
RA27	Soil	12.8%	71.5%	47.4%	4.30%	5.05%	7.33%	1.18%	99.6%	24.5%	37.6%	0.75%	3.50%	5.29%	45.7%
RA29	Soil	10.3%	44.5%	15.4%	< LOD	< LOD	0.45%	< LOD	71.2%	< LOD	< LOD	< LOD	4.25%	0.67%	10.0%
RA30	Soil	< LOD	56.9%	36.8%	< LOD	< LOD	0.08%	< LOD	69.0%	11.3%	< LOD	< LOD	< LOD	0.06%	< LOD
RA44	Soil	< LOD	60.7%	5.61%	< LOD	< LOD	1.04%	< LOD	28.2%	< LOD	< LOD	< LOD	6.02%	1.08%	17.8%
RA45	Soil	< LOD	41.5%	17.2%	< LOD	< LOD	0.26%	1.28%	50.2%	< LOD	0.59%	< LOD	5.49%	0.42%	11.4%
RA46	Soil	< LOD	32.3%	18.2%	< LOD	< LOD	0.07%	< LOD	58.3%	2.70%	0.58%	< LOD	< LOD	0.10%	5.84%
RA47	Soil	< LOD	41.6%	15.9%	< LOD	< LOD	0.05%	< LOD	45.9%	6.51%	< LOD	< LOD	< LOD	0.06%	2.53%
S161 10-30	Soil	3.64%	54.0%	21.5%	< LOD	< LOD	2.64%	n.d.	56.4%	4.51%	0.77%	< LOD	< LOD	3.42%	5.34%
S163 10-30	Soil	1.61%	54.8%	14.1%	< LOD	< LOD	0.84%	n.d.	62.8%	2.00%	0.49%	< LOD	< LOD	0.96%	4.83%
S165 10-30	Soil	0.71%	45.3%	12.0%	< LOD	1.50%	0.44%	n.d.	63.2%	1.62%	0.27%	< LOD	1.59%	0.55%	3.35%
S167 10-30	Soil	0.23%	49.8%	14.9%	< LOD	0.59%	0.11%	n.d.	51.1%	2.31%	0.45%	< LOD	0.85%	0.17%	4.93%
S168 10-30	Soil	0.40%	49.2%	15.9%	< LOD	< LOD	0.12%	n.d.	63.3%	2.71%	0.18%	< LOD	0.48%	0.12%	1.56%
S169 10-30	Soil	0.60%	39.8%	22.5%	0.15%	< LOD	0.43%	n.d.	55.6%	2.36%	1.20%	1.59%	3.12%	0.39%	5.75%
S170 10-30	Soil	0.35%	44.1%	6.72%	< LOD	< LOD	0.21%	n.d.	33.9%	2.48%	0.27%	< LOD	0.76%	0.22%	0.63%
S171 10-30	Soil	0.52%	50.6%	15.6%	< LOD	< LOD	0.62%	n.d.	46.3%	2.85%	1.62%	4.69%	2.53%	0.57%	12.6%
S172 10-30	Soil	3.65%	70.2%	49.8%	3.07%	22.9%	7.11%	n.d.	64.1%	20.9%	68.8%	1.14%	1.85%	5.35%	35.2%
S173 10-30	Soil	0.38%	20.5%	16.6%	0.20%	0.46%	0.23%	n.d.	56.1%	3.18%	1.62%	< LOD	0.96%	0.34%	7.56%

< LOD referred to extracted concentration

LABILE FRACTION		As	Cd	Co	Cr	Cu	Fe	Ge	Mn	Ni	Pb	Sb	Tl	V	Zn
Name	**Type**	%	%	%	%	%	%	%	%	%	%	%	%	%	%
S175 10-30	Soil	0.15%	34.6%	4.20%	0.19%	0.85%	0.12%	n.d.	20.8%	2.65%	0.72%	2.34%	0.88%	0.12%	7.45%
S176 10-30	Soil	0.52%	40.7%	21.1%	< LOD	0.65%	0.47%	n.d.	55.4%	7.76%	5.55%	3.55%	0.84%	0.35%	28.1%
S177 10-30	Soil	0.19%	25.4%	11.7%	0.42%	< LOD	0.20%	n.d.	43.4%	9.16%	0.24%	< LOD	0.43%	0.22%	2.61%
S179 10-30	Soil	0.34%	49.2%	6.87%	< LOD	0.34%	0.14%	n.d.	33.8%	2.65%	0.82%	< LOD	1.37%	0.18%	14.6%
S180 10-30	Soil	0.09%	31.8%	9.80%	< LOD	< LOD	0.11%	n.d.	33.5%	2.41%	1.12%	1.49%	2.15%	0.14%	12.3%
S182	Soil	0.20%	28.4%	24.9%	0.17%	0.86%	0.19%	n.d.	58.3%	6.15%	3.90%	< LOD	0.75%	< LOD	12.9%
C01	Stream sediment	< LOD	1.90%	18.4%	< LOD	< LOD	3.89%	n.d.	3.58%	11.5%	< LOD	17.0%	< LOD	3.21%	< LOD
C02	Stream sediment	0.09%	1.71%	19.0%	< LOD	6.06%	0.19%	n.d.	8.88%	6.49%	0.07%	6.39%	1.96%	< LOD	0.69%
C03	Stream sediment	0.04%	1.99%	13.2%	< LOD	1.05%	0.05%	n.d.	8.52%	3.64%	0.06%	4.39%	8.37%	< LOD	0.35%
C04	Stream sediment	0.03%	0.55%	19.6%	< LOD	< LOD	0.06%	n.d.	5.92%	4.41%	0.07%	4.58%	6.75%	< LOD	0.52%
C05	Stream sediment	0.09%	1.27%	17.8%	0.24%	2.87%	0.10%	n.d.	9.59%	5.30%	0.05%	7.33%	5.34%	0.19%	0.35%
C06	Stream sediment	< LOD	28.8%	n.d.	< LOD	0.69%	0.03%	n.d.	53.7%	< LOD	< LOD	1.26%	1.12%	0.03%	< LOD
C07	Stream sediment	0.09%	2.58%	11.3%	< LOD	< LOD	0.10%	n.d.	8.82%	5.60%	< LOD	6.89%	3.70%	< LOD	0.39%
C08A	Stream sediment	0.10%	1.54%	16.2%	< LOD	< LOD	0.06%	n.d.	9.55%	3.18%	< LOD	5.53%	3.48%	< LOD	0.37%
C08B	Stream sediment	0.06%	0.76%	11.9%	< LOD	< LOD	0.05%	n.d.	7.42%	2.49%	< LOD	5.29%	3.18%	< LOD	0.26%
C09	Stream sediment	< LOD	1.30%	17.7%	< LOD	< LOD	0.09%	n.d.	7.28%	4.91%	< LOD	4.46%	4.07%	< LOD	0.38%
C10	Stream sediment	< LOD	1.65%	17.4%	< LOD	< LOD	0.08%	n.d.	9.67%	3.04%	< LOD	5.38%	2.83%	< LOD	0.36%
RA30	Stream sediment	n.d.	n.d.	n.d.	n.d.	n.d.	n.d.	n.d.	n.d.	n.d.	n.d.	n.d.	n.d.	n.d.	n.d.
RA35	Stream sediment	n.d.	n.d.	n.d.	n.d.	n.d.	n.d.	n.d.	n.d.	n.d.	n.d.	n.d.	n.d.	n.d.	n.d.
RA48	Stream sediment	n.d.	n.d.	n.d.	n.d.	n.d.	n.d.	n.d.	n.d.	n.d.	n.d.	n.d.	n.d.	n.d.	n.d.
RA53	Stream sediment	n.d.	n.d.	n.d.	n.d.	n.d.	n.d.	n.d.	n.d.	n.d.	n.d.	n.d.	n.d.	n.d.	n.d.
RA54	Stream sediment	n.d.	n.d.	n.d.	n.d.	n.d.	n.d.	n.d.	n.d.	n.d.	n.d.	n.d.	n.d.	n.d.	n.d.
RA13	Tailings	0.01%	55.9%	35.4%	1.22%	1.56%	0.02%	n.d.	40.7%	25.1%	3.05%	< LOD	37.4%	0.04%	45.1%
RA16	Tailings	0.00%	60.1%	45.3%	1.30%	4.60%	0.01%	n.d.	27.2%	27.6%	10.0%	< LOD	7.58%	0.10%	57.3%
RA17	Tailings	0.01%	58.6%	39.4%	0.12%	16.6%	0.00%	n.d.	40.6%	25.9%	10.3%	< LOD	18.0%	0.02%	52.5%
RA37	Tailings	< LOD	75.2%	27.0%	< LOD	6.72%	0.03%	0.42%	51.1%	14.6%	28.4%	< LOD	27.9%	< LOD	77.4%
RA38	Tailings	< LOD	52.7%	44.4%	< LOD	6.39%	0.02%	0.35%	37.6%	32.5%	13.6%	< LOD	46.1%	< LOD	47.8%
RA39	Tailings	0.02%	43.3%	52.3%	< LOD	1.04%	0.68%	1.63%	66.0%	37.5%	22.7%	0.11%	2.34%	< LOD	60.5%

< LOD referred to extracted concentration

LABILE FRACTION		As	Cd	Co	Cr	Cu	Fe	Ge	Mn	Ni	Pb	Sb	Tl	V	Zn
Name	**Type**	*%*	*%*	*%*	*%*	*%*	*%*	*%*	*%*	*%*	*%*	*%*	*%*	*%*	*%*
RA18	Waste rock	0.00%	41.6%	45.4%	0.16%	3.09%	0.01%	n.d.	32.4%	21.4%	7.27%	< LOD	17.5%	0.04%	28.3%
RA28	Waste rock	4.23%	43.8%	14.4%	< LOD	0.78%	0.23%	2.15%	64.7%	4.82%	1.80%	1.35%	2.04%	1.03%	24.1%
RA34	Waste rock	0.09%	21.0%	39.8%	< LOD	< LOD	0.71%	2.65%	57.9%	30.5%	34.5%	2.33%	2.25%	0.08%	22.3%
RA36	Waste rock	1.00%	83.8%	51.6%	6.18%	44.8%	7.87%	1.26%	81.5%	25.9%	59.0%	1.42%	9.04%	10.4%	75.6%
RA40	Waste rock	< LOD	74.0%	46.2%	< LOD	1.97%	0.06%	7.33%	28.5%	41.9%	4.92%	1.43%	19.6%	0.33%	66.9%
RA41	Waste rock	< LOD	57.9%	19.8%	< LOD	< LOD	0.02%	0.50%	22.4%	13.1%	5.80%	< LOD	41.9%	0.14%	31.6%
RA42	Waste rock	0.58%	68.5%	30.9%	< LOD	0.98%	0.86%	0.29%	74.9%	11.7%	4.12%	0.55%	9.21%	0.52%	44.2%
RA43	Waste rock	< LOD	54.4%	11.2%	< LOD	< LOD	0.39%	1.89%	29.6%	< LOD	0.91%	< LOD	10.9%	0.62%	29.7%
RA51	Waste rock	27.4%	76.5%	55.8%	7.40%	25.0%	19.5%	0.35%	82.4%	32.0%	58.0%	< LOD	25.1%	25.2%	55.8%
S178 10-30	Waste rock	0.04%	56.2%	29.6%	< LOD	< LOD	0.72%	n.d.	44.6%	18.0%	12.3%	2.32%	4.88%	0.33%	32.4%
S181 10-30	Waste rock	0.27%	39.0%	28.1%	1.02%	1.81%	1.39%	n.d.	41.4%	36.9%	25.3%	1.01%	4.80%	0.10%	41.9%

< LOD referred to extracted concentration

Table A.6 – EMPA microanalysis on tailings minerals in the Zn-Pb Raibl decommissioned mining site (Paper III).

Name	**Type**	**S**	**Fe**	**Zn**	**Pb**
		wt%	*wt%*	*wt%*	*wt%*
63-31_29	Baryte	9.21	0.03	0.03	0.00
63-31_10	Baryte	9.31	0.00	0.04	0.00
250-125_98	Baryte	10.60	0.01	0.06	0.00
250-125_90-b	Baryte	10.83	0.40	0.12	0.00
125-63_6	Dolomite/Calcite	0.00	0.00	0.01	0.00
250-125_81	Dolomite/Calcite	0.02	0.00	0.06	0.02
250-125_38	Dolomite/Calcite	0.02	0.02	1.11	0.00
63-31_39	Dolomite/Calcite	0.02	0.02	0.03	0.00
250-125_88	Dolomite/Calcite	0.04	0.03	0.02	0.03
63-31_11 - b	Fe sulfides (Pyrite/marcasite)	26.57	47.12	4.88	0.31
250-125_50-c	Fe sulfides (Pyrite/marcasite)	38.53	47.79	1.07	1.47
250-125_37	Fe sulfides (Pyrite/marcasite)	49.26	48.33	0.70	0.00
250-125_18-c	Fe sulfides (Pyrite/marcasite)	52.51	46.69	0.04	0.00
250-125_18-r	Fe sulfides (Pyrite/marcasite)	52.73	46.04	0.03	0.00
125-63_128	Fe sulfides (Pyrite/marcasite)	52.79	48.13	0.02	0.00
250-125_45-c	Fe sulfides (Pyrite/marcasite)	52.84	46.39	0.00	0.00
250-125_86	Fe sulfides (Pyrite/marcasite)	55.56	47.07	0.01	0.00
63-31_18	Secondary Fe minerals (Fe oxy-hydroxides)	0.01	18.86	1.47	0.40
125-63_63	Secondary Fe minerals (Fe oxy-hydroxides)	0.01	30.02	3.49	1.06
63-31_84	Secondary Fe minerals (Fe oxy-hydroxides)	0.02	36.13	6.10	3.97
63-31_96	Secondary Fe minerals (Fe oxy-hydroxides)	0.02	51.20	2.07	3.36
63-31_104	Secondary Fe minerals (Fe oxy-hydroxides)	0.03	34.76	5.19	2.21
125-63_49	Secondary Fe minerals (Fe oxy-hydroxides)	0.03	21.85	3.36	1.33
250-125_17	Secondary Fe minerals (Fe oxy-hydroxides)	0.03	41.39	4.22	0.91
63-31_122 - a	Secondary Fe minerals (Fe oxy-hydroxides)	0.03	41.04	6.84	3.60
63-31_144	Secondary Fe minerals (Fe oxy-hydroxides)	0.03	26.07	3.38	1.11
63-31_37	Secondary Fe minerals (Fe oxy-hydroxides)	0.03	31.47	4.96	1.69
250-125_50-r	Secondary Fe minerals (Fe oxy-hydroxides)	0.03	46.02	5.97	8.33
125-63_24	Secondary Fe minerals (Fe oxy-hydroxides)	0.03	37.58	1.90	0.98
63-31_53	Secondary Fe minerals (Fe oxy-hydroxides)	0.04	30.88	4.90	2.93
125-63_21	Secondary Fe minerals (Fe oxy-hydroxides)	0.04	40.40	7.32	3.31
125-63_12	Secondary Fe minerals (Fe oxy-hydroxides)	0.04	46.03	2.33	1.44
250-125_90-a	Secondary Fe minerals (Fe oxy-hydroxides)	0.04	47.02	7.82	2.27
250-125_44	Secondary Fe minerals (Fe oxy-hydroxides)	0.04	49.25	4.99	1.51
63-31_109 - a	Secondary Fe minerals (Fe oxy-hydroxides)	0.04	17.73	4.66	0.80
250-125_130	Secondary Fe minerals (Fe oxy-hydroxides)	0.04	50.91	6.11	1.61
125-63_71	Secondary Fe minerals (Fe oxy-hydroxides)	0.04	43.77	5.38	2.39
63-31_61	Secondary Fe minerals (Fe oxy-hydroxides)	0.04	35.90	4.73	1.78
125-63_115	Secondary Fe minerals (Fe oxy-hydroxides)	0.04	29.42	3.47	4.53
125-63_133	Secondary Fe minerals (Fe oxy-hydroxides)	0.04	37.35	2.43	1.01
63-31_64	Secondary Fe minerals (Fe oxy-hydroxides)	0.04	22.47	1.08	0.46
250-125_46	Secondary Fe minerals (Fe oxy-hydroxides)	0.04	51.54	6.19	1.17
250-125_48-r	Secondary Fe minerals (Fe oxy-hydroxides)	0.04	30.85	3.68	0.45
63-31_83	Secondary Fe minerals (Fe oxy-hydroxides)	0.04	39.93	4.48	1.17
125-63_135	Secondary Fe minerals (Fe oxy-hydroxides)	0.05	46.71	4.57	1.80
250-125_84	Secondary Fe minerals (Fe oxy-hydroxides)	0.05	43.99	6.98	2.07
63-31_107	Secondary Fe minerals (Fe oxy-hydroxides)	0.05	34.80	4.05	0.89
250-125_71	Secondary Fe minerals (Fe oxy-hydroxides)	0.05	47.48	8.01	1.21
125-63_70	Secondary Fe minerals (Fe oxy-hydroxides)	0.05	40.06	1.62	0.93
63-31_57	Secondary Fe minerals (Fe oxy-hydroxides)	0.05	42.61	4.42	1.82
63-31_126	Secondary Fe minerals (Fe oxy-hydroxides)	0.05	31.00	3.89	1.85
250-125_52	Secondary Fe minerals (Fe oxy-hydroxides)	0.05	47.17	6.13	1.42
63-31_90	Secondary Fe minerals (Fe oxy-hydroxides)	0.05	33.70	2.64	1.09
125-63_43	Secondary Fe minerals (Fe oxy-hydroxides)	0.05	37.46	4.62	2.01
250-125_111	Secondary Fe minerals (Fe oxy-hydroxides)	0.05	51.66	5.95	1.33
250-125_64-a	Secondary Fe minerals (Fe oxy-hydroxides)	0.05	45.75	7.99	3.59
250-125_48-c	Secondary Fe minerals (Fe oxy-hydroxides)	0.05	53.67	4.34	0.38
250-125_79-b	Secondary Fe minerals (Fe oxy-hydroxides)	0.05	40.25	4.20	1.97
250-125_67	Secondary Fe minerals (Fe oxy-hydroxides)	0.05	53.25	5.28	0.46
250-125_144-a	Secondary Fe minerals (Fe oxy-hydroxides)	0.06	48.40	7.04	2.64
63-31_98	Secondary Fe minerals (Fe oxy-hydroxides)	0.06	38.52	4.57	1.65

Name	Type	S	Fe	Zn	Pb
		wt%	*wt%*	*wt%*	*wt%*
63-31_44	Secondary Fe minerals (Fe oxy-hydroxides)	0.06	35.91	3.73	1.45
63-31_132	Secondary Fe minerals (Fe oxy-hydroxides)	0.06	45.35	4.03	1.89
250-125_65	Secondary Fe minerals (Fe oxy-hydroxides)	0.06	50.03	7.08	1.55
63-31_68	Secondary Fe minerals (Fe oxy-hydroxides)	0.06	40.99	5.29	2.38
250-125_77	Secondary Fe minerals (Fe oxy-hydroxides)	0.06	51.86	5.41	1.22
125-63_51	Secondary Fe minerals (Fe oxy-hydroxides)	0.06	41.61	6.44	3.16
63-31_101	Secondary Fe minerals (Fe oxy-hydroxides)	0.06	30.24	6.64	2.44
125-63_116	Secondary Fe minerals (Fe oxy-hydroxides)	0.06	48.19	3.52	1.27
250-125_32	Secondary Fe minerals (Fe oxy-hydroxides)	0.06	37.81	3.24	1.13
125-63_56	Secondary Fe minerals (Fe oxy-hydroxides)	0.06	34.08	2.60	1.13
125-63_81	Secondary Fe minerals (Fe oxy-hydroxides)	0.06	52.82	2.58	1.00
63-31_65	Secondary Fe minerals (Fe oxy-hydroxides)	0.06	37.83	4.87	1.62
250-125_7	Secondary Fe minerals (Fe oxy-hydroxides)	0.06	52.16	5.09	2.27
125-63_109	Secondary Fe minerals (Fe oxy-hydroxides)	0.06	45.62	5.13	1.57
63-31_129	Secondary Fe minerals (Fe oxy-hydroxides)	0.06	43.27	7.02	1.55
63-31_27	Secondary Fe minerals (Fe oxy-hydroxides)	0.06	46.30	4.44	1.84
125-63_102	Secondary Fe minerals (Fe oxy-hydroxides)	0.06	42.76	7.32	1.77
250-125_126	Secondary Fe minerals (Fe oxy-hydroxides)	0.06	30.82	3.87	3.63
250-125_28	Secondary Fe minerals (Fe oxy-hydroxides)	0.06	48.61	6.18	2.00
250-125_70	Secondary Fe minerals (Fe oxy-hydroxides)	0.07	50.42	6.47	1.56
125-63_45	Secondary Fe minerals (Fe oxy-hydroxides)	0.07	45.15	4.25	1.44
63-31_51	Secondary Fe minerals (Fe oxy-hydroxides)	0.07	37.36	2.86	1.53
250-125_94	Secondary Fe minerals (Fe oxy-hydroxides)	0.07	49.71	6.02	1.06
63-31_1	Secondary Fe minerals (Fe oxy-hydroxides)	0.07	21.06	4.43	4.63
250-125_22-r	Secondary Fe minerals (Fe oxy-hydroxides)	0.07	50.91	7.20	0.66
250-125_145	Secondary Fe minerals (Fe oxy-hydroxides)	0.07	49.61	7.00	1.94
250-125_123	Secondary Fe minerals (Fe oxy-hydroxides)	0.07	49.49	6.16	2.22
125-63_114	Secondary Fe minerals (Fe oxy-hydroxides)	0.07	42.08	4.96	3.90
250-125_87	Secondary Fe minerals (Fe oxy-hydroxides)	0.07	31.33	2.95	0.54
250-125_16	Secondary Fe minerals (Fe oxy-hydroxides)	0.07	49.66	6.34	2.47
250-125_112	Secondary Fe minerals (Fe oxy-hydroxides)	0.07	47.25	7.66	2.60
63-31_152	Secondary Fe minerals (Fe oxy-hydroxides)	0.07	35.23	2.73	4.47
125-63_68	Secondary Fe minerals (Fe oxy-hydroxides)	0.07	49.81	3.04	3.01
125-63_17	Secondary Fe minerals (Fe oxy-hydroxides)	0.07	42.95	6.99	1.99
125-63_92	Secondary Fe minerals (Fe oxy-hydroxides)	0.07	48.40	4.16	1.61
63-31_79	Secondary Fe minerals (Fe oxy-hydroxides)	0.07	42.61	7.21	1.64
250-125_39	Secondary Fe minerals (Fe oxy-hydroxides)	0.07	49.08	5.94	1.73
250-125_134	Secondary Fe minerals (Fe oxy-hydroxides)	0.07	46.80	2.79	1.20
250-125_107	Secondary Fe minerals (Fe oxy-hydroxides)	0.07	50.00	7.07	1.52
250-125_14	Secondary Fe minerals (Fe oxy-hydroxides)	0.07	46.62	5.98	2.01
250-125_22-c	Secondary Fe minerals (Fe oxy-hydroxides)	0.07	51.21	6.91	0.49
250-125_8	Secondary Fe minerals (Fe oxy-hydroxides)	0.07	56.38	2.18	0.62
63-31_30	Secondary Fe minerals (Fe oxy-hydroxides)	0.07	44.71	3.63	3.54
250-125_76	Secondary Fe minerals (Fe oxy-hydroxides)	0.07	42.36	7.87	1.49
250-125_72	Secondary Fe minerals (Fe oxy-hydroxides)	0.08	43.25	4.75	2.30
125-63_132	Secondary Fe minerals (Fe oxy-hydroxides)	0.08	44.51	3.94	3.46
63-31_143	Secondary Fe minerals (Fe oxy-hydroxides)	0.08	33.17	3.14	1.71
250-125_119	Secondary Fe minerals (Fe oxy-hydroxides)	0.08	54.36	4.13	2.00
125-63_125	Secondary Fe minerals (Fe oxy-hydroxides)	0.08	44.12	5.20	2.45
125-63_83	Secondary Fe minerals (Fe oxy-hydroxides)	0.08	45.29	5.30	1.27
125-63_79	Secondary Fe minerals (Fe oxy-hydroxides)	0.08	38.07	5.63	1.95
63-31_47	Secondary Fe minerals (Fe oxy-hydroxides)	0.08	47.32	3.51	3.73
125-63_11	Secondary Fe minerals (Fe oxy-hydroxides)	0.08	43.42	6.04	1.81
63-31_140	Secondary Fe minerals (Fe oxy-hydroxides)	0.08	36.10	2.69	1.20
63-31_52	Secondary Fe minerals (Fe oxy-hydroxides)	0.08	27.24	2.11	1.17
63-31_118	Secondary Fe minerals (Fe oxy-hydroxides)	0.08	43.01	6.60	1.91
63-31_70	Secondary Fe minerals (Fe oxy-hydroxides)	0.09	35.82	3.16	1.77
250-125_25	Secondary Fe minerals (Fe oxy-hydroxides)	0.09	48.54	3.58	1.07
125-63_8	Secondary Fe minerals (Fe oxy-hydroxides)	0.09	45.27	3.49	2.42
125-63_89 - a	Secondary Fe minerals (Fe oxy-hydroxides)	0.09	44.63	5.98	1.24
250-125_31	Secondary Fe minerals (Fe oxy-hydroxides)	0.09	56.16	3.33	3.32
125-63_18	Secondary Fe minerals (Fe oxy-hydroxides)	0.09	47.82	3.04	1.24

Name	Type	S	Fe	Zn	Pb
		wt%	*wt%*	*wt%*	*wt%*
250-125_59	Secondary Fe minerals (Fe oxy-hydroxides)	0.09	55.10	3.14	1.35
63-31_111	Secondary Fe minerals (Fe oxy-hydroxides)	0.09	34.60	3.88	2.47
250-125_54	Secondary Fe minerals (Fe oxy-hydroxides)	0.09	49.88	4.44	2.17
125-63_90	Secondary Fe minerals (Fe oxy-hydroxides)	0.09	42.78	5.21	2.36
125-63_122	Secondary Fe minerals (Fe oxy-hydroxides)	0.09	47.05	3.48	4.14
250-125_133	Secondary Fe minerals (Fe oxy-hydroxides)	0.09	53.14	3.72	1.27
250-125_35	Secondary Fe minerals (Fe oxy-hydroxides)	0.09	49.73	4.22	0.70
250-125_78-b	Secondary Fe minerals (Fe oxy-hydroxides)	0.09	44.56	3.02	1.35
63-31_40	Secondary Fe minerals (Fe oxy-hydroxides)	0.09	44.49	2.61	1.25
63-31_123	Secondary Fe minerals (Fe oxy-hydroxides)	0.09	39.26	6.44	2.86
63-31_15	Secondary Fe minerals (Fe oxy-hydroxides)	0.09	43.24	5.67	2.54
63-31_99	Secondary Fe minerals (Fe oxy-hydroxides)	0.09	43.28	3.42	2.28
125-63_85	Secondary Fe minerals (Fe oxy-hydroxides)	0.09	45.10	2.69	1.92
250-125_95	Secondary Fe minerals (Fe oxy-hydroxides)	0.09	51.21	6.28	0.72
125-63_35	Secondary Fe minerals (Fe oxy-hydroxides)	0.09	40.53	5.08	7.98
125-63_57 - a	Secondary Fe minerals (Fe oxy-hydroxides)	0.09	45.36	3.10	2.41
63-31_106	Secondary Fe minerals (Fe oxy-hydroxides)	0.09	42.14	7.09	2.40
125-63_97	Secondary Fe minerals (Fe oxy-hydroxides)	0.09	40.47	2.91	2.07
63-31_95	Secondary Fe minerals (Fe oxy-hydroxides)	0.10	43.88	5.84	2.17
63-31_105	Secondary Fe minerals (Fe oxy-hydroxides)	0.10	42.37	6.52	2.77
125-63_137	Secondary Fe minerals (Fe oxy-hydroxides)	0.10	47.25	3.44	0.99
125-63_27	Secondary Fe minerals (Fe oxy-hydroxides)	0.10	46.78	2.60	1.90
250-125_120	Secondary Fe minerals (Fe oxy-hydroxides)	0.10	45.98	1.82	0.75
63-31_134	Secondary Fe minerals (Fe oxy-hydroxides)	0.10	43.81	3.76	2.75
63-31_149	Secondary Fe minerals (Fe oxy-hydroxides)	0.10	42.47	7.24	3.66
125-63_53	Secondary Fe minerals (Fe oxy-hydroxides)	0.10	48.38	3.11	2.10
250-125_55-r	Secondary Fe minerals (Fe oxy-hydroxides)	0.10	55.05	4.18	1.55
250-125_146	Secondary Fe minerals (Fe oxy-hydroxides)	0.10	56.05	2.72	2.83
250-125_106	Secondary Fe minerals (Fe oxy-hydroxides)	0.10	51.70	3.68	2.19
250-125_116	Secondary Fe minerals (Fe oxy-hydroxides)	0.10	47.97	7.71	1.46
125-63_36	Secondary Fe minerals (Fe oxy-hydroxides)	0.10	42.44	5.79	2.76
63-31_146	Secondary Fe minerals (Fe oxy-hydroxides)	0.10	43.38	4.52	1.62
250-125_73	Secondary Fe minerals (Fe oxy-hydroxides)	0.10	54.58	2.07	0.46
250-125_108	Secondary Fe minerals (Fe oxy-hydroxides)	0.11	49.28	5.48	3.04
125-63_30	Secondary Fe minerals (Fe oxy-hydroxides)	0.11	44.48	3.33	1.76
63-31_137	Secondary Fe minerals (Fe oxy-hydroxides)	0.11	41.77	3.20	1.21
250-125_75	Secondary Fe minerals (Fe oxy-hydroxides)	0.11	43.42	3.09	1.56
250-125_139	Secondary Fe minerals (Fe oxy-hydroxides)	0.12	52.88	4.23	1.29
63-31_21	Secondary Fe minerals (Fe oxy-hydroxides)	0.12	42.97	6.71	1.47
125-63_37	Secondary Fe minerals (Fe oxy-hydroxides)	0.12	45.02	3.81	3.11
63-31_135	Secondary Fe minerals (Fe oxy-hydroxides)	0.12	47.08	4.43	1.11
125-63_117	Secondary Fe minerals (Fe oxy-hydroxides)	0.12	41.56	5.66	3.10
125-63_73	Secondary Fe minerals (Fe oxy-hydroxides)	0.12	46.27	3.86	2.27
63-31_92	Secondary Fe minerals (Fe oxy-hydroxides)	0.12	46.51	4.04	1.87
125-63_64	Secondary Fe minerals (Fe oxy-hydroxides)	0.12	43.70	4.41	3.12
250-125_142	Secondary Fe minerals (Fe oxy-hydroxides)	0.12	52.63	4.60	0.98
125-63_69	Secondary Fe minerals (Fe oxy-hydroxides)	0.12	46.64	2.04	2.74
63-31_35	Secondary Fe minerals (Fe oxy-hydroxides)	0.13	45.05	3.96	3.78
125-63_42	Secondary Fe minerals (Fe oxy-hydroxides)	0.13	46.36	3.87	1.43
125-63_141	Secondary Fe minerals (Fe oxy-hydroxides)	0.13	48.02	2.89	1.23
125-63_44	Secondary Fe minerals (Fe oxy-hydroxides)	0.13	38.99	3.96	3.24
63-31_112	Secondary Fe minerals (Fe oxy-hydroxides)	0.13	45.08	4.25	3.00
125-63_140	Secondary Fe minerals (Fe oxy-hydroxides)	0.13	44.65	3.45	1.69
63-31_54	Secondary Fe minerals (Fe oxy-hydroxides)	0.13	48.80	2.71	2.94
125-63_14	Secondary Fe minerals (Fe oxy-hydroxides)	0.13	45.02	4.04	1.89
125-63_136	Secondary Fe minerals (Fe oxy-hydroxides)	0.13	49.43	1.83	1.42
63-31_63	Secondary Fe minerals (Fe oxy-hydroxides)	0.13	45.12	4.10	2.19
125-63_1	Secondary Fe minerals (Fe oxy-hydroxides)	0.14	47.79	3.41	1.06
125-63_124 - b	Secondary Fe minerals (Fe oxy-hydroxides)	0.14	43.08	6.24	1.87
250-125_138	Secondary Fe minerals (Fe oxy-hydroxides)	0.14	49.52	5.89	1.70
250-125_99	Secondary Fe minerals (Fe oxy-hydroxides)	0.14	48.56	7.56	2.69
250-125_41	Secondary Fe minerals (Fe oxy-hydroxides)	0.14	50.86	5.49	2.27

Name	Type	S	Fe	Zn	Pb
		wt%	*wt%*	*wt%*	*wt%*
63-31_88	Secondary Fe minerals (Fe oxy-hydroxides)	0.15	46.00	3.21	2.27
63-31_114	Secondary Fe minerals (Fe oxy-hydroxides)	0.15	45.59	5.59	1.52
125-63_50	Secondary Fe minerals (Fe oxy-hydroxides)	0.15	45.72	4.76	1.66
63-31_24	Secondary Fe minerals (Fe oxy-hydroxides)	0.15	48.80	3.05	0.98
63-31_75	Secondary Fe minerals (Fe oxy-hydroxides)	0.16	43.62	7.22	0.66
125-63_54	Secondary Fe minerals (Fe oxy-hydroxides)	0.17	45.98	3.87	2.20
250-125_27	Secondary Fe minerals (Fe oxy-hydroxides)	0.18	52.23	3.80	1.36
125-63_48	Secondary Fe minerals (Fe oxy-hydroxides)	0.18	42.08	3.36	2.52
250-125_100-a	Secondary Fe minerals (Fe oxy-hydroxides)	0.19	51.51	4.72	3.44
250-125_128	Secondary Fe minerals (Fe oxy-hydroxides)	0.20	54.10	2.35	1.17
63-31_94	Secondary Fe minerals (Fe oxy-hydroxides)	0.22	49.41	3.97	1.54
63-31_136	Secondary Fe minerals (Fe oxy-hydroxides)	0.23	49.60	1.85	1.08
125-63_104	Secondary Fe minerals (Fe oxy-hydroxides)	0.24	42.25	7.11	1.37
63-31_42	Secondary Fe minerals (Fe oxy-hydroxides)	0.30	33.68	3.81	1.81
125-63_86	Secondary Fe minerals (Fe oxy-hydroxides)	0.31	47.43	4.44	2.01
250-125_101-a	Secondary Fe minerals (Fe oxy-hydroxides)	0.32	51.57	4.75	1.81
125-63_77	Secondary Fe minerals (Fe oxy-hydroxides)	0.33	27.00	2.84	1.94
63-31_67	Secondary Fe minerals (Fe oxy-hydroxides)	0.34	42.74	4.09	2.25
250-125_97	Secondary Fe minerals (Fe oxy-hydroxides)	0.36	54.45	3.17	4.53
125-63_55	Secondary Fe minerals (Fe oxy-hydroxides)	0.36	43.67	5.64	2.61
250-125_104	Secondary Fe minerals (Fe oxy-hydroxides)	0.38	50.93	5.18	1.70
63-31_12	Secondary Fe minerals (Fe oxy-hydroxides)	0.47	47.24	2.14	1.61
63-31_73	Secondary Fe minerals (Fe oxy-hydroxides)	0.55	40.24	5.65	8.43
125-63_20	Secondary Fe minerals (Fe oxy-hydroxides)	0.85	40.04	4.36	5.57
250-125_124	Secondary Fe minerals (Fe oxy-hydroxides)	0.90	47.89	6.26	3.65
250-125_36	Secondary Fe minerals (Fe oxy-hydroxides)	0.93	40.26	6.86	0.57
63-31_4	Secondary Fe minerals (Fe oxy-hydroxides)	1.03	42.32	7.37	2.54
125-63_26 - b	Secondary Fe minerals (Fe oxy-hydroxides)	1.21	32.95	3.09	4.07
125-63_87 - a	Secondary Fe minerals (Fe oxy-hydroxides)	1.26	39.01	2.99	6.62
250-125_143	Secondary Fe minerals (Fe oxy-hydroxides)	1.31	48.44	7.62	2.20
250-125_20	Secondary Fe minerals (Fe oxy-hydroxides)	1.41	42.80	3.74	8.03
125-63_33	Secondary Fe minerals (Fe oxy-hydroxides)	1.55	44.01	4.83	5.05
63-31_59 - c	Secondary Fe minerals (Fe oxy-hydroxides)	3.45	23.99	1.13	6.97
63-31_122 - b	Secondary Fe minerals Pb-rich	0.03	30.40	4.03	9.40
125-63_99	Secondary Fe minerals Pb-rich	0.03	36.44	5.65	12.20
63-31_150	Secondary Fe minerals Pb-rich	0.03	34.43	5.45	15.13
125-63_41	Secondary Fe minerals Pb-rich	0.06	39.52	5.16	10.21
63-31_19	Secondary Fe minerals Pb-rich	0.07	37.88	4.67	13.30
250-125_23-c	Secondary Fe minerals Pb-rich	2.22	35.95	3.90	11.72
250-125_9	Secondary Fe minerals Pb-rich	2.74	34.13	2.16	9.71
125-63_87 - b	Secondary Fe minerals Pb-rich	3.02	23.63	1.00	13.68
63-31_74	Secondary Fe minerals Pb-rich	3.48	28.06	1.30	16.40
125-63_138	Secondary Fe minerals Pb-rich	3.69	27.98	1.36	10.93
125-63_26 - a	Secondary Fe minerals Pb-rich	4.55	27.99	2.01	15.09
125-63_60	Secondary Fe minerals Pb-rich	4.92	29.22	1.42	10.98
125-63_84	Secondary Fe minerals Pb-rich	6.44	24.70	0.36	12.30
125-63_98	Secondary Fe minerals Zn-rich	0.00	13.74	36.36	1.04
63-31_56	Secondary Fe minerals Zn-rich	0.02	42.16	8.52	0.69
63-31_124	Secondary Fe minerals Zn-rich	0.02	41.03	7.47	2.36
63-31_93	Secondary Fe minerals Zn-rich	0.03	30.38	6.54	1.02
250-125_33-r	Secondary Fe minerals Zn-rich	0.03	23.79	20.26	0.93
125-63_29	Secondary Fe minerals Zn-rich	0.03	16.87	12.35	0.70
63-31_49	Secondary Fe minerals Zn-rich	0.03	41.30	8.16	2.03
125-63_7	Secondary Fe minerals Zn-rich	0.04	43.62	7.89	0.46
63-31_130	Secondary Fe minerals Zn-rich	0.04	14.70	17.31	0.57
250-125_60	Secondary Fe minerals Zn-rich	0.05	48.59	8.69	1.42
250-125_80	Secondary Fe minerals Zn-rich	0.05	47.93	8.51	1.03
250-125_19-b	Secondary Fe minerals Zn-rich	0.05	8.89	25.75	0.80
250-125_101-b	Secondary Fe minerals Zn-rich	0.05	7.65	43.49	1.42
63-31_8	Secondary Fe minerals Zn-rich	0.05	40.12	7.54	1.30
125-63_80	Secondary Fe minerals Zn-rich	0.06	40.03	8.25	2.06
125-63_19 - a	Secondary Fe minerals Zn-rich	0.06	42.28	7.80	1.82

Name	Type	S	Fe	Zn	Pb
		wt%	*wt%*	*wt%*	*wt%*
63-31_66	Secondary Fe minerals Zn-rich	0.06	38.37	7.98	3.05
250-125_63	Secondary Fe minerals Zn-rich	0.06	23.60	24.60	1.75
250-125_26	Secondary Fe minerals Zn-rich	0.08	45.77	8.38	1.74
63-31_26	Secondary Fe minerals Zn-rich	0.08	39.95	8.34	2.81
125-63_5	Secondary Fe minerals Zn-rich	0.09	40.59	8.15	2.16
125-63_72	Secondary Fe minerals Zn-rich	0.09	41.08	9.44	1.48
250-125_89-b	Secondary Fe minerals Zn-rich	0.11	14.20	10.22	1.48
125-63_32	Secondary Fe minerals Zn-rich	0.12	34.16	9.66	1.44
125-63_126	Secondary Fe minerals Zn-rich	0.21	42.23	7.49	1.89
63-31_127	Secondary Fe minerals Zn-rich	0.39	42.05	8.08	0.84
63-31_11 - a	Secondary Fe minerals Zn-rich	4.36	42.22	7.98	1.89
63-31_43 - c	Secondary Pb minerals (Cerussite)	0.00	0.02	0.00	75.85
63-31_3 - b	Secondary Pb minerals (Cerussite)	0.00	0.07	14.31	55.85
250-125_102-a	Secondary Pb minerals (Cerussite)	0.01	0.12	1.20	0.00
125-63_75 - b	Secondary Pb minerals (Cerussite)	0.01	2.00	12.00	46.79
125-63_47	Secondary Pb minerals (Cerussite)	0.01	0.00	0.00	77.31
125-63_123 - b	Secondary Pb minerals (Cerussite)	0.01	0.00	0.15	69.61
63-31_153	Secondary Pb minerals (Cerussite)	0.87	4.90	0.28	66.19
125-63_61	Secondary Zn minerals (Smithsonite/hydrozincite)	0.00	1.92	48.49	0.21
125-63_65	Secondary Zn minerals (Smithsonite/hydrozincite)	0.00	0.00	39.39	0.23
125-63_4	Secondary Zn minerals (Smithsonite/hydrozincite)	0.00	0.03	38.88	0.26
125-63_107	Secondary Zn minerals (Smithsonite/hydrozincite)	0.00	0.10	42.38	0.08
250-125_140	Secondary Zn minerals (Smithsonite/hydrozincite)	0.00	0.14	53.76	0.51
63-31_25	Secondary Zn minerals (Smithsonite/hydrozincite)	0.00	0.10	43.63	0.18
63-31_34	Secondary Zn minerals (Smithsonite/hydrozincite)	0.00	0.28	44.96	0.05
63-31_82	Secondary Zn minerals (Smithsonite/hydrozincite)	0.00	0.04	38.08	0.42
63-31_14	Secondary Zn minerals (Smithsonite/hydrozincite)	0.00	0.42	41.56	0.18
63-31_109 - b	Secondary Zn minerals (Smithsonite/hydrozincite)	0.00	1.08	44.10	0.23
63-31_55	Secondary Zn minerals (Smithsonite/hydrozincite)	0.00	0.12	46.98	0.00
63-31_113	Secondary Zn minerals (Smithsonite/hydrozincite)	0.00	1.66	44.14	0.55
125-63_103	Secondary Zn minerals (Smithsonite/hydrozincite)	0.00	0.60	44.77	0.24
125-63_119	Secondary Zn minerals (Smithsonite/hydrozincite)	0.00	0.30	39.22	0.63
250-125_89-a	Secondary Zn minerals (Smithsonite/hydrozincite)	0.00	0.74	51.64	0.39
125-63_120	Secondary Zn minerals (Smithsonite/hydrozincite)	0.00	0.09	38.03	0.71
63-31_36	Secondary Zn minerals (Smithsonite/hydrozincite)	0.00	1.03	44.69	0.21
250-125_74	Secondary Zn minerals (Smithsonite/hydrozincite)	0.01	0.02	53.13	0.45
250-125_62	Secondary Zn minerals (Smithsonite/hydrozincite)	0.01	0.07	52.73	0.39
125-63_108	Secondary Zn minerals (Smithsonite/hydrozincite)	0.01	1.52	43.17	0.52
63-31_86	Secondary Zn minerals (Smithsonite/hydrozincite)	0.01	0.12	40.18	0.29
250-125_102-b	Secondary Zn minerals (Smithsonite/hydrozincite)	0.01	0.51	51.24	0.02
250-125_11	Secondary Zn minerals (Smithsonite/hydrozincite)	0.01	0.07	51.36	0.14
250-125_49	Secondary Zn minerals (Smithsonite/hydrozincite)	0.01	1.83	48.34	0.41
250-125_113	Secondary Zn minerals (Smithsonite/hydrozincite)	0.01	0.00	54.21	0.04
125-63_130	Secondary Zn minerals (Smithsonite/hydrozincite)	0.01	0.01	38.19	0.42
250-125_21-r	Secondary Zn minerals (Smithsonite/hydrozincite)	0.01	0.37	51.56	0.40
63-31_85	Secondary Zn minerals (Smithsonite/hydrozincite)	0.01	0.39	41.65	0.13
125-63_15	Secondary Zn minerals (Smithsonite/hydrozincite)	0.01	0.00	37.98	0.18
63-31_89	Secondary Zn minerals (Smithsonite/hydrozincite)	0.01	3.03	43.93	0.39
250-125_96-a	Secondary Zn minerals (Smithsonite/hydrozincite)	0.01	0.31	51.95	1.12
63-31_50	Secondary Zn minerals (Smithsonite/hydrozincite)	0.01	3.25	42.05	0.51
250-125_105	Secondary Zn minerals (Smithsonite/hydrozincite)	0.01	0.57	52.26	0.90
125-63_10	Secondary Zn minerals (Smithsonite/hydrozincite)	0.02	0.21	39.40	0.64
125-63_40	Secondary Zn minerals (Smithsonite/hydrozincite)	0.02	0.09	45.67	0.07
125-63_31	Secondary Zn minerals (Smithsonite/hydrozincite)	0.02	0.42	44.10	0.12
250-125_34	Secondary Zn minerals (Smithsonite/hydrozincite)	0.02	0.00	50.33	0.03
125-63_67	Secondary Zn minerals (Smithsonite/hydrozincite)	0.02	1.83	43.33	0.42
125-63_75 - a	Secondary Zn minerals (Smithsonite/hydrozincite)	0.02	2.15	45.86	0.27
250-125_47	Secondary Zn minerals (Smithsonite/hydrozincite)	0.02	0.02	46.32	0.40
125-63_9	Secondary Zn minerals (Smithsonite/hydrozincite)	0.02	0.10	26.89	0.60
125-63_91	Secondary Zn minerals (Smithsonite/hydrozincite)	0.02	0.14	41.50	0.22
125-63_110 - a	Secondary Zn minerals (Smithsonite/hydrozincite)	0.02	0.75	42.45	0.07
250-125_30	Secondary Zn minerals (Smithsonite/hydrozincite)	0.02	6.97	33.58	0.55

Name	Type	S	Fe	Zn	Pb
		wt%	*wt%*	*wt%*	*wt%*
250-125_21-c	Secondary Zn minerals (Smithsonite/hydrozincite)	0.02	0.07	51.69	0.56
63-31_3 - a	Secondary Zn minerals (Smithsonite/hydrozincite)	0.02	0.10	38.02	0.68
125-63_111	Secondary Zn minerals (Smithsonite/hydrozincite)	0.03	0.25	33.74	1.10
250-125_132	Secondary Zn minerals (Smithsonite/hydrozincite)	0.03	0.03	53.33	0.59
250-125_64-b	Secondary Zn minerals (Smithsonite/hydrozincite)	0.03	0.97	45.87	0.57
125-63_19 - b	Secondary Zn minerals (Smithsonite/hydrozincite)	0.03	4.53	41.38	0.63
250-125_53-r	Secondary Zn minerals (Smithsonite/hydrozincite)	0.03	0.02	26.78	0.54
250-125_15	Secondary Zn minerals (Smithsonite/hydrozincite)	0.03	0.18	42.25	0.62
250-125_144-b	Secondary Zn minerals (Smithsonite/hydrozincite)	0.03	1.75	48.47	0.00
250-125_53-c	Secondary Zn minerals (Smithsonite/hydrozincite)	0.03	0.03	32.95	0.71
125-63_123 - a	Secondary Zn minerals (Smithsonite/hydrozincite)	0.03	0.04	31.08	1.67
250-125_127	Secondary Zn minerals (Smithsonite/hydrozincite)	0.03	1.55	54.38	0.00
125-63_66	Secondary Zn minerals (Smithsonite/hydrozincite)	0.03	0.02	22.77	1.02
125-63_124 - a	Secondary Zn minerals (Smithsonite/hydrozincite)	0.04	0.29	27.60	1.13
250-125_33-c	Secondary Zn minerals (Smithsonite/hydrozincite)	0.04	1.02	31.22	0.69
250-125_61	Secondary Zn minerals (Smithsonite/hydrozincite)	0.04	0.46	30.04	1.05
125-63_93	Secondary Zn minerals (Smithsonite/hydrozincite)	0.04	0.00	24.95	0.37
125-63_89 - b	Secondary Zn minerals (Smithsonite/hydrozincite)	0.05	0.39	21.34	0.29
125-63_16	Secondary Zn minerals (Smithsonite/hydrozincite)	0.08	0.12	44.95	1.76
250-125_131	Secondary Zn minerals (Smithsonite/hydrozincite)	0.11	0.05	52.74	0.53
125-63_25	Silicates	0.02	8.71	1.02	0.23
63-31_62	Silicates	0.03	0.33	0.01	0.00
250-125_92-c	Silicates	0.04	12.16	10.09	0.18
63-31_48	Silicates	0.11	1.23	9.17	7.10

Appendix B: data from the Cu-Sb-Ag Mt. Avanza mining site

Table B.3 - Chemical-physical parameters and concentrations of the major ions of waters in the Cu-Sb(-Ag) Mt. Avanza decommissioned mining site (Paper IV).

Name	**Date**	**Type**	**pH**	**ORP**	**T**	**EC**	**DO**	**Sat. O_2**	**TDS**	**Ca^{2+}**	**Mg^{2+}**	**Na^{+}**	**K^{+}**	**F^{-}**	**Cl^{-}**	**NO_3^{-}**	**SO_4^{2-}**	**HCO_3^{-}**	**CO_3^{2-}**
				mV	*°C*	*µS/cm*	*mg/L*	*%*	*mg/L*	mg/L	mg/L	mg/L	mg/L	mg/L	mg/L	mg/L	mg/L	mg/L	mg/L
MA04	01/06/2021	Mine drainage water	8.5	103	5.2	206	9.1	87.2	100	39.5	5.35	0.84	0.44	0.02	0.30	1.12	7.36	150	< LOD
MA04	18/10/2021	Mine drainage water	7.7	74.0	6.3	127	6.1	61.0	n.d.	39.9	4.16	1.00	0.42	0.05	0.55	1.25	8.08	165	< LOD
MA04	12/11/2021	Mine drainage water	7.8	220	5.6	200	8.7	83.8	100	36.9	4.12	1.07	0.60	0.10	0.50	1.22	7.58	164	< LOD
MA09	01/06/2021	Mine drainage water	8.8	226	6.4	221	11.2	119.3	111	42.1	5.30	1.02	0.66	0.02	0.22	1.07	9.24	171	< LOD
MA09	18/10/2021	Mine drainage water	7.8	74	6.1	130	5.6	57.2	n.d.	37.7	5.84	0.77	0.52	0.08	0.26	0.94	8.17	166	< LOD
MA09	12/11/2021	Mine drainage water	7.6	281	5.5	184	6.7	64.6	92	38.1	3.89	0.66	0.53	0.01	0.24	0.81	4.81	156	< LOD
MA12	01/06/2021	Mine drainage water	n.d.	239	6.5	227	n.d.	n.d.	113	42.4	6.19	0.87	0.57	0.01	0.16	0.71	10.1	168	< LOD
MA12	18/10/2021	Mine drainage water	8.0	97.0	5.2	n.d.	6.0	57.0	n.d.	37.4	2.88	0.49	0.43	0.04	0.24	0.37	2.44	155	< LOD
MA12	12/11/2021	Mine drainage water	7.5	303	5.0	170	6.4	60.6	85	37.5	2.99	0.82	0.52	0.01	0.65	0.66	3.07	148	< LOD
MA12IN	01/06/2021	Mine drainage water	n.d.	238	5.3	114	12.3	118.5	54	41.3	6.49	0.90	0.60	0.01	0.13	0.81	10.2	171	< LOD
MA12IN	12/11/2021	Mine drainage water	8.0	284	5.6	169	7.3	70.3	85	39.0	2.65	0.52	0.42	0.04	0.21	0.96	2.78	148	< LOD
MA28	18/10/2021	Main river	8.4	72	7.0	262	6.6	64.0	*n.d.*	109	17.6	3.41	1.10	0.15	0.88	2.62	181	209	< LOD
MA28	12/11/2021	Main river	8.4	290	5.7	531	7.4	69.3	266	107	17.1	3.27	1.15	0.04	0.46	2.97	172	149	10.8
MA32	12/11/2021	Main river	8.3	288	5.7	427	7.5	71.1	213	82.3	14.0	3.20	1.08	0.02	0.46	2.74	124	143	10.8
MA35	12/11/2021	Main river	8.4	299	7.4	864	8.2	75.8	432	197	26.1	4.65	1.17	0.26	2.15	2.01	316	204	< LOD
MA37	12/11/2021	Main river	8.2	301	7.7	606	7.8	71.7	303	112	25.6	2.85	0.99	0.29	1.76	2.54	196	221	< LOD
MA29	12/11/2021	Tributaries	8.2	288	6.6	225	7.3	70.6	112	34.1	11.7	2.68	1.26	0.03	0.28	1.57	16.2	178	< LOD
MA30	12/11/2021	Tributaries	8.4	287	6.3	226	7.1	67.9	113	42.3	7.71	1.20	0.66	0.03	0.37	4.29	15.9	132	12.0
MA31	12/11/2021	Tributaries	8.5	290	8.2	223	7.6	75.8	111	42.8	8.57	1.51	0.83	0.05	0.30	3.81	16.1	151	6.0
MA33	12/11/2021	Tributaries	8.4	287	7.0	176	6.7	64.5	88	39.8	3.25	0.85	0.57	0.03	0.34	1.04	5.40	156	< LOD
MA36	12/11/2021	Tributaries	8.4	294	6.5	189	8.1	74.7	95	34.9	7.37	1.09	0.46	0.04	0.22	1.85	14.2	164	< LOD

Table B.2 – Trace element concentration of waters in the Cu-Sb(-Ag) Mt. Avanza decommissioned mining site (Paper IV).

Name	Date	Type	As	Ba	Cu	Fe	Hg	Mn	Mo	Pb	Sb	Zn
			µg/L	µg/L	µg/L	µg/L	ng/L	µg/L	µg/L	µg/L	µg/L	µg/L
MA04	01/06/2021	Mine drainage water	11.0	48.6	1.59	12.2	n.d.	2.78	0.29	0.73	4.58	3.81
MA04	18/10/2021	Mine drainage water	14.8	45.4	1.79	10.5	6.96	1.88	0.47	0.33	4.33	2.97
MA04	12/11/2021	Mine drainage water	14.4	46.3	3.31	10.1	12.2	1.80	0.43	< LOD	5.12	11.0
MA09	01/06/2021	Mine drainage water	2.14	99.5	3.74	9.63	n.d.	1.78	0.17	0.72	20.3	9.36
MA09	18/10/2021	Mine drainage water	1.05	90.9	0.29	6.16	2.41	0.77	0.22	< LOD	19.2	< LOD
MA09	12/11/2021	Mine drainage water	0.93	80.4	0.97	5.70	9.23	1.00	0.17	< LOD	16.0	2.53
MA12	01/06/2021	Mine drainage water	3.02	83.8	5.30	7.99	n.d.	1.10	0.17	0.58	20.3	6.11
MA12	18/10/2021	Mine drainage water	0.87	62.2	1.44	14.1	5.11	1.42	< LOD	< LOD	11.0	< LOD
MA12	12/11/2021	Mine drainage water	0.88	59.3	2.32	5.98	4.31	1.41	0.13	0.22	13.8	3.12
MA12IN	01/06/2021	Mine drainage water	3.73	87.6	8.28	7.30	n.d.	0.30	0.17	1.02	19.0	10.9
MA12IN	12/11/2021	Mine drainage water	1.05	42.4	2.24	4.16	13.2	0.11	< LOD	0.44	7.28	1.85
MA28	18/10/2021	Main river	1.04	102	0.38	16.9	6.17	1.62	0.86	< LOD	0.56	< LOD
MA28	12/11/2021	Main river	1.09	103	1.08	27.5	2.70	1.49	0.86	0.59	0.54	3.81
MA32	12/11/2021	Main river	1.02	91.1	0.18	10.5	1.17	0.35	0.58	0.72	0.30	4.30
MA35	12/11/2021	Main river	2.98	56.0	0.17	25.7	6.49	0.90	6.70	< LOD	1.16	0.34
MA37	12/11/2021	Main river	0.60	46.1	< LOD	14.5	2.45	0.27	3.00	< LOD	0.34	< LOD
MA29	12/11/2021	Tributaries	3.89	277	0.12	3.66	1.81	0.15	0.18	< LOD	0.35	0.47
MA30	12/11/2021	Tributaries	1.45	172	0.27	5.21	2.07	0.16	0.37	< LOD	1.51	< LOD
MA31	12/11/2021	Tributaries	1.69	193	0.36	5.42	7.63	0.32	0.34	< LOD	1.39	0.67
MA33	12/11/2021	Tributaries	0.46	96.9	0.41	5.25	7.28	0.33	< LOD	< LOD	1.59	0.83
MA36	12/11/2021	Tributaries	0.18	< LOD	0.35	5.02	10.2	0.37	0.96	< LOD	0.19	1.90

Table B.3 – Trace element concentration of solids in the Cu-Sb(-Ag) Mt. Avanza decommissioned mining site (Paper IV).

Name	Type	Ag	As	Bi	Cd	Cr	Cu	Fe	Ge	Hg	Mn	Mo	Pb	Sb	Tl	Zn
		mg/kg	*mg/kg*	*mg/kg*	*mg/kg*	*mg/kg*	*mg/kg*	*mg/kg*	*mg/kg*	*mg/kg*	*mg/kg*	*mg/kg*	*mg/kg*	*mg/kg*	*mg/kg*	*mg/kg*
MA01	Waste rock pile	3.98	135	0.58	1.39	23.2	806	11179	0.82	56.9	230	0.47	127	230	0.27	180
MA02	Waste rock pile	0.71	47.4	0.20	0.37	18.6	167	8845	0.87	13.3	265	0.38	19.4	40.8	0.27	52.7
MA03	Waste rock pile	0.15	8.20	< LOD	0.17	6.91	31.3	3248	0.20	1.42	138	< LOD	27.4	5.00	0.09	20.3
MA05	Waste rock pile	14.1	654	1.98	6.19	25.5	4019	8196	1.25	473	251	0.54	397	1049	0.34	553
MA15	Waste rock pile	1.13	26.8	0.54	0.33	80.4	144	36895	1.62	10.1	689	0.54	329	26.0	0.93	157
MA20	Waste rock pile	3.57	144	0.84	1.11	88.0	1226	15291	2.26	71.8	172	1.33	178	353	1.07	167
MA06	Soil	0.50	15.6	0.87	0.23	76.0	35.6	32215	1.27	2.35	321	1.35	47.5	6.4	0.82	83.3
MA07	Soil	5.54	160	1.51	2.03	80.3	1557	35700	1.58	132	758	0.90	208	153	0.84	309
MA08	Soil	1.81	162	0.43	1.32	25.0	234	8042	0.84	17.4	285	0.67	1216	31.7	0.31	223
MA10	Soil	0.21	27.8	0.52	0.34	76.3	69.5	39296	1.47	2.21	513	1.45	44.4	19.9	0.81	140
MA11	Soil	0.47	18.6	0.41	0.21	89.0	78.1	36951	1.39	3.52	571	0.68	110	19.9	0.87	92.1
MA12	Soil	1.07	27.2	0.41	0.60	44.2	243	21708	1.24	9.10	346	0.44	68.4	33.2	0.54	133
MA13	Soil	0.66	34.7	0.40	0.34	46.0	155	22829	1.28	15.4	420	0.66	98.7	38.0	0.59	86.3
MA14	Soil	0.85	33.0	0.38	0.35	41.9	139	23529	1.55	9.51	304	0.54	142	40.8	0.62	94.2
MA16	Soil	0.14	21.1	0.41	0.16	52.8	41.5	31447	1.73	1.36	318	0.68	37.5	10.2	0.79	78.9
MA17	Soil	0.48	14.2	0.44	0.09	73.1	15.3	32251	1.29	0.42	273	0.98	50.3	5.33	0.79	62.6
MA18	Soil	0.30	21.1	0.41	0.21	39.4	10.1	24329	1.39	0.52	1227	0.57	50.9	2.74	0.73	83.7
MA19	Soil	6.91	14.9	0.37	1.04	182	269	17858	0.93	28.7	734	1.59	134	21.7	0.31	1204
MA21	Soil	0.31	23.3	0.49	0.09	72.8	27.0	34032	1.26	0.65	437	1.27	121	16.8	0.85	70.2
MA22	Soil	< LOD	12.1	0.32	0.20	78.1	26.8	38733	1.75	1.06	744	0.69	51.5	8.88	0.95	126
MA23	Soil	< LOD	17.3	0.36	0.06	78.1	24.3	31135	1.27	0.37	185	1.09	42.8	5.87	0.80	62.0
MA24	Soil	< LOD	22.7	0.37	0.06	95.1	32.5	32449	1.28	0.21	396	1.17	26.4	8.05	0.93	66.4
MA25	Soil	0.59	51.8	0.44	0.43	61.1	163	30892	1.24	13.4	547	0.82	72.4	32.0	0.82	125
MA26	Soil	0.33	17.0	0.36	0.15	49.7	20.8	28649	1.26	0.88	713	1.10	50.3	6.60	0.78	80.4
MA27	Soil	1.40	38.5	0.51	0.66	79.5	150	37755	1.38	14.5	591	0.71	176	28.9	0.85	159
MA04	Sediment	0.22	212	0.21	0.41	56.5	90.1	30407	2.03	3.24	476	1.27	62.5	15.6	0.75	156
MA12	Sediment	0.65	40.0	0.39	0.54	52.4	242	23753	1.20	9.15	247	0.61	78.8	28.0	0.69	158
MA28	Sediment	< LOD	23.7	n.d.	0.46	89.6	34.9	47006	2.03	0.27	577	1.28	28.5	7.41	0.76	145
MA29	Sediment	0.19	25.7	n.d.	0.16	62.6	33.8	43924	2.83	0.13	537	0.59	33.0	4.04	1.04	121
MA30	Sediment	0.21	28.4	n.d.	0.58	101.6	39.6	49918	1.78	0.18	523	0.99	35.8	8.88	0.90	171

Name	Type	Ag	As	Bi	Cd	Cr	Cu	Fe	Ge	Hg	Mn	Mo	Pb	Sb	Tl	Zn
		mg/kg	*mg/kg*	*mg/kg*	*mg/kg*	*mg/kg*	*mg/kg*	*mg/kg*	*mg/kg*	*mg/kg*	*mg/kg*	*mg/kg*	*mg/kg*	*mg/kg*	*mg/kg*	*mg/kg*
MA31	Sediment	< LOD	23.1	n.d.	0.47	84.3	41.3	44872	1.70	0.15	471	1.08	57.9	7.04	0.76	147
MA32	Sediment	< LOD	19.8	n.d.	0.15	62.3	21.2	36890	1.84	0.04	525	1.22	21.9	3.06	0.74	86.3
MA33	Sediment	< LOD	17.1	n.d.	0.11	60.0	23.8	40387	1.63	0.12	474	0.99	24.2	5.44	0.68	93.2
MA34	Sediment	< LOD	28.7	n.d.	0.51	89.9	35.5	42409	1.85	0.39	532	1.14	42.3	7.93	0.88	139
MA35	Sediment	0.26	31.3	n.d.	0.65	79.8	43.0	38654	1.81	0.62	667	1.69	52.7	8.23	0.85	139
MA36	Sediment	< LOD	12.9	n.d.	0.12	54.8	15.8	22674	1.50	0.18	358	1.32	14.7	1.64	0.50	61.5
MA37	Sediment	< LOD	13.1	n.d.	0.10	49.0	14.0	20816	1.44	0.13	327	1.22	15.6	2.06	0.50	57.1